STUDY OF LONG-TERM BEHAVIOUR OF ACTINIDES IN THE TROPICAL MARINE ECOSYSTEM OF TROMBAY

By

AJAY KUMAR
Enrolment No ((CHEM01200804015)
Bhabha Atomic Research Centre, Mumbai

A thesis submitted to the
Board of Studies in Chemical Sciences

In partial fulfilment of requirements
for the Degree of
DOCTOR OF PHILOSOPHY
of
HOMI BHABHA NATIONAL INSTITUTE

May, 2014

Homi Bhabha National Institute

Recommendations of the Viva Voce Committee

As members of the Viva Voce Committee, we certify that we have read the dissertation prepared by Shri Ajay Kumar entitled "Study of long-term behaviour of actinides in the tropical marine ecosystem of Trombay" and recommend that it may be accepted as fulfilling the thesis requirement for the award of Degree of Doctor of Philosophy.

Date: 16.09.14

Chairman – Prof. A. V. R. Reddy

Date: 16.09.14

Guide/Convener – Dr. R. K. Singhal

Date: 16/Sept/2014.

Examiner – Prof. M. M. Sarin

Date: 16/9/2014

Member – Prof. B. S. Tomar

Date: 16/9/2014

Member – Prof. G. G. Pandit

Date: 16/9/14

Member – Prof. P. K. Mohapatra

Final approval and acceptance of this thesis is contingent upon the candidate's submission of the final copies of the thesis to HBNI.

I hereby certify that I have read this thesis prepared under my direction and recommend that it may be accepted as fulfilling the thesis requirement.

Date:

Place:

Guide

Statement by Author

This dissertation has been submitted in partial fulfillment of requirements for an advanced degree at Homi Bhabha National Institute (HBNI) and is deposited in the library to be made to borrowers under rules of the HBNI.

Brief quotations from this dissertation are allowable without special permission provided that accurate acknowledgement of source is made. Requests for permission for extended quotation from or reproduction of this manuscript in whole or in part may be granted by the Competent Authority of HBNI when in his or her judgment the proposed use of the material is in the interest of scholarship. In all other instances, however, permission must be obtained from the author.

Ajay Kumar

Declaration

I, hereby declare that the investigation presented in the thesis has ben carried out by me. The work is original and has not been submitted earlier as a whole or in part for a degree/diploma at this or any other Institution/University.

Ajay Kumar

List of Publications arising from the thesis

International Journal

1. “Spatial Distribution an Accumulation of ^{226}Ra, ^{228}Ra, ^{40}K and ^{137}Cs in Bottom Sediments of Mumbai Harbour Bay”, Ajay Kumar, R.K. Singhal and P.M. Ravi, *Journal of Radioanalytical Nuclear Chemistry*, **(2013),** *Vol.* 295(2), 835-839.

2. “Adsorption and kinetic behavior of uranium and thorium in seawater-sediment system”, Ajay Kumar, R. K. Singhal and P. M. Ravi, *Journal of Radioanalytical Nuclear Chemistry*, **(2013),** *Vol.* 295(1), 649-656.

3. “Spatial geochemical variation of major and trace elements in the marine sediments of Mumbai Harbor Bay”, Ajay Kumar, R. K. Singhal and P. M. Ravi, *Environmental Earth Science*, **(2013),** *Vol.* 70, 3057 – 3066.

4. “Thermodynamic parameters of U (VI) sorption onto soils in aquatic systems”, Ajay Kumar, R.K. Singhal and P.M. Ravi, *Environmental Earth Science (Springer Plus)*, **(2013).** Vol. 2 (1), DOI: 10.1186/2193-1801-2-530.

5. “Modeling of ^{137}Cs migration in cores of marine sediments of Mumbai Harbor Bay”, Ajay Kumar, R.K. Singhal, P.M. Ravi and R.M. Tripathi, *Journal of Radioanalytical Nuclear Chemistry*, **(2014),** DOI: 10.1007/s10967-012-2166-3.

6. “Inventory, fluxes and residence times from the depth profiles of naturally occurring ^{210}Pb in marine sediments of Mumbai Harbor Bay”, Ajay Kumar, R.K. Singhal, P.M. Ravi and R.M.Tripathi, *Environmental Earth Science*, ***(2014),*** DOI 10.1007/s12665-014-3687-6.

7. “Application of Chemometric Methods for Assessment of Heavy Metal Pollution and Source Apportionment in Riparian Zone Soil of Ulhas River Estuary, India”, Sabyasachi Rout, Ajay Kumar and P.M. Ravi, *International Journal of Environmental Sciences*, **(2013),** *Vol.* 3(5) DOI:10.6088/ijes.2013030500019.

8. “Groundwater Geochemistry Study of Estuarine Aquifer, Western India: Mumbai using Chemometric and Conventional Techniques”, Sabyasachi Rout, Ajay Kumar and P.M. Ravi, *Journal of Advances in Chemical Science*, (2012), *Vol.* 1, 1-9.

9. “Selective separation of iron from uranium in quantitative determination of traces of uranium by alpha spectrometry in soil/sediment sample”, Singhal, R.K., Ajay, K., Ranade, A. and Ramachandran, V., *Applied Radiation and Isotopes*, (2009), *Vol.* 67(4), 501-505.

10. “Mobilization of heavy metals from mineral phase and the speciation in potable aquifers due to saline intrusion”, Sabyasachi Rout, Ajay Kumar, P.M. Ravi and R.M. Tripathi, *Journal of Energy and Environment*, (2013), *Vol.* 64, 19049-19053.

Conferences

1. Estimation of total inventories and atmospheric fluxes of naturally occurring ^{210}Pb from core sediments of Mumbai Harbour Bay using radiometric dating, Ajay Kumar, Sabyasachi Rout, P.M. Ravi and R.M.Tripathi, (2014), International Conference on Radiation Protection, Culture- A global challenge (IRPA- 4) during 23 – 27, June, 2014 at Geneva, Switzerland.

2. A novel approach to determine the recent sedimentation rate in the Mumbai Harbour Bay using ^{228}Ra/^{226}Ra geochronology, Ajay Kumar, Sabyasachi Rout, Manish K. Mishra, P.M. Ravi and R.M. Tripathi, (2014), National conference on Advances in Radiation Measurement Systems and Techniques, (IARPNC-2014), 19 – 21, March, 2014, BARC Trombay, Mumbai.

3. Effective vertical migration velocity and residence times of ^{137}Cs in sediments of Mumbai Harbor Bay using compartment models, Ajay Kumar, Sabyasachi Rout, P.M. Ravi and R.M.Tripathi, (2014), National Symposium on Nuclear Analytical Chemistry (NAC-V), 20 – 24, January, 2014, at BARC Trombay, Mumbai.

4. Salinity effect and pH dependence of chemical speciation and kinetic rate of U (VI) sorption onto soil in groundwater system, Ajay Kumar, Sabyasachi Rout, Rupali Karpe and P.M. Ravi, (2013), National Symposium on Environment (NSE-18), Anantapur (AP), 11-12, March, 2013 (BS Publications, Hyderabad, ISBN:978-81-7800-287-3).

5. A Comparative study of distribution coefficients (K_d) for naturally occurring Uranium (U) and Thorium (Th) in two different aquatic environments, Ajay Kumar, Rupali Karpe, Sabyasachi Rout, Manish Kumar Mishra, Usha Narayanan and P.M. Ravi (2012), Radiation protection and environment. Indian Association of Radiation Protection (IARPNC-2012) , 15-17, March, 2012, Mangalore University, Mangalore.

6. Particle size characterization and distribution of Ra-226 and Ra-228 as a function of depth in Marine sediments, Ajay Kumar, Rupali Karpe, Sabyasachi Rout, Manish K. Mishra, V.M. Joshi and P.M. Ravi (2012), National conference of Indian Aerosol Science and Technology Association (IASTA-2012), 11 – 13, December 2012, Vashi, Navi Mumbai.

7. Sorption characteristics of uranium and thorium in seawater –sediment system, Ajay Kumar, R.K. Singhal, Sabyasachi Rout, Usha Narayanan, Rupali Karpe, and P.M. Ravi (2012), International Conference on Sediment Management, (12SM-2012), 20-22, March, 2012, Alibaug, Raigad . (Received Best Paper award as the best contributory paper presentation).

8. Spatial Distribution of ^{226}Ra, ^{228}Ra, ^{40}K and ^{137}Cs in grab sediments of Mumbai Harbour Bay, Ajay Kumar, R.K. Singhal, Sabyasachi Rout, V.M.Joshi, Rupali Karpe, and P.M. Ravi (2012), International Conference on Sediment Management, (12SM-2012), 20-22, March, 2012, Alibaug, Raigad.

9. Chemical speciation modeling of uranium, thorium and $^{239+240}$ Pu in seawater of Mumbai Harbour Bay, Ajay Kumar, R.K. Singhal, Sabyasachi Rout and P.M. Ravi (2012),

International conference on Sediment Management, (12SM-2012), 20-22, March, 2012, Alibaug,Raigad.

10. Principal Component Analysis (PCA) for Assessment of Heavy Metals Pollution in Sediments of Mumbai Harbour Bay, Ajay Kumar, R.K. Singhal and Sabyasachi Rout, International Conference on Sediment Management, (12SM-2012),20-22, March, 2012, Alibaug, Raigad.

11. Source Apportionment of Heavy Metals in the Groundwater Sediments of Estuarine Regions in Mumbai, Sabyasachi Rout, Ajay Kumar, Manish Kumar Mishra, and P.K.Sarkar (2012), International Conference on Sediment Management, (12SM-2012), 20-22, March, 2012, Alibaug, Raigad (Received Best Paper award as a Young Scientist Presentation Award).

12. A Chemometric Approach to Characterize Chemistry of Estuarine Soil of Mumbai, India, Sabyasachi Rout, Ajay Kumar, P. K. Sarkar, Manish K. Mishra, and P. M. Ravi (2012), Indian Analytical Science Congress, 27-28 January, 2012, Kanyakumari, Tamilnadu.

Ajay Kumar

Dedications

I dedicate this dissertation to

My Parents and Uncle

Acknowledgement

At the outset, I wish to express my deepest sense of gratitude and reverences to my mentor and guide Dr. R.K.Singhal, Analytical Chemistry Division for introducing me to present area of research. His valuable and meticulous guidance with lots of constructive criticisms have served as a vital source of inspiration for bringing the present work in the final shape. His affectionate treatment and magnanimity made it feasible to bring the present work to conclusion.

Further, I am extremely grateful to Dr. D.N.Sharma, Director, Health, Safety and Environment Group, Dr. R.M.Tripathi, Head, Health Physics Division and Dr. P.M.Ravi, Head, Environmental Studies Section, Health Physics Division, BARC for providing much more assistance than deserved, the motivation, the detailed technical attention and support.

I am grateful for Dr. (Smt) Usha Narayanan and Smt. Rupali K., Environmental Studies Section, Health Physics Division for helping me in conducting the laboratory experiments, analyzing samples and providing countless assistance during my experimental works.

I express my sincere thanks to my other colleagues Manish Kumar Mishra, Shri Sabyasachi Rout and V.M. Joshi, Environmental Studies Section, Health Physics Division for their valuable advice and help rendered by them during my experimental works.

I am highly indebted to my doctoral committee chaired by Dr. A.V.R.Reddy, along with other members Dr. B.S.Tomar, Dr.G.G.Pandit, Dr.P.K.Mahopatra, for their constructive remarks that helped significantly in improving the focus of thesis.

It would be incomplete if I do not acknowledge, Shri G.L Teli, Shri A.K.Kazi and Shri S.B.Kamble for giving me a helping hand during collection of samples and experimental works. I am also thankful to the staff of Health Physics Division for providing countless assistance over the years.

Further, I would like to thank the Almighty, without Him I could not do anything. I want to express my heartfelt gratitude to my family, friends and relatives for their endless love, blessings, motivation and support. I would also like to express my extreme thanks to my two sons and wife for their support to complete this work.

(Ajay Kumar)

HBNI, BARC, MUMBAI
Date:

Contents

DESCRIPTION ***Page No***

CHAPTER 1

INTRODUCTION: ACTINIDES IN THE ENVIRONMENT

CHAPTER 2

AN OVERVIEW OF STUDY AREA "MUMBAI HARBOUR BAY (MHB)": NATURAL AND ANTHROPOGENIC SOURCES OF ^{238}U, ^{232}Th & $^{239+240}$Pu IN MHB

CHAPTER 3

CONCENTRATION PROFILES OF U, Th and $^{239+240}$Pu IN SEAWATER AND PREDICTION OF THEIR CHEMICAL SPECIATION USING COMPUTATIONAL METHODS

CHAPTER 4

PARTICLE SIZE CHARECTERISATION, MINERALOGY AND THEIR IMPACT ON SPATIAL AND VERTICAL DISTRIBUTION OF ^{238}U, ^{232}Th and $^{239+240}$Pu IN BOTTOM SEDIMENTS

CHAPTER 5

IMPACT OF SPATIAL GEOCHEMICAL VARIATION OF MAJOR AND TRACE ELEMENTS ON DISTRIBUTION OF ^{238}U, ^{232}Th & $^{239+240}$Pu IN THE MARINE SEDIMENTS OF MUMBAI HARBOUR BAY

CHAPTER 6

ADSORPTION - DESORPTION BEHAVIOUR OF URANIUM AND THORIUM IN SEDIMENT-SEAWATER SYSTEM AND COMPARISON WITH SOIL-GROUNDWATER SYSTEM

CHAPTER 7

PREDICTION OF CHRONICLE DEPOSITION OF ^{238}U, ^{232}Th & $^{239+240}$Pu IN CORE SEDIMENTS USING RADIOMETRIC DATING OF ^{210}Pb, ^{137}Cs and ^{228}Ra/^{226}Ra IN MUMBAI HARBOUR BAY

CHAPTER 8

THERMODYNAMICS PARAMETERS OF U (VI) SORPTION ONTO SEDIMENTS/SOILS IN VARIOUS AQUATIC SYSTEMS

Synopsis

PROLOGUE

Nuclear power is the fourth-largest source of electricity in India after thermal, hydroelectric and renewable sources of electricity. Till 2012, India has 20 nuclear reactors in operation in six nuclear power plants, generating 4,780 MW while seven other reactors are under construction and are expected to generate an additional 5,300 MW_e. In October 2010, India drew up "an ambitious plan to reach a nuclear power capacity of 63,000 MW in 2032", but "population around nuclear power plants sites (NPPS) have certain apprehension regarding its long term environmental impact on flora & fauna of the surrounding environment around the NPPS. Scientists are carrying out various research activities to understand the interaction of various effluents released from nuclear industries with the different environmental matrices (soil, water & air) with an aim to provide factual information that will instill confidence in the public.

As of now more than 70 percent of the reactors are on coastal region. Therefore it is very important to study the impact of environmental releases of long lived radionuclides on the various matrices of the coastal environment, since bays and estuaries are known to be biologically productive and strongly influenced by human activities. Coastal bay is the region of strong land-ocean interaction and their ecological functions are more complicated and vulnerable to the influence by human activities and land-source pollution than the open ocean. The bay at Trombay is called as Mumbai Harbor Bay (MHB). The average area of seawater surface of the bay is about 215 km^2 at high tide level and about 160 km^2 at low tide level.

Work described in this thesis, deals with the interaction of actinides (^{238}U, ^{232}Th & $^{239+240}$Pu) in various matrices of the coastal environment at Trombay, Mumbai India. It is known that the major contribution of actinides in the ambient environment is mainly arises due to atmospheric/underground nuclear weapon testing and major nuclear accidents like Chernobyl (Russia) in 1986 and Fukishima (Japan) in 2011. In addition to this, a small fraction of actinides may come into environment through effluents generated at different stages of nuclear fuel cycle and also through safe disposal/storage of nuclear waste. Actinides once entered into the ambient environment, their occurrence and abundances in the various matrices are controlled by their physicochemical characteristics which in turn are controlled for processes like ion –exchange, sorption, hydrolysis and complexation. In this dissertation, special emphasis was given on chemical speciation, interaction with dissolved or adsorbed components in sea water and migration patterns using various analytical methods and predictive models. As the concentration of these radionuclides in the ambient environment either below detection limit or at ultra trace level. Therefore laboratory based experiments were conducted by simulating the conditions close to the ambient marine environment. The work embodied in this thesis has been divided into eight chapters

- Introduction: actinides in the environment
- An overview of study area “Mumbai Harbour Bay (MHB)”: Natural and anthropogenic sources of ^{238}U, ^{232}Th & $^{239+240}$Pu in MHB
- Concentration profiles of U, Th and $^{239+240}$Pu in seawater and prediction of their chemical speciation using computational methods.
- Particle size characterization, mineralogy and their impact on spatial and vertical distribution of ^{238}U, ^{232}Th and $^{239+240}$Pu in bottom sediments

- Impact of spatial geochemical variation of major and trace elements on distribution of ^{238}U, ^{232}Th and $^{239+240}$Pu in the marine sediments of Mumbai Harbour Bay
- Adsorption - desorption behaviour of uranium and thorium in sediment-seawater system and comparison with soil-groundwater system
- Predication of chronicle deposition of ^{238}U, ^{232}Th and $^{239+240}$Pu in core sediments using radiometric dating of ^{210}Pb, ^{137}Cs and ^{228}Ra/^{226}Ra in Mumbai Harbour Bay
- Thermodynamics parameters of U (VI) sorption onto sediments/soils in various aquatic systems.
- Summary

CHAPTER 1: INTRODUCTION: ACTINIDES IN THE ENVIRONMENT

In this chapter, genesis of actinides (U, Th and Pu) and their introduction in the ambient environment with a special emphasis on coastal marine ecosystems are discussed. Actinides once introduced into the marine ecosystems, they get distributed among various matrices such as seawater, suspended silts, sediments, benthic and pelagic organisms etc. These distribution patterns depend on various physiochemical parameters of the participating matrices. In this regard, oxidation state of the actinides and the characteristics of the sorbing materials play a decisive role.

U and Pu are multivalent actinides under different environmental conditions and exist generally as An^{3+}, An^{4+}, AnO_2^{+} and AnO_2^{2+} species. Reduction of higher valent actinides to An^{3+} and An^{4+} species results in lower solubility and a heigher tendency to sorb on mineral surfaces. The tetravalent actinides form stable aqueous complexes and solid phases with low solubility and pentavalent actinides form the least stable complexes and more soluble solid phases. The high solubilities and hence mobilities of the actinides are generally in a higher oxidation state, which are of primary concern in an environmental context.

The sorption mechanisms of actinides are controlled by aqueous solution properties such as pH, Eh, ionic strength and presence of complexing ligands and characteristics of sorbing materials like mineral compositions, surface area, density of sorptive surface sites and solid/solution ratio. Sediments/soils contain a number of radionuclides adsorbing components in the fine particles such as silt and clay fractions. The most important for the sorption of radionuclides onto sediments/soils are clay minerals such as smectite, illite, vermiculite, chlorite, allophone and imogolite as well as the oxides and hydroxides of silica, aluminium, iron and manganese. Literature pertaining to interaction of actinides in the marine ecosystem and earlier work carried out by various researchers in order to understand the interaction of actinides with different marine components of MHB is summarized.

CHAPTER 2: AN OVERVIEW OF STUDY AREA "MUMBAI HARBOUR BAY (MHB)": NATURAL AND ANTHROPOGENIC SOURCES OF ^{238}U, ^{232}Th & $^{239+240}$Pu IN MHB

The chapter encompasses an overview of the study area which includes the interacting components (biotic and abiotic), water movement, tidal flow patterns and available dilution. The study area (MHB) is extensively exploited for multifarious activities. The bay is characterized by abundant mudflats and exhibits good coverage of mangroves. However, in recent years the mangrove areas are being intensively targeted for dumping garbage, disposal of sewage and also overexploited by salt industries, fishing, navigation and recreational activities. The transportability of suspended particulate matters (SPMs) depends on size, density, organic matter content and current velocity in the sea. The SPMs load in the study area varied from 20 to 950

mgL^{-1} with mean value of 180 mgL^{-1}. The study area is rich in benthic organisms which are frequently harvested and consumed by locals.

The average area of water surface of the bay is about 215 km^2 at high tide level and about 160 km^2 at low tide level. The total volume of water at mean sea-level as calculated from surrounding area is 9.1×10^{11} litres. The average tidal volume is 4.8×10^{11} litres. Water movement in the bay is caused by the following factors: i) Part of water from Ulhas river flowing-in through the Thane creek and water from the Panvel river ii) Monsoon water pouring into the bay and iii) Tidal water. Of these three, Ulhas and Panvel rivers contribute a small fraction towards the movement of water in the bay as compared to the factor caused by the volume of tidal water moving in or out of the bay. Discharges during the monsoon do not affect the tidal curves, as these are small compared to the tidal volume. However the flow into the bay by first two factors during the monsoon causes considerable renewal of water in the bay.

The bay is subjected to wave actions and semi-diurnal tides. Three major streams are noticeable during both high and low tides: i) Stream flowing near the Trombay shore ii) Stream flowing near the Elephanta shore (middle stream) and iii) Stream flowing between Elephanta and Nhava islands.

The actinides elements are the 15 chemical elements with atomic number 89 through 103, the first member of which is actinium and last is lawrencium. In the nuclear industry, Th, U and Pu are some of the important members of actinides series having a long half life and substantial toxicity to living beings. Though U and Th are the natural elements and exist in earth crust with the genesis of the earth. The global average concentration of U and Th in earth's crust is 3.2 and 9 μgg^{-1}. However, Pu isotopes are mainly anthropogenic radionuclides and come into the environment due to nuclear weapons (atmospheric and underground) testing, accidental disposal of high-level radioactive wastes and solvents from nuclear fuel processing, atmospheric and accidental releases from nuclear power plants. The recent reactor meltdown at the Fukishima Daiichi nuclear power plant, Japan in 2011 and the nuclear accidents at Chernobyl, Russia, in 1986, have contributed significantly. Whereas, other noticeable nuclear accidents like Three Mile Island, U.S., in 1979 and Windscale Fire, England, in 1957 could not contribute significantly as far as actinides are concerned.

CHAPTER 3: CONCENTRATION PROFILES OF U, Th AND $^{239+240}$Pu IN SEAWATER AND PREDICTION OF THEIR CHEMICAL SPECIATION USING COMPUTATIONAL METHODS.

The chapter describes concentration profiles of ^{238}U, ^{232}Th & $^{239+240}$Pu in seawater of MHB and prediction of their chemical speciation using computational methods. Seawater samples were collected in pre-acid washed plastic carboy (capacity : 35 L) from sixteen different locations covering an area of about 64 km^2 of Mumbai Harbour Bay as per standard protocols adopted by US EPA and IAEA. A grid sampling was prepared with a sub grid dimensions of 1 km x 1 km The on-site measurement of the physico-chemical parameters such as Oxidation-Reduction Potential (ORP), pH, Dissolved Oxygen (DO), Electrical Conductivity (EC), Salinity, and Total dissolved solids (TDS) in seawater during sample collection were carried out using pre calibrated standard field equipment, AM-200 GPS Aquameter (UK make). The collected sea water samples were filtered through 0.45 μm filter paper, acidified with 0.01M of nitric acid (AR Grade, Merck, Mumbai, India) and stored in pre acid washed, 200 mL capacity polypropylene bottles for cation and anion analysis. The determination of cations (Na^+, K^+, Mg^{2+}, Ca^{2+}) and anions (F^-, Cl^- , SO_4^{2-}, NO_3^-) in seawater was estimated by conductivity suppressed ion chromatography system (DIONEX600). Uranium, thorium and plutonium were sequentially separated using standard radiochemical procedures and the concentration was determined using alpha spectrometry for Th and Pu whereas uranium was determined by both alpha spectrometry and laser fluorimetry. The aqueous speciation of U, Th and Pu at various physico-chemical parameters of seawater was calculated by the speciation code MEDUSA. This code includes an extensive thermodynamic database along with HYDRA (hydrochemical equilibrium constant database) speciation program and three main different algorithms for creating chemical equilibrium diagrams. The ligands such as hydroxide, chloride, nitrate, carbonate, fluoride, sulphate, phosphate and silicate are included.

Seawater of study area was dominated by the following major ions: Na^+, K^+, Mg^{2+}, Ca^{2+}, Cl^-, SO_4^{2-}, HCO_3^- and CO_3^{2-}. Salinity and pH of seawater were found to be ranged from 20.6 ppth (parts per thousand) to 30.2 ppth and 7.5 to 8 respectively. The calculated ionic strength ranged from 0.42 to 0.62 with a mean of 0.53, which was almost comparable with the literature value (0.7) reported for seawater. On-site measurement of dissolved oxygen ranged from 3 to 8.5 mg L^{-1} indicated that there was a good aeration of seawater. The activity concentrations of U, Th and $^{239+240}Pu$ in seawater were ranged from 1 - 4.4 µg L^{-1} (mean: 2.6 ± 0.83 µg L^{-1}), 70 – 250 ng L^{-1} (mean: 143 ± 51 ng L^{-1}) and 47 – 138 µBq L^{-1} (mean: 86 ± 30 µBq L^{-1}) respectively. The reported fallout values of $^{239+240}Pu$ in seawaters ranged between 5.2 – 49 µBq L^{-1}. In general, the concentration of U, Th and $^{239+240}Pu$ in seawater showed a decreasing trend from southern part to northern part of studied area indicates a good dilution and dispersion of low level activity released from effluent treatment plant due to tidal action and water current. The variability of U, Th and $^{239+240}Pu$ in terms of coefficient of variation (CV) along the studied regions were found to be 32%, 36% and 35% respectively indicating a non-homogeneous distribution due to the consequences of meteorological conditions, sediment/suspended silt texture, mineralogical composition, anthropic input etc. The activity ratio of ^{238}U /^{232}Th in seawater along the studied locations ranged from 6.7 to 51.8 with mean value of 20 ± 10.4. Higher values of activity ratio of ^{238}U /^{232}Th in seawater clearly indicate that ^{238}U has relatively greater solubility and hence mobility compared to ^{232}Th. On the contrary, Th is highly particle reactive, immobile and strongly bound to solid matrix. The wide variation in the activity ratio of ^{238}U /^{232}Th in seawater might be influenced by tidal action, time of sampling and sedimentation effect.

In the study area, the chemical species of U, Th and Pu were observed to be associated with either the carbonate or the hydroxide at measured range of pH of seawater. At measured concentration range of uranium, thorium and plutonium, the percentage formation of chemical species as indicated within parenthesis, being $(UO_2)_2(CO_3)(OH)_3^-$ (29-51%), $UO_2(CO_3)_2^{2-}$ (0-24%), UO_2CO_3 (4-10%), $UO_2(OH)_2$ (7-35%), $UO_2(OH)_3^-$ (8-29%), UO_2OH^+ (0-3%), ThO_2 (0-76%), $Th(OH)_4$ (24 -100%), PuO_2^+ (0-6%) and PuO_2CO_3 (94-100%) calculated at Eh = + 0.75V and pH = 8 in the oxidized seawater.

CHAPTER 4: PARTICLE SIZE CHARACTERIZATION, MINERALOGY AND THEIR IMPACT ON SPATIAL AND VERTICAL DISTRIBUTION OF ^{238}U, ^{232}Th AND $^{239+240}$Pu IN BOTTOM SEDIMENTS

The chapter focuses on particle size characterization, mineralogy and their impact on spatial and vertical distribution of ^{238}U, ^{232}Th and $^{239+240}$Pu in the bottom sediments. A total of 64 bottom (grab) sediment samples were collected at different seawater depths (1m –3 m) from 16 different locations covering an area of about 64 km^2 of Mumbai Harbour Bay using an Ekman dredge grab sediment sampler having the collecting capacity of 5 kg. Sixteen core sediments were collected from eight different potential locations within 3 nautical mile area from the discharge point of CIRUS. Both grab and core sediments samples were collected as per standard protocols adopted by US EPA and IAEA. The sampling was done by using in-house fabricated sampler made of acrylic cylindrical pipes having a length of 4 m and 30 mm internal diameter which were inserted by a diver. At each location samples were collected upto a depth of 40 -60 cm. The core sample were sliced into 4 cm each fractions, collected in polyethylene bottles with screw caps and transported to the laboratory and stored at 4^0C till further analysis.

Activity of ^{238}U and ^{232} Th was determined using gamma spectrometry (HPGe, 50% relative efficiency). The ^{232}Th activity was determined from the average concentrations of gamma emitting progeny ^{212}Pb and ^{228}Ac in the samples and that of ^{238}U was determined from the average concentrations of the ^{214}Pb and ^{214}Bi decay products. However, $^{239+240}$Pu, was determined by alpha spectrometry (Ortec detector, 18% efficiency) after detailed radiochemical separation. The particle size distribution of sediment samples was determined using a laser diffraction particle size analyzer (CILAS, France, Model 1190). The various minerals present in the sediments were identified and quantified by the X-ray diffraction (XRD, Model: GNR, Italy). The total carbon in the sediments was estimated using C H N S O elemental analyser (Flash EA 1112 Series, Thermo Finnigan, Italy).

Spatial Concentration Profile

The activity concentrations of ^{238}U, ^{232}Th and $^{239+240}$Pu in the bottom (grab) sediments of all locations ranged from 8.5 to 14 Bq kg^{-1}, dry (mean:11.5 ± 1.7 Bq kg^{-1}, dry), 21.5 to 61.2 Bq kg^{-1}, dry (mean: 40 ± 11.4 Bq kg^{-1}, dry) and 0.16 to 1.5 Bq kg^{-1}, dry (mean: 0.7 ± 0.4 Bq kg^{-1}, dry). The variability of ^{238}U, ^{232}Th and $^{239+240}$Pu in terms of coefficient of variation (CV) along the studied regions have been found to be 15.4%, 28.5% and 63 % respectively. A non-homogeneous distribution of ^{232}Th and $^{239+240}$Pu indicates that both radionuclides are very much influenced by anthropic inputs. Locations nearby discharge point showed relatively higher activity of ^{232}Th and $^{239+240}$Pu than locations which are at far off places. This clearly indicates that both have accumulated in sediments through siltation/sedimentation from nearby discharge locations. Impact of particle size on the concentration of radionuclides were studied by fractionating them in three major categories i.e. sand (> 63 µm), silt (> 2 - < 63 µm) and clay (< 2 µm). Although there were almost homogeneous distribution of silt and clay throughout locations, the ratio of maximum to minimum for Th and U was about 3 and 1.6 respectively whereas $^{239+240}$Pu content varied by one order of magnitude. The activity ratio of ^{238}U /^{232}Th in bottom sediments along the studied locations ranged from 0.2 to 0.4 (mean: 0.3 ± 0.07) respectively. The activity quotient of ^{238}U /^{232}Th in sediments was much below unity. This can be attributed to the fact that, in addition to the greater abundance of thorium in the earth's crust, thorium is a particularly insoluble element in natural waters and is usually found associated with solids.

Mineral content of the sediment samples were evaluated by recording their XRD pattern. The XRD patterns of the sediment samples showed chlorite and illite as predominant clay minerals besides calcite, dolomite Ca–montmorillonite, talc, amphiboles, quartz and Na- montmorillonite were also present. There was not much change in the composition of quartz and (Mg, Ca) bearing minerals except calcite and dolomite throughout the regions.

Vertical concentration profile

The vertical profile of porosity and bulk density in cores ranged from 1.38 to 1.81 gcm^{-3} with a mean value of 1.54 ± 0.06 gcm^{-3}. However, the porosity ranging from 31 – 47.4 % with a mean value of 41.4 ± 2.3 %. The total carbon (TC) in the core fractions ranged from 0.9 – 2.41% with a mean value of 1.98 %. The resulting data showed that in general, bulk density increases and porosity decreases with core depth. The observed increased in bulk density with depth in cores may be due to sediment consolidation. The vertical profile of sand, silt & clay in core samples were studied. Like bottom (grab) sediments, the depth fractions of core sediments were also mainly composed of silt and clay. The overall % of sand, silt and clay in the cores of studied region ranged from 0.19 - 23.71% (mean: 2.58 ± 0.5 %), 64.62-78.30% (mean: 74.12 ± 3.4 %) and 11.67-28.91% (mean: 23.3 ± 4 %) respectively.

In some core samples, the distribution of ^{238}U, ^{232}Th and $^{239+240}$Pu as a function of core depth showed a linear relationship with a strong degree of positive correlation coefficient of r = + 0.74, +0.80 and +0.57 respectively indicating that in general, as depth increases, activity concentration of radionuclides increases. It is interesting that elevated activity levels of radionuclides accumulated in the last 5 - 6 fractions. This might be due to either immediate sorption of the activity by the sediment at the time of discharge or during high siltation rate; the activity gets deposited/embedded in the sediments. In other core samples, overall the vertical concentration profiles of ^{238}U, ^{232}Th and $^{239+240}$Pu with depth showed a decreasing trend from top to bottom of the core fractions as established by negative correlation coefficient of r = -0.16, r = - 0.75 and r = - 0.54 respectively. The poor correlation of ^{238}U with depth indicates that there was no temporal variation in its concentration as seen by the almost constant levels throughout the core fractions. However, $^{239+240}$Pu, at top to middle fractions (4 -24 cm) showed relatively higher concentration ranging from 1.1 – 4.22 Bq kg^{-1}, dry and onwards, an almost constant concentration observed up to the last fractions ranging from 0.17 - 0.63 Bq kg^{-1}, dry. This clearly indicates that an accumulation of $^{239+240}$Pu through siltation from nearby discharge locations. Similarly, ^{232}Th also showed comparatively higher concentration ranging from 35 – 52 Bq/kg, dry at top to middle layers (4- 28 cm) of the core than bottom layers which reflected the lower activity ranging from 22 – 30 Bq/kg, dry. The reason for the higher activity on the top layers could be due to concurrent a fresh discharge and the sampling time.

CHAPTER 5: IMPACT OF SPATIAL GEOCHEMICAL VARIATION OF MAJOR AND TRACE ELEMENTS ON DISTRIBUTION OF ^{238}U, ^{232}Th AND $^{239+240}$Pu IN THE MARINE SEDIMENTS OF MUMBAI HARBOUR BAY (MHB)

Distribution of ^{238}U, ^{232}Th and $^{239+240}$Pu in the marine ecosystem is highly influenced by the concentration profiles of major and minor elements**.** In view of this, concentration profiles of major and minor elements in sediments (suspended, grab and cores) samples collected from ten different location of MHB were recorded. The suspended particulates load was estimated to be ranged from 50 mg L^{-1} to 350 mg L^{-1} in seawater of studied area. Samples were completely destructed in a closed microwave digestion system and analysed for estimation of Na, K, Mg, Ca, Fe, Cu, Ni, Co and Mn using ion-chromatography. The mean concentration of major elements as Na, K, Mg, Ca and Fe in the bed sediment was found to be 34.72 g kg^{-1}, 12.05 g kg^{-1}, 16.80 g kg^{-1}, 54.10 g kg^{-1} and 61.72 g kg^{-1}. However, trace elements as Cu, Ni, Co and Mn estimated to be 90 mg kg^{-1}, 78 mg kg^{-1}, 62 mg kg^{-1} ad 242 mg kg^{-1} respectively.

When compared with continental crustal average abundances, the measured mean concentrations for Na, K, Mg, Ca, Fe, Cu, Ni, Co and Mn in grab sediments differed by a factor of 1.47, 0.58, 0.72, 1.30, 1.09, 1.64, 1.04, 2.4 and 0.25 respectively. The relative abundances with respect to crustal average of these metals in the bed sediments were as follows: Co > Cu > Na > Ca > Fe > Ni > Mg > K > Mn. This variation may be the consequence of a variety of lithological components in the investigated area. The highest values were recorded for Ca, Na and Fe, which generally originated to a large extent from the earth crust via weathering except Ca. Although, Ca and Mg are chemically similar, they do not behave equally in sediment system. The depletion Mn concentration at all locations may be the resulting of its reduction to the soluble form and the concomitant break down of the oxy-hydroxides, leading to release of occluded metals to solution. The low supply of organic matter as seen by the significant negative correlation between C and core depth and consequently under strong reducing conditions, all reactive Mn escaped to the dissolved phases.

Using normalization of metals to Fe, the mean enrichment factor of Cu, Ni, Co and Mn was calculated to be 2, 1.24, 3.04 and 0.32 respectively whereas for Na, K, Mg and Ca the values were 1.76, 0.57, 0.81 and 1.66 respectively. Overall, the order of enrichment factor (EF > 1) in the grab sediment were observed to be Co > Cu > Na > Ca > Ni except Mg, K and Mn. In general, the high enrichment observed at those sampling locations where industrial and harbour activities are intense. Transportation to and from the Port, shipping and harbour activities, industrial and urban waste discharges and dredging etc. could contribute the enrichment of metals in the coastal environment. However, for suspended sediments, overall, the enrichment of Co occurred at all locations and others were under depletion. The depletion of trace elements especially Mn in sediments at all locations may be due to change in redox conditions in the particular system.

The linear association relationship between the spatial and vertical concentration profile of ^{238}U, ^{232}Th and $^{239+240}$Pu and heavy elements (Fe, Cu, Ni, Co and Mn) in bottom sediments was established using Karl Pearson's correlation coefficient analysis. Among heavy metals, in general, the spatial concentration profiles of Fe showed a negative correlation with all elements including ^{238}U and ^{232}Th suggesting a distinguishable behaviour during transport in the sediment system. This reveals that that once Fe ions enter into the sediment profile, other metals are removed out from sediments to seawater column. While in the case of K, Mg and $^{239+240}$Pu, Fe containing minerals are seen to be as scavengers/adsorbent as obtained by a positive correlation. Also, in the marine environment, Fe is generally precipitated in the form of oxy-hydroxide which has the affinity to scavenge/carry other metals as they pass through the water column in the sediments. Though, ferric compounds are known to be effective geochemical sinks for all actinides of interest, they only scavenged $^{239+240}Pu$ as obtained by positive correlation. However, as far as vertical concentration profile of Fe is concerned, its minerals played a decisive role for controlling the transport behavior of actinides and showed a negative association with actinides of interest. On the other hand, Mn, presented an atypical behavior in the sediment profile. In spatial concentration profile, it showed positive correlation with actinides of interest whereas in vertical profile, a negative correlation observed. This behavior might be due to Mn migration near to the sediment–water interface, becoming available to biotic uptake. In addition, MnO_2 in bottom sediments might be also involved in redox reactions of redox sensitive radionuclides by oxidizing. The negative poor relationships of Mn with other metals suggest that Mn-oxide might be only a minor host phase for them in the studied area. An even or uneven pattern of relationship among metals is highly influenced by the sorption-desorption processes such as sedimentation, precipitation and flocculation of particulate substances and hence it is difficult to find the principal one. Some radionuclides especially U remains dissolved and are termed conservative within seawater. Some (Th and Pu) are scavenged out of solution onto particulate material by biological or chemical processes (adsorption and co precipitation) leading to deposition in the bottom sediments. Non-significant correlations of other heavy metals with actinides of interest might be possibly due to the different processes (sorption, complexation and biological) and external inputs operating in sediments.

Other ions like Na^+, K^+, Ca^{2+} and Mg^{2+} in marine sediments may also interfere with actinide sorption. In the marine environment, sorption is generally known to take place primarily as an exchange reaction with metal ions, particularly Ca^{2+}, Na^+ and K^+ present in the clay minerals such as Ca -montmorillonite, Na-montmorillonite and illite respectively. In the study area, these minerals were predominately found which have been described in previous chapter. Like heavy metals, the vertical concentration profile of Na^+, K^+, Ca^{2+} and Mg^{2+} in core sediments also showed either positive correlation or negative correlation with actinides of interest. In general, cations were negatively associated with actinides of interest which might be attributed to predominance of cation exchange process among cations of interest bearing minerals in the study area. Whereas the positive association of cations indicates an occurrences of an adsorption or co-precipitation or complexation processes. In literatures, some Fe and Mn containing oxides minerals which are considered as adsorbants for actinides in marine system are not affected by the major cations of Ca^{2+} and Mg^{2+} unlike Na^+.

CHAPTER 6: ADSORPTION - DESORPTION BEHAVIOR OF URANIUM AND THORIUM IN SEDIMENT - SEAWATER SYSTEM AND COMPARISON WITH SOIL - GROUNDWATER SYSTEM

The marine ecosystem (seawater, sediment and biota) represents an ultimate reservoir for elements which may enter it through several pathways. To understand the role of sediments in scavenging and removing radionuclides from the water, it is necessary to study the processes by which ions are sorbed and desorbed from the surface of the sediments. This chapter mainly focuses on the adsorption-desorption behavior of uranium and thorium in two different systems viz sediment-seawater and soil-groundwater. In this study, the laboratory based batch experiment was conducted to determine the distribution coefficient (k_d) of uranium and thorium in sediments. 5 g dried sediment/soil samples was placed in each of seven empty conical flasks and equilibrated for 7 days with 150 mL of sea water /groundwater containing 10 mgL^{-1} (Set-1), 20 mgL^{-1} (Set-2), 30 mgL^{-1} (Set-3) , 40 mgL^{-1} (Set-4), 50 mgL^{-1} (Set -5), 75 mgL^{-1} (Set-6) and 100 mgL^{-1} (Set-7) of uranium and thorium contents followed by shaking. After equilibration time, the samples of each set were centrifuged, filtered through 0.45 μm filter paper and supernatant analysed for uranium and thorium. Similarly, for desorption, a batch equilibrium experiment was conducted with set-1 (10 mgL^{-1} of U) of each system for the period of 1, 3, 7, 14, 21, 28 and 70 days. Each aliquot was then centrifuged, filtered through 0.45 μm filter paper and supernatant analysed for uranium. Finally, concentration of uranium in each set of the equilibrium solution was determined using laser fluorimetery (Quantalase Indore, India). After detailed radiochemical separation, Th was estimated by gross alpha counter.

The distribution coefficient (k_d) was calculated using batch method formula. For sediment-seawater system, k_d for U and Th ranged from 24970 to 55526 L kg^{-1} (mean: 42140 ± 12865 L kg^{-1}) and 24926 to 38561 L kg^{-1} (mean: 34256 ± 4665 L kg^{-1}) respectively. The resulting coefficient of variation (CV) around mean of k_d values for uranium and thorium determined to be 30.53% and 13.62% respectively. Subsequently, at equilibrium condition, the rate constants (k) for uranium and thorium in seawater-sediment were determined by assuming the first order of kinetics reaction and observed to be very narrow range of 0.96 – 1.07 d^{-1} for uranium and 0.96 – 1.02 d^{-1} for thorium. Similarly, for soil-groundwater system, the obtained k_d values of U and Th were in the range of 3435 – 6430 L kg^{-1} (mean: 5135 ± 938 L kg^{-1}) and 4410 – 8442 L kg^{-1} (mean: 7321 ± 1389 Lkg^{-1}) respectively throughout experimental setup. The mean k_d values of Th showed about 43% higher than U in soil indicating that Th has high affinity to sorption sites in soil which depends on the higher ionic radius and subsequently smaller hydration energy**.** High k_d values indicate high metal retention by the solid phase through chemical reactions, leading to low metal bioavailability.

The variation of k_d as a function of U and Th dosages indicates that initially, at low concentration, k_d increased as a function of their concentration till achieving the saturation stage.

After achieving the saturation stage, it observed to be almost constant and at sufficiently high concentration, k_d values decreased because the partitioning behavior deviates from ideality due to removal of species by precipitation. The higher k_d values obtained in the experiment with lower U and Th concentrations, may be due to their strong associations with the sorption sites of sediment/soil leading to relatively strong bonding energies. The sorption parameters of U and Th obtained from the experimental results for sediment-seawater and soil-groundwater systems were fitted to Freundlich, Linear and Langmuir models. For both systems, all models showed a better fit of the adsorption data due to obtaining very strong degree of the coefficient of determination ($R^2 > 0.8$) for both uranium and thorium.

The results of the kinetic experiments of U in sediment-seawater and soil –groundwater system clearly showed that the removal from soil /sediment increased, as the agitation time increased till equilibrium stage. The removal rate of U increased rapidly for the first 7 days and then continued slowly for up to 70 days in both medium (groundwater and seawater). The values of k for uranium in seawater-sediment and groundwater-soil systems obtained from fitting the experimental results using least square method by were derived to be $0.64d^{-1}$ and $0.83d^{-1}$ respectively. The desorption rate of U in sediment – seawater was about 30% slower than soil-groundwater which might be due to high exchange of U with the calcium bearing minerals present as Ca- montmorillonite, dolomite and calcite in sediments and high composition of silt (79%) and clay (19%).

CHAPTER 7: PREDICTION OF CHRONICLE DEPOSITION OF ^{238}U, ^{232}Th and $^{239+240}$Pu IN CORE SEDIMENTS USING RADIOMETRIC DATING OF ^{210}Pb, ^{137}Cs AND ^{228}Ra/^{226}Ra IN MUMBAI HARBOUR BAY

In this chapter, various migration parameters such as sedimentation rate, sediment accumulation rate, age of sediment, total inventory, annual deposition rate, atmospheric fluxes, residences time, scavenging rate, linear attenuation coefficients, mass relaxation depth etc were obtained for ^{210}Pb and ^{137}Cs using radiometric dating models. ^{210}Pb is a member of the ^{238}U decay series and is continuously introduced into the marine environment by deposition from the atmosphere. This radionuclide is readily attached to airborne particulates and removed from the atmosphere both by wet and dry deposition. Like ^{210}Pb and ^{137}Cs have been introduced into the atmosphere in irregularly varying amounts since 1945 and is also strongly bound by sediments. It is trapped by the uppermost layer of the sediment and as this layer is buried by succeeding ones. Dating of the sediment is thus possible by determination of the ^{137}Cs concentration in each interval in the sediment sequence and by correlation of its resulting concentration pattern with the pattern of atmospheric levels since 1945. In addition to traditional methods, one alternative approach is to utilize the expected in-growth of ^{228}Ra to secular equilibrium with its parent ^{232}Th to provide a new geo-chronometer. With time and burial, radium isotopes grow into secular equilibrium as a function of their half lives, which determines sedimentation rates.

The total signal of ^{210}Pb in recent sediment profile consists of, supported ^{210}Pb$_{sup}$, which is present due to autigenic material of the sediment and unsupported (excess) ^{210}Pb, which originates from the atmospheric deposition. ^{210}Pb$_{sup}$ is usually assumed to be in radioactive equilibrium with its parent nuclide ^{226}Ra (half-life 1600 y). The activity of ^{226}Ra in core fractions was determined by taking the average activity of two separate photopeaks of two radon daughters: ^{214}Pb at 352 keV and ^{214}Bi at 609 keV after attaining the secular equilibrium and the activity of ^{137}Cs was determined using photopeak at 662 keV using gamma spectrometry systems. In the case of ^{210}Pb dating model, the sedimentation rate was determined to be 0.52 ± 0.10 cmy^{-1}, 0.73 ± 0.21 cmy^{-1} and 1.12 ± 0.24 cmy^{-1} by the slope of lines obtained in cores of SCL-3, SCL-5 and SCL-9 respectively.

Besides the ^{210}Pb dating models, ^{137}Cs method utilized to confirm the sedimentation rates in core SCL-3, SCL-5 and SCL- 9 obtained to be 1.04 ± 0.18 cmy^{-1}, 0.69 ± 0.25 cmy^{-1}, 1.25 ± 0.28 cmy^{-1}respectively. The sedimentation rate in the last two cores was highly compatible with the results of the ^{210}Pb dating. The minor discrepancy in the sedimentation rate based on ^{210} Pb and ^{137}Cs dating might be due to continual mixing of the top several centimeters of the sediment column by the action of organisms.

In addition to the traditional methods (^{210}Pb and ^{137}Cs profiles), the sedimentation rate was also determined using a new geo-chronometer as ^{228}Ra/^{226}Ra and found to be 1.76 ± 0.30 cmy^{-1}, 2.52 ± 0.21 cmy^{-1} and 2.05 ± 0.29 cmy^{-1} in cores of SCL-3, SCL-5 and SCL-9 respectively. This method has the potential of providing information on an intermediate time scale, which can enhance our understanding of the process of strata formation.

The age of sediment in cores SCL-3, SCL-5 and SCL-9 obtained from ^{210}Pb was representative of 77 ± 15 y, 55 ± 16 y and 36 ± 8 y time spans respectively. The sediment layer ages in the last two cores were highly comparable to the ages resulted from ^{137}Cs which showed the value of 58 ± 21, y, and 32 ± 7 y time spans for SCL-5 and SCL-9 respectively. To avoid any influence of sediment compaction on the results, the overall sediment accumulation rate due to sedimentation rate of ^{210}Pb in core SCL-3, SCL-5 and SCL-9 was found to be 1.73 gcm^{-2}y^{-1}, 1.54 gcm^{-2}y^{-1} and 1.89 gcm^{-2}y^{-1} respectively. For ^{137}Cs, the same was found to be 1.43 gcm^{-2}y^{-1}, 1.15 gcm^{-2}y^{-1} and 1.95 gcm^{-2}y^{-1} respectively.

The total inventory of ^{210}Pb in cores of SCL-3, SCL-5 and SCL-9 was obtained to be 13.5 kBqm^{-2}, 7.85 kBqm^{-2} and 7.7 kBqm^{-2} respectively. However the total inventory of deposited ^{137}Cs in cores of SCL-3, SCL-5 and SCL-9 was determined to 14.5 kBqm^{-2}, 6.45 kBqm^{-2} and 6.97 kBqm^{-2} respectively. The flux of total ^{210}Pb and excess ^{210}Pb in cores of SCL -3, SCL-5 and SCL-9 was observed to be 0.48 kBqm^{-2}y^{-1}, 0.53 kBqm^{-2}y^{-1} and 0.76 kBqm^{-2}y^{-1} respectively. The corresponding ^{210}Pb$_{ex}$ flux (atmospheric flux) was obtained to be 0.21 kBqm^{-2}y^{-1}, 0.19 kBqm^{-2}y^{-1} and 0.57 kBqm^{-2}y^{-1} for the same respectively. Whereas for ^{137}Cs, the flux derived to be 0.35 kBqm^{-2}y^{-1}, 0.15 kBqm^{-2}y^{-} and 0.16 kBqm^{-2}y^{-1} for the cores of SCL-3, SCL-5 and SCL-9 respectively.

The residence time of ^{210}Pb in SCL-3, SCL-5 and SCL-9 ranged from 30 to 226 y (mean: 78 y), 26 to 72 y (mean: 43 y) and 35 to 41 y (mean: 37 y) respectively. The corresponding scavenging rate for the same ranged to be 0.0044-0.033 y^{-1} (mean: 0.013 y^{-1}), 0.014 – 0.038 y^{-1} (mean: 0.023 y^{-1}) and 0.024 – 0.028 y^{-1} (mean: 0.027 y^{-1}) respectively. Comparatively higher residence time obtained in core SCL-3 indicates that the rate of removal of ^{210}Pb from sediment is slower than in both cores i.e SCL-5 and SCL-9. The depth profile variation in residence time of ^{210}Pb for core SCL-3 showed almost constant values in the range of 30 – 42 years up to the depth of 4-20 cm and onwards increased sharply in the higher depth fractions. Similarly, for core SCL-5, the residence time generally decreases as depth increases upto 4 -28 cm and onwards increases in the succeeding downward core fractions. Overall, residence time in both cores increases as depth increases. The core SCL-9 did not show any significant variation in the residence times of ^{210}Pb as seen by almost uniform values throughout the core depth. It is also obvious that larger the residence time, lower the scavenging rate of radionuclides.

For ^{137}Cs, residence half-time were calculated using the multi compartment model and observed to be the highest at the top layers of all the three cores and decreased with sediment depth with a mean ranging from 1.06 at top layer (0 - 4 cm) to 35.35 years at the bottom layer (32 - 36 cm) throughout the cores. This might be due to occurrences of high content of finer particles in the form of clay and silt in the upper layers and coarser particles in the deeper layers.

The parameter α (cm^{-1}) obtained by fitting the depth profile distribution of ^{210}Pb in the cores of SCL-3, SCL-5 and SCL-5 were derived to be 0.028 cm^{-1}, 0.027 cm^{-1} and 0.027 cm^{-1} respectively. The resulting h_0 (kgm^{-2}) of ^{210}Pb was found to be 169 kgm^{-2}, 175 kgm^{-2} and 227 kgm^{-2} respectively**.** The high value of h_0 obtained in core SCL-9 indicates a deeper penetration into the sediment profile. The greater is the value of the relaxation mass depth (h_0), the deeper the ^{210}Pb penetrates into the sediment profile. The penetration of ^{210}Pb in SCL-3 and SCL-5 cores was fairly similar. Similarly, the values of α for ^{137}Cs in cores of SCL-3, SCL-5 and SCL-9 were found to be 0.022, 0.033 cm^{-1} and 0.020 cm^{-1}. The resulting h_0 values for the same computed to be 252 kgm^{-2}, 138 kgm^{-2} and 370 kgm^{-2} respectively. A greater h_0 values obtained at SCL-9 for the ^{137}Cs than ^{210}Pb indicates deeper penetration of ^{137}Cs into the sediment profile.

CHAPTER 8: THERMODYNAMICS PARAMETERS OF U (VI) SORPTION ONTO SEDIMENTS/SOILS IN VARIOUS AQUATIC SYSTEMS

This chapter describes the thermodynamic parameters of U(VI) sorption in various aquatic systems. In this study, the sorption of U onto sediment in seawater in terms of k_d values was initially examined at three different temperatures viz 298 K, 323 K and 343 K under the similar laboratory conditions and it was compared with other geochemical environments such as undisturbed and disturbed soil in groundwater and deionised water system. Each of 5 g dried sediment/soil samples was placed in PTFE containers and equilibrated for 7 days with each of 150 mL seawater (for sediment) and groundwater and deionised water (for soils) containing 10

mgL^{-1} of uranium prepared from standard solutions (1 g L^{-1}) of uranyl nitrate hexahydrate (USA make) followed by shaking using shaker at 298, 323 and 343 K in an incubator. After equilibration time, the samples of each set were centrifuged, filtered through 0.45 µm filter paper and concentration of U in the equilibrium solution was determined using laser fluorimetery. Thermodynamic parameters (ΔG^0, ΔH^0 and ΔS^0) were obtained using the Vant Hoff equation. In sediment-seawater system, the average extraction rate of U at 298 K was found to be 0.0098 % d^{-1} and reduced to 0.0083 % d^{-1} at 343 K. However for undisturbed soil, at 298 K, the average extraction rate in deionised water and groundwater was obtained to be 0.156 % d^{-1} and 0.081% d^{-1} respectively and at 343 K, it was reduced to 0.107% d^{-1} and 0.074% per d^{-1} for the same respectively. Similarly for disturbed soil, at 298 K, the extraction rate in deionised water (0.162 % d^{-1}) was about 15% more than in groundwater (0.141 % d^{-1}), while at 343 K, the extraction rate decreased to about 50% in both medium. Overall, at 298 K, the extraction rate of uranium in sediment-seawater system was about ten to fifteen times slower than soil-groundwater/deionised water system. Similarly, for undisturbed soil, the extraction rate in groundwater was about 50% slower than in deionised water suggesting that groundwater was observed to be more favorable for high surface sorption of U onto soils.

The measured mean k_d value of uranium in sediment– seawater, soils – deionised water and soils - groundwater system at 298 K was found to be 43448 ± 5280 Lkg^{-1}, 2673 ± 415 $Lkg^{-1}$and 4127± 565 Lkg^{-1}respectively whereas at 343 K, the values were increased to 51381 ± 4800 Lkg^{-1}, 4635 ± 673 $Lkg^{-1}$and 6013 ± 848 Lkg^{-1} for the same respectively. The k_d value in sediments was about 10 - 20 times higher than soils and slightly increased by about 18% at 343 K. The high sorption onto sediment may be due to presence of high amount of finer particles in the form of silt and clay and less content of sand. Similarly, the ratio of obtained k_d values of U for undisturbed soil in groundwater to deionised water was found to be 1.92 and 1.46 at 298 K and 343 K respectively whereas for disturbed soil, this ratio was almost insignificant different (differed by 1.7%) at both temperatures. This clearly indicates that the undisturbed soil has stronger sorption capacity than disturbed soil in both aqueous systems.

The values of ΔH^o were positive in soils/sediments, indicating that it is an endothermic process for U adsorption onto them. One possible interpretation for the endothermic process is that U(VI) ions are well solvated in water. In order to adsorb onto soils/sediments, U (VI) ions are denuded of their hydration sheath to some extent and this dehydration process needs energy. It is assumed that the needed energy for dehydration exceeds the exothermicity of the ions attaching to soil/sediment surfaces. The implicit assumption herein is that the adsorbed U(VI) ions are less hydrated than those in solution. The removal of water molecules from U(VI) ions is essentially an endothermic process and the endothermicity of the desolvation process exceeds the enthalpy of sorption to a considerable extent. Similarly, the values of ΔG^o were also all negative at all temperatures studied herein as expected for a spontaneous process under experimental conditions. The higher the reaction temperature, the more negative the value of ΔG^o, indicating that the adsorption reaction is more favorable at elevated temperatures. At high temperature, U(VI) ions are readily dehydrated and thereby their sorption becomes more favorable. The ΔG^o values for sediments were found to more negative than soils. However, the values of ΔS^o in soils/sediments were all positive, which indicates that during the whole adsorption process, some structural changes occurs on soils/sediments surface and thus leading to an increase in the disorderness at the soil- water interface. The relatively higher values of ΔS^o in disturbed soil revealed a more efficient sorption at higher temperature**.** Overall, it was observed that as temperature increases, sorption of U onto soils/ sediment increases. This may be due to increase in diffusion rate of U(VI) into the pores of soils/sediments. Changes in the soils/sediments pore sizes as well as an increase in the number of active sorption sites due to breaking of some internal bonds near soil/sediment surface edge are generally expected at higher temperatures.

Summary

The work carried out under this dissertation deals with interaction of three important members of the actinides i.e. Uranium (U), Thorium (Th) and Plutonium (Pu) in the marine ecosystem of Mumbai Harbour Bay. The activity concentrations of U, Th and $^{239+240}$Pu in seawater were ranged from 1 - 4.4 μg L^{-1} (mean: 2.6 ± 0.83 μg L^{-1}), 70 – 250 ng L^{-1} (mean: 143 ± 51 ng L^{-1}) and 47 – 138 μBq L^{-1} (mean: 86 ± 30 μBq L^{-1}) respectively. These levels are on lower side compared to others equivalent scenario internationally like La hague, France and Sellafield, UK reprocessing. Whereas in case of bottom (grab) sediments, concentrations of ^{238}U, ^{232}Th and $^{239+240}$Pu in bottom sediments of all locations ranged from 8.5 to 14 Bqkg^{-1}, dry (mean:11.5 ± 1.7 Bq kg^{-1}, dry), 21.5 to 61.2 Bq kg^{-1}, dry (mean: 40 ± 11.4 Bq kg^{-1}, dry) and 0.16 to 1.5 Bq kg^{-1}, dry (mean: 0.7 ± 0.4 Bq kg^{-1}, dry). The spatial variability of ^{238}U, ^{232}Th and $^{239+240}$Pu in terms of coefficient of variation (CV) throughout the studied area has been found to be 15.4%, 28.5% and 63 %. Experimental results clearly indicates that distribution of ^{238}U, ^{232}Th and $^{239+240}$Pu in the marine ecosystem is highly influenced by the concentration profiles of major and minor elements in different matrices of marine ecosystem. k_d values were evaluated under different geochemical conditions to understand the role of sediments in scavenging and removing radionuclides from the aquatic systems. The variation of k_d as a function of U and Th dosages indicates that initially, at low concentration, k_d increased as a function of their concentration till achieving the saturation stage. After achieving the saturation stage, it observed to be almost constant and at sufficiently high concentration, k_d values decreased because the partitioning behavior deviates from ideality due to removal of species by precipitation. The higher k_d values obtained in the experiments with lower U and Th concentrations, may be due to their strong

association with the sorption sites of sediment/soil leading to relatively strong bonding energies. The sorption parameters of U and Th obtained from the experimental results for sediment-seawater and soil-groundwater systems were fitted to Freundlich, Linear and Langmuir models. Thermodynamic parameters were evaluated to understand the sorption of uranium onto sediment in seawater and compared with other geochemical environments such as soil – groundwater/deionised water. The negative value of ΔG^o and positive value of ΔH^o reflects that sorption of uranium onto both sediment/soil systems are a spontaneous and endothermic process under experimental conditions. However, the values of ΔS^o were positive, which indicates that during the whole adsorption process, some structural changes occurs on soils/sediments surface and thus leading to increase in the disorderness at the soil/sediment - water interface. Overall, it was observed that as temperature increases, sorption of U onto soils/ sediment increases. This may be due to increase in diffusion rate of U(VI) into the pores of soils/sediments. The speciation of U, Th and Pu at various physico-chemical parameters of marine environment was calculated by the speciation code MEDUSA. This code includes an extensive thermodynamic data base along with HYDRA (hydrochemical equilibrium constant database) speciation program and three main different algorithms for creating chemical equilibrium diagrams. The ligands such as hydroxide, chloride, nitrate, carbonate, fluoride, sulphate, phosphate and silicate are included. Using HYDRA model, the Eh-pH diagram of uranium, thorium and plutonium was drawn at measured composition of seawater. Since there are many constraints while working with Pu as the concentration were very small, therefore various conclusions were drawn on the basis of uranium.

Publications:

a. Published

1. **Ajay Kumar**, Rupali Karpe' Sabyasachi Rout' V.M.Joshi' R.K. Singhal and P.M. Ravi (2013). Spatial Distribution an Accumulation of ^{226}Ra, ^{228}Ra, ^{40}K and ^{137}Cs in Bottom Sediments of Mumbai Harbour Bay, Journal of Radioanalytical Nuclear Chemistry 295(2): 835-839.
2. **Ajay Kumar,** R. K. Singhal, Sabyasachi Rout, Usha Narayanan, Rupali Karpe and P. M. Ravi (2013). Adsorption and kinetic behavior of uranium and thorium in seawater-sediment system, Journal of Radioanalytical Nuclear Chemistry 295(1):649-656.
3. **Ajay Kumar,** R. K. Singhal, Sabyasachi Rout, P. M. Ravi (2013). Spatial geochemical variation of major and trace elements in the marine sediments of Mumbai Harbor Bay, Environmental Earth Science, DOI 10.1007/s12665-013-2366-3
4. **Ajay Kumar,** Sabyasachi Rout, R.K. Singhal and P.M. Ravi (2013). Thermodynamic parameters of U (VI) sorption onto soils in aquatic systems, Earth and Environmental Sciences (Springer Plus), Vol. 2 (1), DOI:10.1186/2193-1801-2-530.
5. **Ajay Kumar**, Sabyasachi Rout, Manish K. Chopra, D.G. Mishra, R.K. Singhal, P.M. Ravi and R.M. Tripathi (2014). Modeling of ^{137}Cs migration in cores of marine sediments of Mumbai Harbor Bay, Journal of Radioanalytical Nuclear Chemistry, DOI: 10.1007/s10967-012-2166-3.
6. Sabyasachi Rout, **Ajay Kumar**, P.K. Sarkar, Manish K. Mishra, P.M. Ravi, (2013).Application of Chemometric Methods for Assessment of Heavy Metal Pollution and Source Apportionment in Riparian Zone Soil of Ulhas River Estuary, India, International Journal of Environmental Sciences. 3(5) DOI:10.6088/ijes.2013030500019.
7. Sabyasachi Rout, **Ajay Kumar**, P.K. Sarkar, Manish K. Mishra, P.M. Ravi (2012). Groundwater Geochemistry Study of Estuarine Aquifer, Western India: Mumbai using Chemometric and Conventional Techniques, Journal of Advances in Chemical Science**,** 1-9.
8. Singhal, R.K., Narayanan Usha, Karpe Rupali, **Ajay Kumar**, Ranade A and Ramachandran V (2009). Selective separation of Iron. from Uranium in quantitative

determination of traces of uranium by alpha spectrometry in soil/sediment sample, Applied Radiation 67(4):501-505.

b. Communicated:

9. **Ajay Kumar,** Sabyasachi Rout, R.K. Singhal, P.M. Ravi and R.M.Tripathi, (2013). Estimation of total inventories and atmospheric fluxes of naturally occurring ^{210}Pb from core sediments of Mumbai Harbour Bay using radiometric dating models, Environmental Earth Science.

International/National Conferences

1. **Ajay Kumar,** Sabyasachi Rout, Manish K. Mishra, P.M. Ravi and R.M. Tripathi, (2014). A novel approach to determine the recent sedimentation rate in the Mumbai Harbour Bay using ^{228}Ra/^{226}Ra geochronology, National conference on Advances in Radiation Measurement Systems and Techniques, (IARPNC-2014) during 19 – 21, March, 2014, at BARC Trombay, Mumbai.
2. **Ajay Kumar,** Sabyasachi Rout, P.M. Ravi and R.M.Tripathi (2014). Effective vertical migration velocity and residence times of ^{137}Cs in sediments of Mumbai Harbor Bay using compartment models, National Symposium on Nuclear Analytical Chemistry (NAC-V) during 20 – 24, January, 2014, at BARC Trombay, Mumbai.
3. **Ajay Kumar**, R.K. Singhal, Sabyasachi Rout, Usha Narayanan, Rupali Karpe, and P.M. Ravi (2012). Sorption characteristics of uranium and thorium in seawater –sediment system, International Conference on Sediment Management, (12SM-2012), 20-22, March, 2012, Alibaug, Raigad

4. **Ajay Kumar**, R.K. Singhal, Sabyasachi Rout and P.M. Ravi, Chemical speciation modeling of uranium, thorium and $^{239+240}$Pu in seawater of Mumbai Harbour Bay, International Conference on Sediment Management, 2012 (12SM-2012),20-22, March, 2012, Alibaug,Raigad.
5. **Ajay Kumar**, R.K. Singhal and Sabyasachi Rout, Principal Component Analysis (PCA) for Assessment of Heavy Metals Pollution in Sediments of Mumbai Harbour Bay, International Conference on Sediment Management, 2012 (12SM-2012),20-22, March, 2012, Alibaug, Raigad.
6. Sabyasachi Rout, **Ajay Kumar**, Manish Kumar Mishra, and P.K.Sarkar, Source Apportionment of Heavy Metals in the Groundwater Sediments of Estuarine Regions in Mumbai, International Conference on Sediment Management, 2012 (12SM-2012), 20-22, March, 2012, Alibaug, Raigad.

Signature of Student (Ajay Kumar)

Date: 25|9|13

Doctoral Committee:

S.No.	Name	Designation	Signature with Date
1	Prof. A.V.R. Reddy	Chairman	
2.	Dr .R. K. Singhal	Convener	R.K. Singhal 25/9/1
3.	Prof. B.S. Tomar	Member	9/10/2013
4.	Prof. G.G. Pandit	Member	
5.	Prof. P.K. Mohapatra	Member	

LIST OF FIGURES

LIST OF TABLES

LIST OF PLATES

LIST OF ABBREVIATIONS

NAPS	Nuclear Power Plants Site	NOM	Natural Organic Matter
MHB	Mumbai Harbour Bay	HA	Humic Acid
SPM	Suspended Particulate Matters	NORM	Naturally Occurring Radioactive Material
US, EPA	United States Environment Protection Agency	ETP	Effluent Treatment Plant
IAEA	International Atomic Energy Agency	BARC	Bhabha Atomic Research Centre
ORP	Oxidation-Reduction Potential	GPS	Global Positioning System
DO	Dissolved Oxygen	DC	Decontamination Centre
EC	Electrical Conductivity	RSMS	Radioactive Solid Waste Management Site
TDS	Total Dissolved Solids	EDTA	Ethylene-Diamine Tetraacetic Acid
IC	Ion Chromatography	DTPA	Diethyl-Triamine-Pentaacetic Acid
AR	Analytical Reagent	HPGe	High Purity Germanium
MEDUSA	Make Equilibrium Diagram Using Sophisticated Algorithms	FWHM	Full Width at Half Maximum
CV	Coefficient of Variation	UCIL	Uranium Corporation of India Limited
CIRUS	Canada India Reactor Utility Services	PTFE	Poly Tetra Fluoro Ethylene
XRD	X-Ray Diffractrometer	BBOT	2,5-bis (5-tert-butyl-benzoxazol-2-yl)-thiopen
TC	Total Carbon	LDM	Laser Diffraction Method
EF	Enrichment Factor	PSD	Particle Size Distribution
SCL	Sediment Core at Location	PAR	4-(2-pyridylazo) Resorcinol
U	Uranium	PDCA	2, 6-Pyridyl Dicarboxylic Acid
Th	Thorium	CFCS	Constant Flux Constant Sedimentation Rate
Pu	Plutonium	CIC	Constant Initial Concentration

FTIR	Fourier Transformation Infra Red	CRS	Constant Rate of Supply
An	Actinides	FDNPP	Fukushima Dai-ichi Nuclear Power Plant
RS	Raman spectroscopy	STP	Standard Temperature and Pressure
TRLFS	Time Resolved Laser Fluoroscence Spectroscopy	SW	Seawater
EXAFS	Extended X-ray Adsorption Fine-Structure Spectroscopy	DW	Deionised water
TCD	Thermal Conductivity Detector	GW	Groundwater

CHAPTER 1
INTRODUCTION: ACTINIDES IN THE ENVIRONMENT

1.1. Abundances, production and environmental sources of actinides

Actinides (An) consist of a group of radioactive metallic elements with atomic numbers (Z) between 89 (actinium) and 103 (lawrencium) with sequentially filled 5f atomic subshells. The heavier actinides (Z = 97−103) have short half-lives which are produced in low quantities and are thus not considered to pose substantial risks to the environment [1]. As is the case with other environmental contaminants, the solubility, transport properties, bioavailability and toxicity of actinides are dependent on their speciation (composition, oxidation state, molecular-level structure and nature of the phase in which the contaminant element or molecule occurs). Generally, actinides show more variability in their oxidation states which can make their fate in the environment more challenging to study. Although minor in abundance of U and Th in Earth's crust and in seawater, light actinides (Th, Pa, U, Np, Pu, Am, and Cm) are important environmental contaminants associated with anthropogenic activities such as the mining and milling of uranium ores, generation of nuclear energy and storage of legacy waste resulting from the manufacturing and testing of nuclear weapons.

Thorium and uranium are the only naturally abundant actinides with typical crustal concentrations of 10−15 mgkg^{-1} and 2−4 mgkg^{-1} and seawater of 0.7 µgL^{-1} and 3µgL^{-1} respectively, although geochemical processes have concentrated thorium and uranium in particular environments to form economic deposits [2]. Actinides such as ^{232}Th, ^{235}U and ^{238}U are each progenitors of long α- and β-decay chains that result in the production of relatively short-lived ^{231}Pa, ^{230,234}Th, and ^{227,228}Ac daughter radionuclides[3]. In uranium-rich ore deposits, trace amounts of other actinide isotopes, primarily ^{237}Np and ^{239}Pu can be produced naturally by neutron capture of ^{235}U and ^{238}U respectively [4]. Notable examples of neutron capture reactions occurring in nature are the natural fission reactors found at the Oklo and Bagombe uranium deposits in the Republic of Gabon. Approximately 2 billion years ago, when the natural ^{235}U/^{238}U ratio was 3.7% (a value much higher than the current value of 0.725%), sustained fission reactions occurred within these uranium-rich deposits [5]. Over the course of the natural reactor life spans (0.6−1.5 million years), ~ 2−3 tons of ^{239}Pu and ~ 6 tons of fission products were produced [6].

The remaining actinides are only produced in high-energy neutron-rich environments typical of nucleosynthesis, nuclear reactors and nuclear explosions. Models for nucleosynthesis based on the characteristic energy output of a supernova explosion, nuclear structure, decay energies and half-lives require that ^{254}Cm and other actinides were synthesized only via rapid neutron capture during core collapse supernovae [7−9]. Because of the short half-lives associated with neutron-rich nuclei, the majority of the actinides underwent a series of α and β decays and spontaneous fission reactions to form lighter elements with $Z < 92$. The abundance of fission products and other daughter isotopes measured in meteorites (e.g.^{136}Xe from fission of ^{244}Pu) confirms that actinides were more abundant in the early solar system [10].

Today, aside from the naturally occurring actinides (primarily thorium, uranium and their daughters), the global inventory of actinides is derived from nuclear reactors and nuclear explosions [11]. As a result, the majority of actinides in particular plutonium, neptunium, americium and curium are released to the environment from human activities. Although the beneficial and industrial applications for some actinides are growing as targets or byproducts of the nuclear industry and in weapons production, the majority of actinides have been released to the environment at different stages of the nuclear fuel cycle, primarily through (1) improper disposal of mine tailings and effluents, (2) direct discharges from enrichment and processing plants to the atmosphere, (3) disposal of high-level waste and highly contaminated solvents into groundwater and surface waters either directly or as a result of faulty storage containment (4) dispersion from atmospheric and below ground nuclear weapons testing and (5) accidental releases from reactors. Runde and Nue (2010) have summarized the global inventories and releases as a consequence of the above activities [12]. A final important consideration in evaluating the environmental consequences of actinide releases is their activities and their half-lives. Even though uranium is generally abundant at sites on a mass-per-volume basis, the short-lived isotopes of americium and plutonium, even at substantially lower concentrations, can pose a much greater health risk because of their much higher activities [13].

1.2. Actinides in the aquatic systems

Nuclear weapon test conducted globally in the process of development of nuclear weapons are estimated to have released more than 2 x 10^{20} Bq of radioactivity to the environment [14]. Accidental and other releases of radioactive nuclides from nuclear reactors amount to about 0.3% of this total. The majority of the releases from weapon testing have been deposited in the oceans and other aquatic systems. These releases include the residual fissionable nuclides in the weapon (^{235}U, ^{239}Pu) and those which are produced in its explosion as fission products (^{137}Cs, ^{90}Sr and nuclei formed by nuclear reactions, beta decay, etc.). It is estimated that 1.6 x10^{16} Bq of plutonium have been deposited in the oceans of the world from these tests [14]. Subsequently, plutonium concentration in open ocean waters is in the order of 10^{-5} Bq L^{-1}, indicating that most of the plutonium released from natural waters is rather quickly sorbed to suspended particles or to the bottom sediments. It is predicted that only about 7% Pu will move into the oceans from the Sea. Since 99% of the release are sorbed onto sediments and suspended particles [15].

Significant resuspension, remobilization and reprecipitation of actinides occur after the initial sorption. While the nature of actinide sorption, the mode of migration and the potential effects of the radionuclides on marine biota have been the subjects of study and hence more research is needed for a satisfactory understanding of these processes.

Actinide ions often are not in a state of thermodynamic equilibrium and their solubility and migration behavior is related to the form in which the nuclides were introduced into the aquatic system. In general, the mobility of actinides in aqueous systems is dependent on (1) their thermodynamic properties, which determine solubility and speciation as a function of pH and redox potential (2) the availability of inorganic and organic ligands to form soluble complexes and (3) the composition and abundance of minerals and mineral colloids present in the system. Representative actinide isotope concentrations in seawater are given in Table 1.1 [16]. From the table, it is clear that except uranium, all radionuclides have concentration less than $< 10^{-12}$ M.

Various geochemical reactions and migration behavior of actinides is much dependant on their oxidation state .Some of the prominent oxidation state depandent reaction are solubility-limited concentrations, complexation reactions, sorption onto minerals and colloid formation. Thorium, americium, and curium exist in only one oxidation state (Th^{4+}, Am^{3+}, and Cm^{3+}) under all redox conditions. However, some actinides such as uranium, neptunium and plutonium are multivalent and exist generally as trivalent, tetravalent, pentavalent and hexavalent, denoted by An^{3+}, An^{4+}, AnO_2^{+}, or AnO_2^{2+} species respectively. Reduction of higher valent actinides to An^{3+} and An^{4+} species results in lower solubility and a elevated level of tendency to sorb on mineral surfaces. In these lower oxidation states, actinides form hydrated An^{3+} and An^{4+} ions, whereas in the V and VI oxidation states, they are unstable in aqueous solution and hydrolyze instantly to form linear trans-dioxo (actinyl) cations, AnO_2^{+} and AnO_2^{2+} respectively [17−19]. The strength of the actinide complexes for a particular ligand generally decreases in the order: $An^{4+} > AnO_2^{2+} \geq An^{3+} > AnO_2^{+}$. The tetravalent actinides form stable aqueous complexes and solid phases with low solubility and pentavalent actinides form the least stable complexes and more soluble solid phases [20]. The high solubilities and hence mobilities of the actinides are generally in a higher oxidation state, which are of primary concern in an environmental context. Table 1.2 details the available oxidation states for actinides in sea water and indicates which states predominate. Microbes, when present in aquatic environments, can also play a major role in defining the predominant oxidation state of the actinide through enzymatic pathways [21]. Multivalent actinides can be reduced to their lowest oxidation states by microbial processes in suboxic and anaerobic biogeochemical zones. Abiotic reduction of actinides is also possible when the oxidized species accept electrons from Fe^{2+}- containing minerals, as is oxidation when reduced species transfer electrons to Fe^{3+}- containing minerals, which are among the most abundant and important natural inorganic sorbents. Radiolysis of actinides in solution can also produce highly reactive species such as e^{-} (aq), H•, OH• and H_2O_2, which can induce changes in the solute, including the actinide oxidation state [22, 23].

Thorium occurs only in the +4 oxidation state in nature. In aqueous solutions, especially in natural waters, the concentrations of dissolved thorium are very low. Dissolved thorium forms a variety of hydroxyl species and undergoes extensive chemical interaction with water and most anions. Thorium can form various aqueous complexes with inorganic anions such as dissolved carbonate, fluoride, phosphate, chloride, and nitrate. The formation of these complexes will increase the concentrations of total dissolved thorium in the environment. Although the tetravalent Th ion (Th^{4+}) having the radius of approximately 1.0 Å is more resistant to hydrolysis than other tetravalent ions, it forms a variety of hydroxyl species at pH values above 3. The concentration range of ^{232}Th in natural fresh water rarely exceeds 1 ng/L, although mg/L concentrations of ^{232}Th have been detected in high-acid groundwaters beneath uranium tailings sites [24]. The normal ranges of thorium concentrations in igneous, metamorphic and sedimentary rocks are less than 50 mgkg^{-1} whereas in oceanic sand/clays and marine manganese nodules, its concentration was found to be 30 and 300 mgkg^{-1} respectively [3]. These anomalously high concentrations of thorium have been explained by the tendency of thorium to strongly adsorb on clay and oxyhydroxide phases [24].

Table 1.1: Representative actinide isotope concentrations in seawater [16]

Radionuclides	Concentration (M)
^{232}Th	4.3×10^{-13}
$^{234, 238}$U	1.3×10^{-8}
^{238}Pu	3×10^{-18}
^{239}Pu	1×10^{-14}
^{240}Pu	3×10^{-15}
^{241}Pu	8×10^{-17}
^{241}Am	4×10^{-17}
^{237}Np	2×10^{-14}
^{244}Cm	3×10^{-22}

Table 1.2: Available actinide oxidation states in sea water at pH = 8.2, I = 0.7 m

(Most common oxidation states denoted in Bold)

Radionuclides	Oxidation states
Th	**IV**
U	IV, **VI**
Np	IV, **V**, VI
Pu	III, **IV**, V, VI
Am	**III**
Cm	**III**

For uranium, oxidized hexavalent uranium is highly soluble as the uranyl ion UO_2^{2+}, whereas the solubility of U (IV) is largely controlled by insoluble oxides such as uraninite (UO_2). A redox diagrams for U, Np, Pu in seawater at T = 298, pH = 8.1, I = 0.7m (values are reduction potentials vs. standard hydrogen half cell) are presented in **Fig. 1.1.**

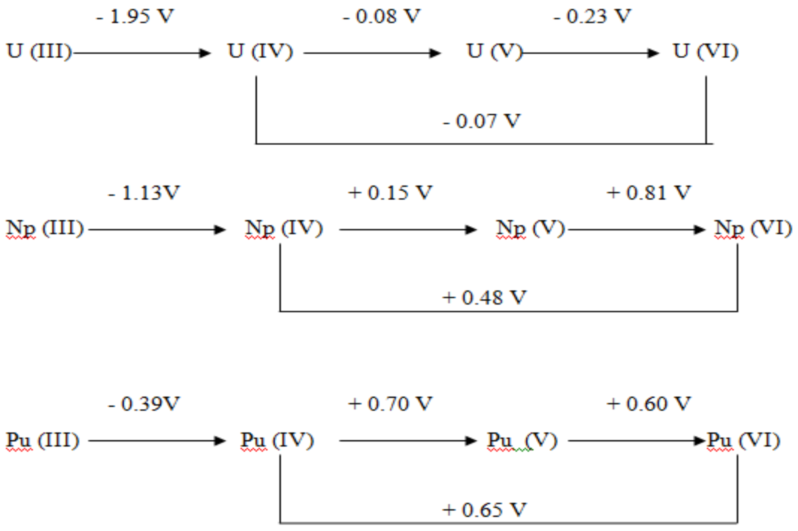

Fig. 1.1: Redox diagram for U, Np, Pu in seawater at T = 298, pH = 8.1, I = 0.7m

Under oxidizing conditions of typical surface and subsurface waters, the aqueous speciation of U(VI) may determine the partitioning of uranium onto mineral surfaces, the reduction of U(VI) to U(IV) and the mode of incorporation of uranium into secondary precipitates such as iron oxy-hydroxides. Hydrolysis of the uranyl ion becomes important above pH = 4, where hydroxo complexes compete with other inorganic and organic ligands in solution, including carbonate, phosphate, sulfate, silicate, n-carboxylic and humic acids [25−28]. In the presence of carbonate and other cations, the uranyl ion forms a series of neutral, anionic binary and polynuclear species that can influence adsorption of uranium on mineral surfaces [29 - 32] and inhibit both the abiotic and biotic reduction of uranium [33–37]. In general, the binary species are the most stable aqueous species, but polynuclear species, particularly in the neutral to alkaline pH range, can be important for uranium mobility. Aqueous complexation of uranium and the other actinides has been studied using a variety of techniques, including calorimetric or potentiometric titration [38, 29 - 32], time-resolved laser-induced fluorescence spectroscopy [39 - 41], Raman spectroscopy [42], attenuated total-reflectance Fourier transform infrared spectroscopy [43] and extended X-ray adsorption fine-structure (EXAFS) spectroscopy [44 - 48] and through application of quantum chemical approaches such as density functional theory [47, 49], The most recent evaluation of thermodynamic data regarding the aqueous speciation of uranium is described in Guillaumont et al. (2003) although data for some species, particularly organic ligands, were not reviewed for this compilation [25]. Berto et al. (2012) also provide a thorough review of the aqueous coordination chemistry of uranyl along with a compilation of stability constants, including the major organic and inorganic ligands [27]. In general, the tendency of actinide ions to form complexes with univalent or bivalent inorganic ligands follows the trends: $OH^- > F^- > NO_3^- > Cl^- >>> ClO_4^-$ and $CO_3^{2-} > SO_3^{2-} > C_2O_4^{2-} > SO_4^{2-}$. Because of their ubiquity in natural waters, hydroxide and carbonate are the most important ligands for actinide complexation.

Chelation of UO_2^{2+} by organic compounds may be as important as inorganic complexation in many natural systems and at contaminated sites where organic chelators were used in actinide processing. Organic ligands from simple carboxylic acids to more complex humic acids are present at variable concentrations in most natural waters [50]. In oilfield brines, acetic acid concentrations can approach thousands of parts per million [51] whereas surface and shallow groundwaters typically contain di- and tricarboxylic acids at concentrations of ∼10−100 ppm [52] and a high proportion of humic acids [53]. Uranium forms stable complexes with a variety of organic ligands and organic-chelated uranyl species can be highly mobile [54 - 56]. Pompe et al. (2000) found that natural and synthetic humic acids complex U [VI] and may also play a role in Pu (VI) complexation [57]. Thorium (IV) humate complexes have also been reported [58]. When the organic chelate has the proper steric arrangement to form small chelate rings with the equatorial oxygen atoms on the uranyl ion (the carboxylate groups in oxalate or citrate), the uranyl chelates can have exceptionally high stability. As a result, the industrial use of chelating agents such as Tiron or citrate, to enhance the mobility of uranyl is common in industrial applications and organic chelation of uranyl has been used to remove uranium from contaminated soils during pump and treat remediation strategies [59]. The mobilization and transport of uranium by carboxylic acids and organic compounds is also thought to be important in the formation of sedimentary uranium ore deposits [60, 61], At low pHs, where uranyl adsorption onto mineral surfaces is not favored by charge considerations, functional groups associated with natural organic matter (NOM) adsorbed to mineral surfaces may enhance UO_2^{2+} sorption [62, 63]. Alternatively, binding of uranyl to the cell envelope of microbial organisms may inhibit cell metabolism [64] or inhibit uranium reduction, with consequences for the effectiveness of bioremedation strategies. In addition, plutonium and americium have been found to associate preferentially with dissolved high molecular weight organic matter [65]. NOM can also cause reduction of redox-sensitive actinides, including neptunium and plutonium [66 - 68] Interactions between natural and amended synthetic organic compounds can thus play a key role in determining the fate of actinides in the environment.

The dominance of the carbonato complexes under natural conditions at near-neutral and basic pHs is a common feature of all the three actinides (U, Np and Pu). However, there are some key differences among uranium, neptunium and plutonium speciation. Plutonium has the most complex redox chemistry of the actinides with multiple valence states stable under typical pH and redox conditions of subsurface environments. Plutonium speciation is thus a strong function of the Eh, pH, ionic strength, organic and inorganic ligands and disproportionation kinetics. Since the redox couples of Pu (III)/Pu(IV) and $Pu(V)O_2^+$/ $Pu(VI)O_2^{2+}$ are less negative than the Pu(IV) /$Pu(VI)O_2^+$ couple therefore multiple oxidation states can be present in solution as a result of plutonium disproportionation which becomes increasingly favorable at elevated temperature and at $pH < 1.5$ and > 7. Although Pu(V) and Pu(VI) predominate under oxic conditions, in general, Pu (IV) is often the most common plutonium ion at neutral pH and mildly reducing conditions, whereas Pu (III) tends to have much lower solubility. Pentavalent plutonium can be reduced to Pu (IV) via adsorption on mineral surfaces including redox-inactive minerals, although the exact mechanism and kinetics are not well established [69 - 72]. In the tetravalent state, the aggregation of hydrolysis products as $[Pu(OH)_n]^{(4-n)+}$ results in the formation of hydroxo-bridged polymers [73]. The formation of stable colloids of polymeric plutonium (IV) hydroxide is known to greatly enhance the mobility of Pu(IV) in the environment. At the concentrations (10^{-9} M Pu_{tot}), Pu-$(OH)_4$(s) is found to control the Pu (IV) solubility [12]. If crystalline PuO_2(s) is considered for the dominant control on plutonium solubility, the concentration of Pu (IV) would be ∼10^{-17} M. PuO_2^+ does not tend to form strong complexes with inorganic anions within the low to neutral pH range, whereas PuO_2^{2+} forms complexes with Cl^- and NO_3^- anions, which are comparatively less stable than Pu(IV) complexes. However, Pu (III), Pu (IV) and Pu (VI) will form mono to polymolecular complexes with many organic ligands such as acetate, oxalate, and ethylenediaminetetraacetic acid [74]. Such complexes would limit the polymerization of plutonium (IV) hydroxides and are thus often used in plutonium separations.

In contrast to uranium and plutonium, pentavalent neptunium is stable under oxic to moderately suboxic conditions as the trans-dioxoneptunyl cation NpO_2^+ or as neptunylcarbonato complexes at high pH [75]. As a result, neptunium is generally the most soluble and mobile of the actinides and perhaps the greatest concern to waste storage sites. Np (IV) is favored in anoxic environments and hydrolyzes to form polymeric hyroxides, similar to Pu (IV). Tetravalent neptunium is commonly incorporated into sparingly soluble solids such as $Np(OH)_4$ or immobilized via the formation of strong surface complexes with suspended solids. Depending on the redox conditions, neptunium solubilities are also likely to be limited to 10^{-8} to 10^{-4} M by poorly crystalline oxyhydroxides [Np(IV)$(OH)_4$(s)] or oxides [Np(V)$_2O_5$(s)] respectively [12, 76]. Although NpO_2 is thermodynamically favored, it has not been identified in solubility experiments involving natural waters - only amorphous Np(IV) solid phases precipitated and hence these are considered to control aqueous neptunium concentrations, at least initially [77, 78].

1.3. Sorption of actinides on sediment surfaces

The term “sorption” encompasses a variety of possible processes and does not make any distinction with regard to the underlying mechanism. Ultimately, the mobility of actinides in near- and far-field environments is known to be a strong function of the competition between dissolved and adsorbed phases. Sediment, in general, conatins more than 70% minerals, thefore sorption on mineral and surface complexation reactions is one of the leading reactions. [78,79]. Reactions of actinides at the mineral−aqueous solution interface have attracted much attention during recent years. Initially research was mainly driven by the need to obtain solid/liquid distribution coefficients (k_d-values) as input data for performance assessment modeling related to nuclear waste repository projects or to the development of remediation technologies for contaminated sites. Very soon it became apparent that profound understanding of reaction mechanisms is required to develop appropriate geochemical sorption models for a reliable description and prediction of actinide environmental behavior. The surface complexation involves chemical binding of aqueous species and direct contact with mineral surface functional groups. However, depending on geochemical conditions and the type of minerals, reactions other than mere sorption such as surface induced redox reactions and actinide incorporation into the solid matrix, are possible. Master parameters controlling sorption mechanisms and determining the extent of sorption are pH, redox conditions, total actinide ion concentration, the type of mineral surface functional groups and the dynamic properties of the mineral in contact with the aqueous solution. Further parameters, such as salinity, ionic strength, the presence of competing cations and actinide ligating anions exert further influence on surface sorption reactions and actinide surface speciation. Table 1.3 summarizes some of the parameters which must be considered in experimental design and which must be consistent with any sorption theories.

To quantify actinide sorption, batch sorption experiments are usually carried out by varying the chemical conditions. Sorption isotherms are determined by measuring the solid−liquid distribution of an actinide ion at the variable concentration but at fixed pH. The pH dependent actinide sorption is studied at constant concentration and provides the so-called “sorption edges” [8 − 10]. Both sorption isotherms and sorption edges provide imperative input data for development of mechanistic geochemical/thermodynamic sorption models, able to account for variable geochemical conditions. Combination of results with complementary spectroscopic and theoretical methods allows for elucidation and verification of sorption mechanisms and actinide surface species.

Even though this approach is elaborated, it is much more appropriate for predicting contaminant mobility under natural conditions than using a single distribution coefficient (k_d value) determined for a specific geochemical environment. Such k_d values are, in general, only applicable at trace concentration ranges for reversible sorption reactions and at invariable geochemical conditions.

The complexity of the actinide aquatic chemistry has a strong impact on sorption. Under naturally relevant conditions, actinide ions can exist in various redox states such as An(III), An(IV), An(V), An(VI). The actinide redox state and speciation of the actinides change due to surface reactions and can form a broad variety of complexes with dissolved constituents in the form of mainly OH^- and CO_3^{2-} in natural waters. While the tri- and tetravalent actinide species form more or less spherical aquo-ions with [80, 81] water molecules in the first coordination sphere, penta and hexavalent cations form actinyl cations with covalently bound axial oxygen atoms and 4 - to 6-fold coordination in the equatorial plane [13]. Steric constraints are thus to be expected for the interaction of actinyl cations with surfaces.

Table 1.3: Factors important to sorption

Parameters	Impact on sorption process
pH	Strong increase in sorption within the middle pH range.
Sorbate concentration	Depending on sorbate concentration, the increase in sorption can be linear or non-linear with concentration.
Temperature	In many cases, increased temperature is likely to reduce sorption
Pressure	Important if sorption leads to a volume change
Ionic concentration	Reduces non-specific sorption through mass action effects.
Complexing ligands	Can reduce or enhance sorption
Eh	Affects the chemistry of redox sensitive sorbates, sometimes significantly affecting sorption.
Solid/liquid ratio	Can influence measured sorption at low solid concentrations.
Specific Surface area	Determines the amount of available surface sites.
Exchange capacity	Determines the total amount of sorption by ion exchange
Type and density of surface sites	Determines the total amount of sorption by surface complexation
Mineral pre-treatment	Sorption results can be affected by the amount of time the mineral is conditioned in the experimental ionic medium

Notably the tetravalent actinide but also the hexavalent actinyl cations tend to form oligomeric or even polymeric species which may interact with surfaces by either electrostatic forces or chemical bonds. This chemical complexity has todate prohibited development of any unified model for dealing with actinide sorption under varying geochemical conditions. A further inherent difficulty is related to the unique properties of different mineral surfaces. Even actinide sorption onto pure and well-defined crystal planes is not entirely understood, demonstrating the need for further study.

Actinide reactions with microbial surfaces are quite comparable to interactions with mineral surfaces. Bacterial cell walls consist of exopolymers, proteins and lipids and thus, contain various surface functional groups potentially capable of interacting with actinide cations. While hydroxyl groups dominate mineral surfaces, bacteria also contain carboxylate, phosphate, thiol and amino moieties where carboxylate and phosphate groups generally exhibit high affinities for actinide cations. The range of possible surface sorption mechanisms, such as outer- sphere binding, inner-sphere surface complexation, surface precipitation and surface induced redox reactions have also been observed for actinide−microbe interactions. Geochemical modeling approaches for quantitative description are virtually the same for metal cation sorption to mineral surfaces and biosorption. Under certain conditions, biomass can dominate actinide solid−liquid interface reactions, for example, in soil systems. Unlike mineral surfaces, living cells can actively take up metal ions and transfer them to the cell interior and sequester them in the intracellular medium.

Due to very low solubility of the tetravalent actinides such as Th(IV), U(IV), Np(IV) and Pu(IV), they have a strong tendency toward hydrolysis under relevant natural aquatic system conditions [82]. This leads to a strong interaction (sorption) with any kind of surfaces, even at low pH [83 - 85]. Precipitation or polymer/colloid formation due to oversaturation [86 - 88] has to be expected as side reactions in sorption studies of tetravalent actinides. Among actinides, only Th is exclusively stable in the tetravalent oxidation state. The other actinides U−Pu are redox active and form different oxidation states depending on electro-chemical boundary conditions for surface induced redox reactions. To avoid associated experimental complications, many sorption studies reported in the literature have been performed with thorium. Typically, An(IV) sorption is modeled with monodentate surface complexes, while spectroscopic investigations suggest rather that bidentate surface complexes form. Thorium sorption onto silica was modeled assuming monodentate complexation at silanol surface sites and considering the different Th(IV) hydrolysis species ($Th(OH)_x^{4-x}$ with $x = 0-4$) [89]. The same surface speciation was used in a surface complexation model to describe Th(IV) sorption onto illite and montmorillonite [90]. In the presence of strongly complexing ligands such as carbonate, phosphate and carboxylic acids, ternary An(IV) surface complexes have been reported. Uptake of Th(IV) and Np(IV) has been studied at high pH (pH = 11.0−13.6), under conditions where γ-Al_2O_3 and SiO_2 surfaces are negatively charged and at elevated carbonate concentrations where tetravalent actinide ions form anionic carbonato complexes. The observed decrease in distribution coefficient with increasing carbonate concentration is explained by the simple assumption that negatively charged complexes will not or barely sorb [91]. Declining Pu(IV) sorption onto calcite with increasing pH was also explained by the competitive formation of aqueous plutonium−carbonate species [92].

Strong hydrolysis and carbonate complexation are known reactions in hexavalent actinide chemistry, as well as the formation of U(VI) silicato species and formation of polynuclear (dimeric, trimeric etc.) species. As uranium aqueous speciation is quite complex, interactions with mineral surfaces are difficult to correctly describe [93]. At increasing pH and uranyl ion concentration, ternary hydroxo and carbonato surface complexes and polynuclear complexes form and finally U(VI) hydroxide/carbonate precipitates. $\equiv SiOUO_2$ type complexes form at surfaces of the minerals silica [94] and albite [95]. Uranium (VI) forms very stable carbonato complexes in solution and as a consequence uranium sorption in the presence of dissolved CO_2 is strongly suppressed in comparison to the carbonate free system [96 - 100]. The effect for U(VI) is much more pronounced than for the trivalent actinides [100]. Description of uranium sorption on natural rocks and sediments in the presence of carbonate is only possible by postulating formation of various ternary uranium carbonato surface complexes [101 - 103]. Different stoichiometries have been proposed in the literature for these species, a portion of these in modeling studies: $\equiv SOUO_2(CO_3HCO_3)^{2-}$ [101, 102], $\equiv SOUO_2(OH)(CO_3)^{2-}$ [93, 94], $\equiv SO(UO_2) - Ca_x - (CO_3)_y$ [104, 105], $\equiv S(CO_3)UO_2(CO_3)_2^{3-}$ [106, 107], $\equiv SOUO_2HCO_3$ [93], $\equiv SOUO_2CO_3^{-}$ [93], $\equiv SOUO_2(CO_3)_2^{3-}$ [93], $\equiv SOUO_2(HCO_3)^{2-}$ [93] and $\equiv SOUO_2OH(CO_3)_2^{4-}$ [93]. In addition to sorption of pure carbonato and bicarbonate complexes, mixed hydroxo-carbonato and carbonato-bicarbonato surface complexes have been proposed. Sorption of Ca-uranium− carbonato species such as $Ca_2UO_2(CO_3)_3$, which dominate aqueous U(VI) speciation in Ca containing systems at neutral/slightly alkaline pH conditions [93] have not yet been experimentally verified but had to be considered in modeling to successfully describe U(VI) uptake data [93, 108]. The existence of bicarbonato surface complexes may be questionable, as bicarbonate is known to be a weak ligand for actinide ions in solution.

Sorption reaction mechanisms and actinide surface speciation now a day can be investigated in great detail with increasing availability of spectroscopic techniques which is described in the previous section (section 1.2). The actinide sorption reactions generally take place at mineral surfaces by various surface phenomena such as outer-sphere attachment and inner-sphere surface complexation of ionic and colloidal actinide species as shown in Fig.1.2. Beyond pure surface attachment and complexation reactions, actinides can also react with minerals by incorporation (mineralization) and surface induced redox reactions.

1.3.1. Outer-sphere sorption

Sorption reactions may involve pure electrostatic attraction of actinide ions or polymeric actinide species to negatively charged mineral surfaces with no or little impact on the metal ions hydration shell. Such reactions are well-known for actinides interactions with permanently charged clay mineral surfaces i.e. the typical “ion-exchange” sites. The origin of the relevant

surface charge for this type of interaction in clay minerals is isomorphic substitution of Al in Al_2O_6 octahedral layers by divalent cations (Mg/Fe(II)) and/or Si in tetrahedral SiO_4 layers by trivalent cations (Al/Fe(III)). The usually weak electrostatic nature of cation attachment to permanently charged surfaces renders this interaction readily reversible and strong competition with other cations takes place. Relative sorption strength is quantified by selectivity coefficients defining the exchange of actinide ions with other cations (e.g., Na^+, Ca^{2+}) bound to the clay mineral planar sites. The mostly outer-sphere binding character of actinide ions sorbed to cation exchange sites has been evidenced by applying various spectroscopies [109 - 112] but can also be derived from the interpretation of results obtained from batch experiments performed at different ionic strengths. Solid/liquid distribution ratios are almost pH independent in the low pH region and decrease strongly if ionic strength increases. A general observation is obviously that actinide outer-sphere sorption to clay-type minerals becomes prevalent at low pH and low ionic strength as is described for An(III), An(V), and An(VI) [113-115]. However, the affinity of An(IV) toward hydrolysis and chemical binding to surface hydroxyl groups is generally considered strong even at low pH so that purely electrostatic interactions with mineral surfaces are considered irrelevant [114].

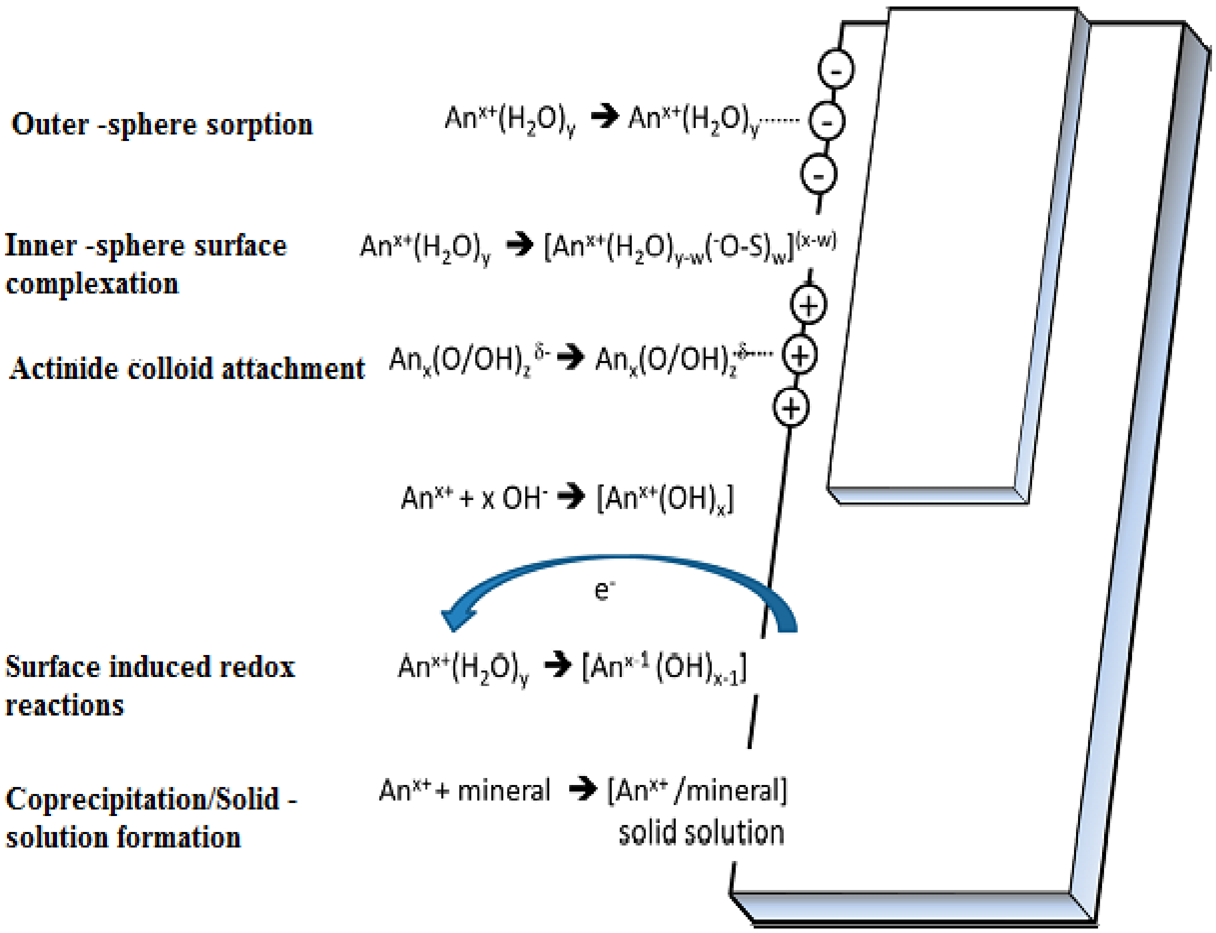

Fig.1.2: Actinide sorption reaction mechanisms

Da□hn et al. (2002) identified only inner-sphere surface complexes for Th(IV) interacted with montmorillonite under very similar conditions of pH = 2 and 3, 0.1 mol dm^{-3} $NaClO_4$ [116]. The strong ionic strength dependence of neptunyl (NpO_2^+) sorption at pH < 6 onto smectite indicates outer-sphere sorption as well [117]. Various studies on UO_2^{2+} sorption to mineral surfaces are available from the literatures, where laser fluorescence and X-ray spectroscopies have been applied to identify sorption mechanisms. At low pH, fluorescence emission spectra for UO_2^{2+} bound to montmorillonite closely resemble that of the aquo ion [108, 118] and are consequently assigned to a purely electrostatically sorbed aquo complex. Interestingly, outer-sphere sorption of UO_2^{2+} onto TiO_2 (rutile) at pH = 3 was also reported [119]. This is certainly surprising because of the expected electrostatic repulsion between the uranyl cation and the positively charged oxide surface. In their ATR-FTIR study, Müller et al. (2012) found outer-sphere binding of UO_2^{2+} at the TiO_2 surface only at higher loading while at low surface coverage an inner-sphere bidentate surface complex was observed [118]. Chang et al. (2006) concluded from deconvolution analysis of their cryogenic TRLFS spectra obtained for UO_2^{2+} adsorbed onto gibbsite a minor contribution from outer-sphere surface species [119]. According to that study the outer-sphere species exists only at the lowest ionic strength investigated (0.001 m) and disappears at higher electrolyte concentrations.

1.3.2. Inner-sphere sorption

The formation of strong actinide ion−surface oxygen atom bonds with significant ionic or covalent contribution results in inner-sphere surface complexes where part of the metal ion's hydration sphere is removed [24]. This strong binding to the mineral surface has a more pronounced effect on reversibility and desorption kinetics compared to outer-sphere sorption [27, 54], While formation of outer-sphere bound actinide species at ion exchange sites of clay minerals is more or less pH independent. Sorption by inner-sphere complexation is considered to take place on amphoteric surface hydroxyl groups and thus varies with their pH dependent protonation/deprotonation. Further parameters affecting inner-sphere sorption are ionic strength, electrolyte composition as well as metal ion concentration, presence of competing cations, complexing ligands and temperature, etc [25, 55]. In general, the extent of sorption at given geochemical conditions follows the effective charge of the actinide ion: $AnO_2^{+} < An_3^{+}/AnO_2^{2+} < An_4^{+}$ [25, 56].

At given geochemical conditions, actinide sorption to various metal oxides generally decreases in the series iron ≈ aluminum > titanium > silicium oxides [55, 57]. The presence of strong complexing organic and inorganic ligands effectively competes with surface complexation. Especially, carbonate and carboxylic acids can significantly suppress actinide uptake by solution complexation or competitive sorption, but also favor formation of ternary surface complexes. The interplay of actinide solution chemistry and reaction with mineral surfaces has been discussed in the literatures. A great number of studies on inner-sphere sorption of trivalent actinide ions onto pure and composite minerals are available as aluminum and iron oxides and hydroxides, clay minerals, igneous rock minerals, titanium oxides, calcite, etc. Am(III) sorption was studied mainly by batch sorption experiments [41, 56, 58-61], while only a few spectroscopic studies have been published [62-64]. In a study of Am(III) sorption onto smectite and kaolinite inner-sphere surface compexation is studied at pH 6.62. The trivalent actinide ions coordinate with 4 oxygen atoms from the surface and 5 remaining hydration sphere water molecules. Am(III) sorption onto ferrihydrite results in a bidentate corner-sharing surface species [63]. Two different inner-sphere surface complexes have been identified also on quartz up to pH 9.4 [65]. In this case the sorption data have been interpreted as bidentate Am/ Cm(III) coordination to the surface. Very often the trivalent lanthanides are used as chemical homologues to simulate the behavior of the trivalent actinides Am(III) and Cm(III) with similar ionic radii. Analogous behavior could be clearly verified for Eu(III), Gd(III), Am(III) and Cm(III) sorption onto γ-Al_2O_3 [58]. Surprisingly, Am(III) binding to Na-illite was reported to be significantly stronger than Eu(III) binding [42]. This finding is currently not understood, but might be explained by the differing sorption properties of different illite batches used for the experiments. Overall, the experimental findings suggest that the pH dependent surface speciation will be controlled by the deprotonation of one surface hydroxyl group. However, because of the surface structure of minerals considered, further coordination to about 3−4 neighboring surface oxygen atoms takes place simultaneously. At higher pH, trivalent metal ion sorption strongly decreases compared to the organic-free system due to An(III)-organic complexation in solution and reduced sorption of organic matter [97]. At pH > 10, dissolved silica increases due to enhanced dissolution of the alumosilicate. This is proposed to cause the appearance of silicato-Cm(III) surface species, identified by additional TRLFS bands. The fraction of these species is enhanced if the silicate concentration increases. Similar spectral features have been recently reported in a study of Cm(III) sorption onto illite and montmorillonite at pH > 10 and attributed to the same mechanism [102].

1.3.3. Competitive sorption

Geochemical modeling of actinide sorption in multi-component systems currently relies on the assumption of competitive metal ion interaction with hydroxyl groups at mineral surfaces. The extent of individual metal ion sorption is determined by the respective complexation constants. Recently, this concept has been put into question by a study on competitive sorption of actinide/lanthanide and other metal ions onto montmorillonite and illite [110]. Interestingly, only metal ions with similar chemistry (e.g., valence state) were observed to compete with one another, whereas metal ions with dissimilar chemical properties were not so that competition seems to be selective [111]. Eu(III), Nd(III), and Am(III) were reported to show competitive behavior. In contrast, competition between Th(IV) and U(VI) was not observed. From these findings, the authors conclude that multiple sets of surface sites exist at the clay mineral surfaces, which are selective with regard to the sorption of certain types of metal ions. Other types of metal ions are not able to compete for sorption on those selective sites.

1.3.4. Actinides - Natural organic matter (NOM) interactions

Generally, natural organic matter (NOM) mainly present in the environment play an important role in the fate and transport behaviour of actinides in which they form strong complexes. The complexation of actinides with NOM may have two opposite effects. If complexed by immobile organic matter, their migration will be retarded. On the other hand if a stable complex is formed with mobile organic matter, migration will be enhanced. The presence of NOM has a strong impact on actinides sorption, is affected by the extent of organic interaction with mineral surfaces and thereby depends on pH [56, 96, 106, 107, 115]. General trends of actinide (IV) partitioning between solid and dissolved organic matter are inherently similar to observed behavior of trivalent actinide ions. The positively charged actinide ions in solution are sorbed on negatively charged mineral surface, thus retarding their migration. Actinides are also capable of forming soluble complexes with dissolved negatively charged organic acids. The organically complexed actinides do not interact as efficiently with mineral surface, thus their rates of transport as neutral species may be enhanced. The evidence that NOMs form very strong complexes with numerous actinides (Th, U, Am) and fission products has been reported [32]. Field observations have suggested that the actinides are mobilized by NOM and rapidly transported with little retention [39]. Depending on geo-chemical parameters, the actinides-organic complexes are able to migrate as colloid or retained through adsorption onto mineral surfaces [40]. Under a condition that limits NOM interaction with minerals due to low affinity or saturated for binding NOM, the presence of the NOM decreases the binding of the metals to the mineral phase and enhances their transport [39]. The mechanism of metal ion binding to organic matter remains a controversial area with ion-exchange, complexation, and surface adsorption being the prevalent theory. Other theories include chemisorption and adsorption-complexation [41]. The same binding mechanism is believed to apply for NOM-radionuclides interactions.

In NOMs, humic acids (HAs) plays a decisive role within natural interaction processes because of their good solubility in the pH range of natural waters and high complexing capacity. Due to their complicated and heterogeneous nature, a thermodynamically based description of the complex formation of HAs with actinide ions is difficult but yet important. There are different thermodynamic models describing the complexation behavior of HAs. However, these models differ from each other in the definition of the complexation reaction and the humic acid ligand concentration. Moreover, the existing database for the interaction between actinide ions and humic acids is incomplete, especially for actinides in the pH and concentration range of natural systems. Humic substances have been shown to interact with metal ions [34, 35], radionuclides [36], organic compounds [37] and minerals [38] through chemical and physical reactions forming soluble and insoluble complexes of widely differing chemical and biological stabilities. These interactions will determine the retention and migration of ions in the environment. The interactions with natural radionuclides are important in speciation and migration studies related to environmental contamination and landfill disposal of naturally occurring radioactive materials (NORM) waste. The ability of humic substances to bind actinides/metal ions comes from their high content of oxygen-containing groups such as carboxylic, phenolic, alcoholic and enolic and carbonyl. Several mechanisms are involved in the association of actinides/metals with HAs : (1) outer sphere complex formation (a relatively weak electrostatic interaction of metals with carboxylic or phenolic groups of humic acids) (2) inner sphere complex formation (strong interaction of dehydrolyzed metals with ligand in humic acids) and (3) physical interactions such as inclusion of inorganic particles in a three-dimensional pocket-like structure in humic acids and precipitation of actinides/metals on humic acid molecules [17, 18]. The stability of metal–humic complexes depends on the nature and properties of humic acids [19, 20]. Humic acids are relatively stable in oxidative environment and relatively immobile [21, 22] because metals are strongly bound to humic acids in a stable form for very long periods of time. According to Blevius et al. (1983), clay–organic interactions are important to change the nature and number of complexation sites [23, 24]. Literature reported that the adsorption of humic acids on positively charged hematite changes the surface charge from positive to negative [25] and the addition of humic acids to clay or Fe oxide can increase colloidal stability [26, 27]. The mechanisms of clay–humic acid interaction depend of the type of clay minerals involved and may be categorized as follows: (1) anion and ligand exchange at the clay edges, (2) cation or water bridges to basal surface, (3) H-bonding to the siloxane or gibbsite sheet, (4) Van der Waals forces, (5) entrapment in the crystal pores, (6) adsorption in interlayer spaces and (7) hydrogen bonds between oxygens or hydroxyl groups of clay and functional groups of humic compounds [28, 33,]. Thus, the stability of radionuclide-humate complexes in solid media in the environment is important to retard the mobilization of radionuclides. In peat lands, humic substances is mineralized very slowly to carbon dioxide and methane because microbial metabolism is restricted to anaerobic pathways in waterlogged and anoxic peat [31] .

1.3.5. Geochemical modeling

Traditionally, distribution coefficients (k_d) are used to describe sorption of actinides and their retention on mineral surfaces in migration processes as well as to assess their mobility and propagation in environmental systems from a given source. k_ds of actinides are affected by numerous geochemical parameters and processes such as pH, sorption to clays, organic matter, iron oxides, oxidation/reduction conditions, major ion chemistry and the physico-chemical form of actinides. The number of significant influencing parameters, their variability in the field and differences in experimental methods result in as much as several orders of magnitude variability in measured k_d values reported in the literature. This variability makes it much more difficult to derive generic k_d values for actinides. Therefore, it is recommended that k_d values to be measured for site-specific conditions. If the k_d is not measured site-specifically, then a conservative k_d should be used for calculation purpose.

At equilibrium, distribution coefficients of interest is given by the following equation,

$$k_d = \frac{C_S}{C_W} \tag{Eq.1.1}$$

Where, C_S is the amount of sorbate adsorbed per unit mass of adsorbent and C_w is the total amount of dissolved sorbate at equilibrium. The following common methods are used frequently for determination of k_d values.

1.3.5.1. Batch method

In batch experiments, the sorbent and the solution containing the sorbate (usually dissolved) are contained in a vessel. After a given reaction time, the solid and liquid are separated and the liquid (or solid) are characterized for sorbate concentration or chemical form. These methods are used for both adsorption and desorption reactions.

1.3.5.2 Column method

In this method, sorbent material is loaded in the column and the solution containing the sorbate is passed through the column. After a given reaction time, the liquid are separated and characterized for sorbate concentration.

1.3.5.3. Adsorption isotherm models

Since the amount of surface available for adsorption on solids is limited, therefore, increases in sorbate concentration will induce competition for these sites and may decrease the value of the measured k_d. The variation of the k_d values with sorbate concentration is known as a sorption isotherm, which can be described with a number of different approaches. The Freundlich equation is often useful for modeling sorption of metals onto solids with heterogeneous surfaces (multi- sites) and has frequently proved superior to the Langmuir equation for cations or anions sorption. The Langmuir isotherm is used for the changes in sorption when the surface becomes loaded with sorbate. It is originally developed to describe monolayer adsorption of gases onto solids. When it was adapted for adsorption from a liquid to a solid, it retained two useful parameters, which were the maximum adsorption capacity, Q^0, and a constant, K_L, related to the binding energy. Furthermore, many other (nonlinear) isotherms exist that rule out the application of a constant distribution coefficient in migration calculations. However, the use of single distribution coefficients may lead to significant error in performance assessment calculations. In principle, the drawbacks of the distribution coefficient concept are overcome by using appropriate adsorption models such as ion exchange and surface complexation/precipitation models. Various general phenomena contribute to sorption from aqueous solutions. For all these phenomena, models are required to go beyond simple distribution coefficients. The adsorption of a sorbate (An^{n+}) to a surface functional group (≡ SOH) of sorbent materials is given by the following equation:

$\equiv SOH + An^{n+} \leftrightarrow \equiv SOAn^{-1+n} + H^+$,

where, $\equiv SOAn^{-1+n}$ are the actinide surface complex formed. The basic charging is due to interactions of the surface hydroxyls with the charge-determining ions (proton and hydroxide ion for oxide minerals). The net charge of various surface species depends on pH and ionic strength and is described by surface chemical reactions, such as

$\equiv SOH + H^+ \leftrightarrow \equiv SOH_2^+ \ (K^+)$ and $\equiv SOH + OH^- \leftrightarrow \equiv SO^- + H_2O \ (K^-)$.

These two reactions generically symbolize protonation and deprotonation of mineral surfaces and are part of the very first surface complexation models which would nowadays be termed 1-site-2-pK models.

1.3.5.4. Transport model

The transport of sorbate in sorbent materials is described using one dimensional differential model which can be derived as follows:

$$R\frac{\partial C}{\partial t} = D\frac{\partial^2 C}{\partial X^2} - V\frac{\partial C}{\partial X} - R\lambda C$$

(Eq. 1.2)

Where, C is the amount of the sorbate in dissolved phases, t is the time during movement of sorbate in sorbent, x is the thickness of sorbent materials, D is the diffusion coefficient, V is the velocity of the fluid, λ is radionuclides decay constant and R is the retardation factor of sorbate which is calculated using the following formula,

$$R = \frac{V_W}{V_X}$$

(Eq. 1.3)

Where, V_W is the velocity at which the sorbate moves in sorbent materials and V_w is the velocity of conveying fluid. Using the value of retardation factor of interest, k_d can be determined by the following equations

$$k_d = \frac{\Phi(R-1)}{\rho_b}$$

(Eq. 1.4)

Where, Φ and ρ_b are the fractional porosity and the bulk density of the sorbent materials respectively.

1.3.5.5. Salinity method

This method is applicable only when there is opposite relation (but strong correlation) between salinity and k_d values. This can be expressed by the following equation:

$$\ln k_d{}^S = b\ln(S+1) + \ln k_d{}^0 \qquad \textbf{(Eq. 1.5)}$$

Where, $k_d{}^S$ is the distribution coefficient at some salinity S, b is a constant and $k_d{}^0$ is a constant that essentially represents the distribution coefficient at zero salinity. A plot of ln k_d vs ln (S+ 1) yields a straight line (not always) with a slope b and intercept ln (S+ 1). These distribution coefficients (correspond to linear and reversible adsorption isotherms) are rather easily implemented in codes that describe the migration of a selected sorbate through sorbent materials. They are neither linked to a retention mechanism nor do they necessarily consider solution and surface speciation explicitly. Both these aspects can be resolved mechanistically by considering their contribution in the sorption reactions.

1.4. Objectives of the thesis

The main objectives are;

1. To study the interaction of actinides (U, Th and Pu) with various matrices of prevailing marine environment of Mumbai Harbour Bay (MHB).
2. Spatial and vertical concentration profile of U, Th and Pu in bottom sediment of MHB.
3. Impact of minerals, trace metals and particle sizes on the association of U, Th and Pu with marine sediments.
4. To study the adsorption-desorption behaviou of U and Th in sediment-seawater sytem and comparision with other geochemical environments.
5. Radiometric dating of ^{210}Pb, ^{137} Cs and ^{228}Ra/^{226}Ra for evualtion of chronicle deposition of U, Th and Pu in bottom sediment of MHB.

6. To evaluate the various thermodynamic parameters for U (IV) sorption onto sediment/soil in various aquatic environments.

1.5. Outline of the thesis

The rest of the thesis is organized as follows:

Chapter 2 encompasses an overview of the study area which includes the interacting components (biotic and abiotic), water movement, tidal flow patterns and available dilution at Mumbai Harbour Bay (MHB). In addition, the various natural and anthropogenic sources of U, Th and Pu in the bay were also discussed in detail.

Chapter 3 describes the concentration profiles of ^{nat}U, ^{nat}Th & $^{239+240}Pu$ in seawater of MHB and prediction of their chemical speciation using computational methods. The chapter also discusses the various physico-chemical parameters such as Oxidation-Reduction Potential (ORP), pH, Dissolved Oxygen (DO), Electrical Conductivity (EC), Salinity, and Total dissolved solids (TDS) in seawater. In addition, the predominant aqueous species of U, Th and Pu at various physico-chemical parameters of seawater was calculated by the speciation code MEDUSA. This code includes an extensive thermodynamic database along with HYDRA (hydrochemical equilibrium constant database) speciation program and three main different algorithms for creating chemical equilibrium diagrams. The ligands such as hydroxide, chloride, nitrate, carbonate, fluoride, sulphate, phosphate and silicate are included.

Chapter 4 focuses on particle size characterization, mineralogy and their impact on spatial and vertical distribution of ^{238}U, ^{232}Th and $^{239+240}Pu$ in the bottom sediments. A total of 64 bottom (grab) sediment samples were collected at different seawater depths (1m –3 m) from 16 different locations covering an area of about 64 km^2 of Mumbai Harbour Bay using an Ekman dredge grab sediment sampler. The particle size distribution of sediment samples was determined using a laser diffraction particle size analyzer (CILAS, France, Model 1190). The various minerals present in the sediments were identified and quantified by the X-ray diffraction (XRD, Model: GNR, Italy). The total carbon in the sediments was estimated using C H N S O elemental analyser (Flash EA 1112 Series, Thermo Finnigan, Italy). Detailed spatial and vertical concentration profile of ^{238}U, ^{232}Th and $^{239+240}$Pu in bottom sediments was also discussed.

Chapters 5 gives the detail of the distribution of major and trace metals (Na, K, Mg, Ca, Fe, Cu, Ni, Co and Mn) in sediments and their correlations with the contration profile of ^{238}U, ^{232}Th and $^{239+240}$Pu. Using normalization of metals to Fe, the mean enrichment factor of Cu, Ni, Co and Mn was also evaluated.

Chapter 6 mainly focuses on the adsorption-desorption behavior of uranium and thorium in two different systems viz sediment-seawater and soil-groundwater. To understand the role of sediments in scavenging and removing radionuclides from the aquatic systems, it is necessary to study the processes by which ions are sorbed and desorbed from the surface of the sediments. In this study, the laboratory based batch experiment was conducted to determine the distribution coefficient (k_d) of uranium and thorium in sediments.

Chapert 7 discusses on the various obtained migration parameters such as sedimentation rate, sediment accumulation rate, age of sediment, total inventory, annual deposition rate, atmospheric fluxes, residences time, scavenging rate, linear attenuation coefficients, mass relaxation depth etc for ^{210}Pb and ^{137}Cs using radiometric dating models.

Chapert 8 describes the various thermodynamic parameters of U(VI) sorption in various aquatic systems. In this study, the sorption of U onto sediment under seawater systems in terms of k_d values was initially examined at three different temperatures viz 298 K, 323 K and 343 K under the similar laboratory conditions and it was compared with other geochemical environments such as undisturbed and disturbed soil in groundwater and deionised water system.

Summary of the study under this dissertation provides important informations about the interaction of three important elements of the actinides i.e. Uranium (U), Thorium (Th) and Plutonium (Pu) with various abiotic components of the marine ecosystem of Mumbai Harbour Bay.

CHAPTER 2

AN OVERVIEW OF STUDY AREA "MUMBAI HARBOUR BAY (MHB)": NATURAL AND ANTHROPOGENIC SOURCES OF ^{238}U, ^{232}Th & $^{239+240}$Pu IN MHB

2.1. Introduction

Mumbai, a metropolitan city, on the west coast of India is surrounded by coastal marine environment comprising of the Arabian Sea to the west and a number of tidal inlets around it such as the Thane creek, Back Bay, Mahim creek, Versova creek, Ulhas estuary and the Bassein creek. Most of the earlier studies carried out in this region have focused more on the main channel of the estuary (Ulhas) or larger creeks (Thane), especially near major industrial units [120 – 123]. The bay is a triangular mass of brackish water which widens out and opens to the Arabian Sea in the South and narrow at the Northern end, where it is fed partially by river Ulhas. The river is connected with the bay through thane creek. Ulhas flows into the Arabian sea through the Bassein creek at the north- western end of Salsatte island and part of it flows through the Thane creek into the bay. The Panvel River flows into the bay from the eastern mainland [124 – 126]**.** The average area of water surface of the bay is about 215 km^2 at high tide level and about 160 km^2 at low tide level. The total volume of water at mean sea-level as calculated from surrounding area is 9.1 x 10^{11} litres [124, 125]**.** The average tidal volume is 4.8 x 10^{11} litres [124]**.** Water movement in the bay is caused by the following factors: i) Part of water from Ulhas river flowing-in through the Thane creek and water from the Panvel river ii) Monsoon water pouring into the bay and iii) Tidal water. Of these three, Ulhas and Panvel rivers contribute a small fraction towards the movement of water in the bay as compared to the factor caused by the volume of tidal water moving in or out of the bay. Discharges during the monsoon do not affect the tidal curves, as these are small compared to the tidal volume. However the flow into the bay by first two factors during the monsoon causes considerable renewal of water in the bay. The bay is subjected to wave actions and semi-diurnal tides. Along the east and west sides of the bay, many industrial units like textile mills of South and Central Mumbai, the petrochemical, fertilizer, thermal plants, the pharmaceutical and chemical industries.

2.2. Water movement in the bay

Water movement in the bay is caused by the following factors;

i) Part of water from Ulhas River flowing through the Thane creek and water from the Panvel River

ii) Monsoon water pouring into the bay and

iii) Tidal water

Of these three, factor i and ii consisting of Ulhas and Panvel rivers contribute a small fraction towards the movement of water in the bay as compared to the factor iii caused by the volume of tidal water moving in or out the bay. Discharges during the monsoon do not affect the tidal curves, as these are small compared to the tidal volume. However the flow into the bay by first two factors during the monsoon causes considerable renewal of water in the bay [124].

2.3. Tidal flow patterns and available dilution

Three major streams are noticeable during both high and low tides;

1. Stream flowing near the Trombay shore
2. Stream flowing near the Elephanta shore (middle stream)
3. Stream flowing between Elephanta and Nhava islands

During high tides, water flowing near Trombay shore and near Elephanta and Nhava moves mainly into the creeks to the east of the bay. The pattern of water movement and dilution availability in the bay was determined in 1959 with a tracer discharge, before CIRUS was commissioned. A total of 4 Ci of ^{24}Na were dissolved in 180000 L of seawater and discharged through a pipeline at the peak of high tide for about 30 hrs. The movement of radioactivity was traced with underwater probes and dilution was measured in water samples collected at various intervals. The observations were

a. discharged radioactivity returned to the outfall on reversal of the tide,

b. There was an immediate dilution by factors of 10^4- 10^5 for a 0.3 L/s discharge

c. Patches of radioactivity remained close to the shore

In a second experiment conducted after CIRUS was commissioned, 20 Ci ^{42}K dissolved in 810000 L of seawater were released in 3 hrs through the CIRUS outfalls (700 Ls^{-1}) at low tide. Observations confirmed the earlier pattern of dilution and tidal oscillations. The net dilution available during a particular tide during the period of a cycle has been calculated to lie between 150 and 300 [124].

2.4. Climate and topography of the study area

Most of the Mumbai city is at sea level and the average ranges from 10 to 15 meters. The northern part of Mumbai is hilly. Soil texture in the proximity of the sea is predominantly sandy. In the suburbs, the soil is largely alluvial and loamy. The underlying rock of the region is composed of black Deccan basalt. The climate of Mumbai is highly erratic as it is a coastal area and the weather is highly influenced by the Arabian Sea. Generally, May is the hottest month of the year and the average temperature ranges between 32°C and 40 °C. January is the coldest month and the average temperature is about 18 °C. The annual rainfall in this region varied from

1800 mm to 2400 mm with an average value of 2170 mm. Because of the southwest monsoon winds, more than 95% of the annual rainfall occurs during four months period of June to September. During monsoon season, the circulation pattern might be altered due to the influx of fresh water. This city has a high humid climate with an annual average relative humidity of more than 60% [127]**.** The city falls in the seismic zone that may experience an earthquake up to a magnitude of 6.5 on the Richter scale.

2.5. Sample collection

The marine environment of Mumbai Harbor Bay [latitude (18^0N – 19.5^0N), longitude (72.5^0E-73^0E)] **(see Table 2.1)** is the recipient of sewerage and effluents discharged from the chemical industries situated along the coast of Mumbai & Navi Mumbai. In addition, the bay also receives the ultra low level liquid effluent discharged from Effluent Treatment Plant (ETP) of Bhabha Atomic Research Centre, (BARC) in Mumbai. The effluents discharged from BARC, meets all the stringent safety standards set by the Atomic Energy Regulatory Board. The discharges are made at about 825 m away from the shore where 1.8 m depth of water is available even at neap tide.

2.5.1. Seawater

A total of 64 seawater samples were collected in pre-acid washed plastic carboy (capacity : 35 L) from 16 different locations covering an area of about 64 km^2 of Mumbai Harbour Bay. A grid sampling was prepared with a sub grid dimensions of 1 km x 1 km. **Fig.2.1** depicts the map of MHB showing all sixteen sampling locations with Unique Identification Code (UID). During collection of samples, all members of team were briefed as shown in **Plate 2.1.** The seawater was collected as per standard protocols of US EPA and IAEA using Niskin sampling bottles as depicted in **Plate 2.2.**

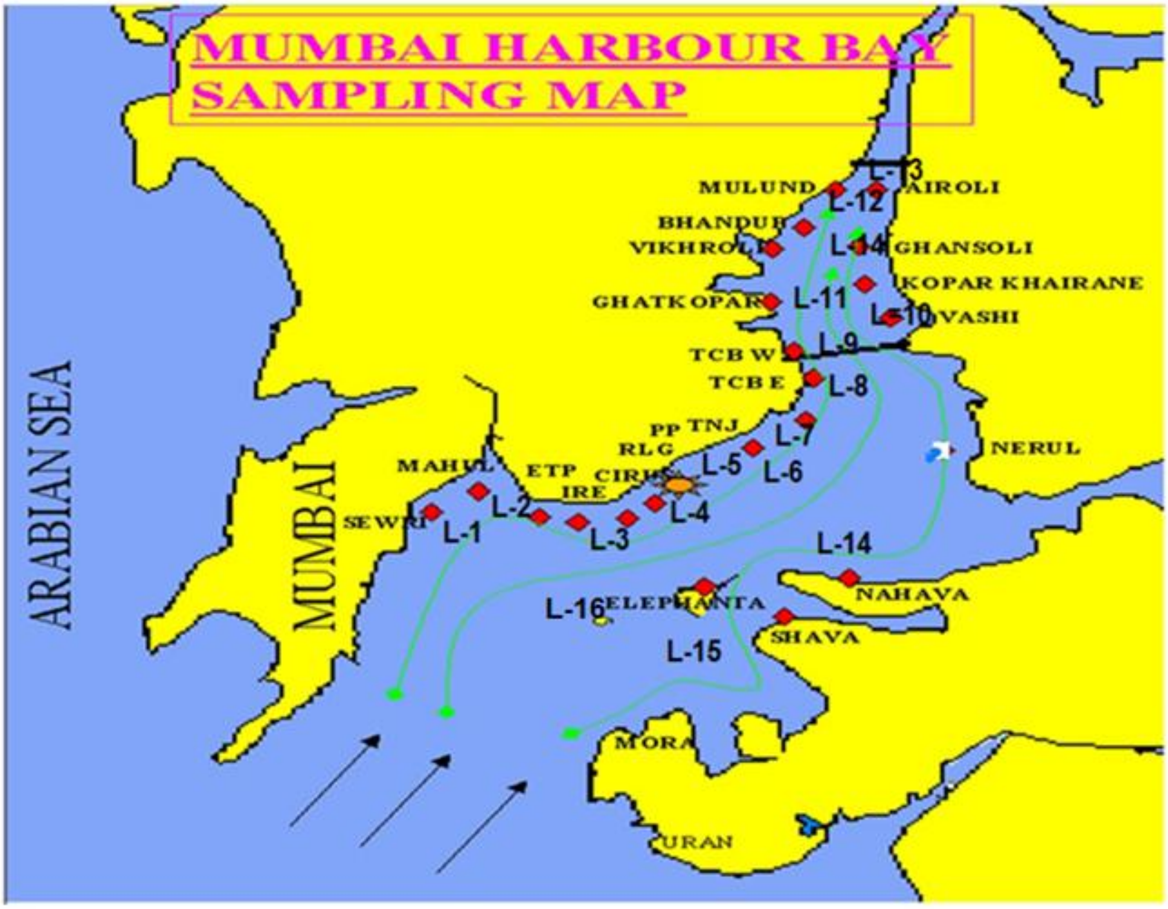

Fig. 2.1: Map of Mumbai Harbour Bay showing various sampling locations with unique identification code

Plate 2.1: Briefing of members during collection of marine samples of Mumbai Harbour Bay

Plate 2.2: Collection of seawater using Niskin sampling bottles

2.5.2. Sediment

A total of 64 bottom (grab) sediment samples were collected at different seawater depths (1m –3 m) from 16 different locations covering an area of about 64 km^2 of Mumbai Harbour Bay using an Ekman dredge grab sediment sampler **(See Plate 2.3)** having the collecting capacity of 5 kg. Sixteen core sediments were collected from eight different potential locations within 3 nautical mile area from the discharge point of CIRUS. Both grab and core sediments samples were also collected as per standard protocols adopted by US EPA and IAEA. The sampling was done by using in-house fabricated sampler **(See Plate 2.4)** made of acrylic cylindrical pipes having a length of 4 m and 30 mm internal diameter which were inserted by a diver. The core samples were sliced (sectioned) into 4 cm fractions as depicted in **Plate 2.5,** collected in polyethylene bottles with screw caps and transported to the laboratory and stored at 4^{0}C till further analysis. The depth of the core was upto 40 – 52 cm.

Plate 2.3: Collection of grab (bottom) sediment using Ekman dredge sampler

Plate 2.4: Collection of core sediment using in-house fabricated core sampler

Plate 2.5: Section of core sediment using core pusher

2.6. Interacting components/phases in the marine system

The marine environment of studied area has three main interacting components such as seawater, sediment and organisms. The interactions of sediment and the organisms are constantly with seawater in two directions: from seawater to sediments/organisms and vice – versa. During interactions, some constituents of seawater are entered into sediment/organisms. The product of such reactions may remain in solution or suspended or precipitate. All of these forms continue to interact, whereas the precipitates may settle down perhaps to disappear from the scene of interaction. The dissolved and the suspended materials will be more exposed for interaction. The nature and both the relative and total concentration of dissolved concentration of the dissolved constituents of seawater are remarkably invariant. In contrast, the nature and concentration of suspended materials in the sea can be highly variable. The chemistry of seawater is known pretty well. There have been innumerable studies on the sedimen

Table 2.1: Sampling locations code with GPS coordinate

L-1	N 18^{0}59.0390’, E 72^{0}53.6111’
L-2	N 18°59.5012'. E 72°54.0130'
L-3	N 18°59.6196', E 72°54.6856'
L-4	N 19°00.0056', E 72°55.2760'
L-5	N 19°00.0002', E 72°55.2795'
L-6	N 19°01.3507', E 72°57.1143'
L-7	N 18^0 59.0385’, E 72^{0}53.6123’
L-8	N 19°04.2287', E 72°57.6107'
L-9	N 18^0 59.0382’, E 72^{0}53.6120’
L-10	N 18^0 59.0391’, E 72^0 53.6122’
L-11	N 19°06.2377', E 72°57.6566'
L-12	N 19°08.5737', E 72°58.8153'
L-13	N 18^0.59.0403’, E 72^{0}53.6124’
L-14	N 18°58.4395', E 72°57.5510'
L-15	N 18^0 59.0382’, E 72^0 53.6124’
L-16	N 18°58.2330', E 72°55.8986'

The role of the suspended particulate materials (SPMs) in transporting and depositing of sedimentary materials in oceans and rivers is universally accepted. These materials are transient constituents which eventually settle out. These are originated from many sources such as atmospheric fall out, wind driven dust particles, in situ weathering and precipitation, excreta of organisms, salting out of colloids, industrial and domestic sewage releases, scouring of bottom sediments etc. and subsequently large variation in their composition. The transportability of SPMs depends on size, density, organic matter content and current velocity in the sea. The SPMs load in the study area varied from 20 to 950 mgL^{-1} with mean value of 180 mgL^{-1} as depicted in **Plate 2.5** [126].

The bay is characterized by abundant mudflats and exhibits good coverage of mangroves. However, in recent years the mangrove areas are being intensively targeted for dumping garbage, disposal of sewage and also overexploited by salt industries, fishing, navigation and recreational activities. In the past, the only source of waste water to the bay was from domestic discharge. But in recent years, development of nearby areas for residential purposes and industrial complexes has resulted in increasing level of pollution in the bay. **Kulkarni et al. (2010)** studied biological and environmental characteristics of mangrove habitats around the creek and found Avicennia marina to be the dominant mangrove species [128]**.** Because of poor abundance and diversity of mangroves, the authors classified the area as a highly stressed environment. The dominance of stress tolerant phytoplankton species such as Skeletonema costatum and benthic fauna such as Polychaetas further strengthened their observations. The dominance of polychaeta in the study area is attributed to increased salinity, temperature and heavy metal concentrations in the bay. The study area is rich in benthic organisms which are frequently harvested and consumed by locals.

2.7. Sources of ^{238}U, ^{232}Th & $^{239+240}$Pu in MHB

The World Ocean covers an area of 361.11 x 10^6 km^2 or 70.8% of the total surface of the earth [129]**.** Hence, the ocean is a major recipient of anthropogenic radionuclides released to the environment by atmospheric as well as aquatic pathways. The oceans may receive radioactive fallout directly from the atmosphere and indirectly as runoff from rivers or land. Radionuclides, however, also can be discharged directly into the ocean as liquid waste or dumped as solid waste, which may later dissolve. Some radionuclides will behave conservatively and stay in the water in soluble form, whereas others will be insoluble or adhere to particles and thus, sooner or later, be transferred to marine sediments. The three main sources of man-made radionuclides are nuclear weapons testing in the atmosphere, the Chernobyl accident and liquid waste discharges on routine basis from nuclear plants.

National weapons tests are estimated to have released more than 2 $x10^{20}$ Bq of radioactivity to the environment. Accidental and other releases of radionuclides from nuclear reactors amount to about 0.3% of this total. The majority of the releases from weapon testing have been deposited in the oceans and other aquatic systems. These releases include the residual fissionable nuclides in the weapon (e.g., ^{235}U, ^{239}Pu) and those which are produced in its explosion (fission products, e.g., ^{137}Cs, ^{90}Sr etc. and nuclei formed by nuclear reactions, beta decay, etc.). It is estimated that 16 PBq of plutonium have been deposited in the oceans of the world from these tests [130]. Plutonium radioactivity in surface sea water is about 10 μBqL^{-1}, indicating that most of the almost 10^{15} Bq of plutonium estimated to have been deposited in the oceans is now incorporated into bottom sediments [130]. Uranium and neptunium are more soluble than plutonium and, hence, are at higher concentrations.

The coastal zone represents the portion of World Ocean which is the most directly affected by human activities. Development of the coastal zone, exploitation of its natural resources and its use as a receptacle for societal wastes are resulting in problems ranging from contamination of sediments and living marine resources to eutrophication. Radionuclides provide tracers for many of the processes related to coastal zone problems. Indeed, increasingly in the last 25 years, natural radionuclides have been used to quantify the rates of coastal ocean processes and many of these results are directly applicable to providing important information in the coastal zone.

At BARC, Trombay, radioactive wastes are generally generated from the operation of research reactors, fuel fabrication, spent fuel reprocessing, research labs, manufacture of sealed sources and labeled compounds. Use of radiation sources in the field of medical, agriculture and industry also leads to generation of assorted solid waste and spent sealed radiation sources which require proper waste management. Waste Management Facilities at Trombay, comprise of Effluent Treatment Plant (ETP), Decontamination Centre (DC) and Radioactive Solid Waste Management Site (RSMS). Low level radioactive liquid effluents are received at ETP having the treatment capacity of 100 m^3d^{-1}. Average yearly releases of low level liquid wastes comprises of gross α wastes (3 - 6 GBq), gross β – γ wastes (50 – 70 PBq) and ^{3}H (27 PBq) in which ^{137}Cs (52% of gross β /γ), ^{90}Sr (30% of gross β/γ), other β/γ nuclides (18% of gross β/γ), ^{3}H (100%), ^{239}Pu (70% of gross α) and other α emitting radionuclides (30% of gross α) are discharged to MHB. Radionuclides discharged into the marine system of MHB get diluted and dispersed by tidal actions. Some radionuclides such as $^{239, 240}$Pu, ^{241}Am and ^{137}Cs are particle reactive and will end up in the sediments. From the sediments, these radionuclides can later be remobilized and transported away by local currents. Other radionuclides, such as ^{99}Tc and ^{90}Sr are not particle-reactive and will follow currents and can be transported large distances away from the discharge point. Thus the input of radioactivity to the MHB from natural and anthropogenic sources is derived from atmospheric fallout due to nuclear weapons tests (conducted mainly in the 1950s and 1960s), the Chernobyl accident in 1986 and low level liquid effluents discharged from ETP.

Natural radioactivity in seawater is primarily derived from the three primordial radioactive parents: ^{238}U, ^{235}U and ^{232}Th which yield over 22 radioactive daughter products with widely different half-lives and reactivities. Along each of these three natural radioactive decay pathways, soluble species, such as uranium, often decay to particle reactive species, such as thorium; one also finds the opposite tendency of a particle reactive species decaying to a soluble species. These discrepancies in particle reactivity lead to ‘secular disequilibrium’ and dramatically different distributions in the water column. Oceanographers have exploited these particle-scavenged ‘clocks’ to derive information on sources and fluxes of marine and terrestrial particles, carbon, and gases as well as on inputs and stirring rates of the present and past ocean. ^{238}U decays with a long half-life, thereby producing ^{234}Th, a short lived daughter. As the ocean is not closed system and thorium is highly reactive, ^{234}Th is easily removed by particulates from the surface. Only in deeper layers, it can in secular equilibrium or equal activity. Since ^{234}U is the next daughter product and is a uranium isotope. Although the isotopic abundance of ^{234}U is very small in terms of mass, the activity of ^{234}U is comparable to that of ^{238}U because the half life of ^{234}U is much shorter. In ocean water, the activity ratio is quite uniform at 1.15 indicating an excess of ^{234}U over ^{238}U. This suggests preferential mobilization of ^{234}U in seawater reflecting results of continental weathering processes and input from sediment pore waters. Due to highly soluble nature of uranium, it has a long mean residence time (10^5- 10^7 years) in the oceans. The long residence time is sufficient to allow studies of oceanic or geochemical processes that cause a radioactive disequilibrium between a parent and its daughter, since the daughter production rate can be accurately determined. ^{226}Ra is produced from ^{230}Th decay in the uranium decay series. It decays to ^{222}Rn. ^{226}Ra in the ocean is released mainly from bottom sediments via pore water exchange and diffusion due to its high mobility and much higher concentration in the sediments. Because of large variation in the deep and bottom water, ^{226}Ra has been used as a tracer for global-scale mixing and circulation studies.

Since the 1960s, thorium isotopes occupy a special place in the oceanographer's toolbox as tracers for determining rates and mechanisms of oceanic scavenging, particle dynamics, and carbon fluxes. Thus, in marine systems, Th has proven to be a very useful tracer of a wide range of oceanographic processes ranging from particle cycling [131 – 134] to boundary scavenging [135 – 138] and paleocirculation [139 -141] **.** This is because Th's chemical properties are relatively simple. Th has only one stable oxidation state, IV, under all redox conditions in natural waters and Th (IV) ions are extremely particle reactive. In seawater, ^{232}Th is present at pM concentrations. A number of other Th isotopes (^{234}Th, ^{230}Th, and ^{228}Th) also exist in seawater, albeit at lower concentrations, e.g., ^{234}Th is present in the ocean at atto-molar (10^{-18}M) concentration levels. These Th isotopes are primarily produced by natural uranium isotopes (^{238}U, ^{235}U and ^{234}U) that are soluble in seawater.

CHAPTER 3

CONCENTRATION PROFILES OF U, Th and $^{239+240}$Pu IN SEAWATER AND PREDICTION OF THEIR CHEMICAL SPECIATION USING COMPUTATIONAL METHODS

3.1. Introduction

Generally, actinides in natural waters are not in a state of thermodynamic equilibrium for long time periods. In seawater, oxidation state distribution of actinides is dependent on pH, Eh and the presence of suspended particulates. Each oxidation state has quite different chemical behavior; consequently, geochemical modeling becomes very challenging. In general, increased pH or Eh favors higher oxidation states. The Eh varies as a function of the amount of dissolved oxygen. The simultaneous presence of more than one oxidation state of actinides in seawater complicates actinide environmental behavior. Actinides in different oxidation states have different migration rates as these rates depend on solubility, sorption/desorption phenomena and interactions with inorganic anions and organic material, all of which are greatly influenced by oxidation state [142]. Uranium shows relatively conservative behavior in seawater because of the formation of stable carbonato complexes, whereas particulate uranium, involved in suspended particles with the particle size of more than 0.45 µm, is a minor constituent [143]**. Miyake et al. (1972)** and **Hodge et al. (1979)** found that less than 0.3% and 0.1 of the total uranium to be in particulate form in Japanese and California coastal waters respectively [144, 145]. **Anderson** showed that in the deep ocean, where the concentrations of particulate materials are much less than in coastal waters, particulate uranium concentrations fall in the range of 10^{-5} to 10^{-4} of the total [146]. **Hirose s**uggested that the chemical form of particulate 'metals in seawater are closely related to that of the corresponding dissolved ones [147]**.** The major features of uranium isotopes in seawater are well known. Uranium is very soluble in oxygenated seawater as a result of the formation of stable uranyl carbonate complexes and shows a fairly homogeneous distribution in the open ocean which is reflected in a long residence time of 2 – 5 x l0^5 years [143, 148, 149]**.** However, seawater is under saturated with respect to precipitation of uranium minerals [150]**.**

U occurs in aquatic systems in a variety of physicochemical forms, including the free metal ion (U^{4+} or UO_2^{2+}) and complexes with inorganic ligands (uranyl carbonate or uranyl phosphate), and humic substances (HS) (uranyl fulvate or humate) in dissolved, colloidal, and/or particulate forms [151]**.** Fine-grained sedimentary rocks typically have higher U concentrations than coarser-grained igneous rocks because of the higher content of clay and organic matter that readily binds U [152]. The geochemical cycle of U begins with the chemical weathering of rocks in the oxidized zone of the terrestrial near-surface environment and continues with mobilization by ground and surface waters. During weathering, ^{238}U and ^{235}U are released to water in a constant isotopic ratio. ^{234}U is produced by the radioactive decay of ^{238}U. However, the preferential mobilization of ^{234}U during weathering (due to α-recoil fractionation) gives rise to a $^{234}U/^{238}U$ activity ratio greater than unity for river (1.2 to 1.3) and seawater (1.14) [153]. In the rocks, ^{234}U and ^{238}U isotopes are generally in radioactive equilibrium and these isotopes are washed by water through rocks, soils and sediments and next is inflowing to rivers. The particles containing uranium are also precipitated from atmosphere as a result of rocks erosion and resuspension of soil [154, 155]. The average concentration of U (as ^{238}U, the most abundant isotope) in river water is 0.3 μgL^{-1} [156, 157] but typically ranges from 0.01 to 6.6 μgL^{-1} depending on contact time with the U bearing strata, the U content of the strata, the amount of evaporation and the availability of complexing ions [158]**.** In estuaries, where river and seawater mix, the concentration of dissolved U usually increases as a linear function of salinity i.e. conservative behavior [159], until it plateaus at around 3.2 μgL^{-1} in seawater [153]. Although U usually behaves conservatively during estuarine mixing (Zaire, Gironde, Tama, and Medway estuaries), it may also behave non-conservatively, such as in the Ganges-Brahmaputra and Amazon estuaries, where U is removed (sink) and added (source) respectively [160]. River water is the only significant input of dissolved U (3 to 5 × 10^7 mol y^{-1}) to the oceans [157, 158].

In seawater, ^{232}Th is present at pM concentrations. A number of other Th isotopes (^{234}Th, ^{230}Th, ^{228}Th) also exist in seawater, although at lower concentrations, ^{234}Th is present in the ocean at atto-molar (10^{-18} M) concentration levels. These Th isotopes are primarily produced by natural uranium isotopes (^{238}U, ^{235}U and ^{234}U) that are soluble in seawater. In marine systems, Th has proven to be a very useful tracer of a wide range of oceanographic processes ranging from particle cycling [161 – 163], and carbon export flux [164], to boundary scavenging [165 – 167] and paleo-circulation [168 – 170]. This is because of relatively simple chemical properties of Th which has only one stable oxidation state, IV, under all redox conditions in natural waters and Th (IV) ions are extremely particle reactive.

$^{239+240}$Pu is known to be the fallout radionuclide present in the marine environment, the concentration varying from region to region, according to the specific sources of contamination and the geographical location since high latitude atmospheric global fallout is smaller than low latitude fallout. A number of factors and processes control the transport and fate of plutonium over the time. The distribution of Pu between water and sediment greatly depends on the oxidation state [171 – 173]. Because the pH of oceans is well buffered, being quite equal, Pu is typically in the Pu (V) or Pu (VI) state in aquatic system under oxidising conditions and as Pu (IV) in sediments. Experimental studies have shown that in shallow water bodies, usually more than 90 % of total Pu is rapidly transferred to sediments associated with particulate materials. In deep oceans, the situation is different. Most of Pu remains in the water phase for a long time due to a slow mixing of water masses and slow sedimentation rates [174 – 176]. In the water phase, plutonium can be either soluble or fixed in particulate fraction depending on the chemical properties of water. For instance, in the Baltic Sea, the proportion of soluble Pu varied from 25 to 70 % of total Pu in the water on different sampling dates [177]. The solubility of Pu in natural waters is complex. The pH, amounts of humic and fulvic acids and many complexing agents affect the solubility of Pu in freshwater. pH can vary greatly and it can be relatively low (about 4). In such conditions, Pu can also be as strong complexes [178, 179]. Several equilibrium reactions affect the distribution of Pu between water and sediment fractions. The main equilibria are the: 1) redox equilibrium between oxidation states in the water column, 2) formation of inorganic and organic complexes (as hydroxides, bicarbonates, carbonates, sulphates etc.), 3) reactions of these complexes with iron-aluminium-manganese compounds in sediments. The typical sediment – water distribution coefficient for Pu in a freshwater environment, as well as in coastal and brackish waters, is $2x10^5$, ranging from 10^4 to 10^6 [180, 181] **.** In the marine environment, the differences between the soluble and particulate phases were noted but the average values of k_d in equilibrium between seawater and sediment was $1\text{-}2x10^5$ [180 – 182]. Generally, the concentrations of ^{239,240}Pu in marine waters originating from global weapons test fallout varied from a few to a few tens μBqL^{-1} and ^{238}Pu & ^{241}Pu are less than 1 μBqL^{-1} and between 20– 40 μBqL^{-1} respectively [183 – 187]. The ^{239,240}Pu concentrations in freshwaters are generally at the same level as in seawaters, when Pu originated from global fallout [187]. However, some exceptional circumstances can increase the normal fallout level of Pu in freshwater. This phenomenon has been observed in organic-rich freshwaters, highly alkaline waters and also anoxic near-bottom waters where a great portion of Pu is in the water phase [179]. In the freshwater system near Chernobyl, the concentrations of ^{238}Pu, and ^{239,240}Pu varied within one decade in rivers and small lakes and were still in 1996 at their highest of 10 µBqL^{-1} and 200 µBqL^{-1} respectively. About 70 % of these nuclides were in particulate fraction of water [188]. The transport of radionuclides depends on several things in an aquatic system: on local current patterns, wave actions, erosion by bottom currents and on bottom configuration. The finest particles can be easily transported long distances into the accumulation basins in deeper parts of the water basin [189 – 195]. The activity concentrations of $^{239+240}$Pu in water samples of the southern Baltic comprise dissolved (2.8 – 145 µBqL^{-1}) and suspended particles (1.6 – 4 µBqL^{-1}) and colloidal (0.8 – 1 µBqL^{-1}) fractions [196]. The largest activities of total $^{239+240}$Pu (150 µBqL^{-1}) were found for Pomeranian Bay area. The average activity concentration of $^{239+240}$Pu in the Baltic Sea water for the year 2000 was reported to be about 1.5 µBqL^{-1} [197]. The estimated sedimentation rate based on measured $^{239+240}$Pu in bottom sediments ranged from 0.2 to 8 mmy^{-1}, maximum activities (4 –12 Bqkg^{-1}) were detected at the depth from 6 to 30 cm [198, 199].

3.1.1. Chemical species of uranium, thorium and plutonium in seawater

Uranium in surface seawater is found in both the tetravalent and hexavalent state, but U (VI) as UO_2^{2+} is dominant. In anoxic waters, U (IV) forms insoluble, polymeric, mixed hydroxides and carbonates in natural waters, which deposit in the seabed. Under oxic conditions, U (IV) is oxidized to U (VI), which is capable of forming more soluble species, allowing more migration. The solubility of the hexavalent UO_2^{2+} in sea water is also limited by hydrolysis; however, it has an unexpectedly high concentration (10^{-8} M) due to primarily formation of strong carbonate complexes [200]. At low pH, adsorption of uranyl cation (UO_2^{2+}) is generally negligible and increases with increasing pH usually in the pH range of 4 to 6. But, in the alkaline region, U (VI) is strongly adsorbed in the absence of dissolved CO_2 [201]. Uranyl (VI) hydrolysis study in the laboratory is complicated by the formation of polymeric species. In concentrations below 10^{-6} M, $UO_2\ (OH)^+$ is the dominant hydrolysis species in solution while above this concentration polymeric forms such as $(UO_2)(OH)_2^{2+}$, $(UO_2)_3(OH)_2^{4+}$ and $(UO_2)_3(OH)_5^+$ exist [200]**.** Uranium concentrations in sea water are in the order of $U_T = 10^{-8}$ M, so hydrolytic polymers are not significant and the monomeric hydrolytic species are less important than the carbonate complexes since it is estimated that 90–100% of the dissolved uranium in ocean waters is present as carbonate species [200]. In uranyl−hydroxide−carbonate system, the $UO_2CO_3^0$, $UO_2\ (CO_3)_2^{2-}$ and $UO_2\ (CO_3)_3^{4-}$ complexes predominate in the pH range of 6−8 [202]. The $(UO_2)_2CO_3(OH)_3^-$ species appears in neutral pH range, varying in significance concentrations of carbonate and uranium in solution.

Thorium (IV) is capable of forming both mono- and polymeric hydrolysis products. In dilute solution ($\leq 10^{-4}$ M), as the pH increases above 2, the species $Th\ (OH)^{3+}$, $Th\ (OH)_3^+$ are present and at higher pH, $Th(OH)_4$ are present [203, 204]. Tetravalent actinide cations do not form carbonate complexes in significant levels as hydrolysis is a much more dominant reaction, leading to the very insoluble $An(OH)_4$ species. Mixed hydroxocarbonato complexes may be present in carbonate rich sea waters, but the concentrations of these species would be very small compared to the concentration of the simple hydrolyzed species of the An(IV) cations. The prevailing inorganic species of Th in seawater at pH 8 are hydroxo [205] and carbonato complexes, in approximately equal proportions [204, 206, 207]. In fact, in organic-free solutions, thorium will strongly hydrolyze to form polyhydroxy colloidal complexes. Other strong ligands include carbonate, humics, phosphate, ethylene-diamine tetraacetic acid (EDTA) and diethyl-triamine-pentaacetic acid (DTPA). The solubility of Th depends on the structure of the ThO_2 solid. The solubility of crystalline ThO_2 is ~10^{-15} M [208, 209] well below the observed 10^{-12} M seawater ^{232}Th concentrations [210]. In contrast, the observed solubility of all forms of Th oxyhydroxides, including $Th(OH)_4$ (am), ranges from 10^{-8} to 10^{-10} M, due to conversion of larger crystalline forms to smaller amorphous colloidal forms during the dissolution and/or precipitation process [208, 209]. There are few studies that have focused directly on organic ligand complexation of Th in natural waters. In general, they indicate that Th forms strong complexes with humic acids [211 – 214], and acid polysaccharides [215 – 217]**.** In fact, thorium generally shows high concentrations in colloidal fractions in marine environments [218]. Since natural particles in seawater are coated with an organic film at the surface, they are mostly negatively charged [219]**.** Thus, it can be expected that metal ion sorption to inorganic surfaces is modified by dissolved organic compounds and dependent on the relative abundance and binding energies of functional groups on particle and in solution phases.

In oxic waters, Pu is found exclusively in one or more oxidation states from IV through VI. At the environmental levels of plutonium in seawaters at neutral-to-basic pH, PuO_2^+ disproportionate into Pu^{4+} and PuO_2^{2+}. The redox potential of Pu (V) and the strong hydrolysis of Pu (IV) limit the concentration of PuO_2^+ in marine and natural waters. The trivalent plutonium ion is present only in anoxic waters. In the open oceans, a more equal distribution between oxidized (V) and reduced (IV) forms has been reported [220, 221], Plutonium sorbs more extensively in the (III) and (IV) oxidation states than in the higher states (V and VI) by over two orders of magnitude [222]**.** In the Baltic Sea, 99% of the total plutonium inventory is sorbed onto sediment as Pu (IV) [223]. Because of the strong affinity of $Pu(OH)_4$ [224] for sediments and suspended particulates, Pu(IV) sorption is the limiting factor in Pu transport processes [224].

PuO_2^+ is a weakly complexing cation whose concentration is predominately determined by its redox equilibrium with the III, IV and VI oxidation states. In both acidic and basic solutions, PuO_2^+ is present only in submillimolar concentrations.

3.1.2. Computational Methods

Speciation methods have been classified into two categories, one is analytical methods which include physical separation (by species, size and charge) electrochemistry/spectroscopy and another is computational methods, including thermodynamic (and kinetic) modeling. Despite the central importance of knowing the full speciation of a chemical in order to predict its behaviour in a system, it is generally not possible to determine a speciation analysis using analytical chemistry methods alone. Most techniques are focused on detection of free metal ion concentrations or total metal concentrations. Direct speciation measurement using traditional analytical methods requires significant complexity and generally hyphenated techniques. Since environmental concentrations of most metals of interest are low, therefore many relevant forms of metals cannot be measured directly and hence analytical techniques often are not effective for determining overall speciation. Thus chemical speciation determination generally relies on utilising analytical methods in conjunction with chemical speciation models.

Due to a lack of analytical methods to directly determine the speciation of actinides in natural surface waters, computational methods have predominantly been used. Much of the available information on the speciation of actinides in aquatic systems has been determined using thermodynamic speciation modeling. A speciation model is a mathematical statement (system of equations) of the methods and assumptions used to describe metal-ligand equilibria [225]. Two distinct, but thermodynamically related methods are used by speciation models to calculate metal-ligand equilibria in aqueous systems: the equilibrium constant method and the Gibbs free-energy method [226]. Both methods are subjected to the conditions of mass balance and chemical equilibrium. The mass balance condition requires that the calculated sum of the free and complexed species of each element be equal to the given total concentration. Chemical equilibrium requires that the most stable arrangement for a given system be found, as defined by the stability constants for all mass action expressions of the system or through the use of Gibbs free-energy values for all components and derived species. In the equilibrium constant method, the mass action expressions are substituted into the mass balance equations, resulting in a set of nonlinear equations that must be solved simultaneously. The Gibbs free-energy method is simply a transformation of variables through the thermodynamic relation, which allows a different numerical approach [226].

A speciation code (MEDUSA, MINTEQA2, PHREEQE, MINEQL, EQ3/6 etc) is the practical realization of the solution to a speciation model which executes calculations based on a model, typically written in a high-level computer language. Most codes employ the equilibrium constant method, which uses measured or calculated stability constants for all mass action expressions of the system [227]**.** The model inputs include pH, redox potential, temperature, total metal (e.g., U, Th, Pu) and ligands (e.g., carbonate, sulfate) concentrations. As output, the percentage formation of relevant species, such as the free metal ion (UO_2^{2+}) and metal complexes (e.g., UO_2CO_3, UO_2SO_4), are calculated for specific physicochemical conditions [225]**.** Although a variety of speciation models are now widely available, all have significant limitations and these are discussed in detail elsewhere [226, 228, 229]**.** One limitation is that most speciation models assume equilibrium conditions i.e. the kinetics of precipitation; oxidation reduction and adsorption are generally ignored. This is not a valid assumption for uranium in some cases, because of kinetically unfavorable chemical processes, biological transformation, and physical transport [230]. There is a lack of kinetic-based speciation models available compared to thermodynamic (equilibrium) models. The modeling of actinides adsorption is not well developed in most speciation models, owing to a general lack of understanding of the phenomenon [231]. Modeling of adsorption processes can be accomplished using stability constants which are frequently estimated in the laboratory and later adjusted in field applications. Natural colloids are also very difficult to include in model calculations and more work is required in this area. The output from a speciation model is only as reliable as the input data. There is a clear requirement for a reliable and internally consistent database of stability constants to model chemical equilibria. Such a database exists for inorganic metals species [225, 232]. In natural waters, however, metals binding by HS, in the form of fulvic and humic acids, are not accounted for by many speciation models, since these macromolecules are chemically ill defined and stability constants are poorly known. Markich and Brown give an overview of the conceptual models that have been incorporated into some speciation codes to predict metal binding with HS, including U [227]. HS may account for a significant portion of the U binding capacity of surface waters and hence, markedly influence the speciation, transport and bioavailability of U [233]. Therefore, U complexes with HS may be greatly under estimated or not considered in surface waters by many speciation models. As a result, such models may markedly overestimate the formation of inorganic U species.

There is no general-purpose speciation model that can be used for all applications. While there are several limitations in using speciation models, the general consensus is that they can provide useful results if applied correctly and with an understanding of the differences between simulated and natural systems [231]. Only one study [234] has attempted to verify, in part, the speciation modeling results of dissolved U (in simulated freshwater) using an analytical technique (e.g., TRLFS). However, to date, the model has not been evaluated with U and this should be a priority for future research.

3.2. Materials and methods

3.2.1. Seawater sampling and field measurements

Seawater samples were collected in pre-acid washed plastic carboy (capacity : 35 L) from sixteen different locations covering an area of about 64 km^2 of Mumbai Harbour Bay. Detailed of sampling and locations were already discussed in **Chapter 2 (Section 2.5.1).**

3.2.2. Measurement of physiochemical parameters

The in-situ measurement of the physico-chemical parameters such as Oxidation-Reduction Potential (ORP), pH, Dissolved Oxygen (DO), Electrical Conductivity (EC), Salinity, and Total dissolved solids (TDS) in seawater during sample collection were carried out using pre calibrated standard field equipment, AM-200 GPS Aquameter (UK make). Measurements of pH were made with a glass sensor calibrated at the sample temperature and using pH 4, pH 7 and pH 9 buffers. The deviation of pH measurements was ±0.2 pH units. The redox potential was measured with a Pt electrode and a calomel reference electrode. ZoBell's solution (220 mV at pH=7) was used as a standard to verify the measured values. When the Pt electrode gave readings within a range of ±5 mV, the steady state potential was regarded as having been reached and data were collected. All electrodes were connected to a multi parametric probe (AP-1000) with which physicochemical variables were recorded.

3.2.3. Seawater sample processing

The collected water samples were filtered through 0.45 μm filter paper using a suction pump. The filtered seawater samples were acidified with 0.01M of nitric acid (AR Grade, Merck, Mumbai, India) and stored in pre acid washed, 500 ml capacity polypropylene bottles for cation, anion and uranium analysis.

3.2.4. Cations and anions

The determination of cations ($Na^{+,}$ K^{+}, $Mg^{2+,}$ Ca^{2+}) and anions (F^{-}, Cl^{-} , $SO_4^{2\ -}$, NO_3^{-}) in seawater was estimated by conductivity suppressed ion chromatography system (DIONEX- 600). **Plate 3.1** and **Fig. 3.1** show the photograph and schematic arrangement of various important components of ion chromatography system.

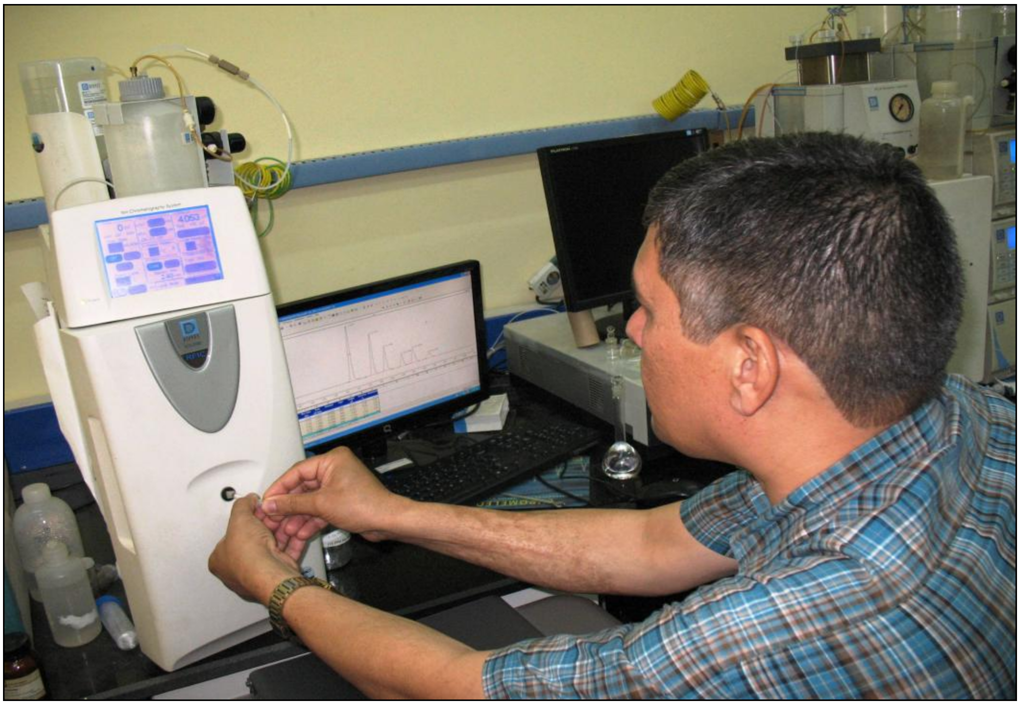

Plate 3.1: Photograph of reagent – free ion chromatography system (Model RFIC, ICS-2100, DIONEX)

Ion chromatography system consists of solvent delivery system (pump, pressure controls, flow controls, inlet filters etc.), sample injection system, column, detector and data control and display system.

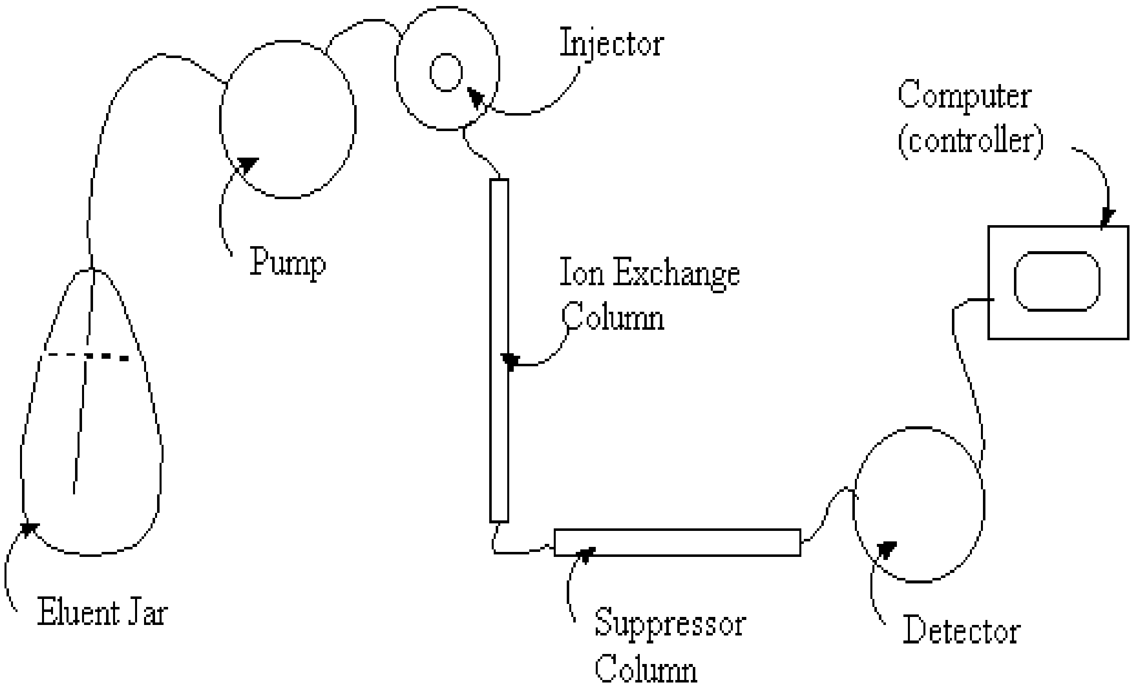

Fig.3.1: Schematic arrangement of basic components of ion chromatography system

The sample is injected into the instrument through the injection system. The eluent, which the pump draws from the eluent jar and forces through the system, then carries the analyte onto the ion exchange column under a pressure of about 1000 psi (65 atm). As the eluent flows through the column, the components of the analyte will move down the column at different speeds and therefore separate from one another, as shown in **Fig. 3.2.**

The instrument was calibrated and standardized with the stock solution of ultra pure Fluka (Switzerland) standards for the above cations and anions. The major cations **(Fig.3.3)** were estimated under following conditions: Sample Volume: 25 µL Loop, Column: IonPac CG17, CS17, 2-mm , Eluent: 6 mM MSA, Eluent Flow Rate: 0.25 mL/min, Temperature: 30°C, Detection : Cation Self-Regenerating Suppressor- ULTRA Auto Suppression - Recycle Mode , Expected Background Conductivity: < 2 µS, Storage Solution: Eluent,

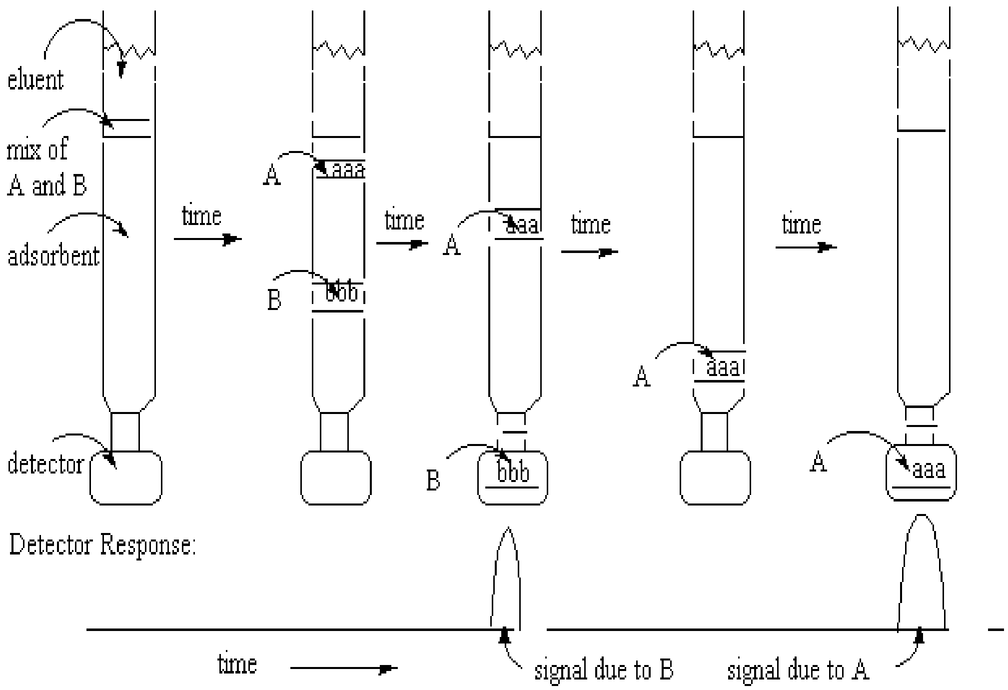

Fig.3.2: Separation of ionic components of the analyte as a function of retention time in ion chromatography system

Similarly, the major anions **(Fig.3.4)** were estimated under following conditions: Sample Volume: 25 µL Loop, Column: IonPac AG17, AS17, 2-mm, Eluent: 14 mM NaOH, Eluent Flow Rate: 0.25 mL/min, Temperature: 30°C, Detection: Anion Self-Regenerating Suppressor-ULTRA Auto Suppression - Recycle Mode, Expected Background Conductivity: < 2 µS, Storage Solution: Eluent,

HCO_3^- was estimated titrimetrically using autotitrator (Metrohm-798 MPT Titrino). CO_3^{2-} was determined with the help of measured concentration of HCO_3^- and pH using an equilibrium relationship for the carbonate system.

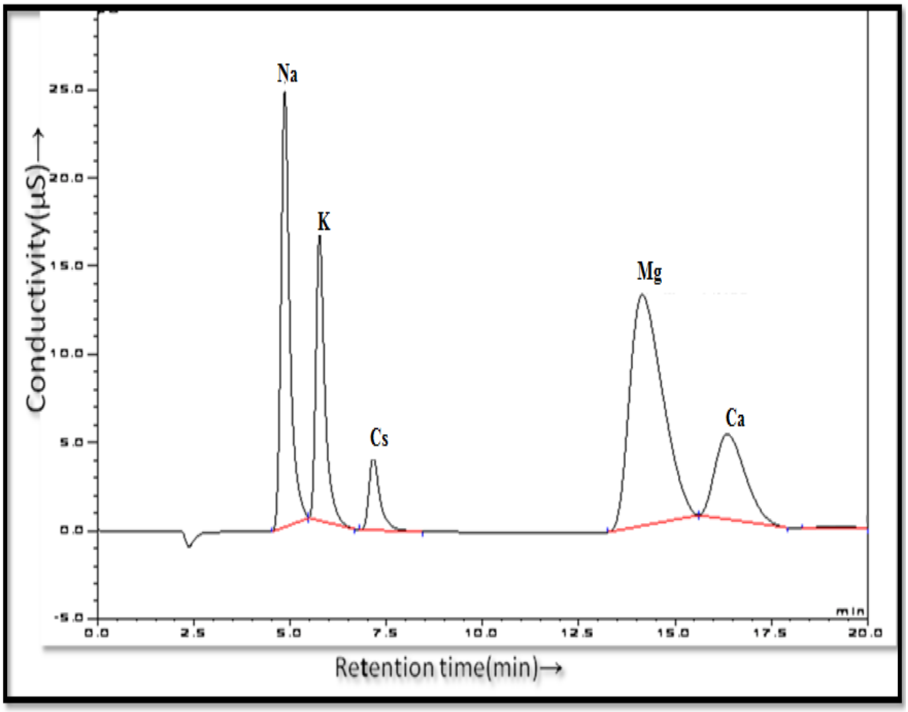

Fig.3.3: Chromatogram of major cations using 5 mg/L of mixed standard solution (Fluka)

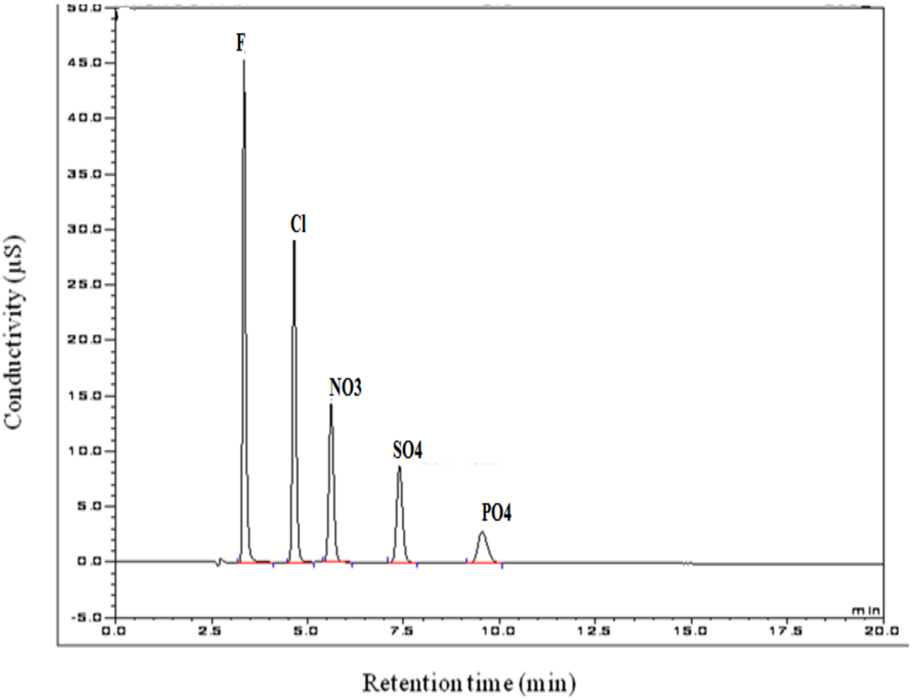

Fig.3.4: Chromatogram of major anions using 5 mg/L of mixed standard solution (Fluka)

3.2.5. Sequential separation of uranium, thorium and plutonium

30 L of filtered seawater acidified with 30 mL conc. HNO_3 and 1dpm of ^{242}Pu tracer, 100 mg Fe carrier was added and kept overnight for equilibrium. $Fe(OH)_3$ was precipitated by adding liquid ammonia till pH >7. The precipitate was separated by centrifugation and then dissolved in 8N HNO_3. The dissolved fractions was evaporated to near dryness and diluted to 1 L by adding deionised water. 0.5g hydroxylamine hydrochloride ($NH_2OH.HCl$) was added and the sample was heated at 80^0 C. 100mg Bi carrier and 10 mL H_3PO_4 were added to get the precipitate of $BiPO_4$. The precipitate was centrifuged, dissolved in 1ml 6N HCl +10 ml 0.2 HCl (normality = 0.75 N) and passed through in preconditioned cation exchange resin (Dowex-50X8, 100-200 mesh) with 0.75 N HCl. Washed the column with 0.75 N HCl. Eluted Pu and Th with 8NHCl. The eluent was evaporated to dryness and converted to nitrate by evaporating with concentrated HNO_3. The residue was dissolved in 8N HNO_3 and 0.5g $NaNO_2$ was added to oxidize Pu^{3+} to Pu^{4+}. This was loaded on a preconditioned anion exchange resin (Dowex-1X8) with 8N HNO_3. Washed the column with 8N HNO_3 and discarded the effluent. Th was finally eluted with 8NHCl and estimated by precipitating with ferric hydroxide followed by centrifugation. The precipitate was washed, dried, weighed in stainless steel planchet and estimated by gross alpha counter. Pu was eluted with 1.5M $NH_2OH.HCl$. The eluent was evaporated and residue destroyed with concentrated HNO_3. Pu was electroplated by using an electrochemical cell in which a stainless steel (SS) buffed planchet acting as cathode and platinum wire as anode. The electrolytic solution of $(NH_4)_2SO_4$ at pH 2.2 was used. The electroplating was done at an applied voltage of 6V and 0.3A current for 3 hours. After that, the planchets were washed with alcohol, heated directly on the flame till red-hot and counted for 80,000s using alpha spectrometry (ORTEC, OCTETE model) with 12% efficiency, 20 keV resolutions and 300 mm^2 areas with a depletion

depth of 100 mm. **Plate 3.2** depicts the schematic photograph of the alpha spectroscopy system showing the sample holder and vaccum chamber.

The supernatant of $BiPO_4$, was allowed to precipitate of $Ca_3(PO_4)_2$ by adding 200mg Ca carrier and liquid ammonia. The precipitate was then dissolved in 8N HCl and loaded on preconditioned anion exchange resin column (Dowex 1 x 8) with 8N HCl. Uranium was finally eluted with 1N HNO_3 and estimated by laser uranium analyser flourimeter (Quantalase Indore, India) which consists of a small nitrogen laser, which emits UV radiation of wavelength of 337.1 nm. This laser excites the uranyl ions present in the sample, which on de-excitation gives out fluorescence peak at 496, 516 and 540 nm. Finally standard addition technique was followed for the estimation of uranium in the samples. The instrument was calibrated in the range of 1-100 µg/L using a stock solution of (1 g/L) of $UO_2(NO_3)_2$ standard (USA). 5% sodium pyrophosphate in ultra pure water was used as fluorescence reagent. Relative standard deviation (RSD) was calculated to be 8-12%. **Plate 3.3** depicts the photograph of compact laser uranium flourimeter (Quantalase Indore, India).

3.2.6. Equilibrium modeling of actinides speciation

Equilibrium distribution of aqueous and solid phase of U, Th and Pu at various physico-chemical parameters of seawater was calculated by the computer code MEDUSA [235]. This code includes an extensive thermodynamic data base along with HYDRA (hydrochemical equilibrium constant database) speciation program and three main different algorithms for creating chemical equilibrium diagrams. The ligands such as hydroxide, chloride, nitrate, carbonate, fluoride, sulphate, phosphate and silicate are included. Using HYDRA model, the Eh-pH diagram of uranium, thorium and plutonium was drawn at measured composition of seawater. This diagram is a useful tool for visualizing the stability fields of the mineral phases that control seawater chemistry.

Plate 3.2: The schematic photograph of the alpha spectroscopy system showing the sample holder and vacuum chamber (Model: OCTETE PLUS, ORTEC)

Plate 3.3: The photograph of compact laser uranium fluorimetery (Quantalase Indore, India) showing the display unit

3.3. Results and discussions

3.3.1. Physicochemical analyses of seawater

Seawater of studied area was dominated by the following major ions: Na^+, K^+, Mg^{2+}, Ca^{2+}, Cl^-, SO_4^{2-}, HCO_3^- and CO_3^{2-}. The typical mean and range of the physico-chemical analyses in sea water are listed in **Table 3.1.** Salinity and pH of seawater were found to be ranged from 20.6 to 30.2%□ and 7.5 to 8 respectively. The calculated ionic strength ranged from 0.42 to 0.62 with mean of 0.53, which was almost comparable with the literature value (0.7) reported for seawater. In situ measurement of dissolved oxygen ranged from 3 to 8.5mgL^{-1} indicated that there was a good aeration of seawater. The mobility of actinides in seawater is extremely sensitive to oxidation-reduction potential (ORP) (approximated by Eh). The present study has estimated the ORP in the range of +30 mV to +100 mV with mean value of +50 mV. The positive range of ORP values again confirms that seawater is in oxic environment. To visualize the stability fields of U, Th and Pu bearing mineral phases, the Eh - pH diagram was constructed under the assumption of oxic (P_{O2} = 1 atm) and anoxic conditions (P_{H2} = 1 atm) of seawater. The Eh values were calculated to be in the range of - 460 mV to + 750 mV at measured pH range of seawater using an Eh - pH equation for water system. In this study, as obtained the positive value of ORP, therefore only positive Eh value (~ 0.75 V) was considered.

On the other hand, carbonate ions (CO_3^{2-}) were calculated in the range of (0.2 – 1.5) x10^{-5} M. The predominant source of carbonate ions might be due to calcite/dolomite whereas carbonic acid results from the dissolution of atmospheric carbon dioxide gas and the decomposition of organic matter in seawater.

3.3.2. Concentration profile of U, Th and $^{239+240}$Pu in seawater

The activity concentrations of U, Th and $^{239+240}$Pu in seawater as illustrated in **Fig. 3.5 – 3.7** were found to vary from 1 to 4.4 µgL^{-1} (mean: 2.6 ± 0.83 µgL^{-1}), 70 to 250 ngL^{-1} (mean: 143 ± 51 ngL^{-1}) and 47 to 138 µBqL^{-1} (mean: 86 ± 30 µBqL^{-1}) respectively. The levels of U and Th in seawater are comparable with the values for other oceans.

The reported values of total concentrations of uranium and thorium in surface seawater of both the Atlantic and Pacific oceans ranged from 2.61 to 3.57µgL^{-1} and ~58 ngL^{-1}. The levels of $^{239+240}$Pu are on lower side compared to others equivalent scenario internationally like La hague, France and Sellafield, UK reprocessing plants. The reported fallout values of $^{239+240}$Pu in seawaters of Baltic Sea ranged between 5.2 – 49 µBqL^{-1} [236] **[95].** The levels of $^{239+240}$Pu in seawater from north east Irish Sea, collected in 1992, were in the range of 170-4300 µBqL^{-1}.

Table 3.1: The mean and range of physico-chemical analyses in seawater

Physico-chemical parameters	Mean	Minimum	Maximum
F^{-1}(mgL^{-1})	8	2	22
Cl^{-1} (mgL^{-1})	9896	5652	16812
Br^{-1}(mgL^{-1})	70.34	37	185
SO_4^{-2} (mgL^{-1})	1392	993	1751
HCO_3^{-1}(mgL^{-1})	150	110	180
CO_3^{2-}(mgL^{-1})	0.18	0.13	0.88
DOC(mgL^{-1})	7.3	1.4	10.8
Na^+(mgL^{-1})	9310	4419	15387
K^+(mgL^{-1})	171	77	312
Mg^{2+}(mgL^{-1})	583	266	971
Ca^{2+}(mgL^{-1})	260	127	538

U (μgL^{-1})	2.6	1	4.4
Th (ngL^{-1})	143	70	250
$^{239+240}$Pu (μBqL^{-1})	86	47	138
pH	7.7	7.5	8
Dissolved Oxygen (mg/L)	5.56	3	8.5
EC (μS/cm)	50500	29178	60349
TDS(mg/L)	32860	18965	39226
Salinity (ppth)	26	20.6	30.2
Ionic strength	0.53	0.42	0.62
ORP (mV)	+ 50	+ 30	+100

The spatial variability of U, Th and $^{239+240}$Pu in terms of coefficient of variation (CV) along the studied area were found to be 32%, 36% and 35% respectively indicating a non-homogeneous distribution. This might be due to the consequences of meteorological conditions, sediment/suspended silt texture, mineralogical composition, anthropogenic input etc. In addition, the distribution pattern of radionuclides also depends on the sorption capacity of suspended particulate matters in seawater. Some radionuclides remain dissolved and are termed conservative within aqueous medium. Some are scavenged out of solution onto particulate material by biological or chemical processes, e.g., adsorption and co precipitation leading to deposition in bottom sediments.

In general, the concentration profile of U, Th and $^{239+240}$Pu in seawater showed a decreasing trend from southern part to northern part of studied area indicates a good dilution and dispersion due to tidal action and water current. The uneven pattern for radionulides might be attributed either due to dynamic nature of the system under the study or local influence due to ultra low level inputs from effluent treatment plants Some environmentally elevated levels of activity were observed at L-14 to L-16 which may be due to stream flowing in opposite direction from the discharge locations. The activity levels near the discharge locations are distinctly higher than other locations confirming that there is net northerly transport of radionuclides through seawater.

3.3.3. Activity ratio of ^{238}U /^{232}Th in seawater

The activity ratio of ^{238}U /^{232}Th in seawater along the studied area ranged from 6.7 to 51.8 with mean value of 20 ± 10.4. **Fig. 3.8** depicts the variation in activity ratio of ^{238}U /^{232}Th in seawater of study area of Mumbai Harbour Bay. Higher values of ^{238}U /^{232}Th in seawater clearly indicate that ^{238}U has relatively greater solubility and mobility compared to ^{232}Th. On the contrary, Th is highly particle reactive, immobile and strongly bound to solid matrix.

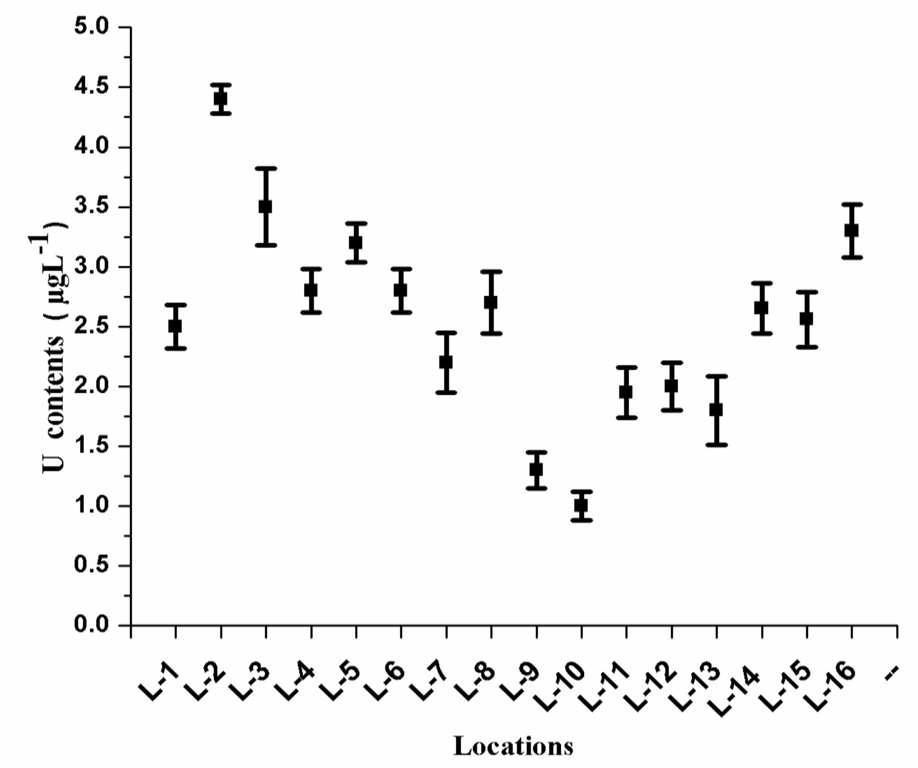

Fig. 3.5: Spatial distribution of U in seawater of Mumbai Harbour Bay

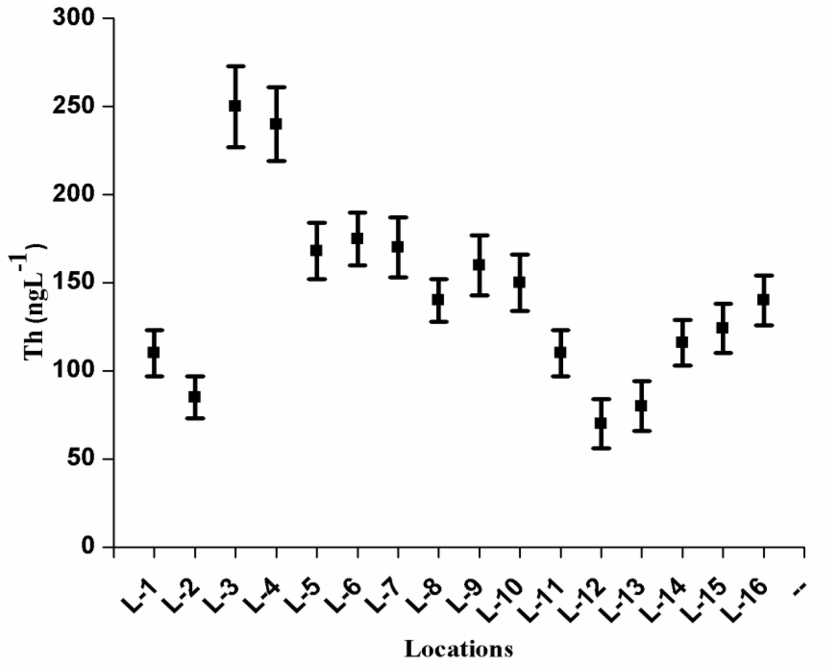

Fig. 3.6: Spatial distribution of Th in seawater of Mumbai Harbour Bay

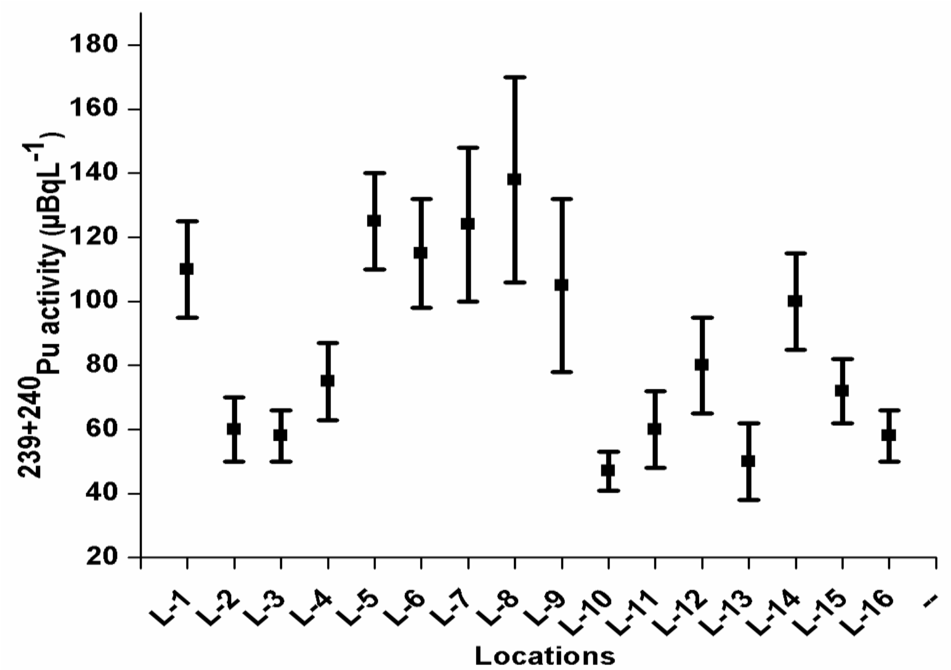

Fig. 3.7: Spatial distribution of $^{239+240}$Pu in seawater of Mumbai Harbour Bay

The wide variation in the activity ratio of ^{238}U /^{232}Th in seawater might be influenced by tidal action, time of sampling and sedimentation effect. The water movement of the bay is controlled by semi diurnal tides. During the process of tidal mixing, uranium scavenging occurs due to extensive flooding of the surface sediments. Initially, the particulate authigenic uranium is formed in surface seawater which is rapidly remineralised in deep water leading to change in activity ratio of ^{238}U/^{232}Th in seawater. Primarily, the radionuclides are sorbed onto suspended particulate matter in the seawater column and then settle down in the seabed sediment. The association of thorium with marine particulate matter has been shown to be reversible and in equilibrium with adsorption/desorption processes**.** In general, the mobility of thorium is quite restricted because its transport along streams can occur by the movement of particulate matter in which the thorium is attached.

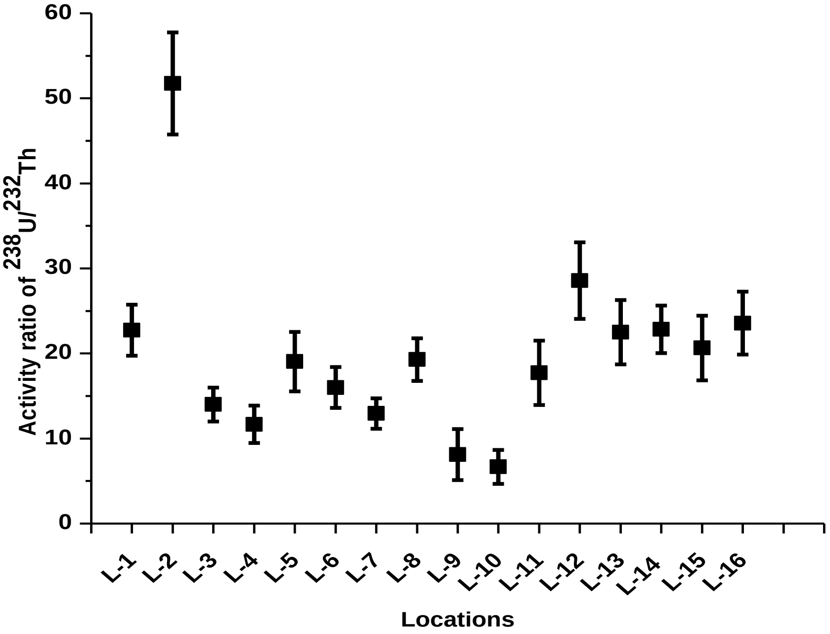

Fig. 3.8: The variation in activity ratio of ^{238}U /^{232}Th in seawater of studied locations of Mumbai Harbour Bay

The activity ratios of $^{238}U/^{232}Th$ in seawater varied within the narrow range throughout the studied area except L-2 location which showed the maximum activity quotient. As the distribution of dissolved uranium in the seawater is generally relatively uniform due to its conservative behavior, the differences in the $^{238}U/^{232}Th$ activity ratios particularly at some locations might be due to releasing of higher activities from nearby discharge locations.

3.3.4. Prediction of chemical speciation of U, Th and Pu in seawater

Under the influence of measured redox conditions and seawater composition, MEDUSA model was used to assess the aqueous speciation of uranium, thorium and plutonium. The dominant aqueous species for especially uranium and plutonium was calculated at 25^0C based on the minimum and maximum concentration of chemical analyses of sea water using Eh- pH diagram as shown in **Fig. 3.9– 3.12.** The speciation of uranium and plutonium was found to be strongly affected by the level of carbonate and chloride in seawater. At uranium concentration below 10^{-9} M in presence of low level of carbonate ($<10^{-5}$ M), hydrolysis species of uranium was found to be the major factor. However, in concentration above 10^{-8} M at $[CO_3^{2-}] > 10^{-4}$ M and $[Cl^-]$ of about 0.5 M, the mixed hydroxo-carbonato complexes including carbonate species were observed to be dominant.

Uranyl carbonate complexes existing as UO_2CO_3, $UO_2(CO_3)_2^{2-}$ and $UO_2(CO_3)_3^{4-}$, in surface seawater are more fully discussed in the literatures. Despite of wide range (10^{-12} - 10^{-9} M) of thorium concentration in sea water, it was found exclusively as the tetravalent species of $Th(OH)_4$ and $ThO_2(c)$ due to its limited solubility. In concentration of $^{239+240}Pu$ above 10^{-14} M, the neutral species of plutonium as plutonyl carbonate (PuO_2CO_3) was the only predominant species. The formation of PuO_2^+ was also observed at low concentration of carbonate and chloride which may be due to its limited solubility by the formation of the insoluble tetravalent species,

$Pu(OH)_4$, (pKsp ~ −56). Generally, in marine system, plutonium is continually being removed from solution by $Pu(OH)_4$ precipitation under redox reactions between Pu(IV), $Pu(V)O_2^+$ and $Pu(VI)O_2^{2+}$ and sorption of the hydrolyzed species to humates, colloids, and mineral surfaces. Thus, in the study area, the chemical species of U, Th and Pu were observed to be associated with either the carbonate or the hydroxide at measured range of pH of seawater. On considering the estimated chemical analyses of seawater, the speciation program of HYDRA, calculated the percentage formation of various chemical species of uranium, thorium and plutonium, accounted for each of 100% of total dissolved uranium (VI), thorium (IV) and Pu (VI) as given in **Table 3.2**.

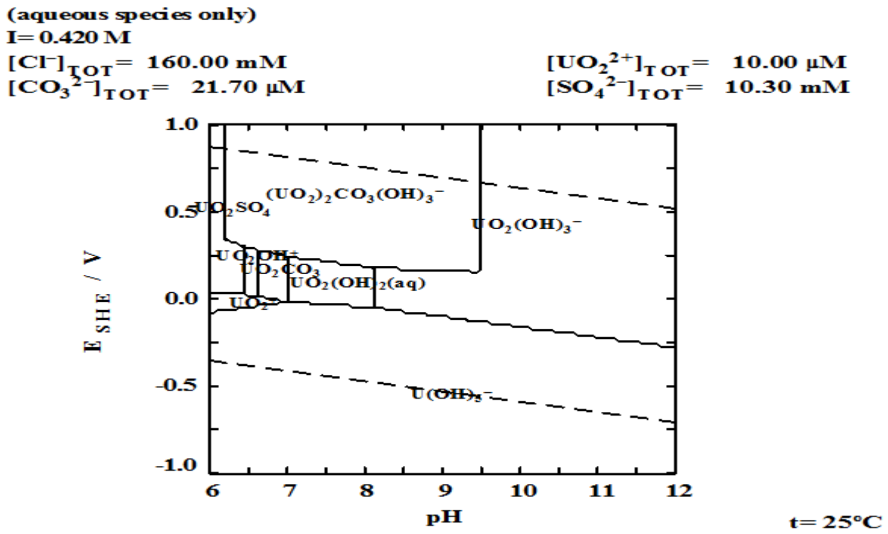

Fig. 3.9: Eh-Ph diagram for the dominant aqueous complexes of uranium in presence of minimum concentration of total dissolved uranium, chloride, carbonate and sulphate

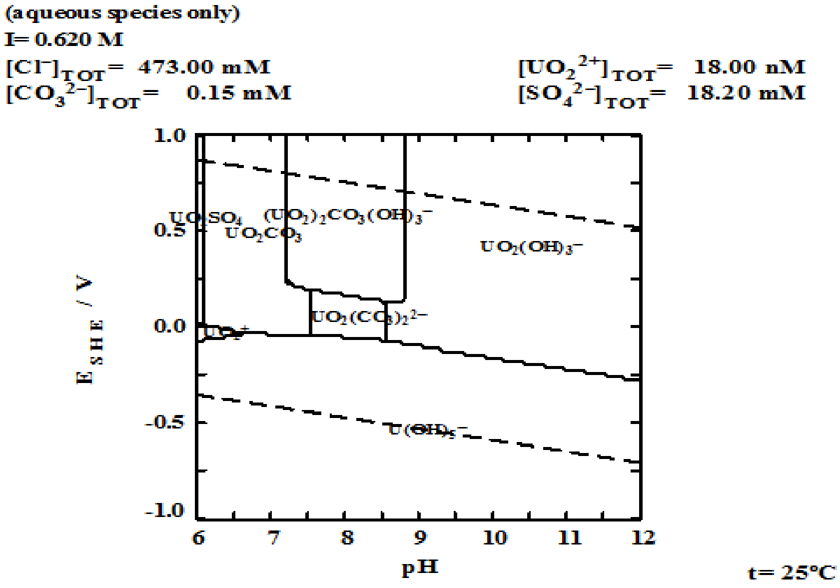

Fig. 3.10: Eh-Ph diagram for the dominant aqueous complexes of uranium in presence of maximum concentration of total dissolved uranium, chloride, carbonate and sulphate

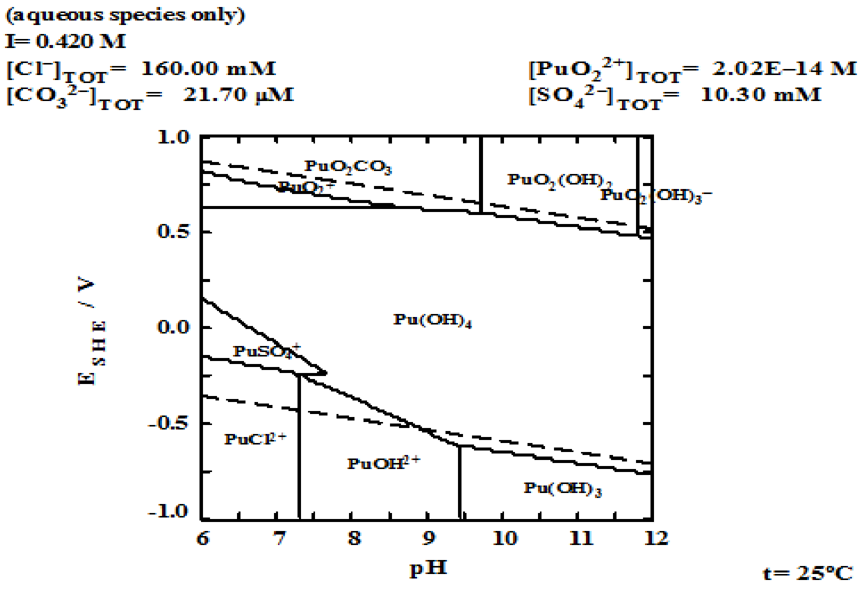

Fig.3.11: Eh-Ph diagram for the dominant aqueous complexes of plutonium in presence of minimum concentration of total dissolved $^{239+240}$Pu, chloride, carbonate and sulphate

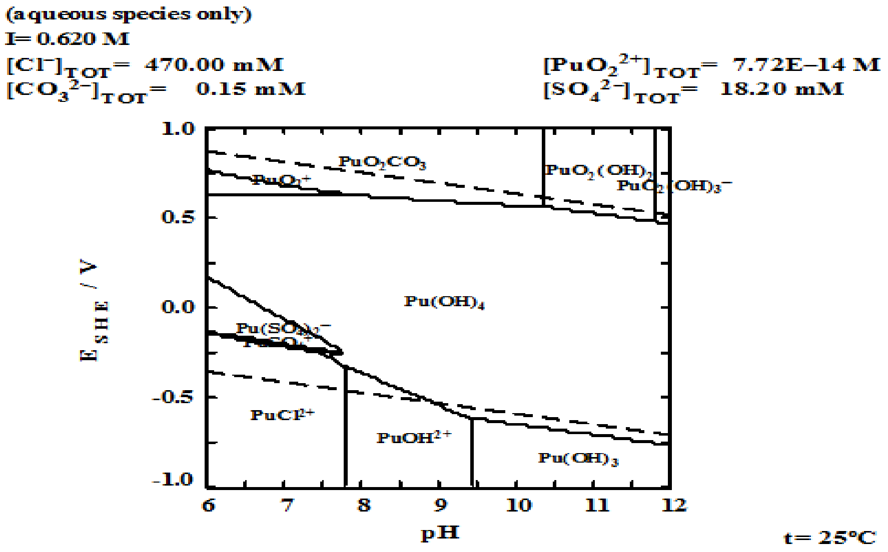

Fig. 3.12: Eh-Ph diagram for the dominant aqueous complexes of plutonium in presence of maximum concentration of total dissolved $^{239+240}$Pu, chloride, carbonate and sulphate

Table 3.2: The percentage formation of uranium, thorium and plutonium species in seawater based on their measured concentration range and other ligands at pH 8 and I = 0.42-0.62 m

Oxidation	Species at pH 8	% formation	% formation
U(VI)	$(UO_2)_2(CO_3)(OH)_3^-$	29 %	51%
	$UO_2(CO_3)_2^{2-}$	-	24%
	UO_2CO_3	4%	10%
	$UO_2(OH)_3^-$	29%	8%
	$UO_2(OH)_2$	35%	7%
	UO_2OH^+	3%	-
Th (IV)	ThO_2 (c)	-	76%
	$Th(OH)_4$	100%	24%
Pu(VI)	PuO_2^+ (Pu-V)	6%	-
	PuO_2CO_3	94%	100%

At measured concentration range of uranium, thorium and plutonium, the percentage formation of chemical species as indicated within parenthesis, being $(UO_2)_2(CO_3)(OH)_3^-$ (29-51%), $UO_2(CO_3)_2^{2-}$ (0-24%), UO_2CO_3 (4-10%), $UO_2(OH)_2$ (7-35%), $UO_2(OH)_3^-$ (8-29%), UO_2OH^+ (0-3%), ThO_2 (0-76%), $Th(OH)_4$ (24 -100%), PuO_2^+ (0-6%) and PuO_2CO_3 (94-100%) calculated at Eh = + 0.75V and pH = 8 in the oxidized seawater. Fig. 3.13 – 3.16 illustrates the speciation diagram for measured concentration range of uranium (VI) and Pu (VI) as a function of pH in oxic seawater.

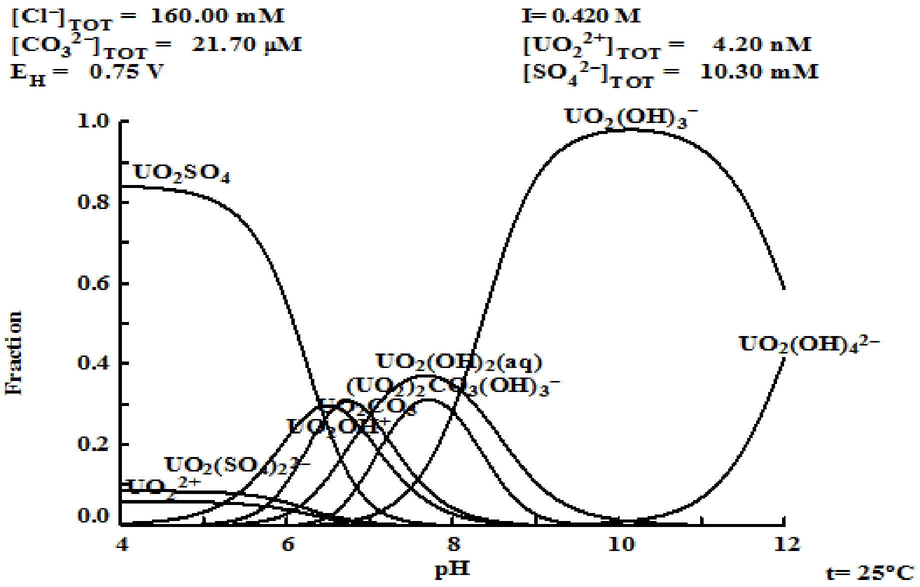

Fig. 3.13: Fraction of U (VI) species as a function of pH in seawater in presence of minimum concentration of total dissolved uranium, chloride, carbonate and sulphate

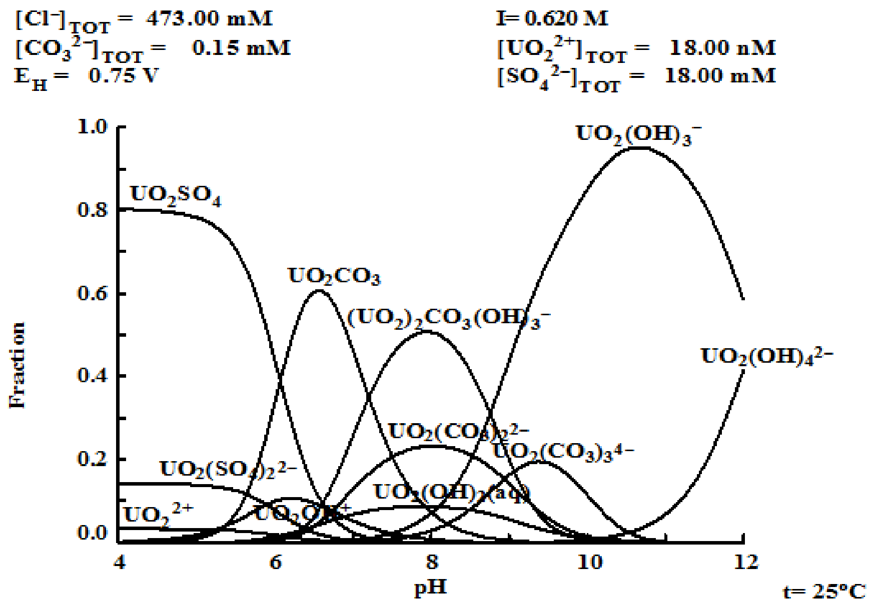

Fig. 3.14: Fraction of U (VI) species as a function of pH in seawater in presence of maximum concentration of total dissolved uranium, chloride, carbonate and sulphate

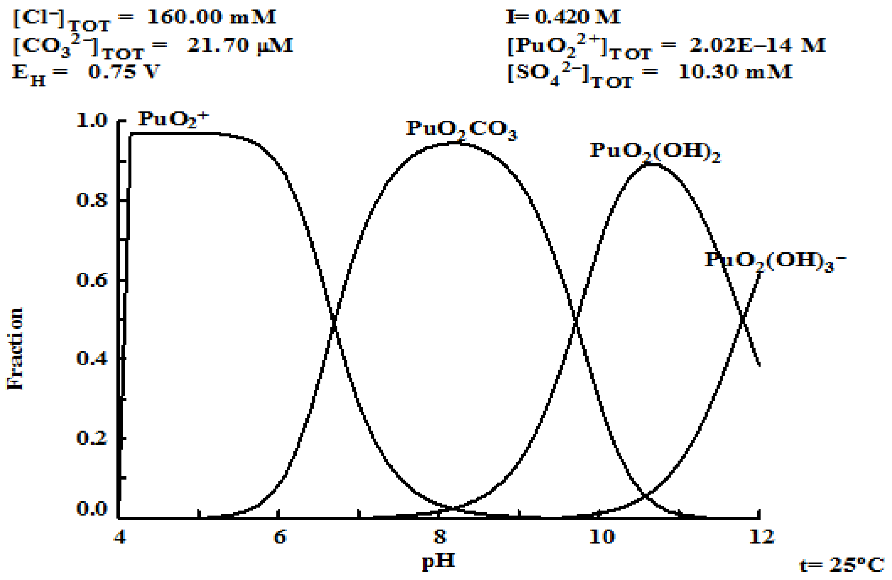

Fig. 3.15: Fraction of Pu (VI) species as a function of pH in seawater in presence of maximum concentration of total dissolved $^{239+240}$Pu, chloride, carbonate and sulphate

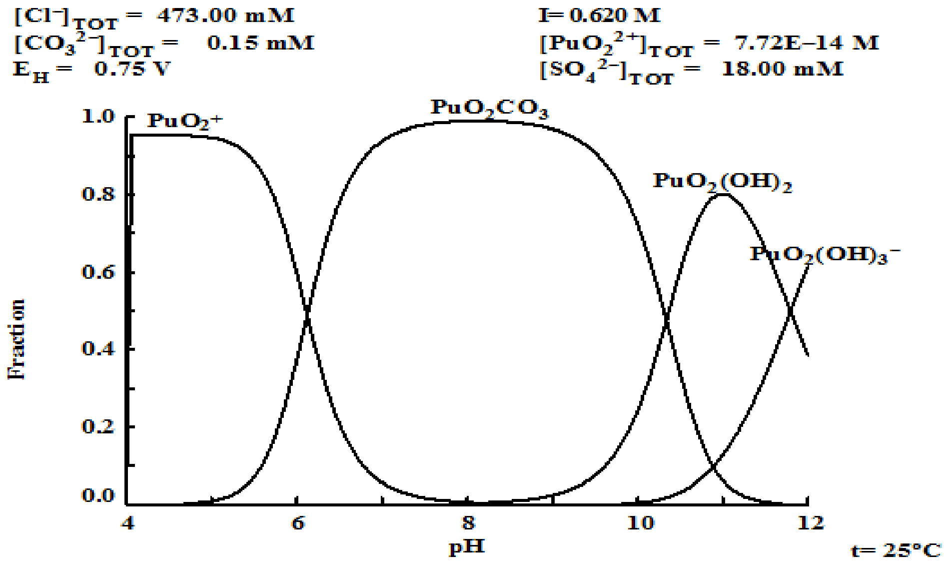

Fig. 3.16: Fraction of Pu (VI) species as a function of pH in seawater in presence of maximum concentration of total dissolved $^{239+240}$Pu, chloride, carbonate and sulphate

3.4. Conclusions

This chapter discussed in detail regarding spatial variation in concentration of U, Th and $^{239+240}$ Pu in MHB along with chemical speciation. The spatial variability in distribution of these radionuclides along the studied regions was found to be a non-uniform. As per stream flow pattern (upstream to downstream direction) , the activity levels of all radionuclides (U, Th and $^{239+240}$Pu) showed a decreasing trend from southern part to northern part of studied area indicates a good dilution and dispersion of low level activity released from effluent treatment plant.

The chemical speciation of actinides in seawater is greatly influenced by the pH, pCO_2, Eh and ligand concentration. The positive range of ORP values indicates that seawater was in oxic environment. The high redox potential of seawater enhances the concentration of dissolved uranium and plutonium due to formation of their soluble carbonate complexes. In sea water, hydrolysis was much more dominant than carbonate complexation reaction for uranium. The formation of predominant species as mixed hydroxocarbonato complexes of uranium may be due to carbonate rich sea waters. Thorium was found exclusively as the tetravalent species which may be due to its limited solubility by the formation of quite insoluble $Th(OH)_4$ species. In case of $^{239+240}Pu$, which is continually being removed from solution by $Pu(OH)_4$ precipitation under redox reactions between Pu(IV), $Pu(V)O_2{}^{+}$ and sorption of the hydrolyzed species to humates, colloids, and mineral surfaces. The speciation of actinides depends on a complex and dynamic set of parameters. Since uranium and thorium are persisted for the time of existence of marine systems, therefore their data on chemical speciation and behavior can be used for predictive models for the long-term behavior of the man-made radionuclides. An accurate characterization of actinide interactions in the oceans requires the expertise of many fields such as chemistry, biology, geochemistry, oceanography, geology etc. Higher values of activity ratio of ^{238}U /^{232}Th in seawater clearly indicate that ^{238}U is relatively more soluble and mobile than ^{232}Th. Alternatively, Th is highly particle reactive, immobile and strongly bound to solid matrix. The wide variation in the activity ratio of ^{238}U /^{232}Th especially in seawater might be influenced by tidal mixing, time of sampling and sedimentation effect. During the process of tidal mixing, uranium scavenging occurs due to extensive flooding of the surface sediment and mobility of thorium is quite restricted due to highly attached with the suspended particulate matters in seawater. The variation in activity levels of thorium along the studied area might be only due to the movement of particulate matter in which the thorium is attached. The significant changes in the $^{238}U/^{232}Th$ activity ratios at some locations might be due to anthropic inputs.

CHAPTER 4

PARTICLE SIZE CHARECTERISATION, MINERALOGY AND THEIR IMPACT ON SPATIAL AND VERTICAL DISTRIBUTION OF ^{238}U, ^{232}Th and $^{239+240}$Pu IN BOTTOM SEDIMENTS

4. 1. Introduction

Radionuclides introduced into the marine surface water either through atmospheric fall-out or discharges of effluents from nuclear installations around the world. Once radionuclide entered into marine environment it is subjected to movement and mixing with tides and current, undergo horizontal dispersion, dilution and get bound to suspended particles by various physical, chemical and biological processes. After a considerable period of time the suspended particles settles down at bottom as sediments which is primarily responsible for the adsorption of radioactivity entering the body of seawater. Thus sediments are complex heterogeneous materials that readily accumulate pollutants from water column and transport them to other parts of the water system. These are considered as major repository of radionuclides released into the water and serve as a main potential source of uptake for water feeding biota [237, 238]. Most radionuclides are sorbed directly to sediments or to other sinking particles within 1–2 years [239]. In freshwater, actinides are tightly bound to the sediment grains, but in saline water, they are bound to the surface of sediment grains readily undergoes ion exchange with other dissolved cations which leads to increase in dissolved actinides in coastal waters [239].

Sediments are complex assemblages of oxides, clay minerals, silts, organic materials and other coatings presenting a variety of surfaces to which metals can sorb [240, 241]. Each of these different surfaces exhibit distinct reactivities and cation sorption which generally follows electrostatic trends: $M^{4+} > M^{3+} > M^{2+} > M^{+}$ [241, 242]. The sorption is generally found to increase as the particle sizes decrease and is influenced by silt load, organic matter content of ambient water and sediments, particle size and clay minerals composition of sediments [243]. Generally, metals are found to be more concentrated in fine-grained sediments than in coarse-grained sediments.

The depth profile study on accumulation of radionuclides in sediments is very important as sediments are the largest reservoir of any pollutants entering into the environment. In general, the uptake of radionuclides by marine sediments is dependent on their physical and chemical properties. The sedimentation rate and the physico-chemical nature of radionuclides are determined by the rate of deposition and accumulation in core sediments. Moreover, it also indicates the temporal variation and the impact of radionuclides released through fallout and discharges from nuclear installations. The distribution of radionuclides within the seabed can provide information on transient and vertical sediment movement, accumulation and global radioactive inventory. The single most important property affecting the characteristic of actinide elements is their oxidation state. Precipitation, complexation, sorption and colloid formation processes depend on the prevailing oxidation state [244]. All four processes contribute to the chemical behavior and environmental transport properties of actinides in the environment.

Uranium and its daughters have been shown to be valuable as geochronometers [245] and paleoceanographic proxies [246]. These studies have suggested that uranium behaves conservatively with the formation of soluble U (VI) carbonate complexes in oxygenated seawater. However under reducing conditions, soluble U (VI) in the overlying seawater can be transformed into insoluble U (IV). This transformation, which can occur in seawater column at the sediment-water interface and within the sediments, resulted in the addition of authigenic uranium to sediments and altered the uranium distribution in the sedimentary records. It is clear that uranium is reactive in some marine environments such as anoxic basins [247] **,** coastal ocean [248], turbidities [249] and pelagic sediments **[14]**. Uranium concentrations may vary depending on the particle size, mineral composition (reflecting regional geology) and the physico-chemistry of the water, particularly for freshwater environments. Substantial U enrichment (up to 100 times) has been reported for sediments sampled from anoxic environments (swamps or deep ocean basins) [251]**.**

Thorium is known as one of the least soluble elements in seawater due to its tendency to hydrolyze and associate with particle surfaces. Indeed, thorium enters the oceans primarily in detrital form derived from continents, although Scott [252] has shown that there is some mobilization of thorium during weathering and soil formation. Owing to the particle reactive nature of thorium, its distribution in solution, suspended particles and sediments as well as the parent/daughter ratios are used extensively to study the rate of sedimentation [253] and mechanism of chemical scavenging in the oceans [254, 255]**.** In Open Ocean, scavenging is usually dominated by biogenic particles and the short-lived ^{228}Th is particularly useful in determining rates of cycling of these particles since its half-life is comparable to the scales of temporal variations in surface ocean processes [256]. The scavenging rates are not constant, however, but increase towards the shore [257, 258]. Thorium is found exclusively as the tetravalent species and its solubility is limited by the formation of quite insoluble $Th(OH)_4$.

Plutonium plays an important role in the extent to which it sorbs to sediments. It can exist in multiple oxidation states with a wide range of cationic charges extending from +1 as the PuO_2^+ moiety to + 4 as the simple tetravalent cation [259] **.** In aqueous solutions with pH and Eh ranges of natural waters, plutonium can be present in four oxidation states: III, IV, V and VI [260]**.** The main part of the dissolved plutonium in natural waters exists in oxidation state Pu(V), while Pu(IV) is present in colloidal form [260] **.** Low pH values promote lower oxidation states while higher oxidation states become more general as the pH increases. Pu(III) is possible in prevailing anoxic conditions, i.e. in lower sediments layers. In most natural aquatic systems, the majority of the Pu is associated with sediments; though trace quantities observed in the water column. The redox equilibria can also coexist between Pu^{4+} in the solid phase as either PuO_2 or $Pu(OH)_4$ or sorbed Pu^{4+} and aqueous forms of PuO_2^+ [261]**.** Literatures have reported that plutonium sorbs more extensively in the (III) and (IV) oxidation states than in the higher V and VI states by several orders of magnitude [262]. In the Baltic Sea, 99% of the total plutonium inventory sorbs onto sediment as Pu(IV) [263] **,** consistent with observations that Pu sorbed onto coastal soils along the Irish Sea exists exclusively as Pu(IV) [264]**.** Because of the strong affinity of $Pu(OH)_4$ for sediments and suspended particulates, Pu(IV) sorption is the limiting factor in Pu transport processes [265] .

The association of Pu with sediment is dependent on particle size: the association favours fine clay or clay-silt particles [266 – 269]. The size of particles can affect 5- 10 fold on the k_d-factor [266, 270, 271]**.** Pu is mainly associated with sesquioxides and undissolved organic complexes such as chelates [272 – 274]**.** The concentrations of Pu in sediments can thus vary according to both the source and the type of bottom, including the sedimentation rate in the area. For instance, in the Baltic Sea, in soft bottom areas, where the sedimentation rate can be more than 20 mmy^{-1}, $^{239,240}Pu$ concentrations were at the highest, about 15 $Bqkg^{-1}$ [275]. However in the Kara Sea area, where the sedimentation rate is usually less than 2 mmy^{-1}, the concentration was typically about 1- 2 $Bqkg^{-1}$ [276, 277]**.** The source in both areas was global fallout, which was slightly smaller in the pole regions.

4.2. Materials and methods

4.2.1. Sediment sampling

A total of 64 bottom (grab) sediment samples were collected at different seawater depths (1m –3 m) from 16 different locations covering an area of about 64 km^2 of Mumbai Harbour Bay. Details of the same were already discussed in **Chapter 2 (Section 2.5.2).** The core sample were sliced into 4 cm each fractions, collected in polyethylene bottles with screw caps and transported to the laboratory and stored at 4^0C till further analysis.

4.2.2. Sample processing

The sediment (grab and core) samples were cleaned by removing any remains of plants, biota and other substances. These samples were dried at 110ºC for 24 h, ground with a mortar and pestle, homogenized and sieved through a 2 mm mesh sieve. For core sediments, two different composite samples were prepared by mixing the same core depth fractions of each of the eight locations. The two composite core samples were categorized into two groups and coded with CCS-1 (L-4 to L-7) and CCS-2 (L-8 to L-11). About 100 - 250 g of both meshed samples were transferred to a pre-weighed cylindrical acrylic container with dimension of 75 mm diameter x 75 mm height ($331cm^3$), sealed and kept for 30 days to allow for growth of radon gas in order to achieve secular equilibrium between ^{226}Ra, ^{214}Pb and ^{214}Bi in the ^{238}U decay chain and between ^{212}Pb, ^{208}Tl and ^{228}Ac in the ^{232}Th decay chain.

4.2.3. Gamma spectroscopy

The activity concentrations of ^{226}Ra, ^{214}Pb and ^{214}Bi in the ^{238}U decay chain and ^{212}Pb, ^{208}Tl and ^{228}Ac in the^{232}Th decay chain in sediments were measured using Gamma spectrometry system based on a co-axial high purity germanium detector (HPGe, 50% relative efficiency) coupled to spectroscopy workstation (integrated assembly of amplifier, high voltage unit and 16 K multichannel analyser) to make it a computerized data acquisition system. **Plate 4.1** depicts the block diagram of schematic arrangement of various components of gamma spectroscopy system (HPGe) with photograph of HPGe including lead shielding

The detector has a resolution (FWHM) of 1.82 keV for the 1332.5 keV γ-ray line of ^{60}Co. The γ -ray spectrometer energy calibration was performed using ^{60}Co, ^{137}Cs and ^{133}Ba disk sources.

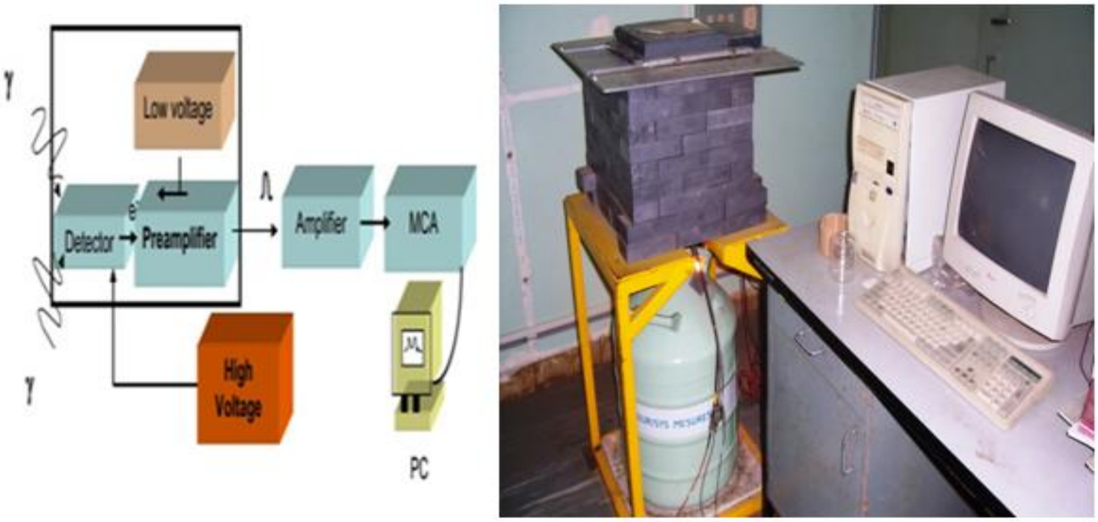

Plate 4.1: The block diagram of schematic arrangement of various components of gamma spectroscopy system (HPGe) with photograph of HPGe including lead shielding

The detector was surrounded by a special heavy lead shield of about 10 cm thickness with inside dimensions 45 cm diameter × 85 cm height. The absolute detection efficiency of the HPGe detector for each γ -ray energy was determined using uranium ore (U_3O_8) standard (UCIL, Jaduguda) with activity concentration of 1154.19 Bq placing in the same identical acrylic container of 331 cm^3 volume and calculated from the well-known formula

$$E\% = \left(\frac{S}{T_1} - \frac{B}{T_2}\right) \mathrm{X} \frac{100}{A} \mathrm{X} \frac{100}{I\%}$$

(Eq. 4.1)

Where, *S* is the count due to sample + background of radionuclide for time of counting T_1 (s), B is count due to background for time of counting T_2 (s), A, the activity of radionuclides (Bq) and I is the absolute intensity of the γ –transition (%).

Finally, the absolute efficiency for unknown radionuclides was determined by plotting the calibration curve between efficiency and each γ -ray energy of uranium ore. The counting time for both activity and background measurements was 80,000 s. The γ -ray transitions used to measure the concentrations of the assigned nuclides are as follows: For ^{232}Th series: 238.39 keV (^{212}Pb), ^{208}Tl (583 keV and 2614 keV), ^{228}Ac (338.5, 463.1 and 911.2 keV), for ^{238}U series: ^{226}Ra (186.1 keV), ^{214}Pb (295.1 and 352 keV) and ^{214}Bi (934, 609 and 1120.3 keV). If there is more than one photo peak of γ energy for a nuclide, then the average of peak activities were taken into account. **Fig. 4.1** shows the typical γ-ray spectrum for measurement of gamma emitting radionuclides in ^{238}U and ^{232}Th decay series of representative sediment sample. Based on the measured gamma-ray photo peaks area of particular radionuclides, the activity concentrations in samples were determined. Calculations relied on attaining the secular equilibrium in the samples, due to the much smaller lifetime of daughter radionuclides in the decay series of ^{232}Th and ^{238}U. More specifically, the ^{232}Th concentration was determined from the average concentrations of ^{212}Pb and ^{228}Ac in the samples and that of ^{238}U was determined from the average concentrations of the ^{214}Pb and ^{214}Bi decay products. Thus, an accurate measurement of ^{232}Th and ^{238}U radiological concentrations was made. Prior to the samples measurement, the environmental background at the laboratory site was determined with an empty cylindrical acrylic container under identical measurement conditions. Background spectral intensities were later subtracted to correct the net γ -ray peak areas for the studied isotopes. Uncertainties of all measurements have been taken into account and are presented at the 68.73% confidence level (1σ).

4.2.4. Sediment digestion and alpha spectroscopy

0.2 g of powdered and dried samples were placed in PTFE (Poly Tetra Fluoro ethylene) digestion vessels with desired amount of HNO_3 (MERCK, 65%), HF (MERCK, 48%) and hydrogen peroxide (H_2O_2) and ^{242}Pu tracer. After that samples were completely destructed in a closed microwave digestion system (Milestone Srl, Model Ethos 1, Italy). The resulting solution after centrifuged was transferred to glass beaker and diluted up to 100 mL with deionised water. 0.5g hydroxylamine hydrochloride ($NH_2OH.HCl$) was added and the sample was heated at 80^0 C. 100mg Bi carrier and 10 mL H_3PO_4 were added to get the precipitate of $BiPO_4$. The precipitate was centrifuged, dissolved in 1ml 6N HCl +10 ml 0.2 HCl (normality = 0.75 N) and passed through in preconditioned cation exchange resin (Dowex-50X8, 100-200 mesh) with 0.75 N HCl. Washed the column with 0.75 N HCl. Eluted Pu and Th with 8NHCl. The eluent was evaporated to dryness and converted to nitrate by evaporating with concentrated HNO_3. The residue was dissolved in 8N HNO_3 and 0.5g $NaNO_2$ was added to oxidize Pu^{3+} to Pu^{4+}. This was loaded on a preconditioned anion exchange resin (Dowex-1X8) with 8N HNO_3. Washed the column with 8N HNO_3 and discarded the effluent. Pu was eluted with 1.5M $NH_2OH.HCl$. The eluent was evaporated and residue destroyed with concentrated HNO_3. Finally Pu was electroplated and estimated by alpha spectrometry with 12% efficiency, 20 keV resolutions and 300 mm^2 areas with a depletion depth of 100 mm [278]. Chemical yields using a ^{242}Pu tracer ranged from 70 to 80%. The typical spectrum of $^{239+240}$Pu in alpha spectrometry system is shown in **Fig. 4.2.**

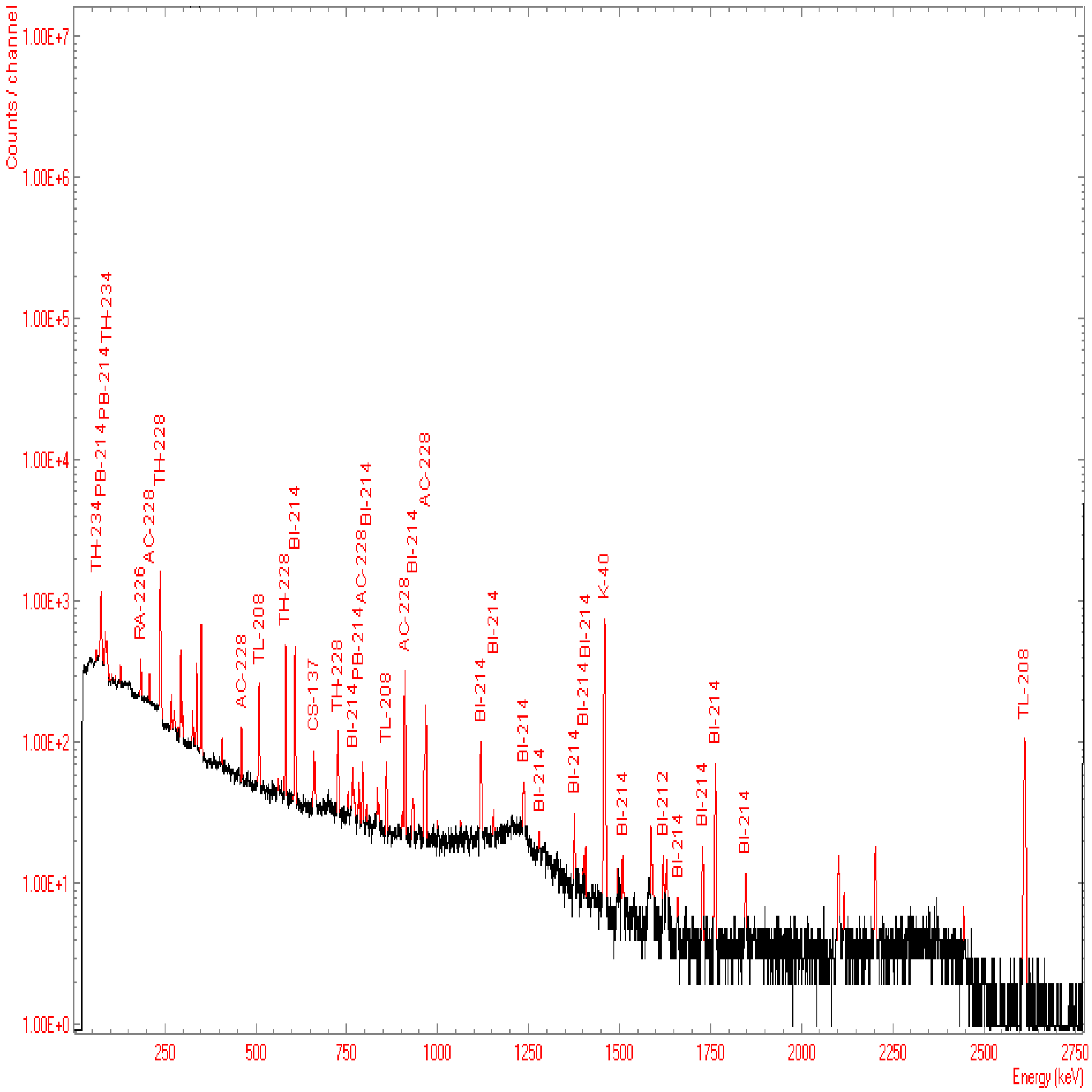

Fig. 4.1: The typical γ-ray spectrum for measurement of gamma emitting radionuclides in ^{238}U and ^{232}Th decay series of representative sediment sample

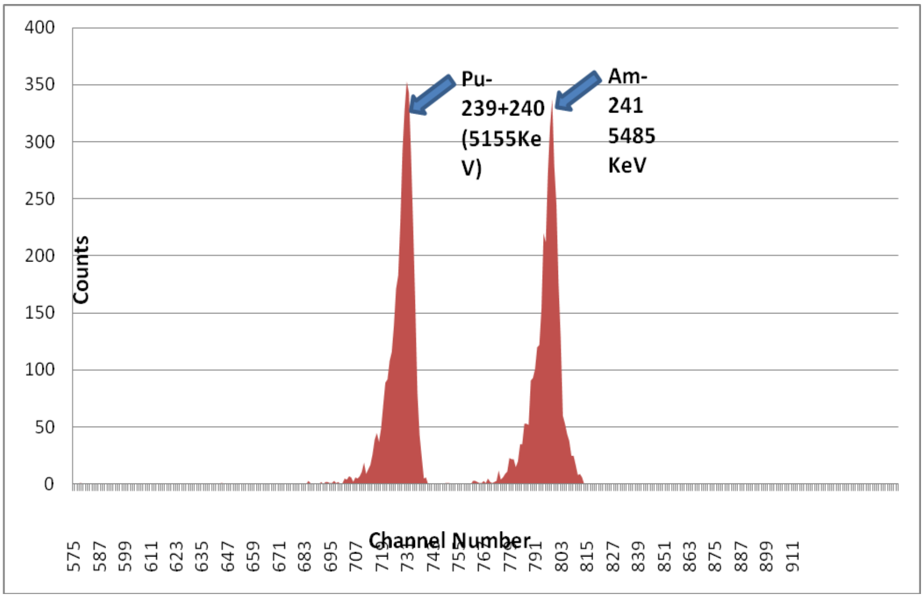

Fig. 4.2: The typical alpha spectrum of mixed standard source of $^{239+240}$Pu and ^{241}Am

4.2.5. Determination of bulk density and porosity

The bulk density and porosity of sediments was calculated from natural moisture content and grain specific gravity values using equations of soil mechanics as given below.

$$\rho_b = \frac{W_s}{V_s} \qquad \textbf{(Eq. 4.2)}$$

$$\varphi = \left[1 - \frac{\rho_b}{\rho_p}\right] \qquad \textbf{(Eq. 4.3)}$$

Where, W_s, V_s, ρ_b, ρ_p and φ are weight, volume, bulk density, particle density and porosity of sediment respectively. The value ρ_p is taken as ratio of mass of dry sediment and volume of sediment particles only (air removed).

4.2.6. Determination of total carbon (TC)

The total carbon in the sediments was estimated using C H N S-O elemental analyser (Flash EA 1112 Series, Thermo Finnigan, Italy) as depicted in **plate 4.2**. About 1.2 mg of dried sediment was tightly wrapped in an already weighed tin container, put into an auto sampler and dropped into the combustion reactor. Sn (tin), in contact with an extremely oxidizing environment, triggers a strong exothermic reaction and temperature reaches approximately 1800^{0}C. Then the gas mixtures (N_2, CO_2, H_2O and SO_2) are allowed to flow into the gas chromatographic column where separation occurs. The eluted gases are conveyed to Thermal Conductivity Detector (TCD) which provides the percentage of C, H, N and S in the sample. The elemental analyser was calibrated using BBOT Standard {2, 5-bis (5-tert-butyl-benzoxazol-2-yl)-thiopen, $C_{26}H_{26}N_2O_2S$, Thermo Finnigan, Italy)}.The minimum detection limit for C was calculated to be 0.08%.

4.2.7. Particle size characterization of sediments

The particle size distribution of sediment samples was determined using a laser diffraction particle size analyzer (CILAS, France, Model 1190) as shown in **plate 4.3**. For analysis of sediment texture, 3 different laser diffraction methods identified as LDM 1, LDM 2 and LDM 3 were considered. In LDM 1, the sediment sample is thoroughly mixed before analysis. In LDM 2, the sand fraction is sieved out and analyzed separately from the silt-clay fraction. LDM 3 is similar to LDM 2 except that the silt-clay fraction is diluted so that a large sample volume can be used while maintaining an acceptable level of obscuration. LDM 2 and LDM 3 improve the particle size distribution (PSD) in comparison to LDM 1, without the need of altering the Mie theory parameters. Finally, the PSD of the silt-clay and sand were quantified in terms of percent (%) based on the relative weight of each fraction. PSD was performed with a small-angle light scattering apparatus equipped with a low-power (2 mW) Helium-Neon laser with a wavelength of 633 nm as the light source. The apparatus has active beam length of 2.4 mm, and it operates in the range 0.04 to 2500 µm. The obscuration levels of samples in the laser diffractometry analysis were kept between 15% and 25%. Maintaining this obscuration levels in sediments with high clay contents (>20%) compelled to use small volumes because of the high optical density of clay. A 2 g aliquot of the dried sample was introduced into the ultrasonic bath. Finally, the particle size distribution was obtained using two optical models, the Fraunhofer diffraction model and the Mie theory. Because the Fraunhofer model is not accurate enough for the determination of the clay - size fraction. The Mie theory applies rigorously to spherical, homogeneous particles and fits less satisfactorily nonspherical or non homogeous particles as commonly found in sediments.

Plate 4.2: The schematic photo of the C H N S-O elemental analyser (Flash EA 1112 Series, Thermo Finnigan, Italy)

4.2.8. Identification and quantification of minerals

The various minerals present in the sediments were identified and quantified by the X-ray diffraction (XRD, Model: GNR, Italy) as shown in **plate 4.4**. The XRD data were collected on an

APD-2000 diffractometer equipped with a 6-position sample holder, theta-theta goniometer, and a NaI (Tl) scintillation detector. A Ni-filtered CuK$_{\alpha}$ radiation at applied voltage of 40 kV and

Plate 4.3: A photograph of a laser diffraction particle size analyzer during keeping the sample on ultrasonic bath with stirrer (CILAS, France, Model 1190)

Plate 4.4: A photograph of X-ray diffractrometer during keeping the sample on holder and taking the diffraction pattern (XRD, Model: GNR, Italy)

current of 30 mA was used. Based on five replicate analyses, counting 2 s per 0.04° 2θ step was found to produce reproducible diffraction data for non-clay minerals in a reasonable registration time. Better statistics are needed for clay mineral quantification because the diagnostic reflections are weaker and broader than are those of non-clay minerals. The goniometer settings for quantitative analysis were as follows: 1° divergent slit, 1° anti-scatter slit and 0.2 mm receiving slit. For phase identification, Search & Match procedure was performed by using GNR's SAX software with ICDD Reference Database.

4.3. Results and discussions

4.3.1. Spatial concentration profile

4.3.1.1. Activity levels of ^{238}U, ^{232}Th and $^{239+240}$Pu

Figs. 4.3 – 4.5 illustrate the spatial mean concentration profile of ^{238}U, ^{232}Th and $^{239+240}$Pu activity levels in grab sediments of MHB respectively. The activity concentrations of ^{238}U, ^{232}Th and $^{239+240}$Pu in grab sediments of all locations ranged from 8.5 to 14 Bq kg^{-1}, dry (mean:11.5 ± 1.7 Bq kg^{-1}, dry), 21.5 to 61.2 Bq kg^{-1}, dry (mean: 40 ± 11.4 Bq kg^{-1}, dry) and 0.16 to 1.5 Bq kg^{-1}, dry (mean: 0.7 ± 0.4 Bq kg^{-1}, dry). The activity levels of ^{238}U and ^{232}Th in sediment of Indian rivers reported to be ranged from 34.1 to 196.7 Bq kg^{-1} and 4.6 to142 Bq kg^{-1} respectively [279]. Uranium concentrations in aquatic sediments typically range from 0.5 to 5 mg kg^{-1}, with an average of 3 mg kg^{-1} [280 – 282]. In addition, the observed values can be compared with some of the reported values in different parts of the world. The ranges of activities observed for ^{238}U and ^{232}Th were 2.71-13.42 Bqkg^{-1} and 3.62-18.73 Bqkg^{-1} from Port Sudan and 3.87 - 24.79 Bqkg^{-1} and 1.13-10.04 Bqkg^{-1}, dry weight from Sawakin, respectively [283]. In sandy sediments of the Irish Sea, ^{238}U and ^{232}Th activity concentrations ranged as 1.8 - 6.5 Bqkg^{-1} and 4.1 - 12.1 Bqkg^{-1} dry weight [284]. 2.6 - 24.2 Bqkg^{-1} (^{232}Th) and 3.6- 32.3 Bqkg^{-1} (^{238}U) for coastal sediments found in the United Kingdom [285] and 3 - 11 Bqkg^{-1} for ^{238}U in sediments of the North Sea [286]. Sediments of coastal zone of southern Scotland showed $^{239+240}$Pu concentration of 2 to 58 Bqkg^{-1} due to Wind scale discharges [287]. Ribble estuary, Barents sea and Petshora sea showed < 4 to 259 Bqkg^{-1}, 0.5 to 3.2 Bqkg^{-1} and 0.27 to 4.3 Bqkg^{-1} respectively [288]. The $^{239+240}$Pu concentration in sediments due to effluent discharges ranged from 0.02 to 2.8 Bqkg^{-1} in Japan [289] Meditarian coastal sediments showed Pu concentrations of 0.025 – 0.1 Bqkg^{-1}, dry due to fall out [287].

The variability of activity concentration of ^{238}U in terms of coefficient of variation (CV) along the studied areas has been found to be within narrow limits of 15.6% indicating that there is an almost uniform distribution throughout the studied area. On the other hand, ^{232}Th and $^{239+240}$Pu showed a wide dispersion with CV of 28.5% and 63% respectively indicates a non-homogeneous distribution. On the other hand, in general, the activity levels of ^{232}Th were observed to be relatively higher at sampling locations from L-3 to L-6, whereas $^{239+\ 240}$Pu activities showed from L-3 to L-9.

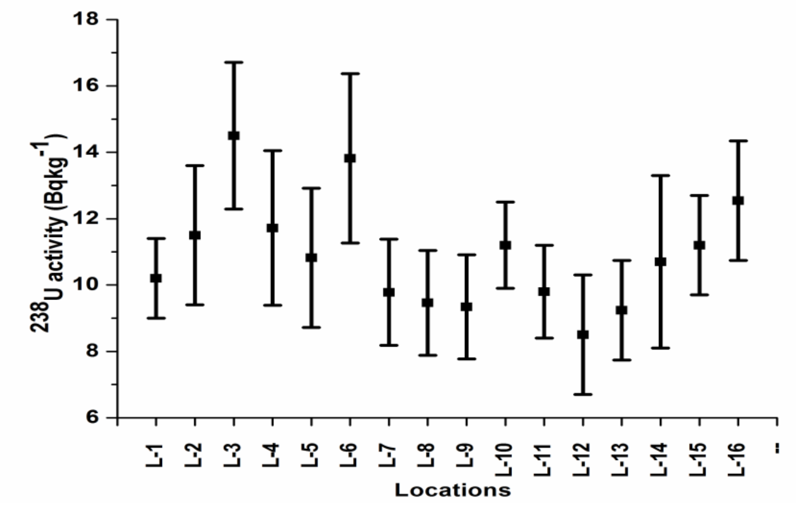

Fig. 4.3: Spatial distribution of ^{238}U in grab sediments

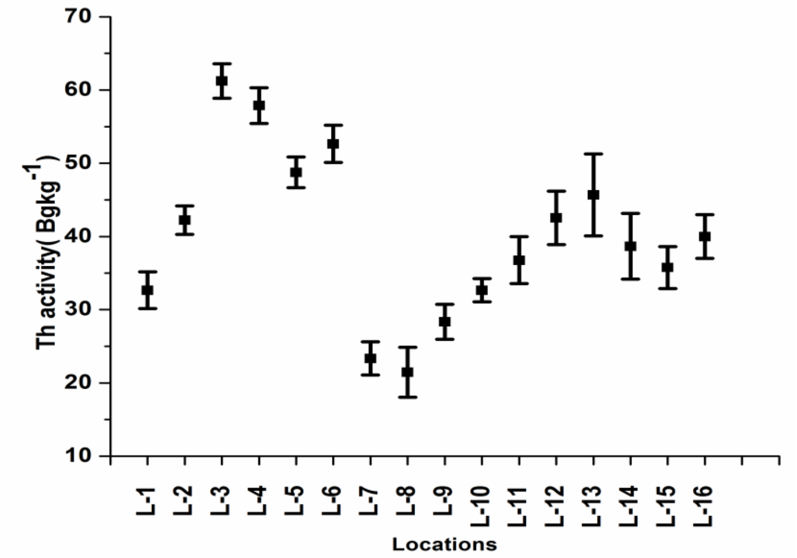

Fig. 4.4: Spatial distribution of ^{232}Th in grab sediments

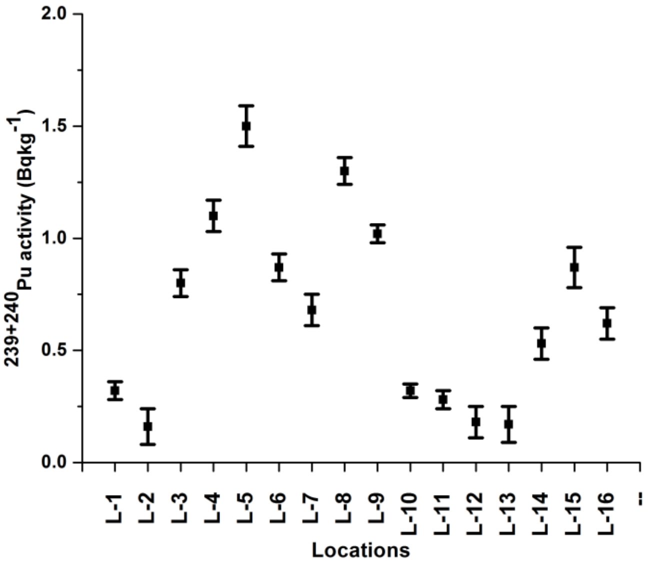

Fig. 4.5: Spatial distribution of $^{239+240}$Pu in grab sediments

This clearly indicates that radionuclides might have accumulated in sediments through siltation/sedimentation from nearby discharge locations. In the past, there were no centralized facilities for discharging the liquid wastes generated from various nuclear facilities at Trombay.

The liquid effluents were directly discharged to the shore near the plants. That is why, the maximum activity levels of ^{232}Th and $^{239+240}$Pu observed at L-3 and L-5. Moreover, the elevated levels of radionuclides could be also very much influenced by the sedimentation rate/ sediment accumulation rate **(**details of same are discussed in Chapter 7**)** which was found to be relatively higher at close proximity of discharge locations than far away locations. In literatures, it is reported that $^{239+240}$Pu concentrations in the Baltic Sea increases as sedimentation rate increases [275 – 277]**.**

The decreasing trend in activity levels of radionuclides from south to north direction indicates a good circulation and movement of water in the bay. Furthermore, due to tidal action, the top layers activity of radionuclides in bottom sediments might be probably transported towards north leading to a good dilution and dispersion.

4.3.1.2. Activity ratio of ^{238}U/^{232}Th

The activity quotient of ^{238}U /^{232}Th in grab sediments along the studied area ranged from 0.2 to 0.4 (mean: 0.3 ± 0.07). These values were comparable with those from coastal sediments of other oceans in the world. The activity quotient of ^{238}U/^{232}Th in Port of Sudan harbor sediments reported to be ranged from 0.22-2.5 with an average value of 0.42 ± 0.20 whereas in Sawakin harbour sediments, the quotient was from 0.42 – 14.28 with an average value of 1.35 ± 1.58 [283, 285]**.** The sediments from Sawakin exhibited activity ratios more than unity whereas in Port Sudan, reverse is true. This opposite trend with respect to ^{238}U /^{232}Th activity quotients probably reflects a variation in the physicochemical composition [290]**. Keating et al. (1996)** reported that the higher activity quotient of ^{238}U /^{232}Th in the sediments of Whitehaven harbor was found due to the highest percentage of silt fraction [291]**.** It is also well known that many radionuclides, in common with stable metals, are concentrated in the finer-grained sediments due to large surface area and mineralogical effects [270]**.** Since ^{232}Th is essentially detrital, the relatively high activity ratios of ^{238}U /^{232}Th might be probably due to the re-mineralization of particulate authigenic uranium. Anderson showed that re-mineralization of uranium fixed to the organic matter in surface sea water is possible except in areas of high organic carbon flux [292] **[56].** In the streambed sediments of the River Nile in Egypt, the activity ratio of U/Th was reported to be ranged from 0.12 to 0.82 with the mean value of 0.31 [293]**.**

Fig. 4.6 depicts the spatial variation in activity ratio of ^{238}U /^{232}Th in grab sediments of studied area. The present study showed the activity ratio of ^{238}U /^{232}Th in grab sediments as much below unity indicating that uranium is more soluble and hence mobile than thorium. Moreover, this can also be attributed to the fact that, in addition to the greater abundance of thorium in the earth's crust; thorium is also a particularly insoluble element in natural waters and usually found associated with solid matrix. Due to particle reactive nature of Th, its concentration in sediments is a function of sedimentation rate which are known to be two to three orders of magnitude higher in coastal regions than in the open sea. A value lesser than unity for ^{238}U/ ^{232}Th ratio, is a feature suggesting high sedimentation rate relative to normal pelagic sediments which generally do not represent a significant sink for uranium.

It is observed that there is no significant variation in activity ratios of ^{238}U/^{232}Th in grab sediments as seen by the almost uniform values throughout the studied locations except locations L-7 and L-8. As the distribution of ^{238}U in the grab sediments seems to be almost homogeneous, the elevated values in the ^{238}U/^{232}Th activity ratios particularly at L-7 and L-8 might be due to drastic fall in ^{232}Th activities at these locations. This might be attributed to the constant flushing activity by tides along with the impact of waves or due to intensive fishing and ferry services using the mechanized boat.

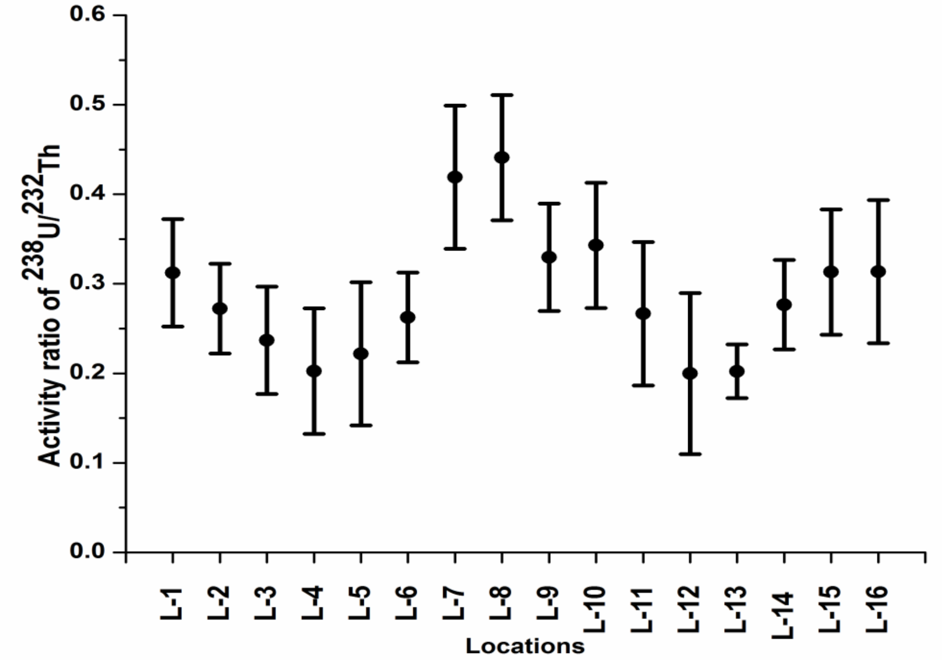

Fig. 4.6: The spatial variation in activity ratio of ^{238}U /^{232}Th in grab sediments

4.3.1.3. Impact of particle size on spatial concentration profile of ^{238}U, ^{232}Th and $^{239+240}Pu$

Sediment particles are generally classified as sand (>63 µm), silt (>2-<63 µm) and clay (<2 µm). However, the particle size ranges are considered differently by many investigators. **Table 4.1** shows the particle size distribution in terms of percentage of sand, silt and clay in grab sediments of studied area. The sand, silt and clay in the studied regions ranged from ND-7%, 76.53-85.69% (Mean: 80.19 ± 2.60 %) and 14.31-22.6% (Mean: 18.29 ± 3.05%) respectively.

In general, the sediments were mainly composed of silt and clay indicating that the resuspension of fine sediments in the harbor bay region might have occurred due to monsoonal activities. The lack of substantial fresh water input and the elongate shape of the bay are also responsible for the high silt and clay content [254]**.** The mean diameter of particle size of bed sediment ranged from 7 to 12.34 µm along the studied area. **Fig. 4.7** shows the analytical results of minimum and maximum value of mean particle size diameter for bed sediment.

Table 4.1: Particle size distribution of the bottom sediments of studied locations

(ND indicates as not detected)

Sampling Locations Code	Sand (%) > 63 µm	Silt (%) > 2 – < 63 µm	Clay (%) < 2 µm
L-1	ND	85.69	14.31
L-2	ND	84.90	15.10
L-3	1.6	81.60	16.80
L-4	ND	78.69	21.31
L-5	ND	78.80	21.20
L-6	ND	79.35	20.65
L-7	ND	77.77	22.23
L-8	ND	77.40	22.60
L-9	7	78.00	15.00
L-10	ND	80.16	19.84
L-11	2.5	81.98	15.52
L-12	3.8	79.82	16.38
L-13	6.5	78.85	14.63
L-14	1.6	76.53	21.87
L-15	ND	81.25	18.75
L-16	1.2	82.27	16.53

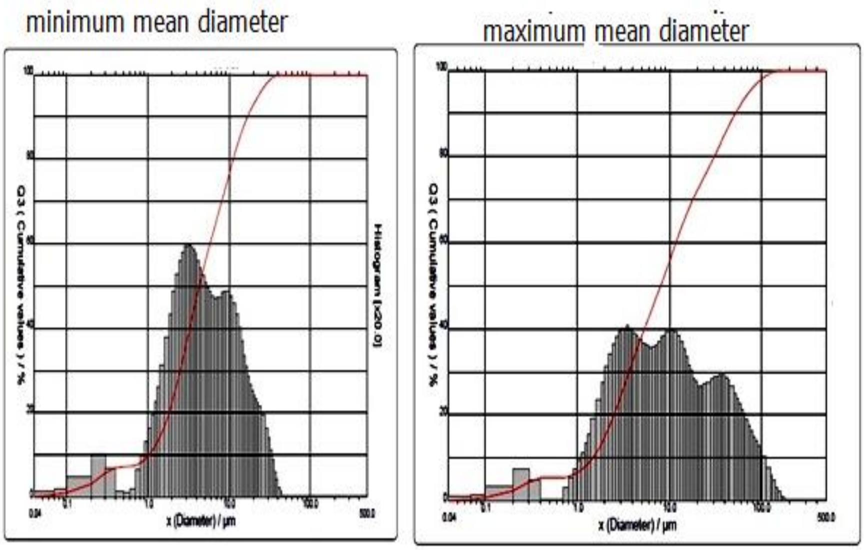

Fig. 4.7: Results of minimum and maximum value of mean particle size diameter for bed sediment using laser diffraction particle size analyzer

Grab sediments in most of locations were mostly free from sand. Only in few locations such as L-9, L-11, L-12 and L-13, sediments were relatively higher abundant with sand sized particles. Though the spatial variability in silt and clay content were within the narrow range (almost uniform) of 3 to 17 %, the activity levels of ^{232}Th and $^{239+240}$Pu varied greatly except ^{238}U throughout the studied area. The activity ratio of maximum to minimum for ^{232}Th and $^{239+240}$Pu was found to be about 3 and 10 whereas for ^{238}U, the ratio was 1.6. The inter-relationship between ^{238}U, ^{232}Th and $^{239+240}$Pu and their correlation with the composition of silt and clay in grab sediments was established using Karl Pearson's correlation coefficient analysis as summarized in **Table 4.2**. $^{239+240}$Pu showed a positive linear relationship (r = + 0.60) with clay fractions while in case of silt, negative correlation (r = - 0.48) obtained indicating that Pu activity is mainly controlled by clay particles during transport. The positive correlation with clays indicates that readionuclides might be mainly concentrated in the fine-grained size fractions of sediments [294, 295] because clay minerals are considered to be the main carriers for radionuclides during mobilizing and diffusing [296]**.** In general, radionuclides have the higher tendency to accumulate in the finest fraction of sediments than the medium-sized and coarse particles.

Table 4.2: Correlation coefficient matrix of U, Th and $^{239 + 240}$Pu with silt and clay in grab sediments (at 5% significant levels)

	Pu	U	Th	silt
U	0.20			
Th	0.10	**0.64**		
silt	**-0.48**	0.25	0.12	
clay	**0.60**	0.13	-0.10	**-0.67**

The strong association of Pu with clay particles might be due to large surface area available for exchange with other metal ions. Generally, it is observed that as particle size decreases, concentration of metal ions increases. In fact, ^{232}Th is also a particle reactive and has a high tendency to fix in the crystal lattice of clay minerals. But in the present study, ^{232}Th showed a very poor degree of positive correlation with silt and negative correlation with clays. This indicates that Th appears to be more attached in medium-sized fractions rather than finer- sized fractions. This may be attributed to agglomeration of smaller- sized particles into larger-sized ones in the sediment. It is also expected that the original particles may not be able to exist as such because of high ionic strength and electrolytes of the medium. On the other hand, ^{238}U showed a positive correlation with both silt and clay fractions indicating that U behaved identical behavior in sorption process onto them. Moreover, silt showed a negative correlation ($r = -0.67$) with clay indicating that their content in sediments are complementary to each other. Also, it can be accomplished that silt particles are not formed by the agglomeration of the clay - sized particles.

4.3.2. Vertical concentration profile

4.3.2.1. Porosity and bulk density

In core CCS-1, bulk density in various depth fractions ranged from 1.49 to 1.81 gcm^{-3} with the mean value of 1.61 ± 0.06 gcm^{-3} (CV : 3.7%), while in the case of CCS-2, the range was from 1.38 to 1.56 gcm^{-3} with mean value of 1.46 ± 0.10 gcm^{-3} (CV: 6.8%). Similarly, the porosity in CCS-1 and CCS-2 was found to be in the range of 31 - 43.4% with mean of 38.7 ± 3.6 % (CV: 9.3%) and 40.4 – 47.4 % with mean value of 44 ± 2.3 % (CV: 5.3%) respectively. The bulk density in CCS-1 was relatively more than in CCS-2 whereas porosity was relatively lesser indicating that lower the bulk density of core depth fractions, higher the fractional porosity. Overall, the means of bulk density and porosity between the both cores was found to be statistically insignificant different. The variability in bulk density and porosity was almost uniform as seen by low CV (< 5 %) from top to middle layers. However, the bottom layers (last 3-4 core fractions) showed a corresponding opposite increasing or decreasing trends as depicted in **Fig. 4.8** and **Fig. 4.9** respectively.

Overall, the bulk density in both cores increases as depth increases while porosity decreases with increasing in depth. The elevated bulk density and subsequently lesser values of porosity at lower layers might be due to sediment consolidation or compaction by the weight (overburden pressure) of upper sediment layers.

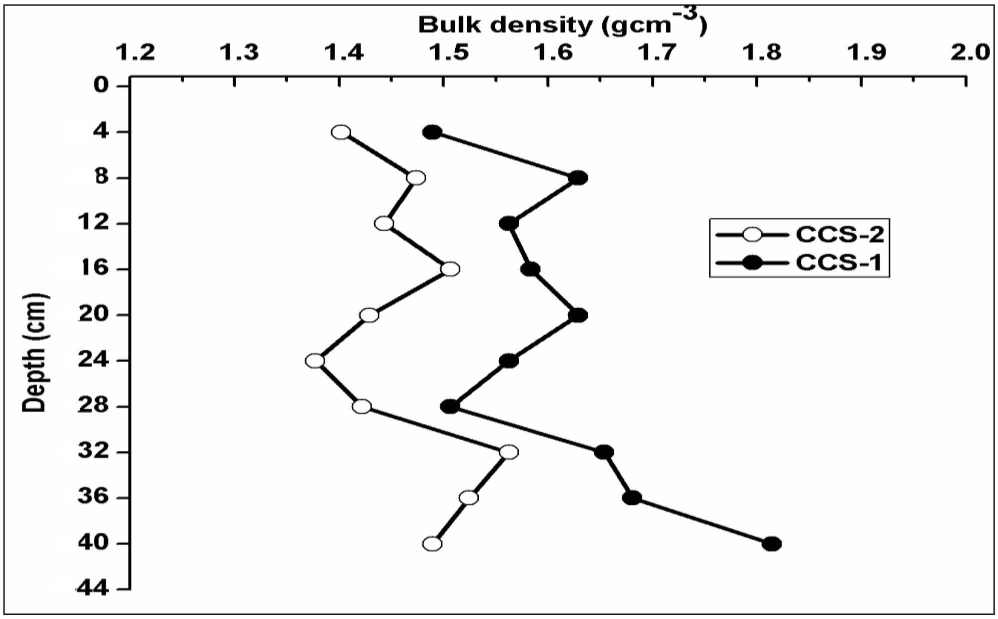

Fig. 4.8: Bulk density of sediments as a function of depth in cores CCS-1 and CCS-2

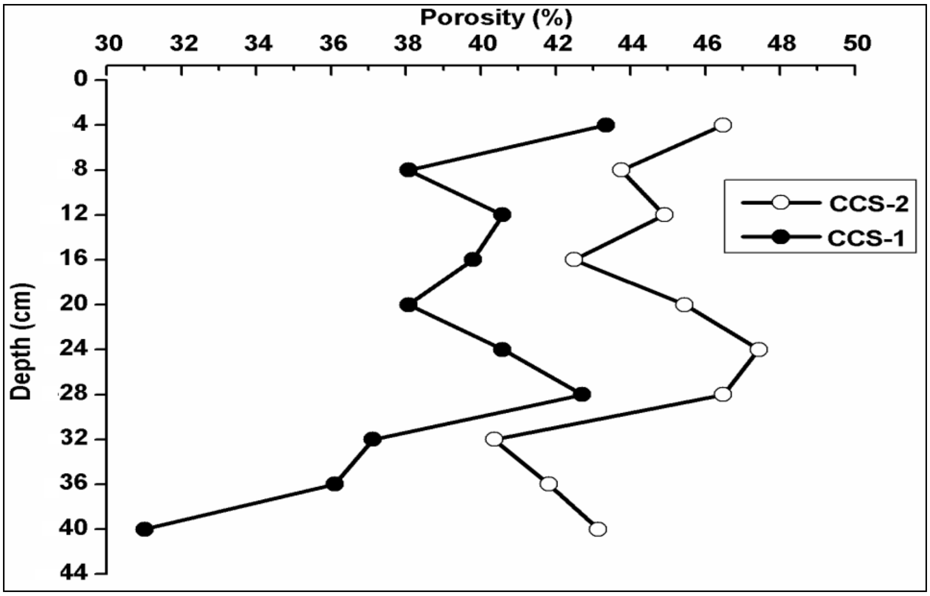

Fig. 4.9: Porosity of sediments as a function of depth in cores CCS-1 and CCS-2

4.3.2.2. Total carbon (TC)

The TC contents of marine sediments reflect processes such as rates of sedimentation and environmental aspects of deposition. Also, as the inner part of the MHB is small and narrow, the waste water drainage from nearby industries and agricultural activities results in relatively high accumulation of external organic matter. The variation in contents of total carbon (TC) as a function of depth for the cores CCS-1 and CCS-2 are given in **Fig. 4.10.** The mean content of the TC in CCS-1 was found to be 1.62 ± 0.4 % whereas in CCS-2, the mean value as 2.41 ± 0.4 %. As can be seen from the figure, the TC in CCS-1 was found to be relatively lower than in core CCS-2. In CCS-1, the carbon content was the highest (2.2%) at top layers and the lowest (0.9%) at bottom layers whereas in CCS-2, the highest (3%) was at 24 cm and lowest (1.8%) at 32 cm depth, In general, the content of TC decreases as core depth increases in both cores. Like porosity and bulk density, TC in bottom layers (last 3-4 core fractions) of both cores was also found to exhibit corresponding opposite trends.

The elevated content of TC at upper layers of cores presumably represents greater input of eroded material from the surrounding land as well as discharge of domestic and industrial wastes. On the other hand, the elevated level of TC observed at the middle layers of cores, might be resulted from rapid sediment deposition due to greater input of eroded material from the surrounding land which in turn protects the buried organic material from contact with the main oxidizing agents found in the overlying seawater such as oxygen, nitrate and sulfate [297]. As a result of rapid deposition, the organic materials are quickly moved below the more diagenetically active zone, thus suffering less degradation.

4.3.2.3. Activity levels of ^{238}U, ^{232}Th and $^{239+240}$Pu

In CCS-1, the activity levels of ^{238}U and ^{232}Th (**see Fig. 4.11)** and $^{239+240}$Pu **(see Fig. 4.12)** ranged from 5.64 to 16.8 Bqkg^{-1} (dry), 25.78 to 56.55 Bqkg^{-1} (dry) and 0.42 to 2.7 Bqkg^{-1} (dry) with averaging being 11.45 ± 3.11 Bqkg^{-1}, 41.45 ± 9.51 Bqkg^{-1}, and 1.12 ± 0.8 Bqkg^{-1} (dry) respectively. Similarly, for CCS-2, the activity levels for the same were found to be in the range of 2.66 - 5.66 Bqkg^{-1} (dry), 22.33 – 52 Bqkg^{-1} (dry) and 0.17 – 4.22 Bqkg^{-1} (dry) with averaging being 3.27 ± 0.8 Bqkg^{-1}, 36 ± 9.60 Bqkg^{-1}, and 1.39 ± 1.27 Bqkg^{-1} (dry) respectively. The mean activity ratio of ^{238}U, ^{232}Th and $^{239+240}$Pu between CCS-1 and CCS-2 was obtained to be 3.50, 1.15 and 0.80 respectively. This confirms that the transport of radionuclides is from south to north direction. The high variability in the activity levels of ^{238}U, ^{232}Th and $^{239+240}$Pu in both cores indicate an almost non-homogeneous distribution throughout the depth fractions. The non-homogeneity might be very much influenced by anthropic inputs. The distribution of ^{238}U, ^{232}Th and $^{239+240}$Pu as a function of depth showed a linear relationship with a strong degree of positive correlation coefficient of r = + 0.74, + 0.80 and + 0.57 respectively **(see Table 4.3).** This clearly indicates that activity levels generally increases, as depth increases.

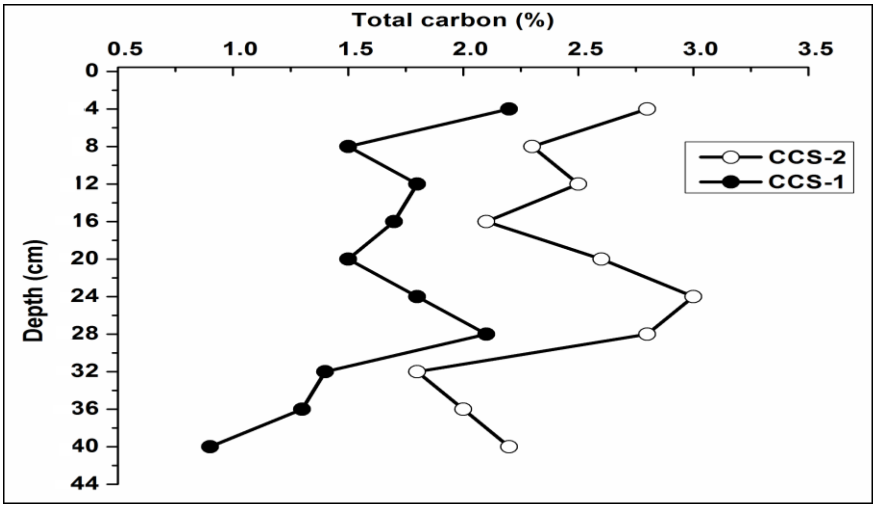

Fig. 4.10: Total Carbon (TC) of sediments as a function of depth in cores CCS-1 and CCS-2

An elevated activity level of radionuclides observed in the bottom layers (last 5 - 6 depth fractions) might be due to either immediate uptake by the sediment at the time of discharge or during high siltation rate, the activity gets deposited/imbedded in the sediments. Thus, high trapping of radionuclides at the bottom layers might be attributed to tidal action, time of sampling and sedimentation effect and sorption capacity of sediments. Another reason might be due to occurring of relatively more adsorption and co-precipitation at bottom layers of cores leading to higher deposition. A significant positive correlation between U and Th (r = + 0.86), Pu and Th (r = + 0.63) and U and Pu (r = + 0.41) suggested that their concentration were very much influenced by a similar origin of sources and identical behavior during transport in the cores.

On the contrary, the vertical profiles of ^{238}U and ^{232}Th (**Fig. 4.13)** and $^{239+\ 240}$Pu (**Fig. 4.14)** for CCS-2 showed a decreasing trend in general from top to bottom as established by negative correlation coefficient of r = -0.16, r = - 0.75 and r = - 0.54 respectively **(see Table 4.4).** ^{238}U did not show any temporal variation as seen by an almost uniform level (CV: ~ 13%) throughout the depth fractions except top layers.

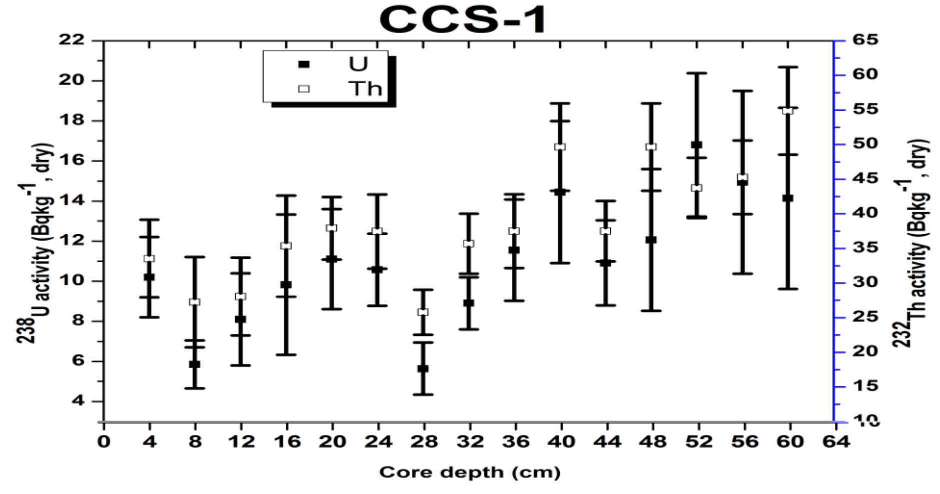

Fig. 4.11: Depth wise distribution of ^{238}U and ^{232}Th in core CCS-1

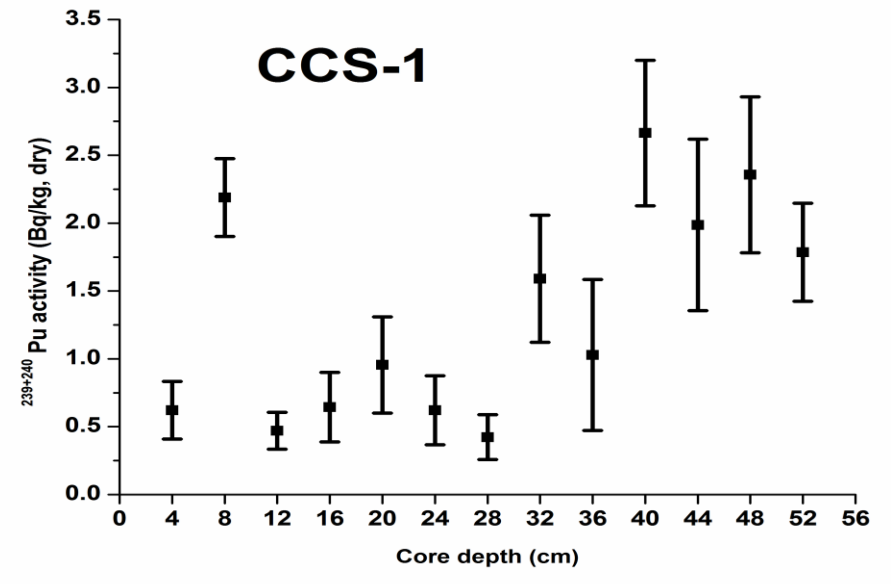

Fig. 4.12 Depth wise distribution of $^{239+240}$Pu in core CCS-1

Table 4.3: Correlation coefficient matrix of U, Th and $^{239+240}$Pu with sand, silt and clay in CCS-1 (at 5% significant levels)

	Depth	sand	silt	clay	U	Th
sand	0.93					
silt	-0.90	-0.97				
clay	-0.91	-0.98	0.90			
U	0.74	0.04	-0.03	-0.05		
Th	0.80	0.22	-0.19	-0.22	0.86	
Pu	0.57	0.06	0.02	-0.13	0.41	0.63

As in the case of ^{232}Th, a decreasing trend observed upto the depth of 16 cm which increased sharply to 28 cm and again decreases in the higher depth fractions. However, $^{239+240}$Pu, showed relatively higher concentration from top to middle layers (4 -24 cm) and onwards, an almost uniform distribution observed upto the last fractions. The reason for the higher activity levels at the top layers could be due to concurrent between a fresh discharge and the sampling time. It is also predicted that in anoxic sediments, radionuclides concentration generally decrease with increase in core depth. In addition, the uptake rate of radionuclides by the sediment is also influenced by changes in sediment composition, pre and post-depositional processes (physical mixing, redox changes and bioturbation), the adsorption on oxides of heavy metals and hydroxides from the seawater, re-mineralisation under the highly reducing conditions, incorporation inside the carbonates framework, scavenging during tidal mixing and as a detrital phase from the downstream floods with different intensities**.** Also, the vertical distribution of ^{238}U, ^{232}Th and $^{239+240}$Pu in cores were poorly correlated with each other indicating that their content were very much influenced by mixed origin of sources such as anthropogenic as well as natural.

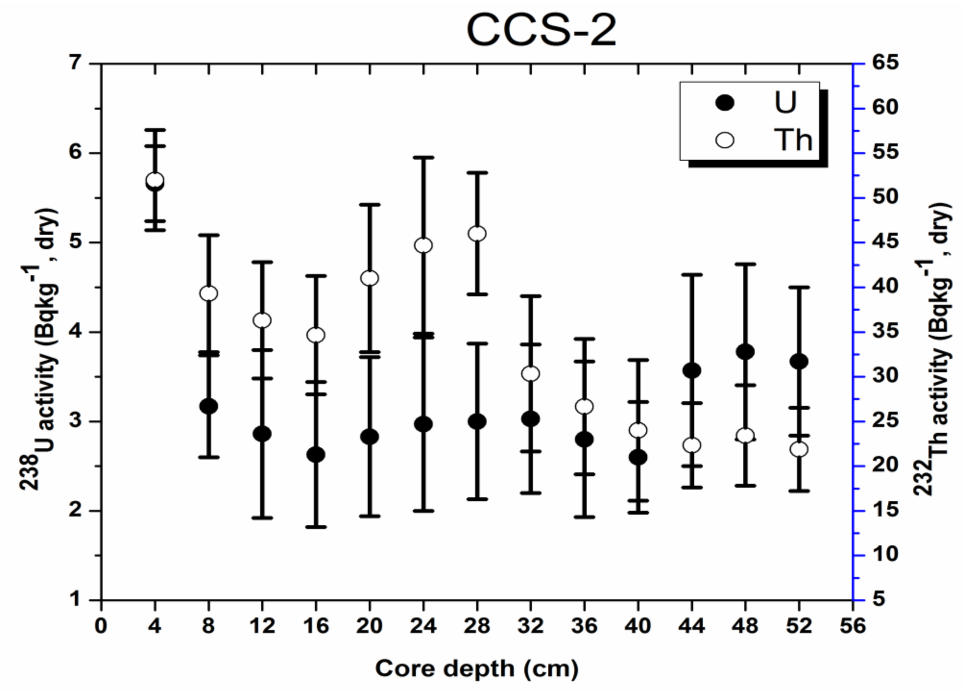

Fig. 4.13: Depth wise distribution of ^{238}U and ^{232}Th in CCS-2

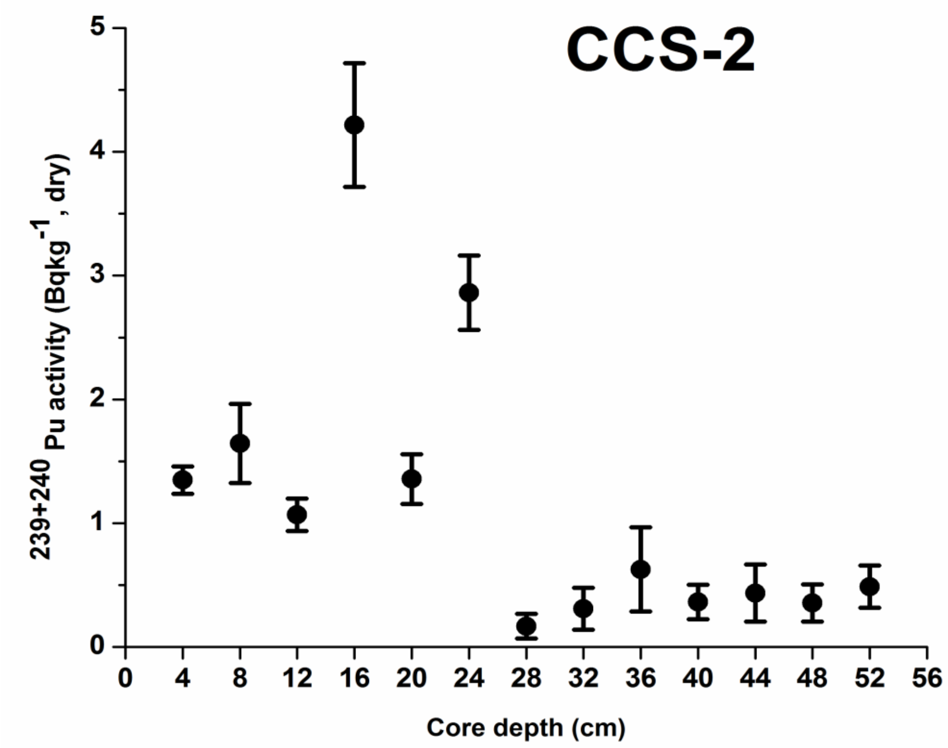

Fig. 4.14: Depth wise distribution of $^{239+240}$Pu in CCS-2

Table 4.4: Correlation coefficient matrix of U, Th and $^{239+240}$Pu with sand, silt and clay in CCS-2 (at 5% significant levels)

	Depth	silt	clay	U	Th
silt	0.10				
clay	-0.10	-0.98			
U	-0.16	-0.27	0.27		
Th	-0.75	-0.47	0.47	0.13	
Pu	-0.54	0.12	-0.13	-0.15	0.34

4.3.2.4. Activity ratio of $^{238}U/^{232}Th$

In CCS-1, the activity ratio of ^{238}U /^{232}Th ranged from 0.22 to 0.38 (mean: 0.28 ± 0.04). **Fig. 4.15** depicts the depth profile variation in activity ratio of ^{238}U /^{232}Th in core CCS-1. In general, there was a gradual decrease in the activity quotient of ^{238}U /^{232}Th from top to middle layers of cores (4 – 24 cm) and onwards, activity ratio increased with depth steadily. Overall, there was an almost uniform distribution in the activity ratio of ^{238}U /^{232}Th as obtained by the low CV (~ 14 %) throughout the core depth fractions and established by strong degree of correlation between them as discussed in previous section **4.3.2.3** .

Similarly, in CCS-2, the activity ratio of ^{238}U /^{232}Th varied from 0.06 to 0.17 (mean: 0.10 ± 0.04). **Fig. 4.16** depicts the variation in activity ratio of ^{238}U /^{232}Th as a function of depth in core CCS-2. The distribution of activity ratio from top to middle layers of CCS-2 showed a significantly decreasing trend with increasing the depth and onwards, there was sharply increasing trend to bottom layers. Overall, the activity ratio of ^{238}U /^{232}Th increases as depth increases due to obtaining strong degree of positive correlation with coefficient of r = + 0.74. The mean activity ratio of ^{238}U /^{232}Th in CCS-1 was about 3 times higher than in CCS-1. Though the activity levels of ^{232}Th in both cores were insignificantly different, the significantly lower activity ratio of ^{238}U /^{232}Th in CCS-2 might be due to lower abundance of uranium caused by far off places from discharge locations. Another reason could be attributed to the fact that uranium is relatively less adsorbed onto the surfaces of settling particles and thorium is almost exclusively transported on particulate matters. This reflects the high probability of thorium to be more concentrated in the streambed sediments by the settling particulates. The main factors controlling uranium concentrations of seawater are the prevailing Eh–pH condition [298] **[62]** and availability of HCO_3^- complex, where uranyl-carbonate plays a crucial role in uranium migration.

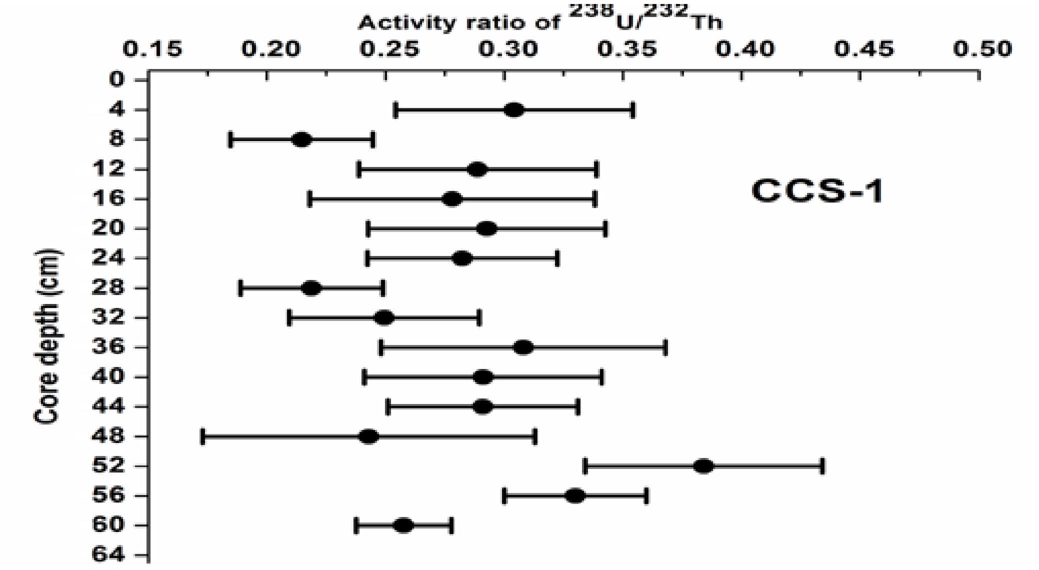

Fig. 4.15: Depth profile distribution of activity ratio of ^{238}U /^{232}Th in CCS-1

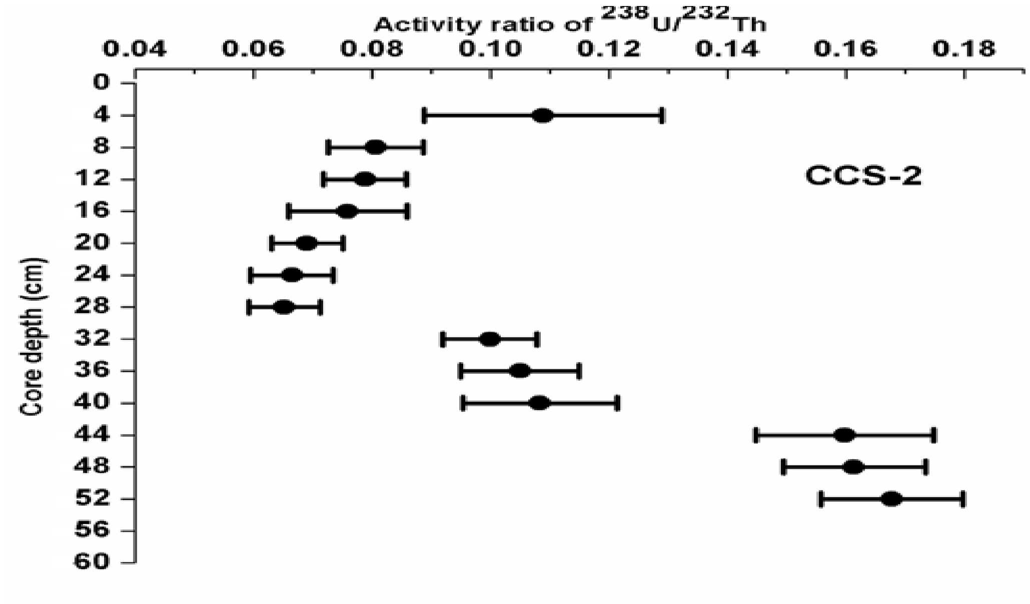

Fig. 4.16: Depth profile distribution of activity ratio of ^{238}U /^{232}Th in CCS-2

4.3.2.5. Impact of particle size on vertical concentration profile of ^{238}U, ^{232}Th and $^{239+240}$Pu

The overall content of sand, silt and clay in both cores (CCS-1 and CCS-2) ranged from 0.19 - 23.71% (mean: 2.58 ± 0.5 %), 64.62-78.30% (mean: 74.12 ± 3.4 %) and 11.67-28.91% (mean: 23.3 ± 4 %) respectively. The vertical profile of sand, silt & clay in CCS-1 and CCS-2 was tabulated in **Table 4.5** and **Table 4.6** respectively. The content of silt & clay in cores of CCS-1 and CCS-2 as a function of core depth are also depicted in **Fig. 4.17 and Fig. 4.18** respectively. Like grab sediments, the cores were also mainly composed of silt and clay.

Table 4.5: Depth profile content of sand, silt and clay in CCS-1

Depth (cm)	Sand	Silt	Clay
4	0.21	74.43	25.36
8	0.75	74.51	24.74
12	0.19	75.22	24.59
16	1.40	75.12	23.48
20	5.10	71.00	23.90
24	12.85	67.11	20.04
28	19.21	64.02	16.77
32	23.71	64.62	11.67
36	20.00	65.55	14.45

In CCS-1, the depth core fractions were dominated by silt ranging between 64.02 to 75.22 % averaging being 70.17 ± 4.83%. Sand was relatively more abundant in the last four fractions being a range from 12.85 to 23.71% than top fractions. Generally, sand content was found to increase as core depth increases confirming a greater input of eroded material from the surrounding land. The clay content varied between 11.67 to 25.36%, averaging being 20.50 ± 5.14%. The variation in silt content was almost uniformly as seen by low CV (~ 7 %) throughout the core depth fractions. However, clays were non-homogeneously abundant as obtained by significant CV (~25%). In general, the silt and clay in CCS-1 were relatively more abundant at top layers (3- 4 depth fractions) than bottom layers and showed a corresponding opposite increasing and decreasing trend to each other upto depth fraction of 16 cm and onwards follow the same trend i.e. decreases to almost the bottom fractions. Overall, the distribution pattern of both silt and clay exhibited a decreasing trend with increasing depth as obtained by a strong degree of negative correlation coefficient of r = - 0.90 and - 0.91 respectively.

Table 4.6: Depth profile content of sand, silt and clay in CCS-2

Depth (cm)	Sand	Silt	Clay
4	ND	74.06	25.94
8	ND	77.92	22.08
12	0.11	74.53	25.47
16	ND	77.84	22.05
20	ND	73.34	26.66
24	ND	73.96	26.04
28	0.16	75.13	24.87
32	ND	78.30	21.54
36	ND	75.68	24.32
40	ND	75.64	24.36

Similarly**,** in **CCS-2**, the depth core fractions were almost free from sand. Since, core fractions did not show any measurable quantity of sand, therefore no trend followed. On the other hand, silt and clay ranged between 73.64 to 78.30 % averaging being 75.64 ± 1.91% and between 21.54 to 26.66%, averaging being 24.33 ± 1.95% respectively. Moreover, both silt and clay were found to be homogeneously abundant as obtained by low CV (~ 8 %) throughout the core depth fractions. Unlike CCS-1, the vertical profile of silt and clay exhibited correspondingly opposite increasing and decreasing trend to each other throughout the core depth fractions. Clay particles showed a prominent peak of 26.66 % and 26.04 % in the middle depth core fractions of 16 -20 cm and 20 – 24 cm respectively which corresponds to the lowest percentage of silt with 73.34% and 73.96% respectively. Similarly, silt was highly abundant as 78.30% at fractions of 28 – 32 cm which corresponds to the lowest abundance of clay with 21.54%. On establishing the correlation between vertical concentration profile of ^{238}U, ^{232}Th and $^{239+240}$Pu and the composition of sand, silt and clay in both cores, it was observed that these particle sizes did not show any particular significant correlation with uranium or thorium or plutonium. Nevertheless, in CCS-1, all radionuclides were positively associated with silt clearly indicates that medium sized particles are the main scavenger during the transport of radionuclides. Whereas for CCS-2, ^{238}U and ^{232}Th showed a positive association with clay and negative association with silt reflecting that clay minerals are the main carriers during mobilizing and diffusing of radionuclides. In contrast, the positive association of Pu with silt and negative association with clays indicate that the migration of Pu is influenced by medium-sized fractions of sediment.

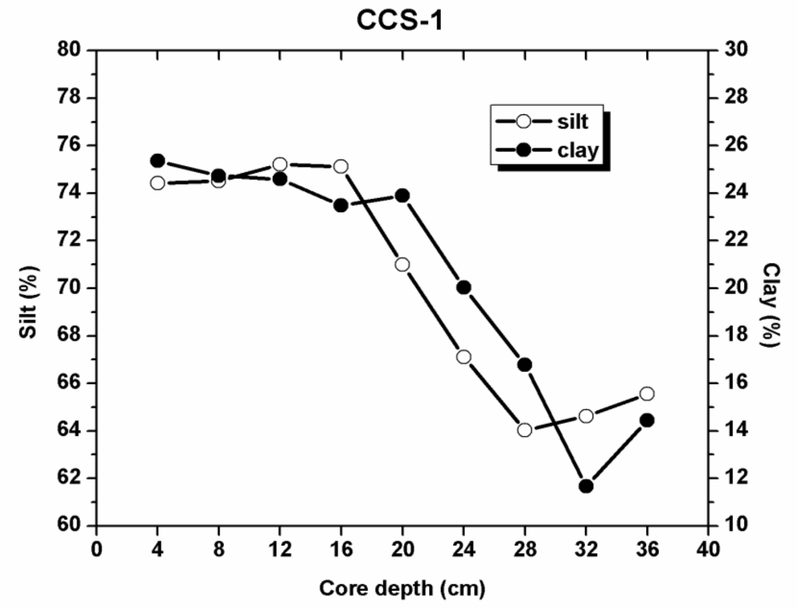

Fig. 4.17: Silt & clay of sediments as a function of depth in CCS-1

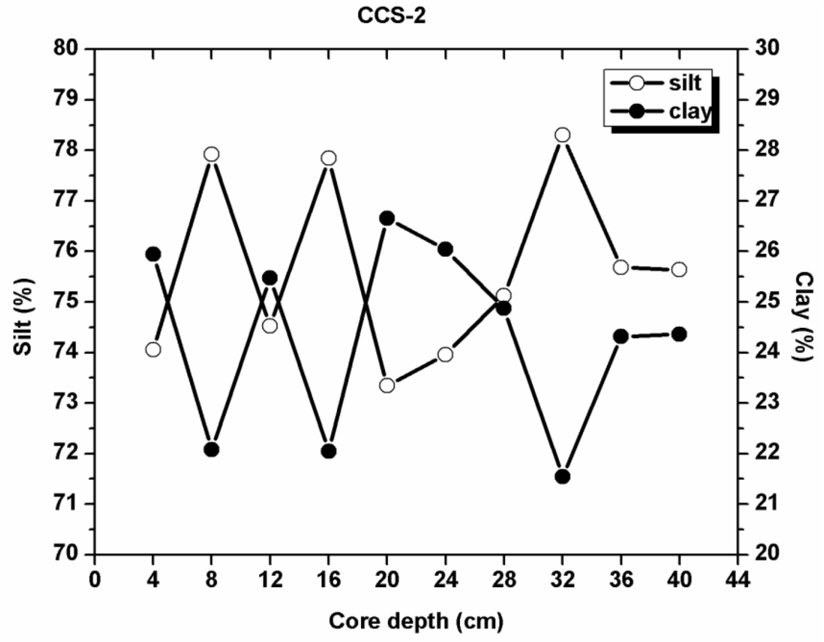

Fig. 4.18: Silt & clay of sediments as a function of depth in CCS-2

4.3.3. Mineralogical composition of sediments

Table 4.7 depicts the range of composition of various minerals in the sediments determined by the X-ray diffraction (XRD). The XRD patterns of the sediment samples showed chlorite and illite as predominant clay minerals in the sediments of studied regions [299, 300].

Overall quite appreciable amounts of calcite, dolomite Ca–montmorillonite, talc, amphiboles, quartz and Na- montmorillonite were present in the studied area. There was not much significant changes in the composition of quartz and (Mg, Ca) bearing minerals except calcite and dolomite throughout the regions. A typical X-ray diffractogram of sediment in Mumbai Harbour Bay is shown in Fig. 4.19 – 4.21.

Table 4.7: Mineralogical composition of sediments

Mineral Name	Formula	Range of Content (%)
Quartz	SiO_2	5-8
Calcite	$CaCO_3$	5-30
Dolomite	$CaMg(CO_3)_2$	ND-30
Ca-montmorillonite	$Ca_{0.2}(Al, Mg)_2Si_4O_{10}(OH)_2.4H_2O$	30-40
Na-montmorillonite	$Na_{0.3}(Al, Mg)Si_4O_{10}(OH)_2.xH_2O$	5-8
Talc	$Mg_3(OH)_2Si_4O_{10}$	30-40
Amphiboles	$Al_{3.2}Ca_{3.4}Fe_4K_{0.6}Mg_6NaSi_{12.8}O_{44}(OH)_4$	1-2
Chlorite	$(Mg_{11.06}Fe_{0.94})((Si_{5.22}Al_{2.78})O_{20}(OH)_{16})$	1-2
Illite	$(K,H_3O)(Al,Mg,Fe)_2(Si,Al)_4O_{10}[(OH)_2,(H_2O)]$	1-2

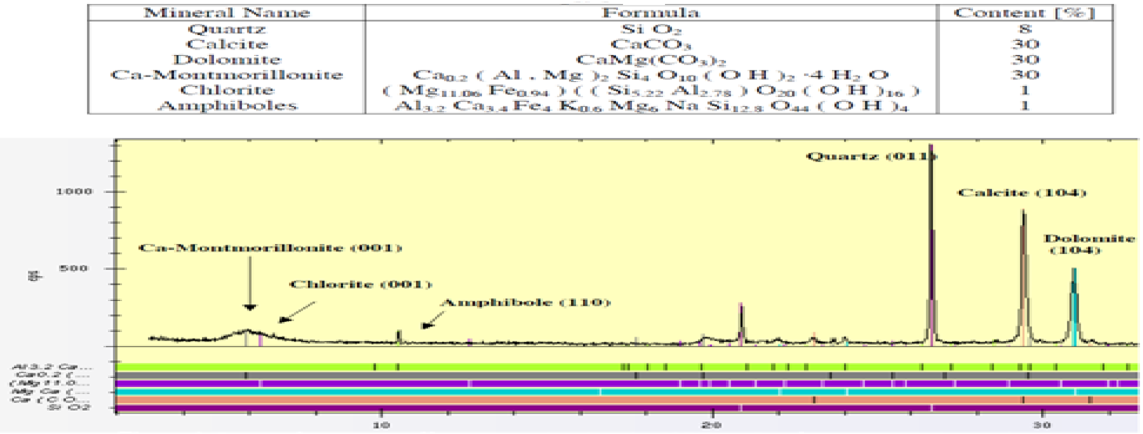

Mineral Name	Formula	Content [%]
Quartz	$Si\ O_2$	8
Calcite	$CaCO_3$	30
Dolomite	$CaMg(CO_3)_2$	30
Ca-Montmorillonite	$Ca_{0.2}\ (\ Al\ .\ Mg\ )_2\ Si_4\ O_{10}\ (\ O\ H\ )_2\ \cdot 4\ H_2\ O$	30
Chlorite	$(\ Mg_{11.06}\ Fe_{0.94}\ )\ (\ (\ Si_{5.22}\ Al_{2.78}\ )\ O_{20}\ (\ O\ H\ )_{16}\ )$	1
Amphiboles	$Al_{3.2}\ Ca_{3.4}\ Fe_4\ K_{0.6}\ Mg_6\ Na\ Si_{12.8}\ O_{44}\ (\ O\ H\ )_4$	1

Fig. 4.19: Diffractrogram of sediment samples (Set 1) showing the 100% peaks of the minerals detected

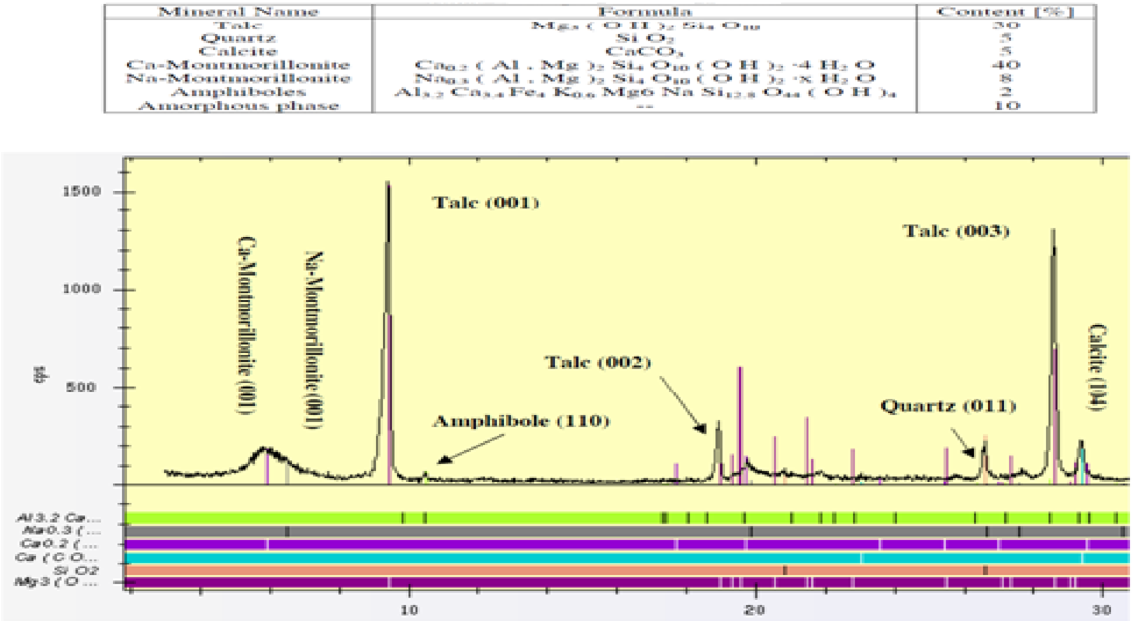

Mineral Name	Formula	Content [%]
Talc	$Mg_3\ (\ O\ H\ )_2\ Si_4\ O_{10}$	30
Quartz	$Si\ O_2$	5
Calcite	$CaCO_3$	5
Ca-Montmorillonite	$Ca_{0.2}\ (\ Al\ .\ Mg\ )_2\ Si_4\ O_{10}\ (\ O\ H\ )_2\ \cdot 4\ H_2\ O$	40
Na-Montmorillonite	$Na_{0.3}\ (\ Al\ .\ Mg\ )_2\ Si_4\ O_{10}\ (\ O\ H\ )_2\ \cdot x\ H_2\ O$	8
Amphiboles	$Al_{3.2}\ Ca_{3.4}\ Fe_4\ K_{0.6}\ Mg6\ Na\ Si_{12.8}\ O_{44}\ (\ O\ H\ )_4$	2
Amorphous phase	--	10

Fig. 4.20: Diffractrogram of sediment samples (Set 2). The preferred orientation for Talc along (001) direction is apparent

In this case the less-than-2 µm fraction was extracted and then prepared in order to achieve a strongly-oriented powder with the purpose of highlighting clay minerals.

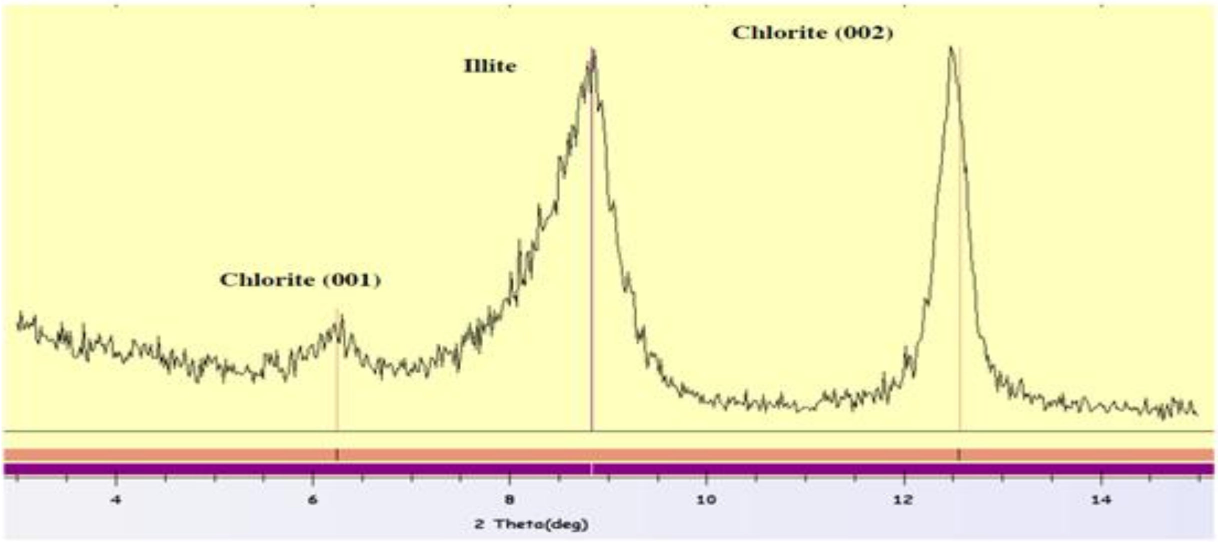

Fig. 4.21: Diffractrogram of clay minerals (<2µm) in sediment samples

4.4. Conclusions

In this chapter, the spatial and vertical concentration profile of ^{232}Th, ^{238}U and $^{239+240}$Pu in both grab and core sediment samples collected from different locations of Mumbai Harbour Bay were discussed in details. The obtained data was compared with some of the similar work carried out in different parts of the world. In addition, an inter correlation between concentration of studied radionuclides, sediment textures, associated minerals and organic carbon content were also established.

The spatial distribution of ^{238}U in grab sediments has been found to be an almost homogeneous throughout the studied area while in the case of ^{232}Th and $^{239+240}$Pu, the concentration profile showed a non-homogeneous distribution. The decreasing trend in activity levels of radionuclides from south to north direction is a good indication that, the bay has a good circulation and movement of water and the activity gets a good dispersion and transport in the seawater. The higher values obtained in the south direction can be attributed to the presence of some hot particle trap at that site. The erratic variation in the activity levels within the studied area might be due to their sorption/desorption processes onto the surface of sediment materials. Furthermore, the activity ratio of ^{238}U /^{232}Th in grab sediments of studied area was much below unity indicating that uranium is more soluble and hence mobile than thorium. Conversely, Th is a high particle reactive, immobile, high abundant in sediment. The spatial variation in the activity ratio of ^{238}U /^{232}Th in grab sediments along the studied area were within the statistical fluctuations except one or two locations. As far as sediment textures are concerned, the sediments were in general, mainly composed of silt and clay indicating that the resuspension of fine sediments might have occurred due to monsoonal activities. The lack of substantial fresh water input and the elongate shape of the bay are also responsible for the high silt and clay content. Sediments in most of locations were mostly free from sand content. Very few locations were comparatively higher sand abundant indicating a greater input of eroded materials from the surrounding land. Though the spatial variability in silt and clay content were within the narrow range (almost uniform), the activity levels of ^{232}Th and $^{239+240}$Pu varied greatly except ^{238}U throughout the studied area. The positive association of $^{239+240}$Pu with clay and negative association with silt indicate that clay minerals are the main carriers during mobilizing and diffusing. However, Thorium appeared to be highly bound to medium size fractions and uranium was partly associated with both size fractions. The relatively more association of Th in medium-sized particles might be attributed to agglomeration of smaller size particles into large size ones in the electrolyte medium of the bay.

On the other hand, the vertical concentration profile of ^{238}U, ^{232}Th and $^{239+240}$Pu in studied area were found to be an almost non-homogeneous distribution as seen by high value of CV. The non-homogeneity might be very much influenced by anthropic inputs. The trend of depth profile distribution of radionuclides in both cores was contrary to each other. In core CCS-1, activity generally increases, as depth increases whereas in CCS-2, an inverse trend followed. High activity levels at the bottom layers of CCS-1 might be attributed to tidal action, time of sampling and sedimentation effect and sorption capacity of sediments. On the contrary, the higher activity levels at the top layers of CCS-2 could be due to concurrent between a fresh discharge and the sampling time and also influence of anoxic sediments caused by waste water drainage from nearby industries. Moreover, in general, the content of TC decreases as core depth increases in both cores. The elevated content of TC at upper layers of cores presumably represents greater input of eroded material from the surrounding land as well as discharge of domestic and industrial wastes. Also, the bulk density of both cores generally increases and porosity decreases as depth increases. This may be due to compaction of lower layers of sediments by the weight (overburden pressure) of upper sediment layers. The mineralogical composition of sediments showed chlorite and illite as predominant clay minerals in the sediments of study regions. Overall quite appreciable amounts of calcite, dolomite Ca–montmorillonite, talc, amphiboles, quartz and Na- montmorillonite were present in the study regions. There was not much change in the composition of quartz and (Mg, Ca) bearing minerals except calcite and dolomite throughout the regions.

CHAPTER 5

IMPACT OF SPATIAL GEOCHEMICAL VARIATION OF MAJOR AND TRACE ELEMENTS ON DISTRIBUTION OF ^{238}U, ^{232}Th & $^{239+240}$Pu IN THE MARINE SEDIMENTS OF MUMBAI HARBOUR BAY

5.1. Introduction

With the rapid industrialization and economic development in coastal region, heavy metals are continuing to be introduced to estuarine and coastal environment around the world [301, 302]. Presence of major & trace elements in turn influence the adsorption & desorption behaviour of ^{238}U, ^{232}Th and $^{239+240}$Pu in marine environment of Mumbai Harbour Bay. Various studies have demonstrated that sediments from coastal areas are greatly contaminated by heavy metals. Therefore, the evaluation of metal distribution in surface sediments is useful to assess pollution in the marine environment [303, 304]**.** These heavy metals participate in various biogeochemical mechanisms that have significant mobility, which affects the ecosystems through bioaccumulation and bio-magnification processes and are potentially toxic for environment and human life [305, 306]**.** Metals such as Fe, Ni, Cu, Co, Mn, Cd, Cr and Zn, etc. are used in contamination studies in marine systems due to their relationship with anthropogenic activities.

Sediments are important carriers of trace metals in the hydrological cycle because metals are partitioned with the surrounding waters; they reflect the quality of an aquatic system. Coastal and estuarine regions are the important sinks for many persistent pollutants and they accumulate in organisms and bottom sediments [307]. Thus, geochemical characteristics of the sediments can be used to infer the weathering trends and the sources of pollution [308 - 311]. Because of their large adsorption capabilities, fine-grained sediments represent a major repository for trace metal and a record of the temporal changes in contamination. Thus, they can be used for historical reconstruction. Vertical profiles of pollutant species in sediment cores have been commonly used as “pollution records” over the last decades [312]. Over the last few decades, the study of sediment cores has shown to be an excellent tool for establishing the effects of anthropogenic and natural processes on depositional environments. Metals enter the environment and oceans by two means: natural processes (including erosion of ore-bearing rocks, wind-blown dust, volcanic activity and forest fires) and processes derived from human activities by means of atmospheric deposition, rivers, and direct discharges or dumping [313]**.** The measurement of trace element concentrations and distribution in marine environment leads to better understanding of their behaviour in the aquatic environment and is important for detecting sources of pollution [314].

The metals ions including radionuclides in sediments are subjected to sorption or ion-exchange processes. These processes change the size and charge characteristics of the metals/radionuclides and thereby, influence their transport, mobility and bioavailability. The mobility of actinides in sediments is generally controlled by precipitation and sorption reactions with mineral surfaces and in particular with smectite, illite, vermiculite, chlorite, allophone, imogolite and oxides/ hydroxides of silica, aluminium, iron and manganese. Sediments with a high content of illite, smectite, vermiculite or mica within the clay fraction adsorb large amounts of cations due to their intrinsic negative charge. Due to their increasing positive charge (outer sphere complex), anions are adsorbed by aluminium and iron oxides at pH values of 8–9, i.e. below the “zero point of charge”. Water-soluble anionic compounds, such as phosphate, selenite, molybdate and arsenate are especially adsorbed due to the formation of stable complexes and the exchange of ligands with iron and aluminium oxides (inner sphere complexes). Important anion adsorbing components are clay minerals such as halloysite and imogolite. Organic matter reduces anion adsorption due to the formation of organic coatings on the surface anion adsorbing minerals.

Bivalent cations, such as Ca and Mg may also affect the adsorption of redox sensitive actinides in several ways, including competing with actinide cations for sorption sites, changing the surface charge or potential of minerals and affecting their aqueous speciation. Since other metal ions (major and trace) play a significant role to control the occurrences and abundances of actinides in natural waters. Therefore, the main objectives are to evaluate the spatial/vertical distribution of major and trace elements in the sediments and to assess their impact on distribution of actinides of interest by establishing the correlation between them.

5.2. Materials and methods

5.2.1. Study area

For this study, representative sediment samples (suspended, grab and cores) were collected from 10 locations of Mumbai Harbour Bay **(see Fig.2.1 in Chapter 2**). The grab sediments were sampled using grab sampler from water depth of 1m to a maximum depth of 3 m in the aquatic region. The suspended sediments were collected (about 2 g) after filtering the large volume of seawater through 0.45µm filter paper. The silt load was estimated to be ranged from 50 mg/L to 350 mg/L in seawater of studied area. During collection of sediment samples, cross contamination were taken care of to avoid any discrepancies. The samples were frozen after collection and later thawed, dried at 50–60°C in an oven and disaggregated in an agate mortar before chemical treatment for total metal analysis.

Details of sample collection were already discussed in Chapter 2 **(section 2.5.2)**. The core samples were sliced into 4 cm fractions. These fractions were dried for 48 h, at 50–60°C and disaggregated in an agate mortar before chemical treatment for total metal analysis. A composite sediment sample was prepared by mixing the same core depth fractions of all locations.

5.2.2. Sample digestion and analysis

0.2g of powdered and dried samples were placed in PTFE (Poly Tetra Fluoro ethylene) digestion vessels with 5 mL of HNO_3 (MERCK, 65%), 3 mL of HF (MERCK, 40%) and 2 mL of hydrogen peroxide (H_2O_2) in Teflon beakers. After that samples were completely destructed in a closed microwave digestion system (Milestone Srl, Model Ethos 1, Italy) under sediment digestion program setting accordingly to manual from manufacture. The resulting solution after centrifuged was transferred to polypropylene tubes and diluted up to 50 mL with deionised water. The concentration of Na, K, Mg Ca in sediments were determined by Ion-chromatography system (DIONEX, 600) using suppressed conductivity while Fe, Cu, Ni, Co and Mn elements using UV-Visible detector respectively. **Plate 5.1** depicts a photograph of complete setup of ion chromatography system (DIONEX-600). The total carbon in percent was estimated using C H N S-O elemental analyser (Flash EA 1112 Series, Thermo Finnigan, Italy). Quality assurance was made by spike recovery, replicate analysis and cross method checking. Blank samples, standard samples and duplicated samples were simultaneously performed in the two analyses as quality control.

5.2.3. Preparation of standards, post column PAR reagent and complexing agent as eluent

In a well ventilated fume hood, 0.12g of PAR (4-(2-pyridylazo) resorcinol) was thoroughly dissolved in 185 mL of NH_4OH and 400 mL of Elix water. 58 ml of acetic acid was added in 600 mL of Elix water to prepare 1.7 MCH_3COOH which was added slowly to the PAR solution. For preparation of eluent, 1 gm of PDCA (2, 6-Pyridyl dicarboxylic acid), 3.2g of 50% NaOH and

5.4mLof glacial acetic acid were added in 1 L of elix water and pH was maintained to 4.8. Prepared reagents were stored under an inert gas, such as nitrogen and used within two weeks of preparation. Finally, the transition metals **(see Fig. 5.1)** in bed and suspended sediment were analyzed under the following conditions: Columns: Ion Pac CS5A Analytical and CG5A Guard, Eluent: MetPac PDCA eluent, Flow Rate: 1.2 mL/min, Injection Volume: 50 µL, Mixing Device: 375- µL knitted reaction coil, Postcolumn Reagent: 0.5 mM PAR, in MetPac PAR Postcolumn Diluent Reagent Flow Rate: 0.45 mL/min, Detector Wavelength: 530 nm.

Plate 5.1: A photograph of complete setup of ion chromatography system (Model DIONEX-600)

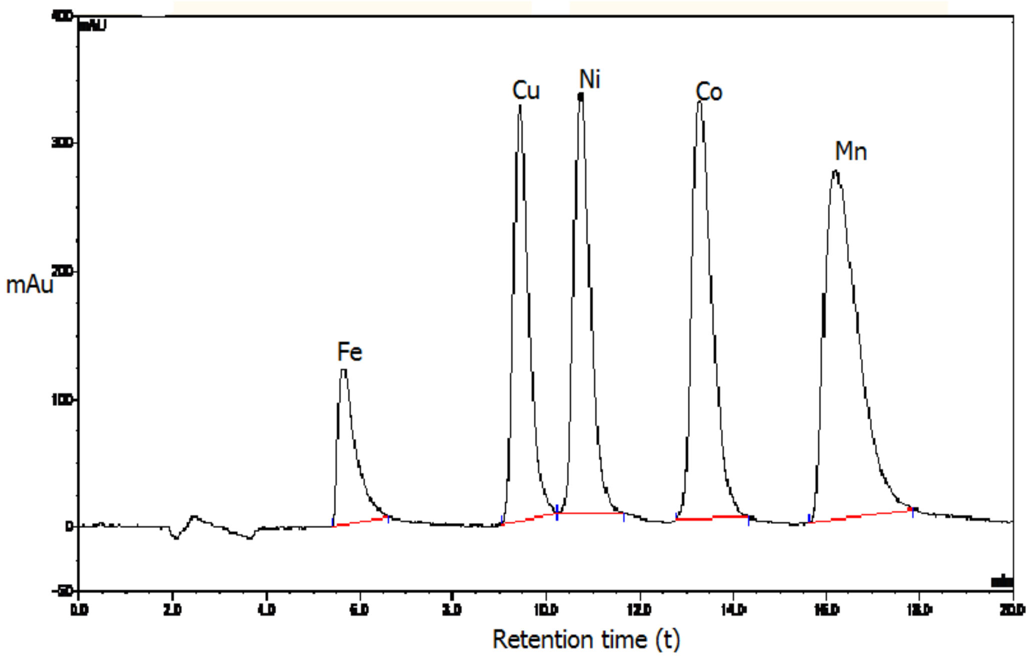

Fig. 5.1: Ion-chromatogram (mAu vs Retention time) for mixed standard of 10 mgL^{-1} each of Fe, Cu, Ni, Co and M

5.2.4. Enrichment Factor (EF)

Enrichment Factor (EF) of elements is used as an index to evaluate their anthropogenic influences in sediments and is generally defined as the observed metal to Al ratio in the sample divided by the background metal to Al ratio. Commonly geochemical normalization of the heavy metals data to a conservative element such as Al or Fe, whose levels are unaffected by contaminant inputs, is employed in order to identify anomalous metal concentration. The conception is that Al or Fe is a major mineral-forming element and combined closely with fine-sized fraction of total suspended material due to its participation in aluminum silicates [315, 316]. Al concentration in the sediment samples were not measured in this study. Therefore, we used Fe instead to calculate the EF. Fe is also an abundant element in the structure of clay minerals and is associated with particle surfaces as oxide coatings. Fe in marine sediment is mainly from natural weathering processes and has been broadly used to normalize the metal concentrations in order to reduce particle grain size influence. Several authors have successfully used iron to normalize heavy metals contaminants [316 - 318];

$$EF = \frac{\left(\frac{C_X}{Fe}\right)_{sediment}}{\left(\frac{C_X}{Fe}\right)_{crustal average}} \qquad \textbf{(Eq.5.1)}$$

Where, C_x is the concentration of metal X in sediment. The world's crustal average value and world's average suspended sediments value have been considered for bed sediment and suspended sediment as a reference element respectively. When $0.5 \leq \mathrm{EF} \leq 1.5$, it suggests that the trace metals may be entirely from crustal materials or natural weathering processes. When EF >1.5, it suggests that a significant portion of trace metals are provided by other sources [318]. EFs can give an insight into differentiating an anthropogenic source from a natural origin. EFs close to 1 point to a crustal origin while those greater than 10 are considered to have a non-crustal source [319]. Further, EFs can also assist the determination of the degree of metal contamination.

5.2.5. Statistical analyses

In basic statistical analysis, mean, skewness and coefficient of variation (CV) were carried out. CV, which is SD/mean, was used to reflect the degree of discrete distribution of different elemental concentrations and to indicate indirectly the activeness of the selected element in the examined environment. Skewness was also utilized to reflect different distributions of the metals. In addition, Pearson correlation coefficients were calculated to determine relationships among different elements.

5.3. Results and discussions

5.3.1. Spatial geochemical variation of elements

Average concentrations of major and trace elements in the grab and suspended sediments of different locations including crustal average abundances [320, 321] are depicted in **Table 5.1**. The mean concentration of metals as Na, K, Mg, Ca, Fe, Cu, Ni, Co and Mn in the grab sediments was found to be 34.72 gkg^{-1}, 12.05 gkg^{-1}, 16.80 gkg^{-1}, 54.10 $gkg^{-1}$and 61.72 gkg^{-1}, 90 $mgkg^{-1}$, 78 $mgkg^{-1}$, 62 $mgkg^{-1}$ and 242 $mgkg^{-1}$ respectively. However, the overall mean activity concentrations of ^{238}U, ^{232}Th and $^{239+240}Pu$ in grab sediments of studied area were estimated to be 11.3 ± 2 $Bqkg^{-1}$, dry, 44.3 ± 11.5 $Bqkg^{-1}$, dry and 0.73 ± 0.47 $Bqkg^{-1}$, dry respectively.

Mean values obtained for TC varied from 1.7% to 3.4%, with an average of 2.7%. The carbon content in grab sediments of L-11 and L-12 was obtained to be relatively lower than other locations. The low carbon values might be the result of marine sedimentation and mixing processes at the sediment water interface where the rate of delivery and rates of degradation by microbial-mediated processes are high [322]. In addition, this is also due to the poor absorbability of organics on negatively charged quartz grains, where they predominate in sediments. On the contrary, the high content of carbon may be due to the discharging of sewage effluents from the outer part of the bay and the finer sediments in this region, which also support the deposition of organic matter.

When compared with continental crustal average abundances, the measured mean concentrations for Na, K, Mg, Ca, Fe, Cu, Ni, Co and Mn in grab sediments differed by a factor of 1.47, 0.58, 0.72, 1.30, 1.09, 1.64, 1.04, 2.4 and 0.25 respectively. The relative abundances with respect to crustal average of these metals in the bed sediments were as follows: Co > Cu > Na > Ca > Fe > Ni > Mg > K > Mn. This variation may be the consequence of the variety of lithological components in the investigated area. The highest values were recorded for Ca, Na and Fe, which generally originated in a large extent from the earth crust via weathering except Ca. Although, Ca and Mg are chemically similar, they do not behave equally in sediment system. The low abundances of Mg in compared to crustal average at all locations might have been due to its greater attraction towards the dissolved phases due to ion exchange of minerals with sea water. In presence of particularly high salinity and sodium–dominated sediments, Mg deteriorates the sediment structure. In addition, the uptake of Mg^{2+} by sediments from dissolved phase is strongly depressed by competing cations, such as K^{+}, $NH_4^{+,}$ Ca^{+2}, Mn^{2+} as well as by pH. The magnitude of Mg and Ca incorporation into carbonates depends on their concentration of the solution, where the carbonates precipitate, culminating in the formation of dolomite.

Moreover, high abundances of Ca and Na in the sediment might be attributed to cation exchange among minerals. During the cationic exchange process, the following types of reactions take place:

$$Na^{+}/K^{+}/Mg^{2+}/AnO_2^{2+} + ½\ Ca\text{-}X_2 \leftrightarrow ½\ Ca^{2+} + Na^{+}/K^{+}/Mg^{2+}/AnO_2^{2+}\text{-}\ X$$

Where, X indicates the sediment exchanger (site). The enrichment of Ca may also be due to its presence in plagioclase and marine sediments in the form of apatite—a Ca-phosphate formed from fish bones and other biogenic debris [323]. The high K content in sediments may be due to its trapping in illite, feldspar and smectites and thereby contributing to its limited mobility [324]. The high relative abundance of Co and Cu in sediments at all locations may be due to either the precipitation of insoluble sulphides onto the sediment particles surface or formation of metal sulphide complexes that attach to the surface of silicate particles.

In some literatures, it was observed that Cu has the strong binding characteristics in the clay fraction and its association with high organic matter content leading to high enrichment in sediments. In addition, the retention of substantial portion of Co in sediments may be due to remineralisation of organic matters, which are known to contain up to 100 ppm Co and has high flux rates of organic carbon. Similarly, the high relative abundances of Fe and Ni observed at the study area. The increase in abundance of Fe may be due to leaching from the Fe-rich basalts of the Deccan Traps which is underlain by basaltic lava flows of upper cretaceous to lower Eocene age. While in case of Ni, there is high tendency to bind to metals, especially sulfides to Fe (pyrite). The second factor affecting Ni concentrations in sediments is the consequences of strong correlation between Ni and the nutrient H_4SiO_4 content found in marine organic matter [325]. In contrast, the depletion in Fe and Ni concentration in sediments found at 40% study area and Mn at all locations may be the resulting of their reduction to the soluble form and the concomitant break down of the oxy-hydroxides, leading to release of occluded metals to solution. Increase in Mn concentration at the upper surface layer (0-12 cm), probably might be due to the reoxidation of upwardly diffused Mn^{2+}. The low supply of organic matter or under strong reducing conditions, all reactive Mn is escaped to the dissolved phases.

The spatial variation in activity concentration of ^{238}U, ^{232}Th and $^{239+240}Pu$ in grab sediments of MHB are shown in **Fig. 5.2.** In general, the activity levels of radionuclides in grab sediments observed at locations (L-3 to L-6) was relatively higher than other locations indicating an occurrence of high siltation/sedimentation rate nearby discharge locations. Also, generally, the decreasing trend of activity levels of radionuclides was seen from southern part (L-2 to L-8) to northern part (L-11 to L-14) of study area indicates a good dilution and dispersion of low level activity released from discharge location due to tidal action and water current.

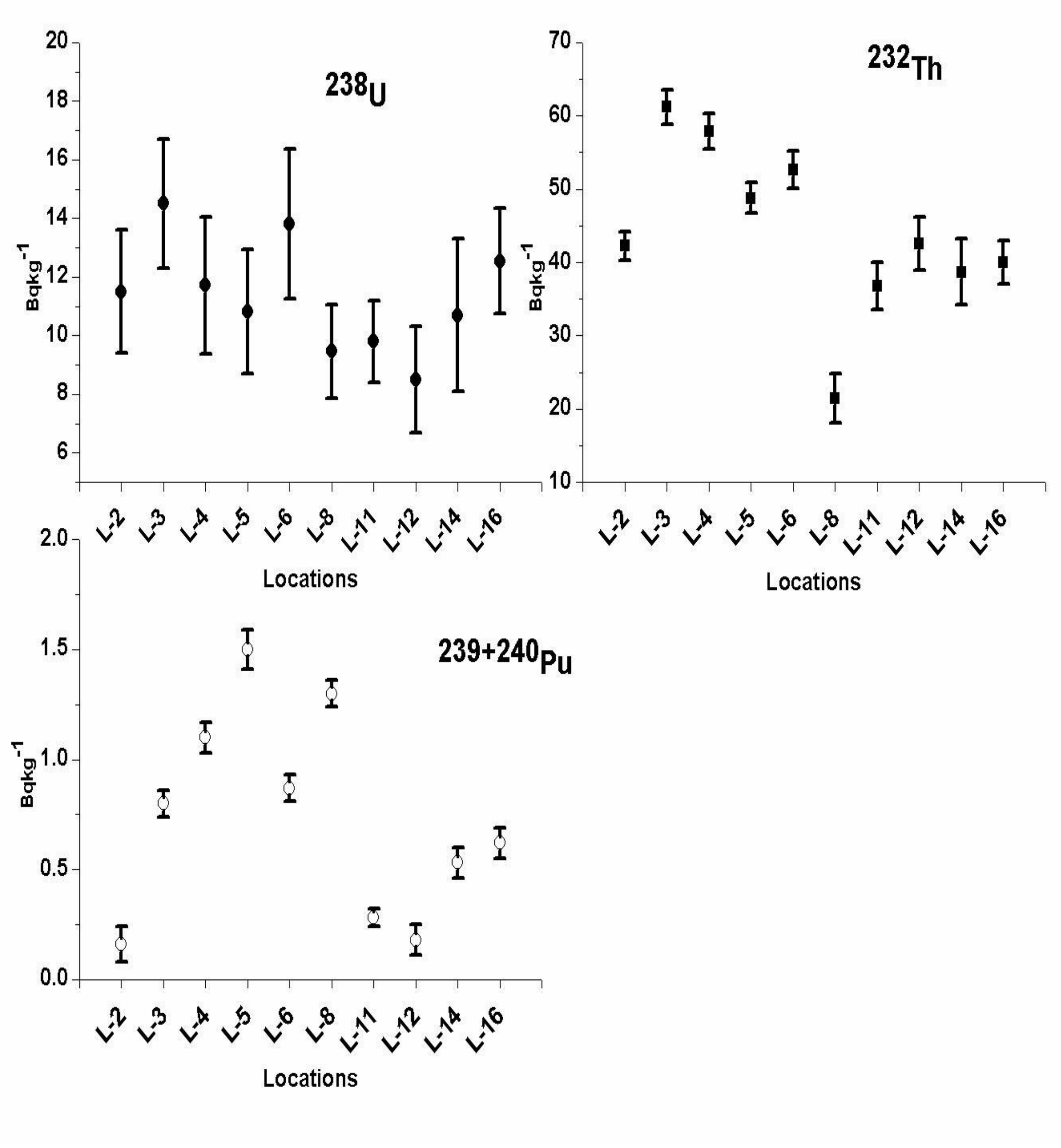

Fig. 5.2: The spatial variation in activity concentration of ^{238}U, ^{232}Th and $^{239+240}$Pu in grab sediments of MHB

Table 5.1: Measured concentration of major and trace elements in grab and suspended sediments along studied area

Sampling Location Code	Sediment code	Fe (gkg^{-1})	Cu ($mgkg^{-1}$)	Ni ($mgkg^{-1}$)	Co ($mgkg^{-1}$)	Mn ($mgkg^{-1}$)	Na (gkg^{-1})	K (gkg^{-1})	Mg (gkg^{-1})	Ca (gkg^{-1})	C (%)
L-2	GSL2	25.60	131	73	77	382	46.20	9.26	12.19	79.93	3.2
	SSL2	24.18	14	10	14	123	NA	NA	NA	NA	NA
L-3	GSL3	39.312	143	109	63	256	45.07	12.42	15.17	36.82	2.8
	SSL3	40.38	27	17	18	267	NA	NA	NA	NA	NA
L-4	GSL4	49.87	91	76	84	416	29.97	13.48	13.95	35.03	2.2
	SSL4	55.08	32	16	38	83	NA	NA	NA	NA	NA
L-5	GSL5	69.31	85	86	41	325	23.98	12.56	11.96	36.31	3.1
	SSL5	34.00	24	17	14	70	NA	NA	NA	NA	NA
L-6	GSL6	83.20	58	61	105	306	17.67	17.76	21.98	48.05	2.6
	SSL6	48.78	32	85	86	234	NA	NA	NA	NA	NA
L-8	GSL8	83.04	111	93	51	69	45.88	15.54	23.30	49.64	2.9
	SSL8	37.58	30	25	12	268	NA	NA	NA	NA	NA
L-11	GSL11	74.55	97	20	20	116	36.87	14.57	15.21	62.13	1.8
	SSL11	38.10	42	74	23	246	NA	NA	NA	NA	NA

Sampling Location Code	Sediment code	Fe (gkg^{-1})	Cu $(mgkg^{-1})$	Ni $(mgkg^{-1})$	Co $(mgkg^{-1})$	Mn $(mgkg^{-1})$	Na (gkg^{-1})	K (gkg^{-1})	Mg (gkg^{-1})	Ca (gkg^{-1})	C (%)
L-12	GSL12	93.87.	83	136	57	123	38.75	15.49	18.23	52.36	1.7
	SSL12	36.94	53	21	18	242	NA	NA	NA	NA	NA
L-14	GSL14	76.06	42	37	54	207	30.80	6.20	15.48	59.05	3.3
	SSL14	36.67	132	59	10	59	NA	NA	NA	NA	NA
L-16	GSL16	22.43	60	92	71	224	32.00	3.23	20.54	81.62	3.4
	SSL16	24.09	89	51	40	270	NA	NA	NA	NA	NA
Mean concentration for grab sediments (CV)		61.72 (41%)	90 (36%)	78 (42%)	62 (37%)	242 (48%)	34.72 (28%)	12.05 (38)	16.80 (24)	54.10 (31)	2.7 (0.22)
Mean concentration for suspended sediments (CV)		37.58 (25%)	48 (75%)	38 (71%)	27 (85%)	186 (48%)					
Crustal Average [320]		56.30	55	75	25	950	23.60	20.90	23.30	41.50	
World's Average Suspended Sediment [321]		48.00	100	90	20	600					

NA: Not Analyzed, GSL: Grab Sediment at Location, SSL: Suspended Sediment at Location

5.3.2. Spatial variation in enrichment factors (EF) of elements

With the increase of industrialization and urbanization around the coastal zone, the sediments are becoming more and more prone to contamination, as they effectively sequester hydrophobic chemical pollutants entering water bodies. Sediments can be sensitive indicators for monitoring contaminants in the aquatic environments. The concentration of trace metals in coastal estuaries get rise due to high inputs from natural, as well as anthropogenic sources. Thus, understanding the transport and distribution of trace metals in estuaries is an important goal of environmental chemists. One of the most distinguishing features of metals from other toxic pollutants is that, they are not biodegradable. Many metals entering bodies of natural water can get incorporated and accumulated in the sediments. The favorable physicochemical conditions of the sediment can remobilize and release the metals back to the water column. It has been observed that specific local sources such as discharge from smelters, metal based industries from electroplating, paint and dye formulators, petroleum refineries as well as effluents from chemical manufacturing plants are some of the major contributor of metals into the water bodies.

Fig. 5.3 and **Fig. 5.4** depict the variation in enrichment factor of major and trace elements in grab sediments of various locations of Mumbai Harbour Bay respectively**.** Using normalization of metals to Fe, the mean enrichment factor of Cu, Ni, Co and Mn was calculated to be 2, 1.24, 3.04 and 0.32 respectively whereas for Na, K, Mg and Ca the values were 1.76, 0.57, 0.81 and 1.66 respectively. Overall, the order of enrichment factor (EF > 1) in the grab sediment were observed to be Co > Cu > Na > Ca > Ni except Mg, K and Mn.

In general, the high enrichment observed at those sampling locations where industrial and harbour activities are intense. Transportation to and from the Port, shipping and harbour activities, industrial and urban waste discharges and dredging etc. could contribute the enrichment of metals in the coastal environment. However, for suspended sediments, overall, the enrichment of Co occurred at all locations **(see Fig.5.5)** and others were under depletion (EF <1). The depletion of trace elements especially Mn in sediments at all locations may be due to change in redox conditions in the particular system.

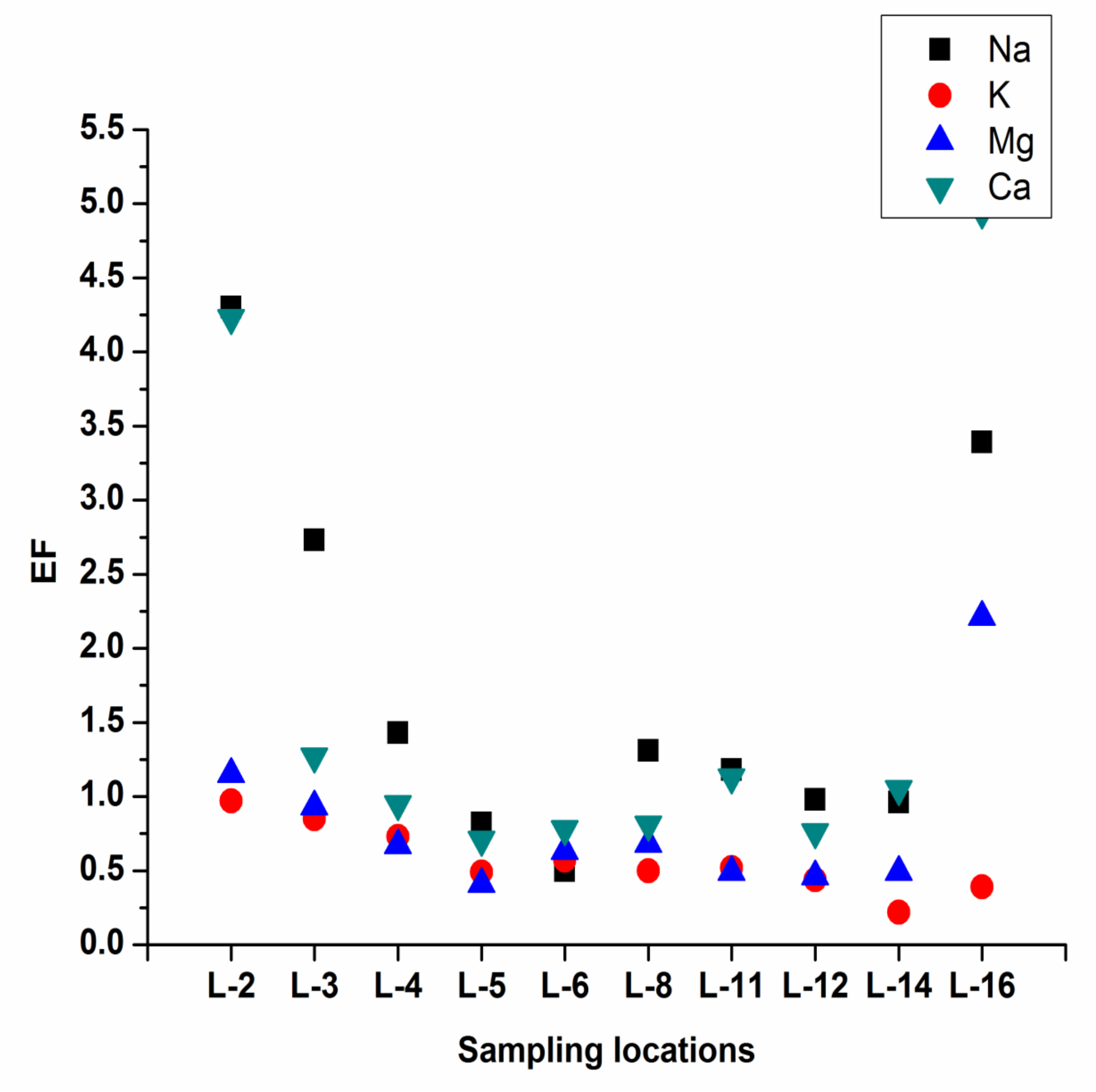

Fig. 5.3: Variation in enrichment factor of major elements in grab sediments along the studied area

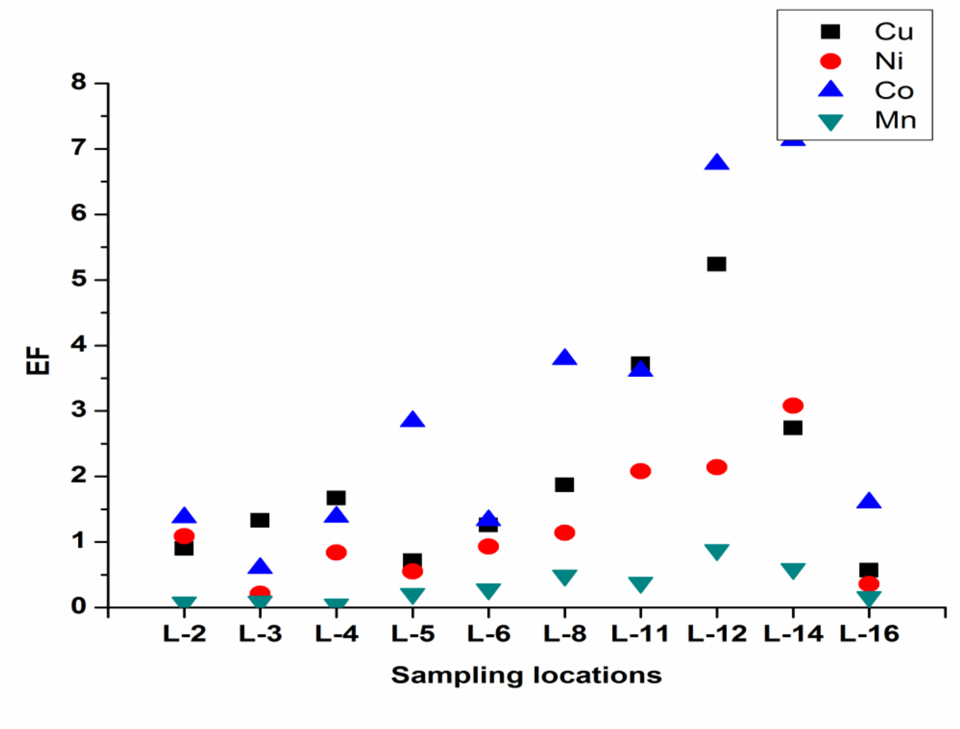

Fig. 5.4: Variation in enrichment factor of trace elements in grab sediments along the studied area

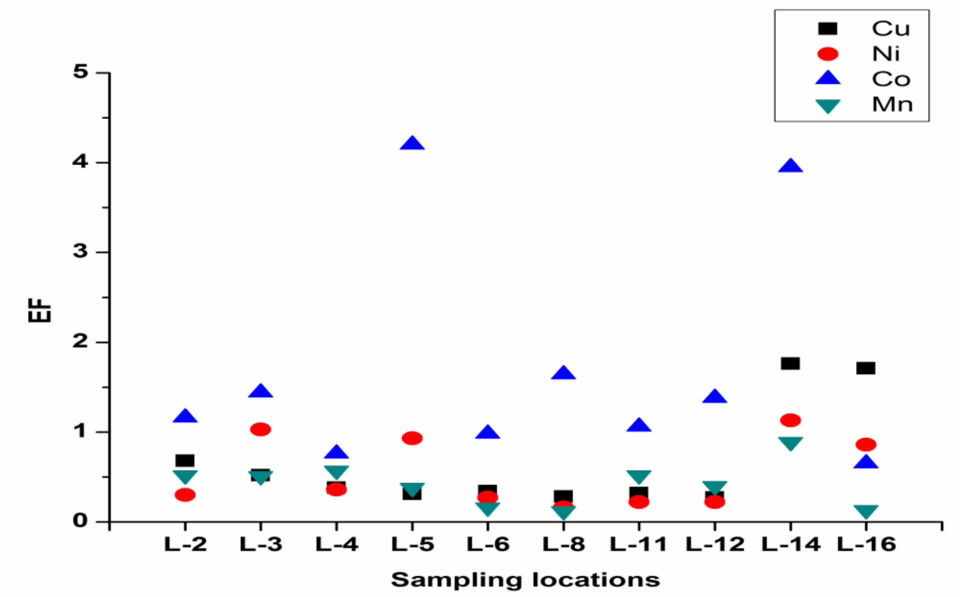

Figure 5.5: Variation in enrichment factor of trace elements in suspended sediments along the studied area

5.3.3. Impact of spatial distribution of elements on actinides

In the marine environment, sorption is generally known to take place primarily as an exchange reaction with metal ions, particularly Ca^{2+}, Na^{+} and K^{+} present in the clay minerals such as Ca -montmorillonite, Na-montmorillonite and illite respectively. In the study area, these minerals were predominately found which have been described in previous chapter. Thus the presence of other metal ions (major and trace) may control the occurrences and abundances of actinides in the marine system. In the presence of high concentration of other metal ions, the actinides ions might be adsorbed or desorbed from mineral surface sites of sediments. Thus due to the diverse compositions of metal ions, the uptake of actinides by marine sediments depends on their physical and chemical properties. Pearson's correlation coefficients between spatial distributions of elements including actinides in MHB are summarized in Table 5.2. An even or uneven pattern of relationship among metals is highly influenced by the sorption-desorption processes such as sedimentation, precipitation and flocculation of particulate substances and hence it is difficult to find the principal one.

In general, the spatial distribution of Fe showed a negative correlation with all elements including U and Th suggesting a distinguishable behaviour during transport in the sediment system. This reveals that that once Fe ions enter into the sediment profile, other metals are removed out from sediments to seawater column. While in the case of K, Mg and $^{239+240}$Pu, Fe containing minerals are seen to be as scavengers/adsorbent as obtained by a positive correlation.

Also, in the marine environment, Fe is generally precipitated in the form of oxy-hydroxide which has the affinity to scavenge/carry other metals as they pass through the water column in the sediments [326]. Though, ferric compounds are known to be effective geochemical sinks for all actinides of interest, they only scavenged $^{239+240}$Pu as obtained by positive correlation. In the marine system, U generally behaves conservatively with the formation of soluble U (VI) carbonate complexes in oxygenated seawater. However under reducing conditions, soluble U (VI) in the overlying seawater can be transformed into insoluble U (IV) resulted in addition of authigenic uranium to sediments.

Th is also conservative in sediments due to its particle reactive nature and essentially locked in the lattice structure of minerals. Hence, due to conservative behavior of U and Th, they could not associate with Fe-containing minerals in the dynamic system of marine system as seen by negative correlation. Moreover, Th and Pu are scavenged out of solution onto particulate material by biological or chemical processes (adsorption and co precipitation) leading to deposition in the bottom sediments. Non-significant correlations of other heavy metals with actinides of interest might be possibly due to the different processes (sorption, complexation and biological) and external inputs operating in sediments. Similarly, Ni, Co and Mn were observed to be positively associated with ^{238}U, ^{232}Th and $^{239+240}$Pu indicating that their minerals in the sediments also might be the probable regulator for actinides of interest in the sediment. In fact, the presence of Mn near the sediment-water interface is available to biotic uptake. Also, MnO_2 in sediments play a decisive role in redox reactions of redox sensitive radionuclides by oxidizing.

The negative poor relationships of Mn with other metals suggest that Mn-oxide might be only a minor host phase in the study area. This is not surprising taking into account its opposite behaviour in the marine environment, which means that when Mn shows an increase in concentration to the sediments due to redox cycling, the other metals concentrations show a decrease. Due to degradation of organic debris in the oxygenated surface layer, metals are normally released from the sediment and escaped to the water phase [327]. However, if this process is valid for oxygen rich surface sediments, it may explain the very high and constant metals concentrations found in the sediments. If reducing conditions exist in sediments, the low Mn content is a result of this situation.

Like Fe, Ca also exhibited generally, a negative association with all metals including ^{238}U, ^{232}Th, $^{239+240}$Pu except Na, Mg and C indicating that the metals/actinides might be participated in the cation exchange processes among Ca-bearing minerals in sediments. However, C, showed both positive correlation with Co, Mn, Ca, ^{238}U and $^{239+240}$Pu and negative correlation with Fe, Cu, Ni, Na, K, Mg and ^{232}Th. This clearly indicates that organic matter contents are important controlling factors in the abundance of trace metals [328]. Generally, in presence of high organic load, metals in sediment are scavenged out to water column leading to poor sorption with sorbent. Diagenesis of the organic matter creates a reducing environment and mobilizes the adsorbed elements which are subsequent transported from the shelf to the continental margin [329] results in a metal poor environment. A positive correlation with C and Ca indicates that the sediments are source of carbonates in the study area. This was also evidenced by higher concentrations of calcite and dolomite observed in the sediments.

5.3.4. Impact of vertical concentration profile of elements on actinides

Most radionuclides are sorbed directly to sediments or to other sinking particles within 1–2 years. However, small fractions of the radionuclides may later be remobilized from the sediments to the water column and subsequently taken up by biota or exported hydrologically from the system. Overall, the mean concentration of elements as Na, K, Mg, Ca, Fe, Cu, Ni, Co, Mn and C in the cores of all locations was found to be 27.68 gkg^{-1} (CV: 27.31%), 12 gkg^{-1} (CV: 21.83%), 14.74 gkg^{-1} (CV: 15.26%), 54.10 gkg^{-1} (CV: 14.37%), 47.55 gkg^{-1} (CV: 26.80%), 79 mgkg^{-1} (CV: 19%), 62 mgkg^{-1} (CV: 26.37%), 67.5 mgkg^{-1} (CV: 15.80%), 333 mgkg^{-1} (CV: 21%) and 2% (CV: 20%) respectively. However, the mean activity concentrations of ^{238}U, ^{232}Th and

$^{239+240}$Pu in core sediments were estimated to be 6.38 Bqkg^{-1}, dry (CV: 22%)), 36.2 Bqkg^{-1}, dry (CV: 10%) and 0.73 Bqkg^{-1}, dry (CV: 50%) respectively.

The mean and range of vertical distribution of elements/actinides throughout the cores of MHB are given in Table 5.3. A wide dispersion (high CV) or non-uniform distribution of elements throughout the core depth indicates that they are not only derived from sediment texture and mineralogical composition but also from anthropic input.

The variation in mean depth distribution of major and trace metals (Fe, Cu, Ni, Co, Mn, Na, K, Mg, Ca), actinides (^{238}U, ^{232}Th and $^{239+240}$Pu) and C in core sediments of Mumbai Harbour Bay is given in Figs. 5.6 – 5.8 respectively.

The mean concentration of metals of interest in cores of MHB were found to be in the order of Ca>Fe>Na>Mg>K>Mn>Cu>Co>Ni. Thus, among selected metals, Ca showed the highest mean concentration in the cores followed by Fe. In general, Th, Pu, Cu, Ni, Co, Mn, K and Mg showed the maximum concentration at the middle layers (16-28 cm) of the cores while in case of Fe, Na and C, maximum values obtained at the top layers (0-12cm) of the cores.

However Ca, showed relatively higher concentration at the bottom layers (36 – 40cm) than the middle layers. The elevated concentration of elements (Fe, Na and C) at upper layers might be due to the erosion of terrestrial matters, intensive fishing and ferry services and domestic/ industrial sewage drainage from the mainland. The other factors like fouling of sediments by frequent dredging activities to maintain the navigation channel along the international shipping line, use of mechanized boat for fishing and erosion due to prawn seed catch by the local inhabitants might be also caused for elevated concentration of elements at top layers of sediment profile. In particular, Fe might be enriched due to the presence of floating old rusty and stranded barges which settle down and mix with the sediments.

Table 5.2: Pearson's correlation coefficient (r) between spatial distributions of elements/actinides of interest (at 5% significant level)

Variables	Fe	Cu	Ni	Co	Mn	Na	K	Mg	Ca	C	^{238}U	^{232}Th
Cu	-0.35											
Ni	-0.06	0.31										
Co	-0.27	-0.14	0.20									
Mn	-0.53	0.08	-0.06	0.60								
Na	-0.27	0.76	0.30	-0.32	-0.35							
K	0.65	0.25	0.11	0.03	-0.14	-0.08						
Mg	0.33	-0.30	0.20	0.26	-0.56	-0.06	0.20					
Ca	-0.42	-0.14	-0.22	-0.002	-0.14	0.25	-0.61	0.11				
C	-0.51	-0.10	-0.06	0.20	0.27	-0.03	-0.68	-0.02	0.32			
^{238}U	-0.43	0.06	0.45	0.68	0.45	-0.21	-0.02	0.08	-0.16	0.39		
^{232}Th	-0.41	0.08	0.44	0.67	0.46	-0.20	-0.02	0.07	-0.15	-0.12	0.77	
$^{239+240}$Pu	0.38	-0.05	0.52	0.02	0.04	-0.31	0.39	0.18	-0.74	0.27	-0.06	0.10

Table 5.3: Mean and range of vertical distribution of elements/actinides of interest

Elements	Mean	Range
Fe (gkg^{-1})	47.55 ± 12.74	26.56 –69.31
Cu ($mgkg^{-1}$)	79 ± 15	61 - 103
Ni ($mgkg^{-1}$)	62 ± 16	37 – 81
Co ($mgkg^{-1}$)	67.5 ± 10.65	51 - 83
Mn ($mgkg^{-1}$)	333 ± 70	207 - 416
Na (gkg^{-1})	27.68 ± 7.56	14.72 – 37.3
K(gkg^{-1})	12 ± 2.62	8.72 – 17.76
Mg (gkg^{-1})	14.74 ± 2.25	10.87 – 19.12
Ca (gkg^{-1})	63.85 ± 9.18	53 - 79
C (%)	2 ± 0.4	1.6 -2.5
^{238}U($Bqkg^{-1}$)	6.38 ± 1.4	8.5-14.5
^{232}Th ($Bqkg^{-1}$)	36.2 ± 3.5	21.5-61.2
$^{239+240}$Pu ($Bqkg^{-1}$)	1.26 ± 0.63	0.16-1.5

The enrichment of metals/radionuclides at the middle portion of cores might be resulted from rapid sediment deposition due to greater input of eroded material from the surrounding land which in turn protects the buried metals from contact with the main oxidizing agents found in the overlying seawater such as oxygen, nitrate and sulfate. As a result of rapid deposition (high sedimentation rates), the metals are quickly moved below the more diagenetically active zone, thus suffering less degradation. The high sedimentation rates might be occurred from coagulation effect due to mixing of salt and freshwater because bay experiences a lot of churning by the wave and tidal effects. A relatively lower abundance of metals at the top sediment surface (0–8 cm) at the study sites could be attributed to the constant flushing activity by tides along with the impact of waves.

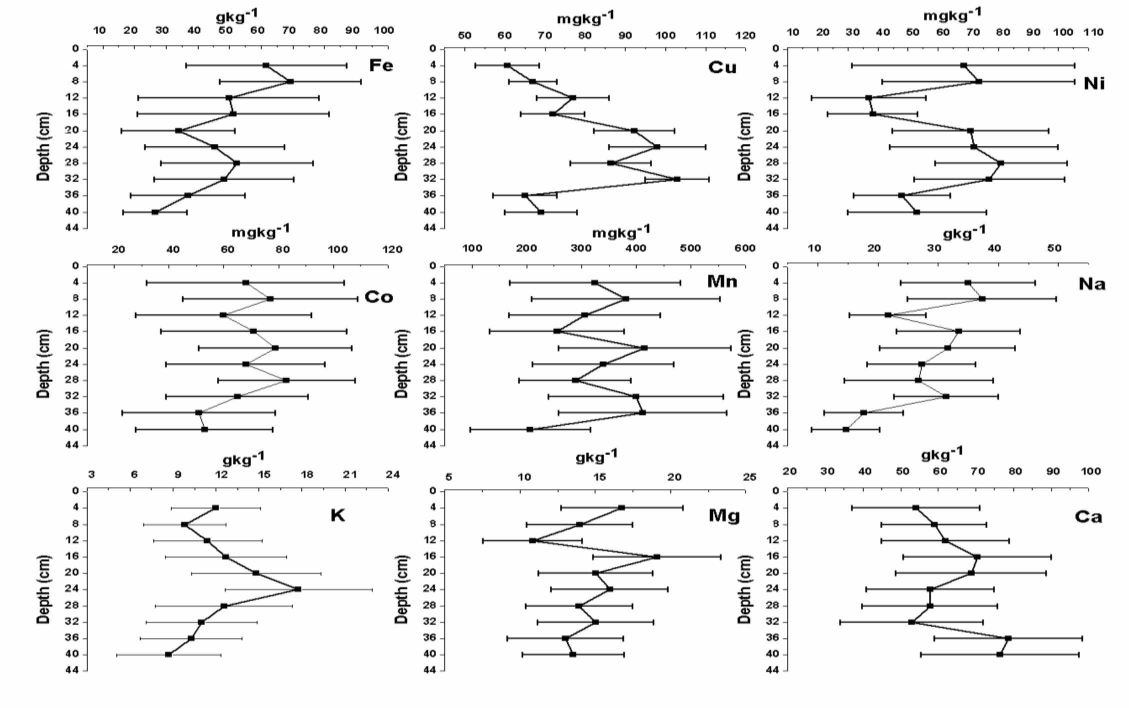

Fig. 5.6: Variation in mean depth profile of major and trace elements along studied area

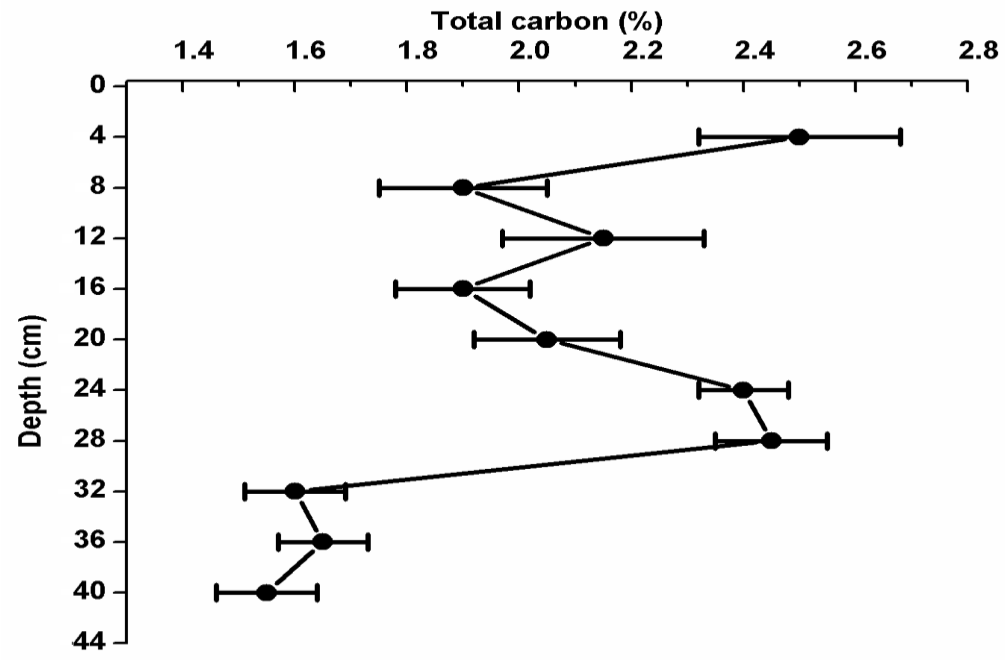

Fig. 5.7: Variation in mean depth profile of total carbon (%) along studied area

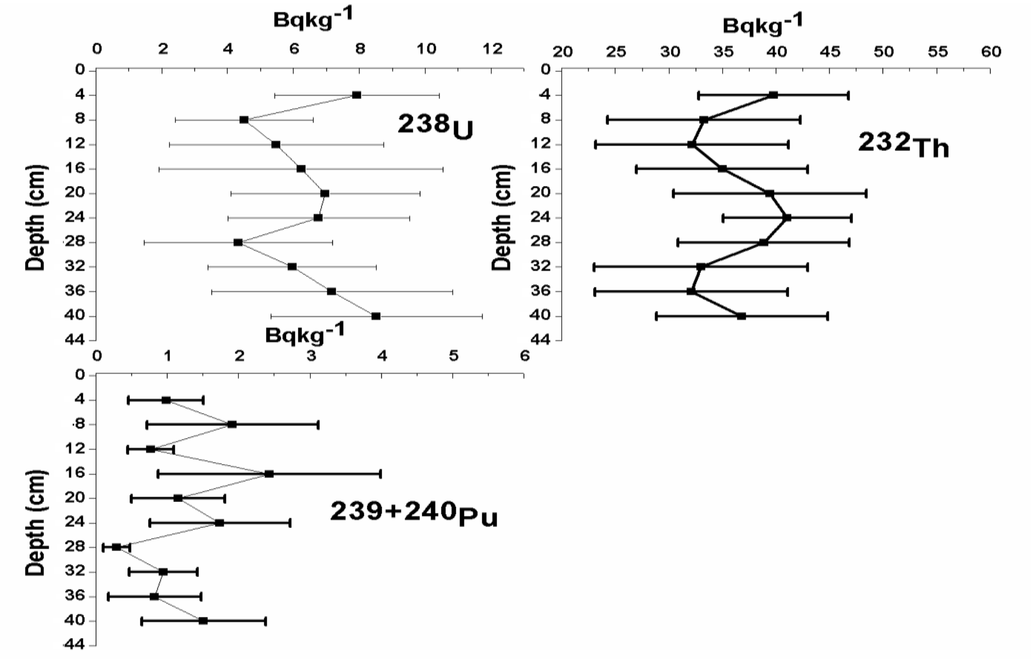

Fig. 5.8: Variation in mean depth profile of ^{238}U, ^{232}Th and $^{239+240}$Pu along studied area

Based on the obtained CV values for actinides, ^{232}Th showed an almost homogeneous distribution throughout the depths. Conversely, the significant variation in the activity levels of ^{238}U and $^{239+240}$Pu in cores might be due to their sorption/desorption processes onto the mineral surfaces of sediment materials. Overall, the concentration profile of $^{239+240}$Pu, Fe, Co, Na and total C, generally showed a decreasing trend with increasing in depth as obtained by significant negative correlation coefficients. Pearson's correlation coefficients of vertical distribution of elements/actinides of interest are given in Table 5.4. On the other hand, the profile of ^{238}U, Ca and Cu was found to increase as depth increases. In addition, there was no statistically significant variation in vertical profile of ^{232}Th, K, Mg, Ni and Mn as seen by almost poor degree of correlation and homogeneous/uniform distribution throughout the cores. An occurrence of uniform distribution in sediments indicates that once they enter into the crystal lattice of core sediments, they are fixed into it and not regulated by adsorption-desorption processes. A significant positive correlation of ^{238}U, ^{232}Th, Fe, Co, Na and K with C indicates that these elements are strongly associated with a high organic load for sinking particles leading to an anoxic environment. A fairly close distribution profiles observed between Ni and Cu/Co/Na/^{232}Th, Fe/Co/Mg and Na, K and Cu/^{232}Th, C and Fe/Co/Na/K/^{232}Th/^{238}U due to obtaining a strong degree of positive correlation between them. On the other hand, Ca showed a negative significant correlation with Na, Fe, Ni, Co and C suggesting a dissimilar origin of their geochemical sources and distinguishable behaviour during transport in the sediment system. The association or dissociation of elements depends on multiple factors such as, differences in hydrodynamics, churning, erosion, bioturbation, periodic dredging activities etc. This association is not unusual and has been previously recognized by several authors [330 - 332].

In general, the vertical profile of $^{239+240}$Pu and ^{238}U were observed to be negatively associated with metal ions. This might be attributed to predominance of cation exchange process among minerals in the sediments. Whereas the positive association of metal ions including ^{232}Th indicates an occurrences of an adsorption/co-precipitation/complexation processes. Generally, some Fe and Mn containing oxides minerals considered as adsorbants for actinides in marine system are not affected by the major cations of Ca^{2+} and Mg^{2+} unlike Na^{+}.

Table 5.4: Pearson's correlation coefficient (r) between vertical distributions of elements/actinides of interest (at 5% significant level)

Variables	Depth	Fe	Cu	Ni	Co	Mn	Na	K	Mg	Ca	C	^{232}Th	$^{239+240}$Pu
Fe	-0.84												
Cu	0.38	-0.28											
Ni	0.20	0.12	0.61										
Co	-0.50	0.53	0.38	0.65									
Mn	-0.24	0.26	0.35	0.35	0.18								
Na	-0.68	0.80	0.41	0.52	0.85	0.41							
K	-0.17	-0.03	0.52	0.18	0.38	0.14	0.24						
Mg	-0.16	0.17	0.09	0.25	0.36	-0.03	0.60	0.40					
Ca	0.50	-0.67	-0.31	-0.61	-0.50	-0.18	--0.63	-0.23	-0.13				
C	-0.57	0.63	-0.06	0.32	0.64	0.09	0.51	0.60	0.15	-0.54			
^{232}Th	-0.31	-0.15	0.13	0.57	0.48	-0.15	0.21	0.61	0.48	-0.23	0.66		
$^{239+240}$Pu	-0.17	-0.06	-0.25	-0.4	-0.1	-0.21	0.21	-0.02	0.55	0.15	-0.23	0.03	
^{238}U	0.58	-0.80	-0.17	-0.24	-0.67	-0.22	-0.54	0.02	0.21	0.39	0.41	-0.01	0.07

5.4. Conclusions

The resulting data on concentration, distribution and possible sources of major and trace elements and organic carbon in the sediments reveals the importance of geochemical processes and possible environmental impact on distribution of ^{232}Th, ^{238}U and $^{239+240}$Pu in marine environment of Mumbai Harbour Bay. High abundances of organic carbon might be due to the discharging of sewage effluents from the outer part of the MHB and the finer sediments which also support the deposition of organic matter. The low carbon values obtained might be the result of marine sedimentation and mixing processes at the sediment - water interface where the rate of delivery and rates of degradation by microbial-mediated processes are high. Looking at the mean concentrations of elements in sediment profiles, an overall metal content in grab sediments were generally higher than in cores. Overall, the order of enrichment factor (EF > 1) in the bed sediment were observed to be Co > Cu > Na > Ca > Ni except Mg, K and Mn while for suspended sediments, only Co has a high enrichment factor. The depletion of Mn in sediments at all locations may be due to change in redox conditions in the particular system. The high abundances of Na and Ca in sediments might be a cause for seawater salinization factor. In addition, the other possible sources for enriched metals might be due to transportation to and from the Port, shipping, harbour activities, industrial and urban waste discharges, dredging etc. in the bay.

A strong degree of positive correlation between elements indicates the fairly close distribution profiles during transport in the coastal environment. In contrast, a negative correlation between Ca and other metals indicate that CaO is mainly hosted within carbonates, thus precluding a significant presence of CaO-bearing silicates. The occurrences of high amount of carbonate in the study area have a diluting effect of elements which are of terrigenous origin.

Among vertical profile of metals, Ca showed the highest mean concentration in the cores followed by Fe. The enrichment at the middle portion of cores might be resulted from rapid sediment deposition due to greater input of eroded material from the surrounding land which in turn protects the buried metals from contact with the main oxidizing agents found in the overlying seawater such as oxygen, nitrate and sulfate. A relatively lower abundance of metals at the top layers could be attributed to the constant flushing activity by tides along with the impact of waves. Overall, the concentration profile of $^{239+240}$Pu, Fe, Co, Na and total C, generally showed a decreasing trend with increasing in depth while the profile of ^{238}U, Ca and Cu was found to increase as depth increases. In addition, there was no statistically significant variation in vertical profile of ^{232}Th, K, Mg, Ni and Mn indicating that once they enter into the crystal lattice of core sediments, they are fixed into it and not regulated by adsorption-desorption processes. A poor degree of negative correlation between Mn and other metals/ radionuclides reflects that the depth profile of Mn is being regulated by redox cycling. This means that when Mn shows an increase in concentration to the core sediments, the other metals concentrations show a decrease. Mn, generally shows low abundances in the reducing conditions. The negative poor relationships of Mn suggest that Mn-oxide might be only a minor host phase for them in the study area.

In general, the vertical profile of $^{239+240}$Pu and ^{238}U were observed to be negatively associated with metal ions. This might be attributed to predominance of cation exchange process among minerals in the sediments. Whereas the positive association of metal ions including ^{232}Th indicates an occurrences of an adsorption/co-precipitation/complexation processes. A positive association between actinides and Fe indicates that Fe-bearing minerals might be the probable adsorbant/scavenger in the sediments. In the marine environment, Fe is generally precipitated in the form of oxy-hydroxide which has the affinity to scavenge other metals as they pass through the water column in the sediments. An even or uneven pattern of relationship among metals is highly influenced by the sorption-desorption processes such as sedimentation, precipitation and flocculation of particulate substances and hence it is difficult to find the principal one. Some radionuclides (^{232}Th and $^{239+240}$Pu) are scavenged out of solution onto particulate material by biological or chemical processes (adsorption and co precipitation) leading to deposition in the grab sediments. Non-significant correlations of other heavy metals with actinides might be possibly due to the different processes (sorption, complexation and biological) and external inputs operating in sediments.

CHAPTER 6

ADSORPTION - DESORPTION BEHAVIOUR OF URANIUM AND THORIUM IN SEDIMENT-SEAWATER SYSTEM AND COMPARISON WITH SOIL-GROUNDWATER SYSTEM

6.1. Introduction

To predict the long term behavior of actinides in the marine system, it is utmost important to understand the adsorption - desorption behavior in sediment - seawater system. To see the impact of high salinity in marine system, it was compared with other geochemical environment such as soil-groundwater system by conducting the laboratory experiment. With the genesis of mother earth, Th and U in the ambient environment are present over the time of existence of marine systems. On account of this, their chemical speciation and sorption behavior can provide the data for development of predictive models for the long-term behavior of the synthetic radionuclides [333].

The sorption of uranium and thorium in soil/sediment is a result of several processes such as adsorption, chemisorptions and ion exchange [334]. In soil/sediment, the most important oxidation states of uranium are U (IV) and U (VI). At Eh < 200 mV, U (IV) dominates for water-logged/wet soils/sediments whereas U (VI) predominates in sufficiently aerated soil/sediments [335]. Detailed investigations about the speciation of uranium in soils/sediments are very scarce. Uranium (IV) is rather insoluble and can form complexes by various inorganic ligands such as fluoride, chloride, sulphate and phosphate. However, the greater solubility of U (VI) as the uranyl (UO_2^{++}) compounds is due to its ability to form stable complexes with various organic and inorganic ligands. The mobility of uranium in groundwater/seawater and soils/sediments is markedly enhanced due to the formation of uranium-carbonate-complexes, a main inorganic form of transport at pH values > 6.5.

The uranium contents and its mobility in aqueous systems is mainly controlled by the pH, alkalinity, the oxidation reduction potential (ORP) and the type of complexing agents present, such as carbonates, phosphates, vanadates, fluorides, sulfates and silicates, etc. [336]**.** The main oxidation states of uranium in natural water systems are U (IV) and U (VI). Under reducing aquatic environment (anoxic waters), usually, U (IV) minerals are the most abundant in uranium ore (uraninite, pitchblende, coffinite, etc.), but lead to low concentrations due to formation of its low solubility aqueous complexes. In contrast, in oxidized waters (Eh >200 mV), dissolved uranium mainly occurs as uranyl ions (UO_2^{2+}), which form highly soluble hydroxide and carbonate complexes of varying stoichiometry as a function of pH and the partial pressure of CO2(g). At low pH, adsorption of uranyl cation (UO_2^{+2}) is generally negligible and increases with increasing pH usually in the pH range of 4 to 6 [337]**.** In pure carbonate free aquatic environment with a uranium concentration of 10^{-8} M, mononuclear species (UO_2^+, UO_2OH^+ and $UO_2\ (OH)_2^0$ dominate at all pH values. But in case of high U (VI) concentrations, the polynuclear species like, $(UO_2)_3(OH)_5{}^+$) become the major hydroxyl complexes. In most natural waters, the uranyl carbonate complexes replace the U(VI)-hydroxyl complexes above pH 6 to 7 with a partial pressure of CO_2 of $10^{-3.5}$ bar (normal atmospheric pressure) and with a typical ground water CO_2 pressure (10^{-2} bar). In uranyl−hydroxide−carbonate system, the $UO_2CO_3^0$, $UO_2\,(CO_3)_2^{2-}$ and $UO_2\,(CO_3)_3^{4-}$ complexes predominate in the pH range of 6−8 [338]**.** Studies on the effect of temperature, bicarbonate concentration and uranium concentration on the sorption of uranium to a number of pure minerals were conducted where idealized distribution coefficients are calculated from Freundlich isotherms [336 – 339]**.**

The soluble and mobile U (VI) can be reduced to its less soluble and less mobile U (IV) by the organic matter present in the environment and thus, can retard the transport of uranium [340, 341]**.** However, the solubility of U (IV) can be increased through the formation of stable [342] and water soluble complexes [341]. Uranium-humates are the major species present in natural waters. The concentration of humic substances is a controlling factor in determining the level of uranium organic species formed. Uranium-humic species in the environment is quite stable due to its slow dissociation rate [342, 343]**.** At uranium mine pile site, the concentration of stable fulvic and humic acid species of uranium were reported to be between 5% and 20% in the flow path of waste dumps, subsoil and aquifer and the distribution coefficients of uranium increased with increasing pH from 4 to 8 [344]**.** The sorption of uranium onto mineral surfaces in the presence of humic substances had been reported by many researchers [345, 346]**.** The U (VI) sorption onto the rock phylite was influenced by the pH-dependent sorption behavior of the humic acids. The strong uranyl sorption on phylite (95 – 97%) was not significantly changed by the presence of humic acid in the pH range from 6 to 7.5.

Thorium is found in the nature only as a tetravalent cation concentrating in natural soils/sediments either in detrital reinstate minerals such as monazite, rutile and thorianite, or adsorbed onto natural colloidal sized materials**.** These minerals are resistant to weathering and do not dissolve readily in ground and surface waters. Hydrous thorium oxide, the dominant forms of Th (IV) in aqueous environments, is known to precipitate in the natural environment and is likely to alter with time to a more crystalline solid that has a lower solubility. The solubility of hydrous Th(IV) oxides decreases with increasing pH . At higher pH values, the hydrous oxides precipitate and dissolved thorium concentrations decrease rapidly. It is rather immobile in the aqueous environment owing to the low solubility of thorianite but the high particle reactivity of thorium shows strong colloidal characteristics, hydroxide and silicate colloids allowing transport of thorium in insoluble form. The movement of thorium is therefore controlled mainly by physical processes [347].

Thorium ion is largely hydrolyzed at pH above 3.2 and the hydroxy complexes as $Th(OH)_2^{2+}$, $Th(OH)_3^{+}$ and $Th(OH)_4(aq)$ are involved in the sorption process. In addition to undergoing hydrolysis, thorium can also form various aqueous complexes with inorganic anions such as fluoride, phosphate, chloride and nitrate. Between pH 5 and 7, dissolved thorium is predicted to be dominated by thorium phosphate complexes and this phosphate complexation is expected to have a role in the mobility of thorium over this range of pH values [348]. At high pH, the dissolved thorium concentrations are very low and only the unhydrolysed Th^{4+} ion and mononuclear divalent hydrolysis species ($Th(OH)_3^{+}$, $Th(OH)_2^{2+}$) are expected to be important in the absence of other ligands [349]. However, thorium concentrations may become elevated owing to formation of thorium–carbonate complexes. The adsorption of thorium on clays, oxides and organic matter increases with increasing pH and is completed at pH 6.5. In neutral to acid waters, thorium adsorption is less on clays than on solid humic acid.

Adsorption is one of the most important chemical processes in soils/sediments. Sorption also affects the electrostatic properties of suspended particles and colloids. The electrostatic properties affect coagulation and settling [350]. Sorption reactions on sediment/soil mineral surfaces potentially attenuate toxic sediment solution [351]. Sorption isotherm techniques provide useful information about the soil/sediment retention capacity and the strength by which the sorbate is held onto the soil/sediment.

Since the amount of surface available for adsorption on solids is limited, therefore, increases in sorbate concentration will induce competition for these sites and may decrease the value of the measured sorption coefficient. The variation of the sorption coefficient with sorbate concentration is known as a sorption isotherm, which can be described with a number of different approaches. The Freundlich equation is often useful for modeling sorption of metals onto solids with heterogeneous surfaces (multi- sites) and has frequently proved superior to the Langmuir equation for cations or anions sorption [348]. Although, there is disagreement regarding the effectiveness of Freundlich and Langmuir models to interpret sorption of metal cations [352], some parameters of these models, such as maximum sorption quantity and the distribution coefficient are widely acceptable in characterizing metals sorption capacity of soils and other materials [353]**.** The Langmuir isotherm is used for the changes in sorption when the surface becomes loaded with sorbate. It is originally developed to describe monolayer adsorption of gases onto solids. When it was adapted for adsorption from a liquid to a solid, it retained two useful parameters, which were the maximum adsorption capacity, Q^0, and a constant, K_L, related to the binding energy.

Batch sorption methods in various configurations provides the largest fraction of sorption data because of their relative simplicity, lower cost and lack of complicating factors associated with dynamic experiments that involve diffusion and advective transport. In batch experiments the sorbing solid and the solution containing the sorbate (usually dissolved) are contained in a vessel. After a given reaction time the solid and liquid are separated and the liquid (or solid) are characterized for sorbate concentration or chemical form. Batch methods are used for both adsorption and desorption reactions.

Distribution coefficient is a useful parameter for comparing the sorptive capacity of different soils or materials for any particular ion, when they are measured under the same experimental conditions [354]**.** The mobility of metals in the environment are directly related to their partitioning between solid and liquid phases and therefore, are directly related to their distribution coefficients, which indicate the capability of a sorbent to retain a solute and the extent of its movement to the liquid.

6.2. Materials and methods

6.2.1. Sampling and pretreatment

Four bulk composite bottom sediment (grab) samples from Mumbai Harbour Bay and two bulk composite surface soil (depth upto15cm) samples of 1 kg each from BARC, Trombay, were collected in polyethylene bags with screw caps and transported to the laboratory and stored at 4^0C till further analysis.

6.2.2. Laboratory analyses

The collected samples were dried at 110^0C for 24 h, powdered, homogenized and sieved through 110 mesh sizes. The powdered samples were thoroughly mixed with each other and prepared for two sets. The powdered sediment/soil materials were washed thrice with deionised water for 7 days. The solid phase was allowed to settle by gravity and the washing solution was discarded. After washing, samples were further dried at 110^0C, placed in conical flasks and stored as stock samples for experimental work. The particle size distribution of sediment/soil samples was determined using a laser diffraction particle size analyzer (CILAS, France, Model 1190). Clay minerals and other minerals present in soils/sediments were identified and quantified using powder X-ray diffractrometer (APD 2000 PRO, Italy make). The total carbon, nitrogen and hydrogen in soil and sediment were estimated using C H N S-O elemental analyser (Flash EA 1112 Series, Thermo Finnigan, Italy).

A batch equilibrium method was used to determine the distribution coefficient of uranium and thorium in sediments/soils because it offered more rapid data, through a simpler way [336] .

This method consists of shaking an amount of adsorbed phases with dissolved phases containing a certain radionuclide concentration until equilibrium is attained. Experiments were conducted with desired strength of uranium and thorium standards which were prepared using stock solutions (1g/L) of $UO_2(NO_3)_2$ $6H_2O$ and $Th(NO_3)_4$. In this study, 5 g dried sediment/soil samples were placed in each of seven empty conical flasks and equilibrated for 7 days with 150 mL of sea water /groundwater containing 10 mgL^{-1} (Set-1), 20 mgL^{-1} (Set-2), 30 mgL^{-1} (Set-3) , 40 mgL^{-1} (Set-4), 50 mgL^{-1} (Set -5), 75 mgL^{-1} (Set-6) and 100 mgL^{-1} (Set-7) of uranium and thorium contents followed by shaking using end-over end shaker (model: 300, Korea make) at 25±1°C.

After equilibration time, the samples of each set were centrifuged, filtered through 0.45 µm filter paper and supernatant analysed for uranium and thorium. The ionic composition of equilibrium solutions in Set 1 in both aqueous media was determined by Ion-chromatography system (DIONEX, 600) using conductivity suppressor as given in **Table 6.1.** HCO_3^- and CO_3^{2-} were estimated titrimetrically using autotitrator (Metrohm-798 MPT Titrino). Using an Eh - pH equation for water electrode, Eh values in dissolved phases of seawater and groundwater determined to be 0.75 V and + 0.8 V at P_{O2} = 1 atm respectively. Sample preparations, procedures and conditions for the experiments were the same to produce reproducible results in order to make comparisons. Prior to the experiments, thorium and uranium concentrations in sediments/soils as a background concentration were determined using gamma spectrometry system.

To determine the kinetic rate constant (k) of uranium in seawater - sediment and groundwater-soil system, experiment was conducted with set-1 (10 mgL^{-1} of U) of each system for the period of 1, 3, 7, 14, 21, 28 and 70 days.

In the similar fashion, a batch experiment was also conducted to determine the distribution coefficient of U in soils/sediments as a function of humic acid (HA) concentrations (0, 2.5, 5, 10, 25, 50, 100 and 125 mgL^{-1}) spiked with 1 mgL^{-1} of uranium standard. The pH of the equilibrated solution was maintained within the range of 5.5 to 6 throughout all experiments after addition of desired amount of NaOH and HNO_3. Blank samples were also run in absence of soils/sediments at different HA concentrations. Humic acid purchased from Aldrich was used for the experiment without further purification. A stock solution of 250 mgL^{-1} of HA (Aldrich) was prepared by dissolving 125 mg of humic acid in 500 mL of 0.1 M NaOH solution prepared in deionized water. The pH (1: 2.5) of soil and sediment in deionized water was measured to be 5.96 and 7.6 respectively.

The concentration of U in the equilibrium solution of each set and aliquot during different time intervals was determined using laser uranium fluorimetery (Quantalase Indore, India). The more details of the system are discussed in Chapter 3 (section 3.3.5).

In the cross checking method, uranium was also determined using differential pulse adsorptive stripping voltammeter (DPASV) in the equilibrium solution of the same set. DPASV is an electro analytical technique in which the relationship between current and voltage is observed during electrochemical processes. In adsorptive stripping voltammetry, the metal ions are first deposited in a hanging mercury drop for a fixed period of time, with the potential at the mercury drop set to a value sufficiently negative to ensure reduction of the ions. The potential is next scanned back towards more positive values. During this scanning process, each of the deposited metals are re-oxidised at a characteristic voltage and a current signal can be measured for quantitative analysis. Voltammetric measurements were performed using a Metrohm Autolab 30 in conjunction with the 663 VA stand. A multi-mode electrode was used for the reproducible production of hanging mercury drop electrode (HMDE) as the working electrode. The three-electrode system was completed by Ag/AgC1 (3 mol/l KCl) reference electrode and a platinum auxiliary electrode.

Table 6.1: Ionic composition of equilibrium solution (Set-1) and particle size characterization of adsorbed phases

Para meters	Dissolved phases		Adsorbed phases		
	Ground water	Sea water	Geochemical characteristics	Soil	Sediments
Dissolved U (µg L^{-1})	273	40	Sand (%)	23	2
Cl^{-1} (mgL^{-1})	22.22	16872	Silt (%)	72	79
NO_3^{-1} (mgL^{-1})	0.17	20	Clay (%)	5	19
SO_4^{-2} (mgL^{-1})	49	1741	Calcite (%)	5	5-30
PO_4^{-3} (mgL^{-1})	0.64	ND	Dolomite (%)	2	30-40
HCO_3^{-1} (mgL^{-1})	248	145	Quartz (%)	32	5-8
CO_3^{-2} (mgL^{-1})	1.8	0.70	Total Carbon (%)	1.90	2.28
Na^{+1} (mgL^{-1})	26	15400	Total Nitrogen (%)	2.10	1.88
K^{+1} (mgL^{-1})	1.2	312	Total Sulpur (%)	0.88	0.95
Mg^{+2} (mgL^{-1})	12	971	Total Hydrogen (%)	1.50	1.62
Ca^{+2} (mgL^{-1})	38	531			

Uranium (VI) is preconcentrated as a chloranilic acid complex at - 50 mV at the hanging mercury drop electrode (HMDE) at a pH of about 2. The determination of uranium (VI) is specific and selective, as the positive deposition potential means that other metal-CAA complexes or organic matrix components of natural waters are either not adsorbed at all or hardly adsorbed on the HMDE. All measurements were carried out in the differential pulse (DP) mode using pulse amplitude ranged from −0.6 to −0.2 V, a pulse time of 30 ms and a potential step of 4 mV. The concentration of the chloroanilic acid solution was 1×10^{-4} mol/L. The pH of the sample in the reaction vessel was adjusted at 2 using supra-pure 7.5 M HNO_3. Plate 6.2 shows the schematic arrangement of various components of Differential Pulse Adsorptive Stripping System (DPASV) with photograph during analysis of uranium.

Similarly, Th was determined by loading the aliquots of the equilibrium solution on anion exchange column (Dowex resin, 100-200 mesh, 1 cm dia x 8 cm long) preconditioned in 8N HCl. The column was then eluted with 8N HCl which contains Th, Ra and other divalent effluents. This fraction was again allowed to reload with 8N HNO_3 to separate Ra and eluted with 8N HCl. Th in eluents was estimated by precipitating with ferric hydroxide followed by centrifugation. The precipitate was washed, dried, weighed in stainless steel planchet and estimated by gross alpha counter. For assuring the purity of Th an aliquot of the separated sample was also electroplated and estimated by alpha spectrometry system. The details of the system have already been discussed in Chapter 3 (section 3.2.5).

6.2.3. Distribution coefficient (k_d) and rate constant (k)

The distribution of an element between two phases can be described by the distribution coefficient, k_d (mLg^{-1}), defined as the ratio between the concentration of the element in the solid phase and the concentration in the liquid phase after equilibrium achievement. The distribution coefficient k_d was calculated according to

$$k_d\left(\frac{mL}{g}\right)=\left[\left(\frac{C_i-C_{eq}}{C_{eq}}\right)\right]\mathrm{X}\,\frac{V}{m} \qquad \textbf{(Eq. 6.1)}$$

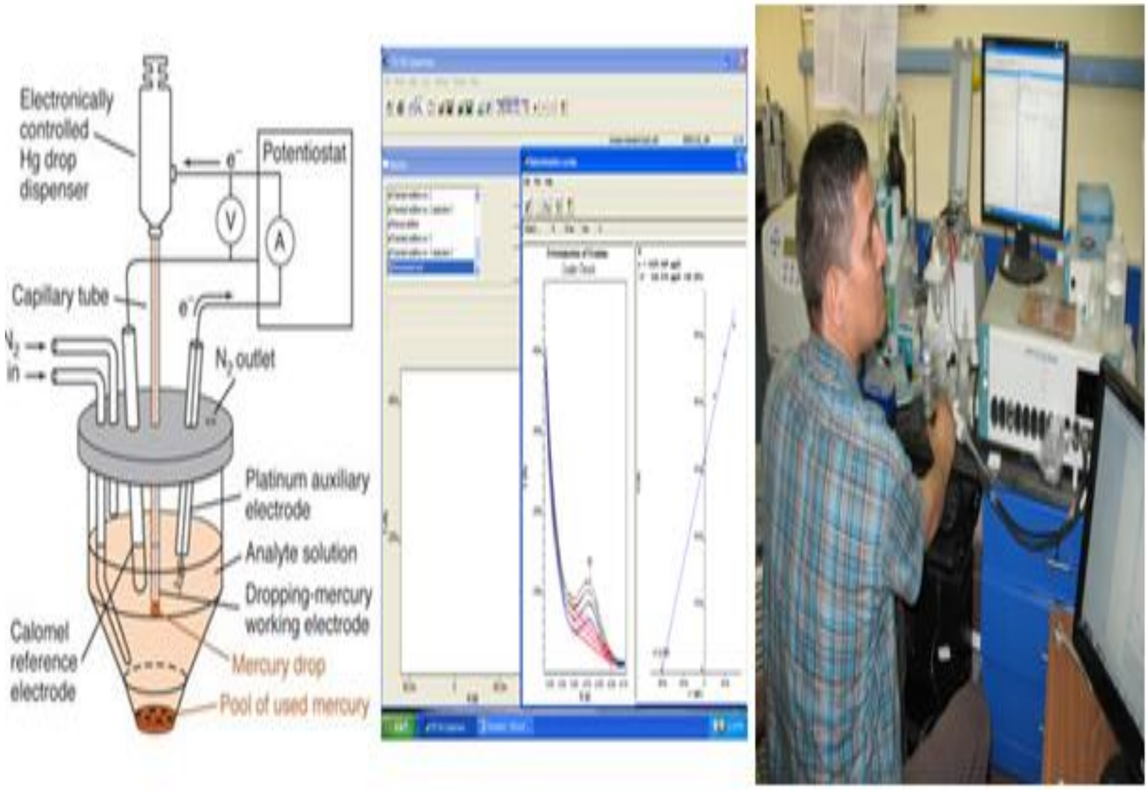

Plate 6.1: The schematic arrangement of various components of Differential Pulse Adsorptive Stripping System (DPASV) with photograph during analysis of uranium

Assuming radioactive decay of uranium and thorium in seawater-sediment system follows first-order process. The kinetic rate (k) for U adsorption onto adsorbed phases after achieving equilibrium was determined using first order kinetic reaction, by the following equation,

$$C_{eq} = C_i e^{-kt} \qquad \textbf{(Eq. 6.2)}$$

Similarly, the kinetic rate for U desorption from adsorbed phases was determined using the following equation

$$C_t = C_i (1 - e^{-kt}) \qquad \textbf{(Eq. 6.3)}$$

Amount of uranium and thorium adsorbed by the sediments was calculated using the following equation,

$$\%A = \left[\left(\frac{C_i - C_{eq}}{C_i}\right)\right] X100$$

(Eq. 6.4)

Where, A = Adsorption of contaminants in sediment; C_i = initial concentration of contaminant in the solution; C_{eq} = final concentration in solution after reaching equilibrium, V = volume of the contact solution (mL) and m = mass of the sediments (g). C_s is the equilibrium mass of adsorbed substance per unit mass of adsorbent.

6.2.4. Adsorption isotherm models

Adsorption isotherms represent the partitioning of particular species between an aqueous phase and solid particles (sorbate). Adsorption values, over the range of uranium and thorium concentrations studied, were utilized to fit Freundlich, Linear and Langmuir models. In Freundlich equation, a plot of log C_s versus log C_{eq} gives a straight line with a slope of 1/n, which often has a value of unity or less. If n is unity then K_f becomes identical to k_d . Values of n greater than unity suggest precipitation from solution rather than sorption [355]**.**

Freundlich isotherm is used for modeling the adsorption on heterogeneous surfaces. This isotherm can be explained by the following equation:

$$C_S = K_f C_{eq}^{\frac{1}{n}}$$

(Eq. 6.5)

Where, K_f is the Freundlich constant and 1/n is an arbitrary constant called as the adsorption intensity.

The linear form of the above equation can be written as:

$$\log C_S = \log K_f + \frac{1}{n} \log C_{eq}$$

(Eq. 6.6)

If 1/n approaches 1, then K_f = k_d (partition coefficient) and the equation would be linear.

The linear model can be written as

$$C_S = k_d C_{eq}$$ **(Eq. 6.7)**

Langmuir isotherm model is used for the single coating layer on adsorption surface. This model supposes that the adsorption takes place at a specific adsorption surface. The attraction between molecules decreases as they are getting further from the adsorption surface. Langmuir isotherm can be defined according to the following formulas:

$$C_S = \frac{Q^0 K_L C_{eq}}{1 + K_L C_{eq}}$$ **(Eq.6.8)**

Q^0 and K_L are adjustable parameters. As classically defined, Q^0 is the adsorption maxima or monolayer capacity, having the units of C_S. The adsorption constant, K_L, is a measure of the intensity of the adsorption isotherm (in units of Lkg^{-1} of adsorbent).

Eq. (6) can be written in the following linear form:

$$\frac{1}{C_S} = \frac{1}{Q^0 K_L C_{eq}} + \frac{1}{Q^0}$$ **(Eq. 6.9)**

6.2.5. FTIR spectroscopy

FTIR Spectroscopy is a technique based on the determination of the interaction between an IR radiation and a sample that can be solid, liquid or gaseous. It measures the frequencies / wave number at which the sample absorbs and also the intensities of these absorptions. The frequencies/wave numbers is helpful for the identification of the sample’s chemical composition due to the fact that chemical functional groups are responsible for the absorption of radiation at different frequencies/wave numbers. The concentration of component can be determined based on the intensity of the absorption. The spectrum is a two-dimensional plot in which the axes are represented by intensity and wave number of sample absorption.

FT-IR spectra for sediment soil and HA were obtained using attenuated total reflection **(ATR)** technique. All spectra were obtained using a resolution of 4 cm^{-1} (wave number) and equal measurement conditions (3900–450 cm^{-1}, 40 scans, scans means 16 repetitions of a single FT-IR measurement). **Plate 6.2** shows the schematic photograph of FTIR (Alpha-T**,** Bruker, Germany) during analysis of samples.

6.3. Results and discussions

6.3.1. Distribution coefficients (k_d) as a function of uranium and thorium concentration

The k_d values varies with the properties of sediment/soil like texture (sand, silt, clay, loam), organic matter content, pH values, the presence of competing cations, anions and complexing agents. Because of its dependence on many sediment/soil properties, k_d values of uranium and thorium in sediment/soil can range over several orders of magnitude under different conditions. Thus, it is very essential to study the geo-chemical characteristics of sediment/soil (see **Table 6.1)** over a time period. The adsorption of uranium and thorium in sediments/soils has been studied by obtaining the mean value of distribution coefficients (k_d) using the batch method. **Fig. 6.1** and **Fig. 6.2** show the variations of k_d with concentration of uranium and thorium spiked in seawater and groundwater respectively. For sediment/soils, k_d values have been reported as the mean from two sets of experimental determinations.

For sediment-seawater system, k_d for uranium and thorium ranged from 24970 to 55526 L kg^{-1} (mean: 42140 ± 12865 Lkg^{-1}) and 24926 to 38561 Lkg^{-1} (mean: 34256 ± 4665 Lkg^{-1}) respectively. The resulting coefficient of variation (CV) around mean of k_d values for uranium and thorium determined to be 30.53% and 13.62% respectively. Similarly, for soil-groundwater system, the obtained k_d values of U and Th were in the range of 3435 – 6430 Lkg^{-1} (mean: 5135

± 938 Lkg^{-1}) and 4410 – 8442 Lkg^{-1} (mean: 7321 ± 1389 Lkg^{-1}) respectively throughout experimental setup.

Plate 6.2: The schematic photograph of FTIR (Alpha-T, Bruker, Germany) during analysis of samples

The mean k_d values of Th showed about 43% higher than U in soil indicating that Th has high affinity to sorption sites in soil which depends on the higher ionic radius and subsequently smaller hydration energy**.** High k_d values indicate high metal retention by the solid phase through chemical reactions, leading to low metal bioavailability. Similarly, low k_d values indicate that a high metal amount remains in the solution.

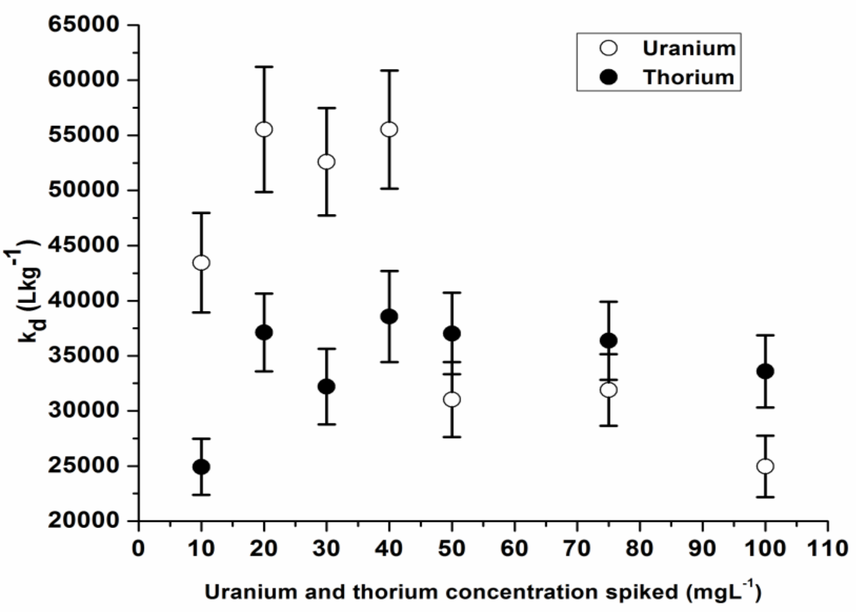

Fig 6.1: Variations of k_d with concentration of uranium and thorium spiked in seawater (pH: 7.8-8.1, m: 5 g, V: 150 mL, t: 7days, T: 25^0C)

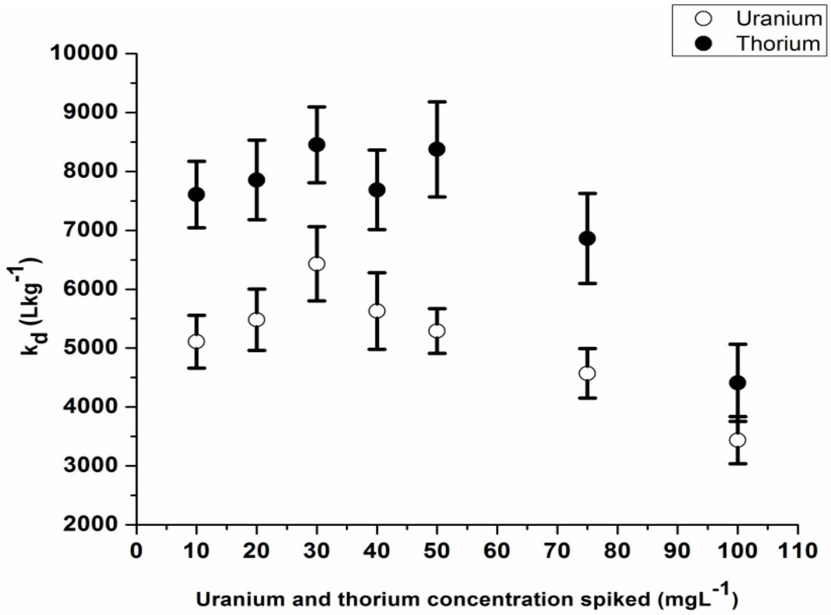

Fig 6.2: Variations of k_d with concentration of uranium and thorium spiked in groundwater (pH: 8.2-8.6, m: 5 g, V: 150 mL, t: 7days, T: 25^0C)

From the resulting data set of k_d values, it is obvious that initially, at low concentration, k_d values of U and Th increased as a function of their concentration till achieving the saturation stage. After achieving the saturation stage, distribution coefficient observed to be almost constant and at sufficiently high concentration, k_d values decreased because the partitioning behavior deviates from ideality due to removal of species by precipitation. The higher k_d values obtained in the experiment with lower U and Th concentrations, may be due to their strong associations with the sorption sites of soil leading to relatively strong bonding energies. In contrast, when the specific bonding sites become increasingly occupied, sorption becomes unspecific at high concentrations, resulting in lower k_d values [356 – 358]**.** Increasing concentration of U and Th to the sediment/soil may result in saturation of their sorption sites, thereby decreasing the sorption capacity. In addition, the sorption characteristics of U and Th in sediment/soil could be attributed to different mechanisms of ion-exchange processes and adsorption processes. During the ion-exchange process, U and Th move not only through the pores of the sediment/soil, but also through channels of the crystal lattice which results to replace exchangeable cations (mainly sodium and calcium).

6.3.2. Adsorption isotherm for sediment and soil

The sorption parameters of U and Th obtained from the experimental results for sediment-seawater and soil-groundwater systems were fitted to Freundlich, Linear and Langmuir models as given in **Table 6.2 and Table 6.3** respectively. For both systems, all models showed a better fit of the adsorption data due to obtaining very strong degree of the coefficient of determination ($R^2 > 0.8$) for both uranium and thorium. Therefore we cannot assume that the adsorption behavior fit one of them better and it is a homogeneous or a heterogeneous one. The % adsorption yields were found to be > 99 % for both U and Th at the same pH and temperature.

In Freundlich model, K_f and adsorption intensity (1/n) for uranium and thorium were calculated from the intercepts and slopes of the curve respectively and n were found to be very close to unity for both systems. Therefore linear model was observed to be more preferably and the distribution coefficient (k_d) of thorium was found to be about 50% and 31% higher than uranium for sediment and soil respectively indicating that the adsorption of thorium is more favorable than uranium onto sediments/soils at the same pH and temperature. This may be due to the decrease of hydration ($-\Delta H_h$) and increase of the ionic radius.

Table 6.2: Adsorption isotherm parameters of uranium and thorium in sediment- seawater

Sediment	Freundlich Model			Linear Model		Langmuir Model		
	K_f (Lkg^{-1})	n	R^2	k_d (Lkg^{-1})	R^2	K_L (Lkg^{-1})	Q^0 ($mgkg^{-1}$)	R^2
U	9.55×10^4	1.35	0.95	22540	0.96	2.88×10^5	16502	0.96
Th	2.40×10^4	0.91	0.97	34590	0.99	6.90×10^6	3623	0.94

Table 6.3: Adsorption isotherm parameters of uranium and thorium in soil – groundwater

Soil	Freundlich Model			Linear Model		Langmuir Model		
	K_f (Lkg^{-1})	n	R^2	k_d (Lkg^{-1})	R^2	K_L (Lkg^{-1})	Q^0 ($mgkg^{-1}$)	R^2
U	1.15×10^4	1.19	0.96	3359	0.91	1.65×10^4	3.2×10^5	0.98
Th	1.82×10^4	1.22	0.93	4400	0.80	2.88×10^5	1.96×10^4	0.98

Thorium has lower hydration energy ($-3332\ kJmol^{-1}$) and high ionic radius ($1.19A^0$) than uranium ($-3958\ kJmol^{-1}$, $0.97A^0$), which means thorium can exchange easily at the sediment/soil surface. Furthermore, thorium is more electropositive than uranium which means that thorium binding onto the negative surface and binding strength should be stronger and higher respectively, than uranium.

The plot of the linear form of all the three models for thorium and uranium adsorption onto sediment is shown in **Figs.6.3 – 6.5 and Figs. 6.6 – 6.8** respectively. Values of K_f constant in Freundlich model were calculated to be 95500 Lkg^{-1} for U and 23988 Lkg^{-1} for Th indicating that sorption of uranium in sediments were observed to be higher than thorium. In contrast, the values for K_L(bonding energy coefficient, Lkg^{-1}) constant for thorium were about one order of magnitude higher than uranium. Moreover, Langmuir adsorption maxima (Q^0, sorption maxima, $mgkg^{-1}$) for uranium were 4.5 times greater than thorium.

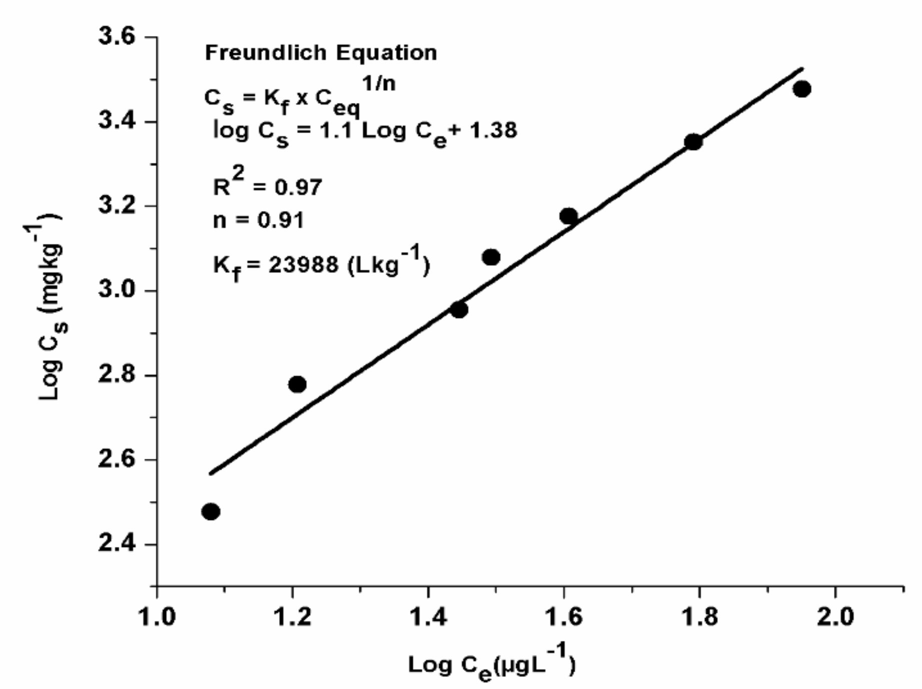

Fig. 6.3: Freundlich model for thorium adsorption on sediment

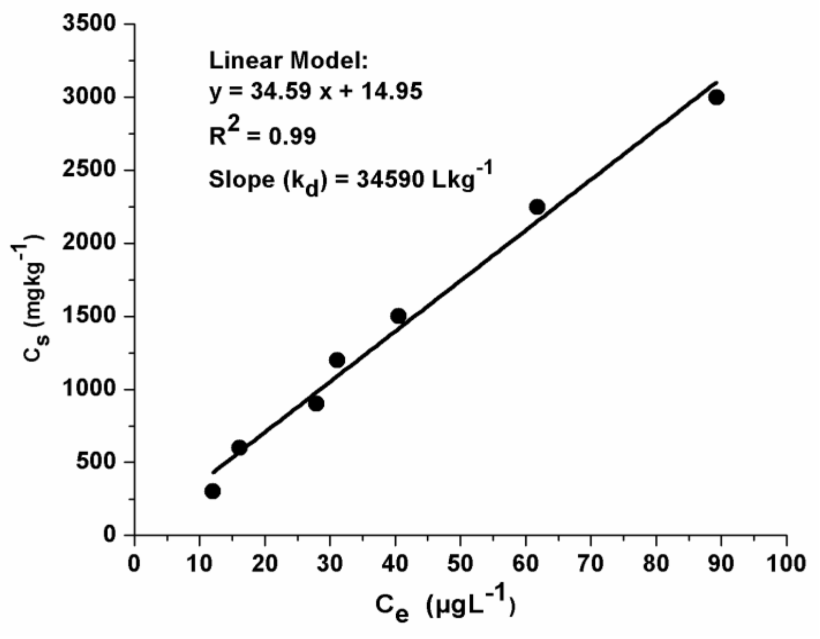

Fig. 6.4: Linear model for thorium adsorption on sediment

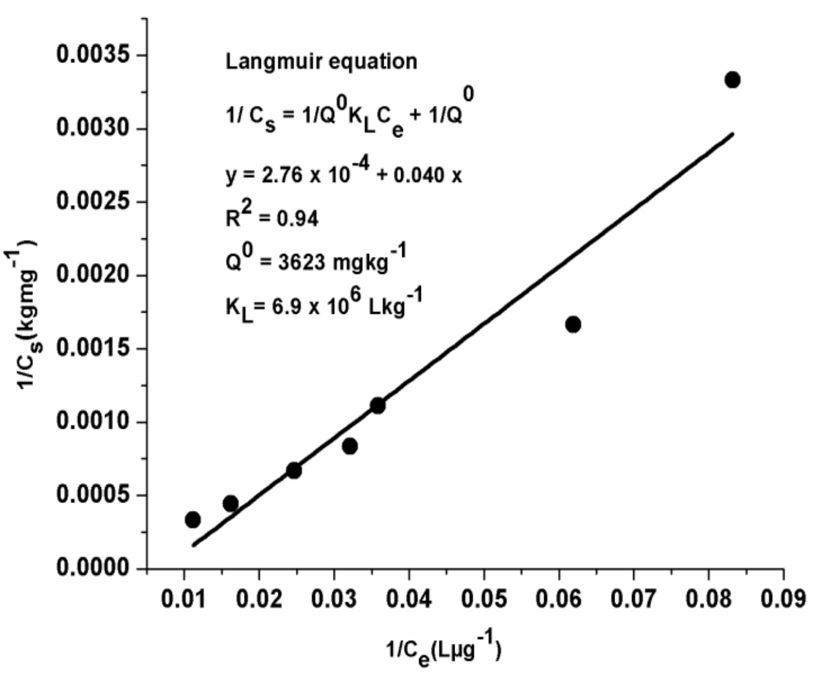

Fig. 6.5: Langmuir model for thorium adsorption on sediment

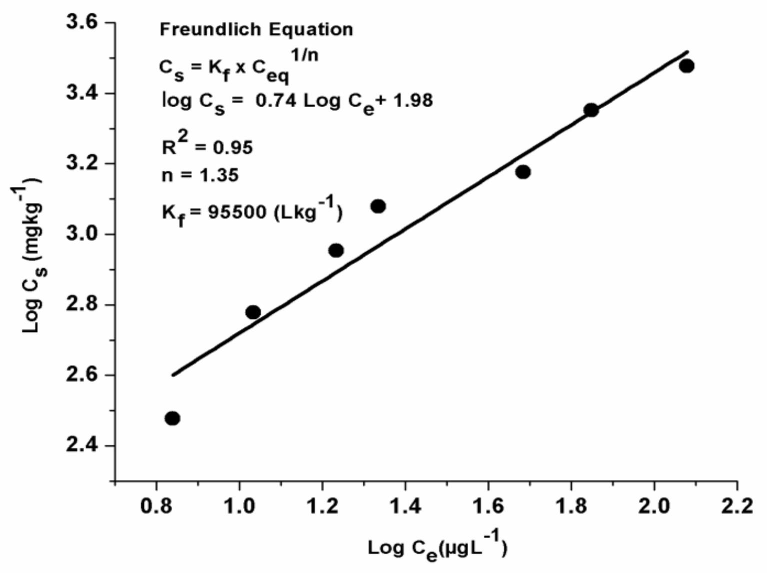

Fig. 6.6: Freundlich model for uranium adsorption on sediment

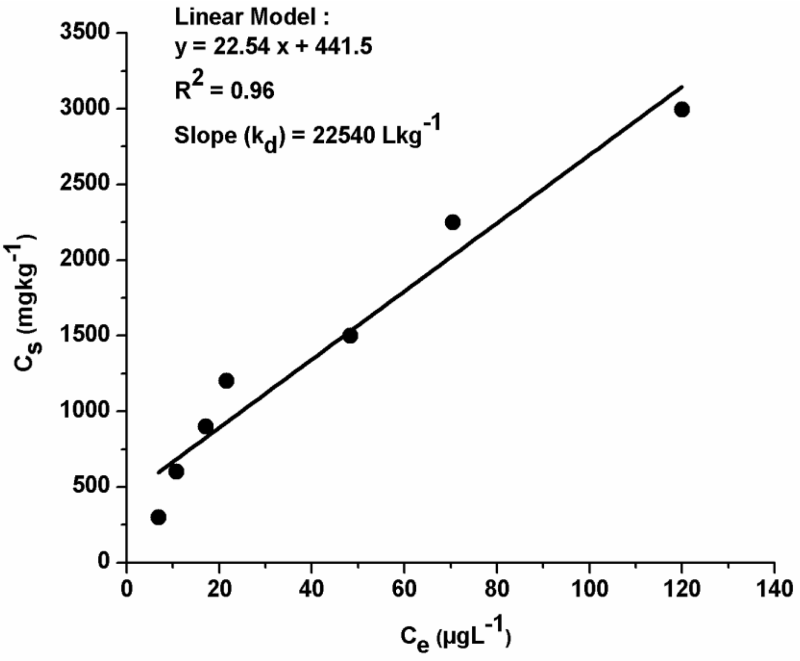

Fig. 6.7: Linear model for uranium adsorption on sediment

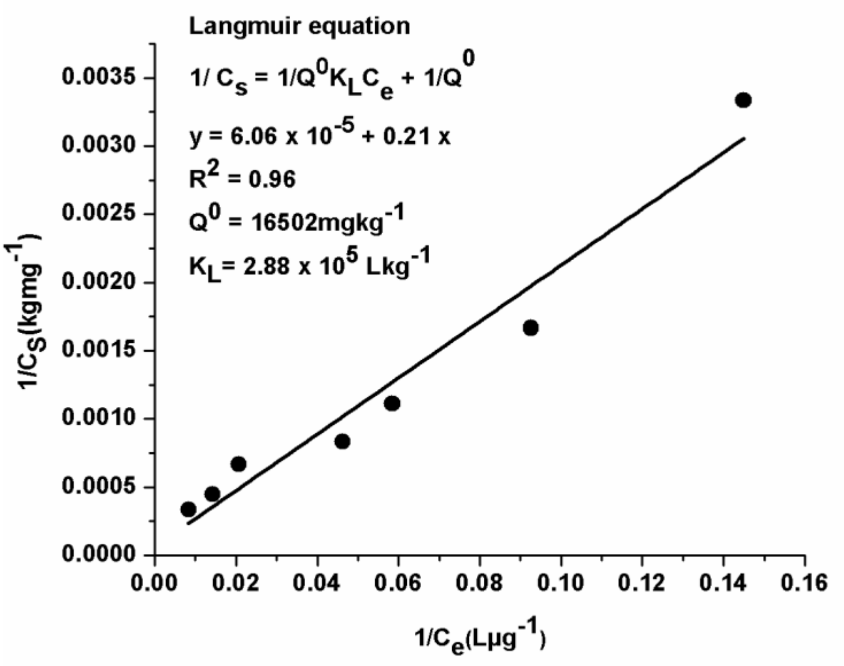

Fig. 6.8: Langmuir model for uranium adsorption on sediment

Similarly, for soil as depicted in **Figs. 6.9 – 6.11** for Th and **Figs. 6.12 – 6.14** for U, values for K_f constant for U and Th obtained in opposite to sediment and were determined to be 18200 Lkg^{-1} for Th and 11500 Lkg^{-1} for U, indicating that the sorption capacity of Th onto soil was about 58% higher than U. Values of K_f and K_L have shown the same trend for both U and Th which confirmed that U has low affinity to sorb onto soil as compared to Th. In addition, Langmuir adsorption maxima for U were found to be about 16 times higher than for Th.

6.3.3. Kinetic rates of uranium and thorium

At equilibrium condition, the rate constants (k) for thorium and uranium adsorption in seawater - sediment were determined using Eq. (7.2) and found to be in narrow range of 0.96 – 1.02d-1 (0.99d-1) for thorium and 0.96 – 1.07d-1 (mean: 1.01d-1) for uranium. Similarly, in soil-groundwater system, the values of k for thorium and uranium obtained to be in the range of 0.77 – 0.79 d-1(mean: 0.78d-1) and 0.73 - 0.77 d-1(mean: 0.74d-1).

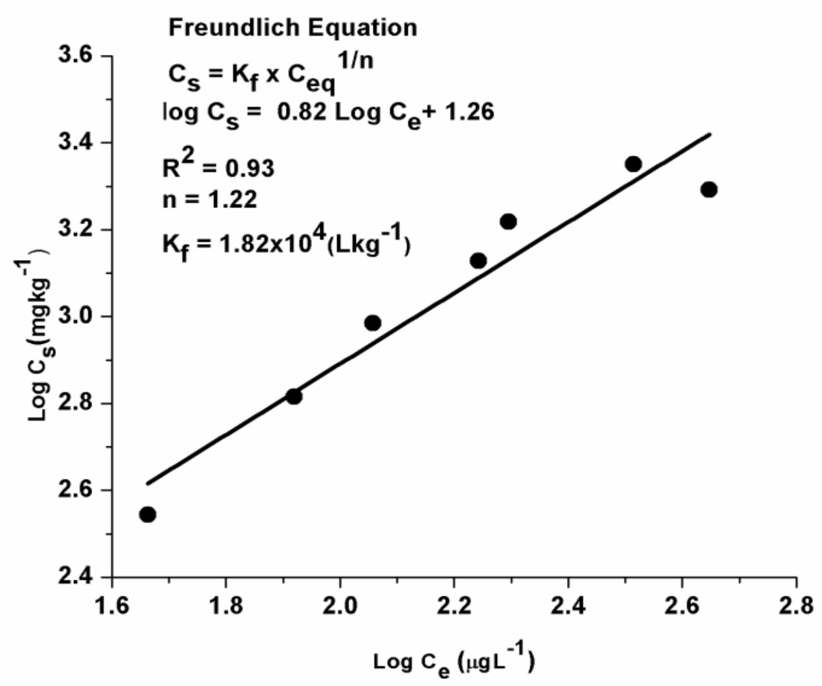

Fig. 6.9: Freundlich model for thorium adsorption on soil

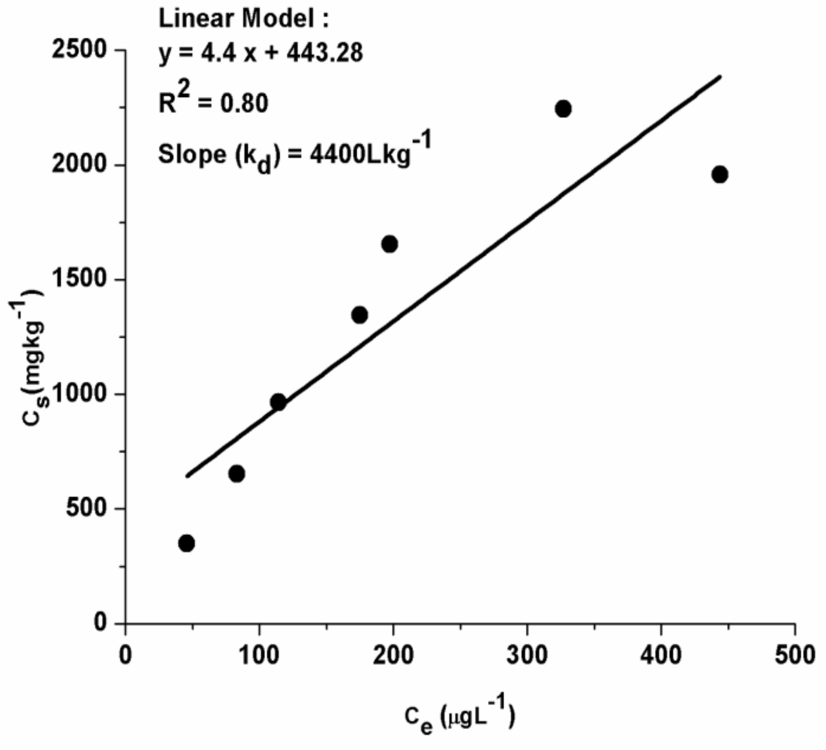

Fig. 6.10: Linear model for thorium adsorption on soil

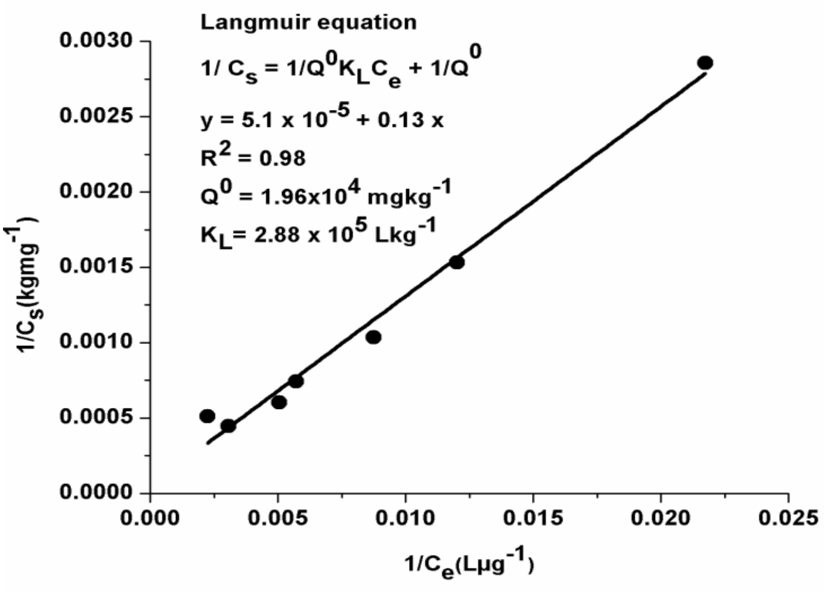

Fig. 6.11: Langmuir for thorium adsorption on soil

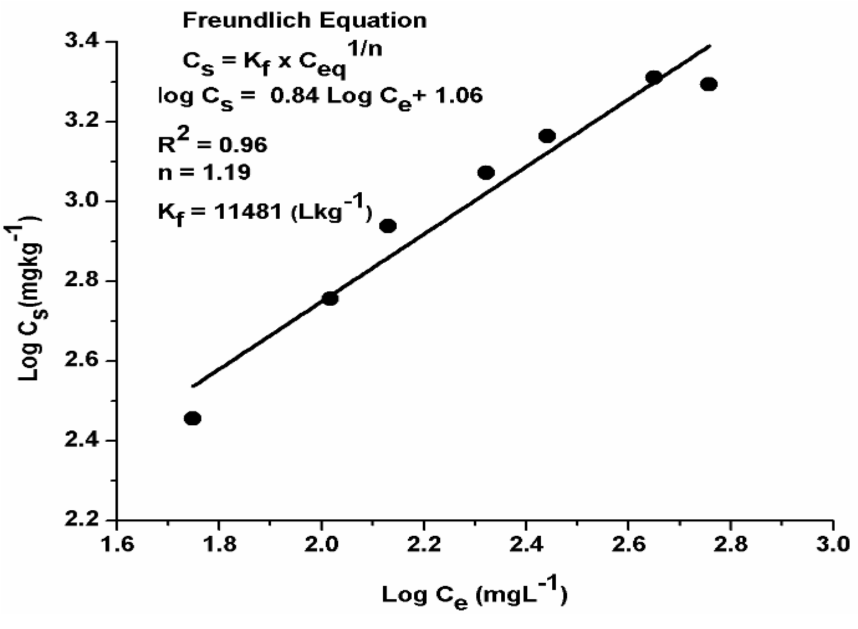

Fig. 6.12: Freundlich model for uranium adsorption on soil

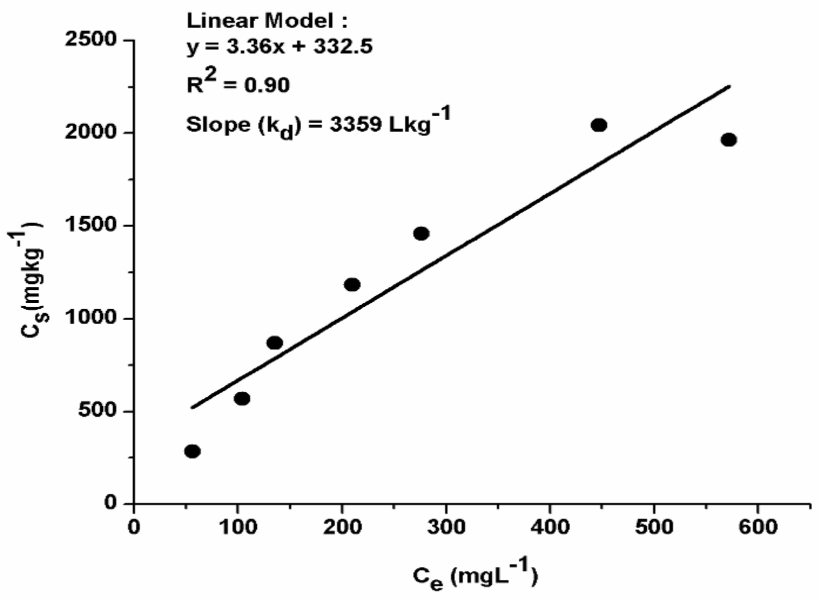

Fig. 6.13: Linear model for uranium adsorption on soil

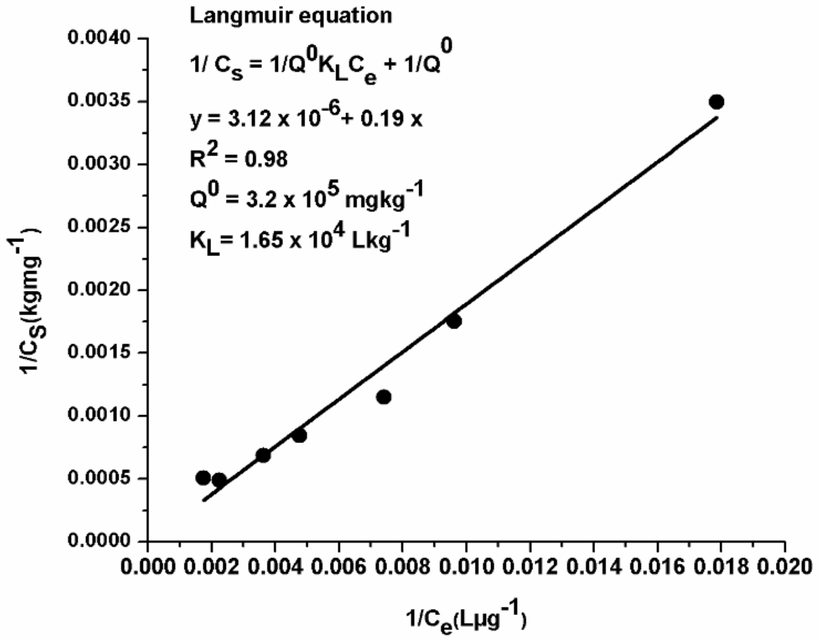

Fig. 6.14: Langmuir model for uranium adsorption on soil

Conversely, the values of k for uranium in seawater-sediment (**Fig. 6.15**) and groundwater-soil systems **(Fig. 6.16)** obtained from fitting the experimental results using least square method by **Eq. (7.3)** were derived to be 0.64d^{-1} and 0.83d^{-1} respectively. Initially, the amount of uranium in dissolved phases (seawater and groundwater) increased rapidly for the first 7 days and then continued slowly for upto 70 days.

In general, the dissolved uranium increased exponentially with time. The kinetic rate of U in sediment – seawater was about 30% slower than in soil-groundwater which may be due to high exchange of U with the calcium bearing minerals present as Ca- montmorillonite, dolomite and calcite in sediments and high composition of silt (79%) and clay (19%). This clearly shows that sediment has higher binding capacity and greater availability of exchange surfaces for U than soil. In soil, the percentage distribution of particle size in the form of sand, silt and clay was determined to be 23 %, 72% and 5% respectively. Due to high content of sand, availability of exchange surfaces for U in soil is small and subsequently it released into the groundwater.

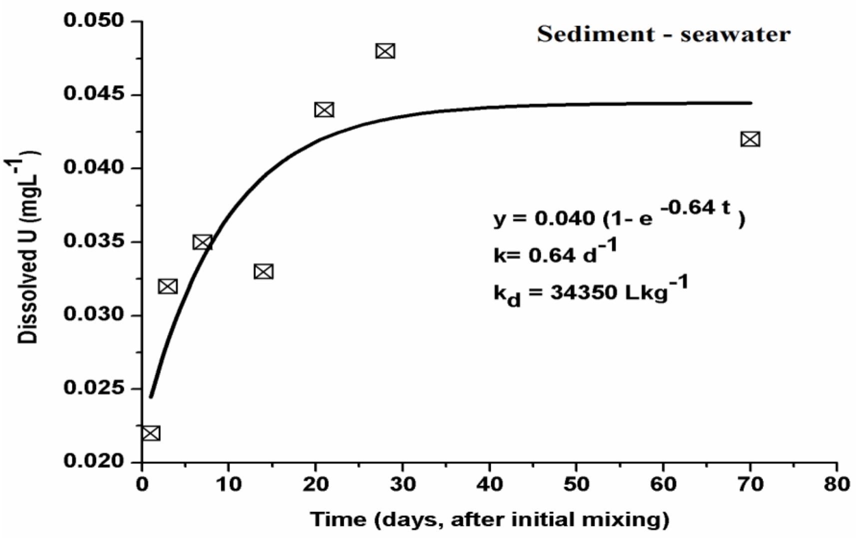

Fig. 6.15: Total dissolved uranium concentration as a function of time in sediment-seawater system

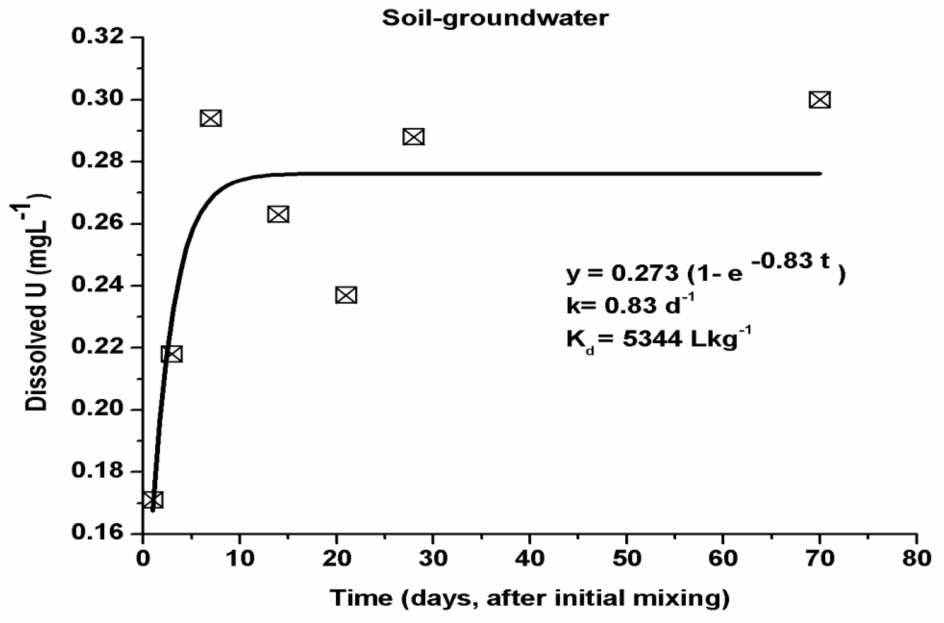

Fig. 6.16: Total dissolved uranium concentration as a function of time in soil-groundwater system

6.3.4. Speciation of U in equilibrium solution

The mean concentration of uranium in equilibrium solution of sediment-seawater and soil-groundwater system for Set-1 at 25^0C was determined to be 40 μgL^{-1}(~ 1.7 x 10^{-7}M) and 273 μgL^{-1}(~1.2 x 10^{-6}M). The pH of the equilibrated solution of seawater and groundwater ranged from 7.8-8.1 and 8.2-8.6 respectively. In equilibrium solution of groundwater, the predicted aqueous species as $(UO_2)_2CO_3\ (OH)_3^-$(aq) accounted for about 92% of the total dissolved U at the measured pH range. However in seawater, this species accounted for about 77% only. Since the major aqueous species is mixed hydroxo-carbonato complexes of U, therefore it is assumed that the complex is adsorbed onto sediment/soil surface and caused the removal of U. Under alkaline conditions, uranium forms anionic complexes and therefore cannot be efficiently adsorbed onto soil surface.

6.3.5. Impact of kind of minerals in sediment

In chapter 4, the various minerals present in the sediments were identified and quantified by the X-ray diffraction (XRD) technique which showed chlorite and illite as predominant clay minerals. In addition, significant amount of calcite, dolomite Ca–montmorillonite, talc, amphiboles, quartz and Na- montmorillonite were also present in the sediments. The slightly higher k_d values for uranium may be due to the presence of Ca-montmorillonite mineral in sediments which might be responsible for the uranium sorption because these minerals have high affinity for sorption of uranium due to exchange with Ca^{2+} ions in the mineral lattice [337]. Generally, sorption of the uranium and thorium is known to take place primarily as an exchange reaction with metal ions, particularly Ca^{2+}, Na^+ and K^+ present in the clay minerals such as Ca - montmorillonite, Na-montmorillonite, illite respectively. Vermiculites and zeolites, are known for their high adsorption capacity for many cations, however, are unable to adsorb relatively high concentration of both thorium and uranium [337].

6.3.6. Impact of humic acid (HA)

In presence of high inorganic carbonate concentration, there is little effect of HA on uranium adsorption. These inorganic carbonates with their high complexing ability towards uranyl ions predominate the influence of HA at pH 3.5 to 9.5. At acidic pH (3.5 - 6), the sorption of uranyl generally increased in the presence of HA which is due to increase in the negative sorption active sites on HA. However, sorption decreases at higher pH (> 6), probably due to formation of soluble uranyl humate complexes species [359]. As pH increases, the increased deprotonation makes the HA more negatively charged. This negative charge creates an electrical field which influences the complexation reaction. HA concentration must be high enough to influence the uranium adsorption onto minerals due to the competition from other anionic ligands especially in the slightly acidic to alkaline pH range.

In the present study, k_d values of U as a function of HA concentration for soil and sediment as depicted in Fig. 6.17 and Fig. 6.18 were obtained to be in the range of 1722 - 6677 Lkg^{-1} (mean: 3543 ± 2133 Lkg^{-1}) and 69 - 184 Lkg^{-1} (mean: 156 ± 39 Lkg^{-1}) throughout entire experimental respectively. However, in the absence of HA, the mean value of k_d observed to be 3050 ± 325 Lkg^{-1} and 48 ± 8 Lkg^{-1} for the same respectively. In soil, it is obvious that initially, in general, at low concentration (2.5 - 5 mg/L) of HA, k_d values of U was found to be maximum and thereby decreased as the HA concentration increased. Increasing concentration of HA to the soils may result in saturation of their sorption sites, thereby decreasing the sorption capacity due to surface precipitation. In general, for soil, k_d values sharply decreased as a function of HA concentration whereas sediment showed an opposite trend to soil i.e. as HA concentration increased, k_d values also increased.

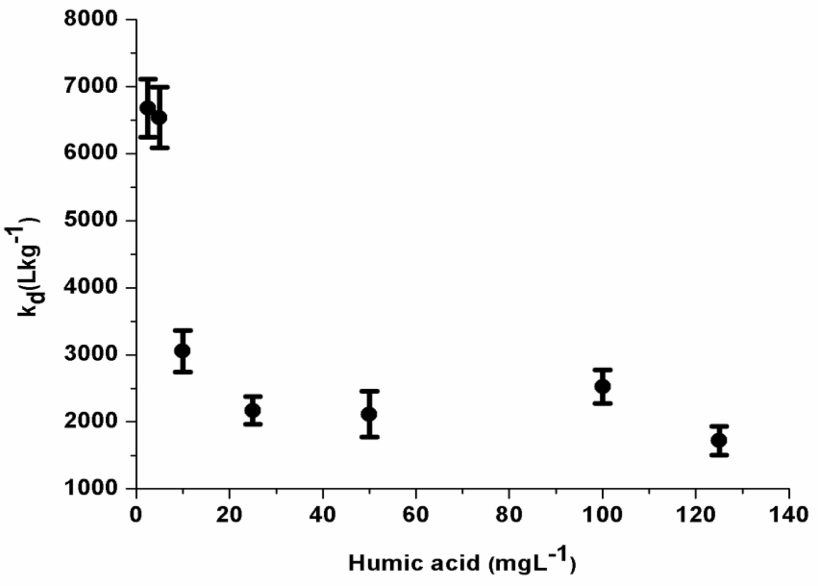

Fig. 6.17: Variation of k_d of uranium in soil as a function of HA concentration

The cationic uranyl ion (UO_2^{2+}) is weakly sorbed onto sediment, as indicated by the small k_d values in the absence of HA, so that it remains in the solution after sorption. The cationic uranyl ion remaining in the solution can be associated with HA which either is sorbed onto the soil (reaction f) or is dissolved (reaction a). The increasing trend of k_d values in sediment might be attributed to providing additional adsorption sites by HA due to their complexing ability or due to adsorption of uranyl humate complexes on mineral surface [360]. In fact, the sorption processes of reactions e and f possibly causes the increase in the k_d of uranium with an increase in the HA concentration (see Fig. 6.18). The various reaction processes predicted in the sorption experimental system in which 'M' represents a metal ion.

$$
\begin{aligned}
&M^{n+}(solution) \xrightarrow{reaction(a)} HA - M(solution) \\
&HA - M(solution) \xrightarrow{reaction(b)} M^{n+}(solution) \\
&M^{n+}(solution) \xrightarrow{reaction(c)} soil / se\dim ent \\
&Soil / Se\dim ent \xrightarrow{reaction(d)} M^{n+}(solution) \\
&HA - M(solution) \xrightarrow{reaction(e)} Soil / Se\dim ent \\
&M^{n+}(solution) \xrightarrow{reaction(f)} HA(Soil / se\dim ent)
\end{aligned}
$$

The FTIR spectra of soil (Fig.6.19) and sediment (Fig.6.20) were compared with the spectra of HA (Fig.6.21). The intensity of absorption bands depends on the amount of absorbing functional groups. This means that a high absorption indicates a high content of the corresponding functional group whereas a low absorption band indicates a low content of this group. The wave number indicates the kind of functional groups which are due to absorption.

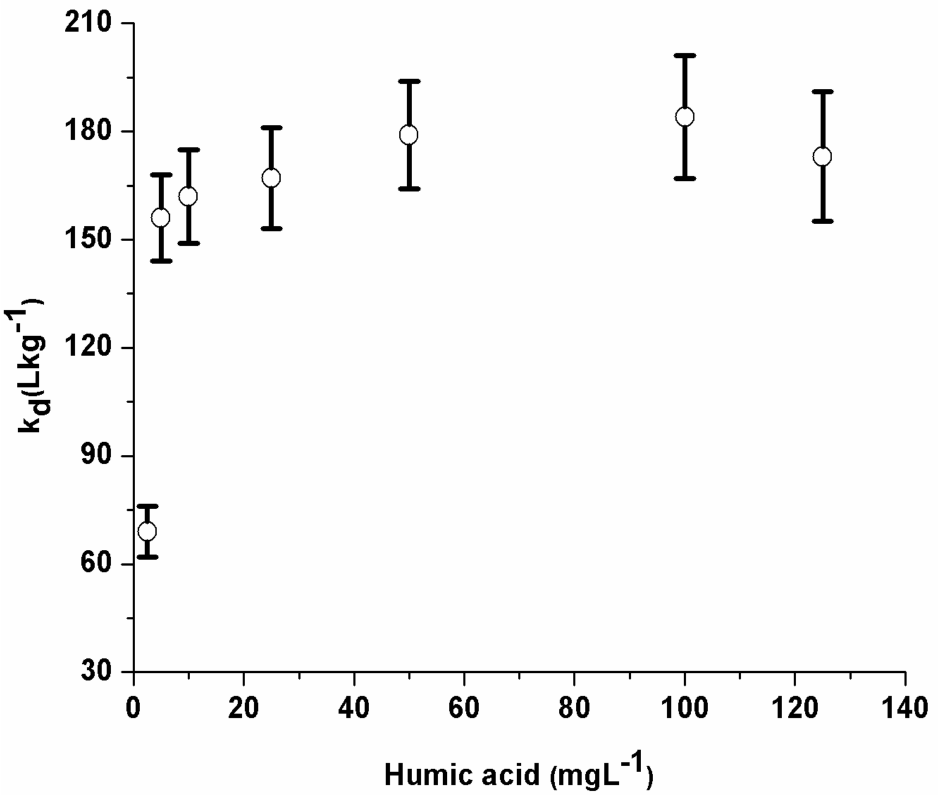

Fig. 6.18: Variation of k_d of uranium in sediment as a function of HA concentration

The wave number indicates the kind of functional groups which are due to absorption.

3500–3200 cm^{-1} due to hydroxyl groups (alcohols, phenols, water molecules),

2922–2926 cm^{-1} due to CH_3, CH_2, and CH groups of alkyls,

1701—1698 cm^{-1} and 1400 cm^{-1} due to carboxyls and carbonyl groups,

1600–1613 cm^{-1} due to aromatic C=C bonds conjugated with C=O bonds of unsaturated ketones or amides, and

1010 and 960 cm^{-1} due to C-O vibration of ether groups or symmetric stretching vibration of silicate group.

The FTIR spectrum of HA revealed the main absorption bands at 3317 cm^{-1} which represents H-bonded OH groups (alcohols, phenols, water molecules), the band at 1635 cm^{-1} related to C=0 stretching vibration of carboxylic (COOH) and ketonic (C=O) groups and the band at 670 cm^{-1} due to aromatic C=C and aliphatic C = C).

The FTIR spectra of sediment and soil have shown the main absorption band at the range of 3361-3374 cm^{-1}, 1634-1674 cm^{-1} and 996 cm^{-1} indicating that they represent H-bonded OH groups (alcohols, phenols, water molecules) and C=O stretching vibration of carboxylic and ketonic groups. In addition, the band at 996 cm^{-1} represents due to symmetric stretching vibration of silicate group, However, HA did not show any absorption band at this wave number. One can notice that first two absorption bands for soil and sediment were in very good agreement with the HA.

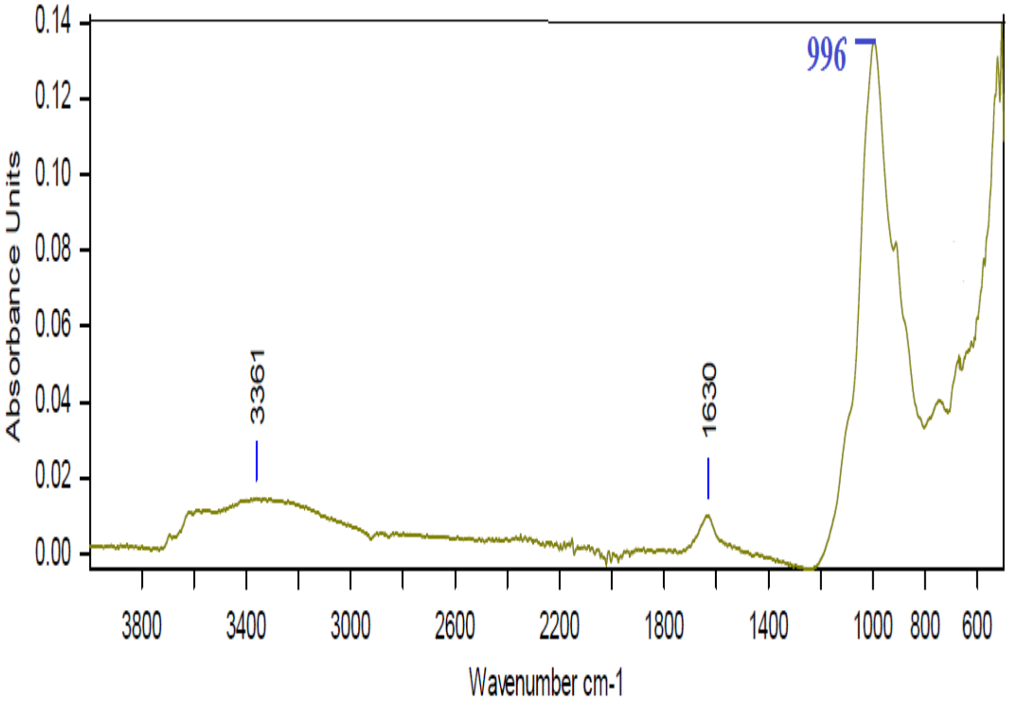

Fig. 6.19: FTIR spectra of soil

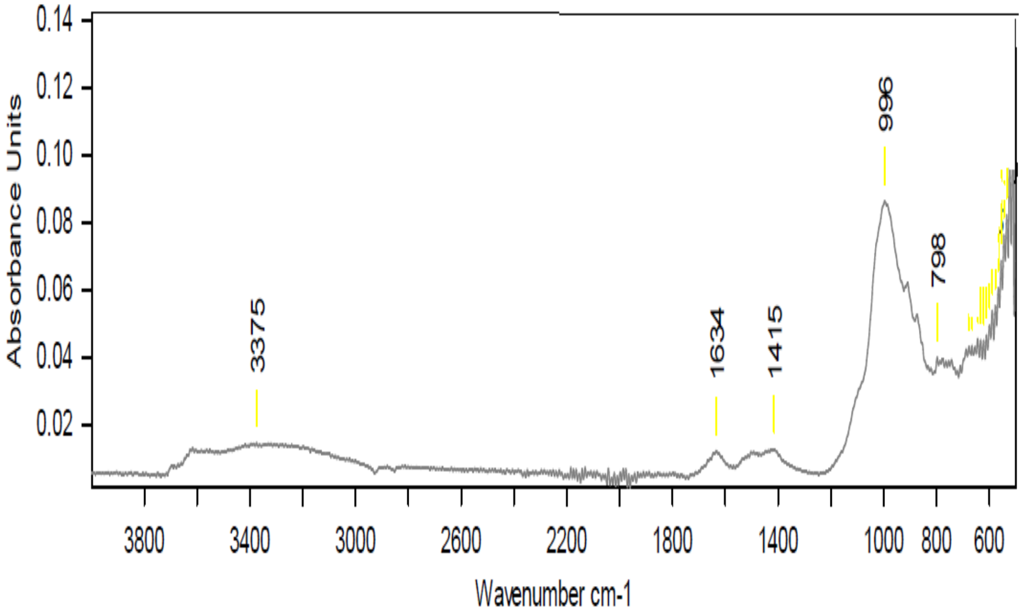

Fig. 6.20: FTIR spectra of sediment

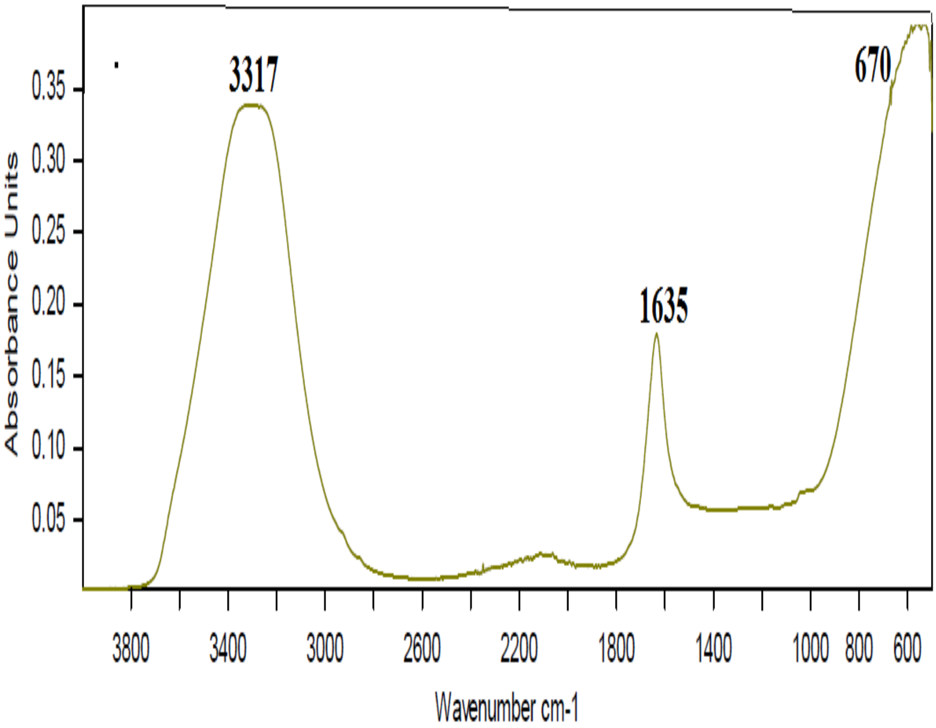

Fig. 6.21: FTIR spectra of HA

6.4. Conclusions

The sorption – desorption of uranium and thorium in sediment-seawater and soil-groundwater environment clearly indicates that k_d values are not only dependent on sediment/soil properties but also on the kinds of minerals present in sediments/soils. Among minerals, Ca bearing minerals such as Ca-montmorillonite, dolomite, calcite in sediments were estimated as predominant minerals in sediments which might be responsible for high uranium sorption. The high k_d values obtained for sediments revealed that they have higher binding capacity and greater availability of exchange surfaces for metals of interest than soil. The resulting data set showed that generally, at low concentration, k_d values of U and Th increased as a function of their concentration till achieving the saturation stage for both systems. After achieving the saturation stage, distribution coefficient observed to be almost constant and at sufficiently high concentration, k_d values decreased because the partitioning behavior deviates from ideality due to removal of species by precipitation. At high concentration, adsorption onto sediment/soil seems to be unspecific as seen by lower k_d values. The experimental results indicate that the U and Th sorption data for sediment/soil can be described satisfactorily by Freundlich and Langmuir adsorption isotherm models because both models showed a significant correlation. This indicates that there are more complex relationships with adsorption behavior of uranium and thorium on sediment/soil surface. Since, the Fruendlich constant (n) for uranium and thorium in both systems was found to be closer to unity. Therefore linear model was observed to be highly suitable. Based on the linear model, Th showed higher binding capacity for sediment/soil than U. According to Freundlich model, sorption of uranium in sediments observed to be higher than thorium while in the case of soil, thorium has shown more sorption capacity. The values for

K_L constant for thorium in sediments/soils were observed to be about one order of magnitude higher than uranium confirmed that Th has high affinity to sorb onto sediment/soil as compared to U. But as far as sorption maxima (Q^0) is concerned, U has shown high values of Q^0 for both system as compared to Th. It is also suggested that sorption experiments must be performed at low U/Th concentration to avoid precipitation of their hydroxides/carbonates. At the measured pH values of equilibrium solution, the speciation of U(VI) was dominated by hydrolysis and carbonate complexation under the measured redox potential which were caused for increasing the solubility of uranium in ground water/seawater. Because anions do not readily adsorb to mineral surfaces at basic pH conditions, the anionic charge of the aqueous U(VI) carbonate complexes at pH values greater than 6 result in decreased adsorption and thus increased mobility of uranium.

In addition, the humic-acid appears to be a key-component in studying the sorption processes of uranium onto soils/sediments. In soil, k_d values generally showed a decreasing trend with increasing the HA concentration whereas sediment exhibited an opposite trend to soil. The presence of humic substances in the soils considerably influences the soil acidity and the soil U(VI) retention properties, as shown by batch experiments.

CHAPTER 7

PREDICTION OF CHRONICLE DEPOSITION OF ^{238}U, ^{232}Th & $^{239+240}$Pu IN CORE SEDIMENTS USING RADIOMETRIC DATING OF ^{210}Pb, ^{137}Cs and ^{228}Ra/^{226}Ra IN MUMBAI HARBOUR BAY

7.1. Introduction

To predict the long term behavior of actinides in the marine environment, it is essential to know their chronological deposition in the bottom sediment of Mumbai Harbour Bay. Normally, three types of radioactive isotopes are present in the environment: those of primordial, cosmic ray and artificial origins. Although, the primordial origins are the most widely used in radiometric dating methods which are based on changes in the isotopic composition with time as a result of radioactive decay.The time elapsed can then be determined from the initial and final isotopic compositions. Isotopes of artificial origins, such as ^{137}Cs, ^{60}Co, and ^{54}Mn have also been used in radiometric dating which are based on their irregular rate of influx or their absence in the environment before 1945 [361]**.** In the present study, the chronological deposition of actinides in sediment system was studied using radiometric dating of both primordial (^{210}Pb and ^{226}Ra/^{228}Ra) and artificial (^{137}Cs) radionuclides.

Sediments at the bottom of lakes, seas and oceans can serve as a unique archive of climate and environmental data. These are collected and studied by a variety of geophysical and geochemical in order to obtain proxies of different parameters for water bodies and the climate in the past times. Past conditions can be reconstructed using these indicators and compared to the present situation. Estimation of the age profile of sediment cores is an important part of climate and environmental research, because the obtained data would be often worthless without information about the age of a specific sample. The chronological methods used in environmental research for determination of sedimentation rate at Holocene scale have been classified into two important categories; a) radiometric and b) non-radiometric.

Sedimentaion rate at a moderate time scale i.e 50 -150 years can be determined by using excess ^{210}Pb methods. ^{210}Pb ($T_{1/2}$ = 22.3 years), a naturally occurring radioisotope is a member of the ^{238}U decay series and is continuously introduced into the marine environment by deposition from the atmosphere. Radioactive disequilibrium between ^{210}Pb and its precursor ^{226}Ra (half-life 1600 years) arises through the mobility of the intermediate gaseous radionuclide ^{222}Rn. A proportion of the ^{222}Rn formed by ^{226}Ra decay in continental soils diffuses into the atmosphere where it decays to ^{210}Pb [362]**.** This radionuclide is readily attached to airborne particulates and removed from the atmosphere both by wet and dry deposition/precipitation.

Fallout over the sea is subsequently transported through the water column and incorporated in the bottom sediments. Total activity in sediments will include both the atmospherically-derived ^{210}Pb and the supported ^{210}Pb derived from the in situ decay of ^{226}Ra. The supported component is usually assumed to be in equilibrium with the parent ^{226}Ra. The unsupported atmospheric component used in sedimentation rate is determined by subtracting the ^{226}Ra activity from the total ^{210}Pb activity. This is plotted against depth and the slope of this line can be used to calculate the sedimentation rate, knowing the radioactive decay constant of ^{210}Pb. The sedimentation rate can be obtained by dividing the ^{210}Pb decay constant by the slope of the log-linear plot of unsupported ^{210}Pb versus depth [362].

Several observations have directed to assess the unsupported ^{226}Ra concentrations in coastal marine sediments as a geochronometer. First of all, a radioisotope with a half-life of thousands of years is desirable for slope and shelf sediments whose rates of accumulation may be intermediate between those of the open ocean (millimeters to centimeters per thousand years) and those of the inshore zone (millimeters to centimeters per year).

One of the most promising methods for estimation of sedimentation rate on a time scale of 100 years is by means of ^{210}Pb [363, 364]**.** The ^{210}Pb method was initiated by Goldberg (1963**)**, then applied to lake sediments by Krishnaswamy et al. (1971) [365] and subsequently introduced to marine sediments by Koide et al. (1972) [366]. It has been very popular in estimating the sedimentation rate of marine sediments [367 – 370]. $^{\mathbf{210}}$Pb has previously been applied as a tracer of various marine processes in the western Mediterranean basin [371 – 375] and other oceanic regions. In fact, ^{210}Pb is one of the most widely used radiotracers to study environmental processes. It has been commonly used to study biogeochemical processes in the oceans [376, 377], atmospheric deposition and anthropogenic contamination [378,379]**,** sedimentary processes [380, 381] and sediment geochronology [382 – 384]**.** A major concern in dating sediments is the problems of mixing and redeposition which may affect the distribution of the radionuclides. This is due to the dynamic nature of the system as opposed to the normal application to areas such as lakes and estuaries which have a well-behaved depositional pattern. As ^{210}Pb method performs best in relatively quiet depositional environment such as marsh lands [385, 386], bays and lakes [387, 388]**.**

One of the key parameters of the ^{210}Pb cycle in the environment is its atmospheric flux, knowledge of which is required for dating recent reservoirs and assessment of soil erosion, sediment processes and biogeochemical processes in the oceanic water column. It is well known that the ^{210}Pb deposition to the Earth’s surface is higher over continents than oceans and varies with season, longitude and local meteorological conditions [389]. The most common procedure to estimate the ^{210}Pb flux is by collecting wet and dry deposition during periods long enough to accommodate seasonal and episodic variations. The ^{210}Pb flux is also determined in natural repositories such as ice cores, lake/ocean sediments and soils that integrate long-term deposition [389, 390].

Like ^{210}Pb, ^{137}Cs (artificial radioisotope formed by nuclear fission with half-life of approximately 30 years) which has been introduced into the atmosphere in irregularly varying amounts since 1945 [391] is also strongly bound by sediments. It will therefore become trapped by the uppermost layer of the sediment and as this layer is buried by succeeding ones. Dating of the sediment is thus possible by determination of the ^{137}Cs concentration in each interval in the sediment sequence and by correlation of the resulting pattern of ^{137}Cs concentrations with the pattern of atmospheric levels since 1945**.** The concentration of ^{137}Cs in the atmosphere peaked sharply (at levels more than an order of magnitude higher than in previous years) in 1958-1959 and 1962- 1963 with a further peak in 1971 [392]**.** As a result, these intervals have shown a significant correlation with the first appearance of detectable amounts of ^{137}Cs in the late 1940's or early 1950's. This method has also been used to date a variety of sediment and non-sediment samples.

^{137}Cs is known to be the most abundant fallout radionuclide present in the marine environment, the concentration varying from region to region, according to the specific sources of contamination and the geographical locations. In most sedimentary environments, ^{137}Cs is deposited as fallout which is rapidly and strongly fixed by sediment particles [393]**.** Further, ^{137}Cs redistribution occurs in association with sediment particles. Dating with ^{137}Cs data is based on assumptions of certain ages for particular parts of its depth profile [394, 395]**.**

Robbins and Edgington (1975) have used both ^{210}Pb and ^{137}Cs to establish anthropogenic inputs of lead from coal and gasoline used in Lake Michigan sediments [396]. Benninger (1978) has used ^{210}Pb to determine lead fluxes in Long Island Sound [397] and Smith and Walton (1980) have used ^{137}Cs to determine the sedimentation rate in a fjord in Quebec [398]**.** A major concern in dating sediments will be problems of mixing and redeposition which may affect the distribution of the radionuclides. This is due to the dynamic nature of the system as opposed to the normal application to areas such as lakes and estuaries which have a well-behaved depositional pattern. It has also been shown by a number of authors that ^{210}Pb [399], ^{137}Cs [396, 398] and various other radionuclides are significantly affected by the finest size fractions (silt and clays) of sediments.

Although the annual flux of ^{210}Pb to sediments has been shown to remain relatively constant from year to year [361, 397], the same is not necessarily true over shorter periods of time. The atmospheric concentrations of both ^{210}Pb and ^{137}Cs [400] in fact, have been shown to fluctuate at some sites by nearly an order of magnitude over periods of several days and also from season to season. Such behavior is indeed not surprising, as weather conditions will clearly affect the transport of nuclides such as ^{222}Rn, ^{210}Pb and ^{137}Cs within the atmosphere as well as the emanation of radon from crust. By scavenging locally available ^{210}Pb and ^{137}Cs, rainfall can also be expected to cause temporarily increased (and later decreased) fluxes of both of these isotopes [361]**.** As mentioned by Krishnaswami, this effect has not been significant in most previous studies because deposition has been continuous and individual samples have typically represented a year or more of such deposition.

Generally, ^{210}Pb and ^{137}Cs are important tools in the determination of sediment accumulation rates or sedimentation rates and in the understanding of processes which control sediment deposition [401, 402]. One alternative approach is to utilize the expected in-growth of ^{228}Ra to secular equilibrium with its parent ^{232}Th to provide a new geo-chronometer. On interaction with the higher ionic strength of ocean water, radium partially desorbs from sediment through ion exchange, resulting in an activity deficit between the radium isotopes and their respective parent isotopes in recently deposited sediment [403]. With time and burial, radium isotopes grow into secular equilibrium as a function of their half lives, which determines sedimentation rates. In-growth of ^{228}Ra ($t_{1/2}$ = 5.8 y) relative to longer-lived ^{226}Ra ($t_{1/2}$ = 1600 y) with depth in the seabed could be a viable geo-chronometer on about a 30 year time scale.

7.2. Materials and methods

7.2.1. Sampling and pretreatment

A total of three core sediment samples in duplicate were collected at seawater depth (1.5 m) from three potential locations viz SCL-3, SCL-5 and SCL-9 **(see Fig.2.1)** within 3 nautical mile area from the discharge location of CIRUS using a sediment corer. Detailed of sampling were already discussed in section 2.5.2 (Chapter 2). The core samples were sliced into 4 cm fractions, collected in polyethylene bottles with screw caps and transported to the laboratory and stored at 4^0C till further analysis. The depth of the core was up to 40 - 44 cm.

7.2.2. Laboratory analyses

Each fraction was dried at 110ºC for 24 h, ground with a mortar and pestle, homogenized and sieved through a 2 mm mesh sieve. About 100 - 250 g of meshed samples were transferred to a pre-weighed cylindrical acrylic container with dimension of 75 mm diameter x 75 mm height (331cm^3), sealed and kept for 30 days to allow for growth of radon gas in order to achieve secular equilibrium between ^{226}Ra, ^{214}Pb and ^{214}Bi in the ^{238}U decay chain and between ^{212}Pb, ^{208}Tl and ^{228}Ac in the ^{232}Th decay chain. The activity of ^{226}Ra in each core fraction was determined using Gamma spectrometry system by taking the average activity of two separate photopeaks of two radon daughters: ^{214}Pb at 352 keV and ^{214}Bi at 609 keV. Similarly, ^{228}Ra activity was estimated by average gamma peaks of ^{228}Ac (911 and 969 keV) and ^{232}Th activity, from the average concentrations of ^{212}Pb (238.39 keV), ^{208}Tl (583 keV and 2614 keV). The activity of ^{137}Cs was determined using photopeak at 662 keV. The details of gamma spectroscopy are discussed in section 4.2.3 (**Chapter 4).**

7.2.3. Analytical methods and alpha spectroscopy

^{210}Pb (assuming secular equilibrium with ^{210}Po) measurements in core fractions were carried out on 1 g of dried, ground sediment sample which was digested in a microwave digestion system with a ^{209}Po tracer with HF and HNO_3 (1:1) and H_2O_2 in Teflon beakers under sediment digestion program setting accordingly to manual from manufacture. ^{210}Po and ^{209}Po were chemically plated onto silver discs from 0.5 N HCl solutions at 90^0C for three hours after reducing Fe using ascorbic acid. ^{210}Po activity was measured at alpha energy of 5.30 MeV using ^{209}Po (4.88 MeV alpha emission) as the internal tracer by alpha spectrometry (ORTEC, OCTAT) with 13% efficiency, 20 keV resolutions and 300 mm^2 areas with a depletion depth of 100 mm Chemical yields using a ^{209}Po tracer ranged from 87 to 92%. **Fig.7.1**.depicts the typical spectrum of ^{210}Po and tracer ^{209}Po in sediment samples using alpha spectrometry system.

7.2.4. Estimation of sedimentation rate, fluxes and residence time

The total ^{210}Pb activity in sediments is comprised by the supported and unsupported components. Supported ^{210}Pb, derives from in situ decay of the parent radionuclide ^{226} Ra and unsupported ^{210}Pb derives from the atmospheric flux. Measured ^{210}Po activity gives the total ^{210}Pb. Unsupported ^{210}Pb is determined by subtracting supported concentration at every levels**.** Extensively used mathematical models in determining sediment chronology are CFCS (Constant Flux Constant Sedimentation Rate), CIC (Constant Initial Concentration) and CRS (Constant Rate of Supply). CFCS model assumes that the unsupported ^{210} Pb concentrations in each section along the core are the same and equal its initial ^{210}Pb concentration and sediment accumulation rate are constant. First, logarithmic plots of unsupported ^{210}Pb concentrations versus sediment depths are made. Then, if the profile distribution of unsupported ^{210}Pb concentrations exponentially decreases, this model is applicable to determine the recent chronology [404]**.**

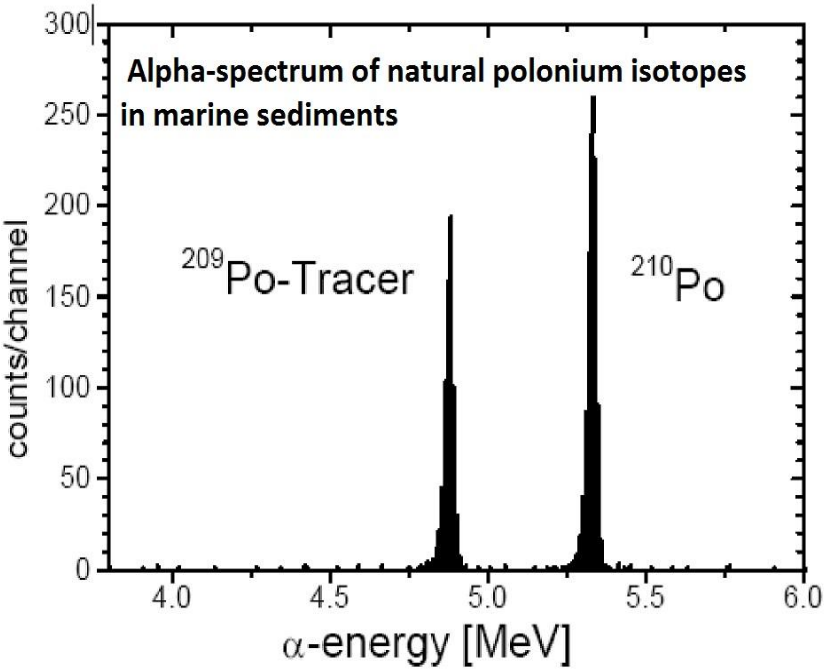

Fig.7.1: The typical spectrum of ^{210}Po and tracer ^{209}Po in sediment samples using alpha spectrometry system

The CRS model allows the sedimentation rate to vary as long as fluxes of unsupported ^{210}Pb to the surface sediment remain constant. McDonald and Urban, (2007) abbreviated the model as it relies on the ratio of the cumulative residual unsupported ^{210}Pb beneath a given depth to the total unsupported ^{210} Pb activity in the sediment column [405]**.** According to the Appleby (2001) CIC model suppose that sediments have a constant initial ^{210}Pb concentration but varying ^{210}Pb flux to the sediment surface and varying sediment accumulation rates due to the non-monotonic decrease in profile distribution of unsupported ^{210}Pb concentrations.

Generally, the depth distribution of radionuclides in undisturbed sediment is expected to exhibit an exponential decline with depth [406] and can be written by the following equation,

$$C_x = C_0 e^{-\alpha x}$$
$$or$$
$$\log C_x = \log C_0 - \frac{\alpha}{2.303} x \qquad \textbf{(Eq.7.1)}$$

The sedimentation rate of radionuclides (eg. ^{137}Cs), can be calculated using the following equation;

$$C_x = C_0 e^{-\left(\frac{\lambda}{S}\right)x}$$
$$or$$
$$\log C_x = \log C_0 - \frac{\lambda}{2.303 * S} x \qquad \textbf{(Eq.7.2)}$$

In the case of ^{210}Pb, the sedimentation rate in the sediment profile can be determined using the following modified equation;

$$\log(^{210}Pb_{ex}) = \log(^{210}Pb_{ex}^{0}) - \frac{\lambda_{210}}{2.303 * S} x_i \qquad \textbf{(Eq.7.3)}$$

Plotting log (^{210}Pb$_{ex}$) versus linear depth (x), the sedimentation rate can be obtained from slope of the line m = $-\lambda_{210}/2.303*S$. In the above equations, C_x and C_0 are the activity concentration of the radionuclide (Bq kg^{-1}) at depth x (cm) and at x = 0 respectively, S = sedimentation rate (cm y^{-1}), λ = radioactive decay constant of radionuclides (y^{-1}), α (cm^{-1}) is the linear attenuation coefficient representing the characteristics of the distribution. The value of α depends on the chemico-physical properties of the radionuclide, the sediment type and the elapsed time since deposition.

In ocean water, radium partially desorbs from sediment through ion exchange, resulting in an activity deficit between the radium isotopes and their respective parent isotopes in recently deposited sediment. Thus sedimentation rates (S) are calculated using the general in- growth equation, for ^{228}Ra to secular equilibrium with its parent ^{232}Th and subsequently applied to the vertical profile of activity ratio of ^{228}Ra/^{226}Ra in the seabed. The equation is as follows;

$$\frac{^{228}Ra}{^{226}Ra} = \frac{^{232}Th}{^{226}Ra}\left(1 - e^{-\lambda t}\right) \qquad \textbf{(Eq.7.4)}$$

$$\frac{^{228}Ra}{^{226}Ra} = \frac{^{232}Th}{^{226}Ra}\left(1 - e^{-\lambda \frac{x_i}{S}}\right) \qquad \textbf{(Eq.7.5)}$$

Where, λ is decay constant for ^{228}Ra (0.121 y) and t is the time (y), Rearranging the above equation, the general equation gives:

$$\ln\{1 - \left[\left(\frac{^{228}Ra}{^{226}Ra}\Big/\frac{^{232}Th}{^{226}Ra}\right)\right] = -\lambda \frac{x_i}{S} \qquad \textbf{(Eq.7.6)}$$

Plotting ln {1 - [(^{228}Ra/^{226}Ra)/(^{232}Th/^{226}Ra)]} versus depth (x), the sedimentation rate can be obtained from slope of the line m = -λ/S.

Also, the age of sediment (*t*) can be determined using the following formula

$$t = \frac{x_i}{S} \qquad \textbf{(Eq. 7.7)}$$

The radionuclides content above certain depth sediment profile can be described by the Profile-Distribution Model [407 – 409]. The amount of radionuclides declines exponentially with depth and their cumulative amount with depth can be expressed as:

$$A(x) = A_{ref}(1 - e^{-x/h_0})$$

(Eq. 7.8)

Where, *A(x)* and A_{ref} are the inventory of ^{210}Pb (Bq m^{-2}) above depth *x* (kgm^{-2}) and the total one in sediment, respectively. The coefficient h_0 is a relaxation mass depth (kgm^{-2})

representing the radionuclides penetration into the sediment. The method of least squares was used to determine the h_0 for radionuclides.

Alternatively, the inventory of radionuclides at particular depth x (cm) is calculated as follows [410, 411],

$$A(x) = \sum_{i=1}^{n} C_i . \times \rho_{b\,i} \times x_i \qquad \textbf{(Eq. 7.9)}$$

i is the sample index, n is the number of the deepest sample with detectable activity of radionuclides, x_i is the thickness of core fractions at i^{th} layer, ρ_b is the dry bulk density of the sediments.

Since, radionuclides content in sediment profile also changes with cumulative relaxation mass depth (h_0), therefore, sediment accumulation rate (ϖ) in terms of $gcm^{-2}y^{-1}$ can be obtained by plotting the logarithmic function of activity ($Bq\ kg^{-1}$) of radionuclides as a function of h_0 (kgm^{-2}) using the following equation [364],

$$\log C(h_0) = \log C(0) - \frac{\lambda}{2.303 * \omega} h_0 \qquad \textbf{(Eq. 7.10)}$$

Finally, sedimentation accumulation rate (ω) can be determined from the obtained value of slope ($-\dfrac{\lambda}{2.303 * \omega}$) of the profile using a least-square fit procedure.

The cumulative deposition rate or flux (F) of ^{210}Pb or $^{210}Pb_{ex}$ in terms of $kBqm^{-2}y^{-1}$ was calculated as

$$F = \frac{A_x * S}{x_i} \qquad \textbf{(Eq.7.11)}$$

However, the deposition rate or flux of ^{137}Cs was calculated as

$$F = A_{ref} \times \lambda_{Cs} \qquad \textbf{(Eq. 7.12)}$$

For a system at steady sate, the activity of the radioactive parent equals to the activity of radioactive progeny plus the activity lost when the progeny is removed from the system by particle scavenging. The radioactive decay equation can be written in terms of the radioactive progeny

$$\frac{dN_2}{dt} = \lambda_1 N_1 - \lambda_2 N_2 \qquad \textbf{(Eq.7.13)}$$

Where, N_1 and N_2 are the number of parent and progeny atoms and λ_1 and λ_2 are the respective decay constants.

Rate of change of ^{210}Pb activity is calculated by taking the difference between its parent ^{226}Ra activity and the sum of activity of ^{210}Pb and its physical removal rate from the system which is given by the following equation

$$\frac{dN_{210}}{dt} = \lambda_{226} N_{226} - \lambda_{210} N_{210} - kN_{210} \qquad \textbf{(Eq.7.14)}$$

Assuming there is no change in the amount of ^{210}Pb, then under steady state of a system,

$$\frac{dN_{210}}{dt} = 0$$

Therefore, the value of removal rate/scavenging rate (*k*) in y^{-1} can be calculated as,

$$k = \lambda_{210} \left[\frac{A_{226}}{A_{210}} - 1 \right] \qquad \textbf{(Eq.7.15)}$$

Since, in sediment, $A_{226} < A_{210}$, therefore, in this study, only magnitude value of k has been considered.

Subsequently, the residence time (R_t) for ^{210}Pb with respect to scavenging in sediment will be as,

$$R_t = \frac{1}{k} \qquad \textbf{(Eq.7.16)}$$

Where, N_{226} and N_{210} are the number of ^{226}Ra and ^{210}Pb atoms respectively, λ_{226} and λ_{210} are their respective decay constants in y^{-1}. A_{226} and A_{210} are the activity concentration of ^{226}Ra and ^{210}Pb in Bqkg^{-1}. In the above equations, deep mixing is assumed to be negligible; hence the calculated migration sedimentation rate represents the upper limit of the true sediment accumulation rate [397].

7.3. Results and discussions

7.3.1. Depth distributions

7.3.1.1. Concentration profile of ^{226}Ra and ^{210}Pb

The activity levels of ^{226}Ra in cores of SCL- 3, SCL-5 and SCL-9 varied from 16.3 to 26.3 Bq kg^{-1}, dry (mean: 22.2 ± 3 Bqkg^{-1}, dry) and 6.7 to 15.7 Bqkg^{-1}, dry (mean: 11.2 ± 3 Bqkg^{-1}, dry) and 1.75 to 6 Bqkg^{-1}, dry (mean: 2.58 ± 1.4 Bqkg^{-1}, dry) respectively. However, in the case of total ^{210}Pb, the activity levels for the same ranged from 20.2 to 48 Bqkg^{-1}, dry (mean: 37 ± 10.8 Bqkg^{-1}, dry), 10.2 to 28.6 Bqkg^{-1}, dry (mean: 21.5 ± 7.2 Bqkg^{-1}, dry) and 10 to 28 Bqkg^{-1}, dry (mean:18.7 ± 6.2 Bqkg^{-1}, dry) respectively. The depth distributions of ^{226}Ra and ^{210}Pb concentrations in the cores are plotted against depth from the sediment surface as shown in **Fig. 7.2 and Fig.7.3** respectively. The mean activity ratios of ^{210}Pb/ ^{226}Ra in cores of all the three locations was found to be 1.67, 1.91 and 7.25 respectively indicating that ^{210}Pb is highly particle reactive, immobile and less soluble than ^{226}Ra. The comparatively higher activity of ^{210}Pb might be due to atmospheric fall-out by ^{222}Rn decay, addition of significant amount of rainwater by heavy rainfall and preferential accumulation in the mud containing fine particles due to industrial activities. **Pillai et al. (1988)** have reported the ^{210}Po activity in the rainwater at the studied area as 0.04 BqL^{-1} [412].

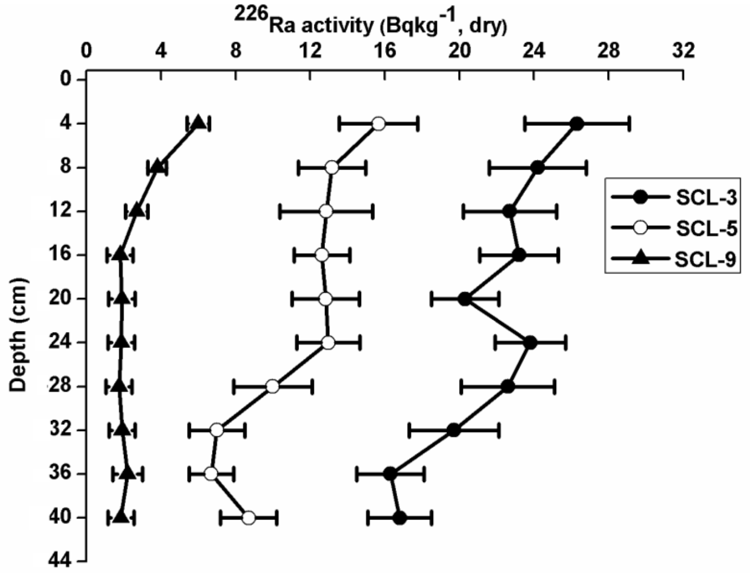

Fig.7.2: Depth profile distribution of ^{226}Ra in cores of SCL-3, SCL-5 and SCL-9

Due to high particle-reactive nature of ^{210}Pb (^{210}Po), it could be easily removable from seawater to the sediment by chemical scavenging, the process which is believed to be dominated by biogenic particles in the open sea. It is also observed that aerosol ^{210}Pb falling directly on surface waters is rapidly scavenged by suspended matter and is subsequently removed to sediments where it may be buried by subsequent accumulations [413]. However, for ^{226}Ra, it has long been established that in the oceans, it is primarily derived from sediments by radioactive decay and lost to seawater by diffusion. In cores of SCL-3, SCL-5 and SCL-9, overall the profile distributions of ^{226}Ra and ^{210}Pb showed a linear decreasing trend with increasing depth. This suggests that the bottom layers of cores are in more compact undisturbed sedimentary environment

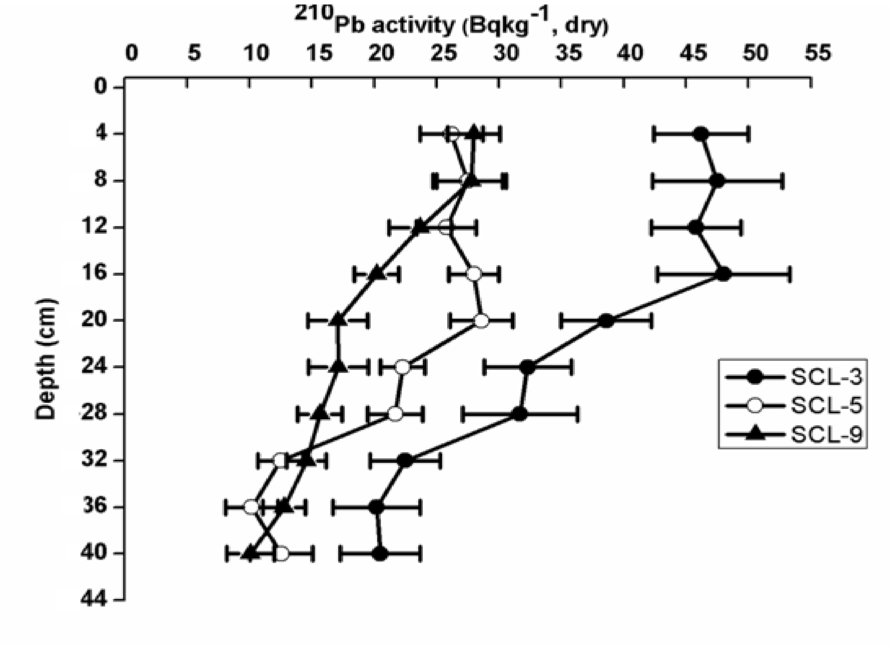

Fig. 7.3: Depth profile distribution of total ^{210}Pb in cores of SCL-3, SCL-5 and SCL-9

An elevated value of ^{210}Pb activity on the surface sediment might be caused by the settling particles produced from the atmosphere and land or the older sediment issued from the resuspension processes [414]. On the other hand, in some literatures, it is observed that ^{210}Pb increases monotonically with depth due to the particulate scavenging [415]. The factors that influence the accumulation of ^{210}Pb include sediment grain-size and organic matter content [416]**.** Linear or irregular profile of ^{210}Pb activity is an indication of complex hydrodynamics and changing sedimentary environment or rapid changes in sediment supply, source or energy conditions [417]**.** It may also be due to disruptions in the normal process of sediment accumulation or mixing of the surficial sediments by physical or biological processes. The accumulation of radionuclides in the studied area might be also affected by the changes in the silt/sediment load.

7.3.1.2. Concentration profile of ^{137}Cs

The depth profile activity concentration of ^{137}Cs in core sediments of SCL-3, SCL-5 and SCL -9 as depicted in **Fig.7.4** ranged from 126 to 562 Bqkg^{-1}, dry (mean: 271.4 ± 148 Bqkg^{-1}, dry), 9 to 39 Bqkg^{-1}, dry (mean: 19 ± 10 Bqkg^{-1}, dry) and 42 to 90 Bqkg^{-1}, dry (mean: 58 ± 17 Bqkg^{-1}, dry) respectively These levels are on lower side as compared to others equivalent scenario internationally like La hague, France and UK nuclear reprocessing plants.

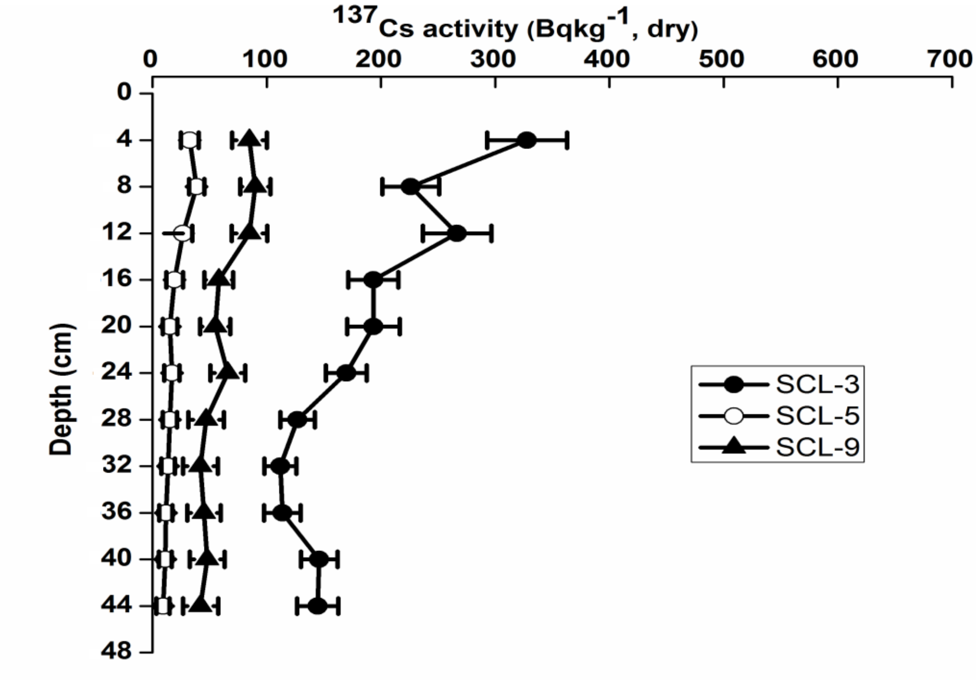

Fig. 7.4: Depth profile distribution of ^{i37}Cs in cores of SCL-3, SCL-5 and SCL-9

The levels of ^{137}Cs in the cores of Arctic waters were reported to be 8 ± 3.7 Bqkg^{-1} (Barents Sea) and 13.6 ± 6.8 Bqkg^{-1}dry weights (Kara Sea) and for surface marine sediments from the Bay of Ghazaouet on the Algerian coast as 6.9-8.6 Bqkg^{-1} [418 - 420].

Overall, ^{137}Cs concentrations at the top layer (upto 8 cm) were quite uniform which might be influenced by diffusion, bio accumulation factor and organisms originated mechanical changes in the sediment profile. The high activity of ^{137}Cs may be attributed to fallout from atmospheric nuclear tests, releases from nuclear reprocessing plants and the accident at the Chernobyl power station. In general, the ^{137}Cs concentrations in all cores were observed to be declined with depth. In most situations, sediment cores generally show the maximum levels of ^{137}Cs at the top layers (4 -8 cm) and expected to exhibit an exponential decline with depth [406, 421].

A number of studies have shown that ^{137}Cs can sorb strongly onto clay and organic particles [420]**.** In general, ^{137}Cs has the higher tendency to accumulate in the finest fraction of sediments than the medium-sized and coarse particles. However, it was also reported that coarse particles also adsorb ^{137}Cs especially when their relative percentage in the sample is high. In the present study, the activity profiles of ^{137}Cs also showed a strong degree of correlation with the coefficients of r = + 0.73 and + 0.80 with silt and clay respectively. This clearly indicates that ^{137}Cs is mainly concentrated in the fine-grained size fractions of sediments

7.3.1.3. Activity ratio of ^{228}Ra/^{226}Ra and ^{232}Th /^{226}Ra

The mean activity levels of ^{226}Ra, ^{228}Ra and ^{232}Th throughout the cores ranged from 8.35 to 16.60 Bqkg^{-1}, dry (mean: 12 ± 3 Bqkg^{-1}, dry), 22 to 48 Bqkg^{-1}, dry (mean: 37.5 ± 10 Bqkg^{-1}, dry) and 43 to 55 Bqkg^{-1}, dry (mean: 46.5 ± 3.3 Bqkg^{-1}, dry) respectively. However, depth profiles of activity ratios of ^{228}Ra/^{226}Ra for the same were observd to be in the range of 1.37 - 2.30 (mean: 1.72 ± 0.28), 2.75 - 5.2 (mean: 3.44 ± 0.82) and 7.67 - 29.72 (mean: 17.52 ± 7.02) and for ^{232}Th /^{226}Ra, the quotient was from 1.67 to 2.63 (mean: 2.16 ± 0.33), 2.81 to 6.43 (mean: 4.38 ± 1.28) and 8.01 to 33.25 (mean: 21.5 ± 7.34) respectively. Thus, in general, the vertical mean concentration profiles of ^{226}Ra, ^{228}Ra and ^{232}Th **(Fig.7.5)** showed a decreasing trend from top to bottom as established by negative correlation coefficient of r = -0.93, r = - 0.80 and r = -0.15 respectively. On the contrary, the profiles of activity ratios of ^{228}Ra/^{226}Ra (**Fig.7.6)** and ^{232}Th /^{226}Ra **(Fig.7.7)** increases as core depth increases. In addition, the mean activity ratio of ^{228}Ra/^{232}Th **(Fig.7.8)** less than unity at each layer of cores indicates an activity deficit of ^{228}Ra throughout the depth leading to not attaining the secular equilibrium with ^{232}Th. Overall, the activity ratio of ^{228}Ra/^{232}Th decreases as depth increases.

Though, ^{232}Th did not show any significant variation as seen by an almost uniform level (CV: ~ 7%) throughout the depth, the only significant changes in the activity ratio of ^{232}Th /^{226}Ra might be controlled by ^{226}Ra (CV: ~25%). Although chemical behavior of ^{226}Ra and ^{228}Ra is virtually identical, the activity ratio of ^{228}Ra/^{226}Ra varied greately throughout the studied area. This confirms that the solubility of ^{226}Ra is relatively higher than ^{228}Ra and their contents in sediments are the function of their parents ^{238}U and ^{232}Th respectively. In literature, it was found that, radium is not strongly particle reactive and about 38 % of both ^{228}Ra and ^{226}Ra is lost from suspended sedimentary particles in sea water [403].

7.3.2. Sedimentation rate and age of sediment

7.3.2.1. $^{210}Pb_{ex}$

Deposition of ^{210}Pb from the atmosphere takes place on a timescale much shorter than its half-life [361]**,** therefore, the ^{210}Pb that settles on the sea is adsorbed by suspended solids and subsequently incorporated in the bottom sediments as excess (unsupported) radionuclide.

Total ^{210}Pb activity in sediments will include both the atmospherically-derived ^{210}Pb and the supported ^{210}Pb derived from the in situ decay of ^{226}Ra. The values of un-supported ^{210}Pb thus were calculated by subtracting ^{226}Ra concentration (supported ^{210}Pb) from total ^{210}Pb in each fraction of the core.

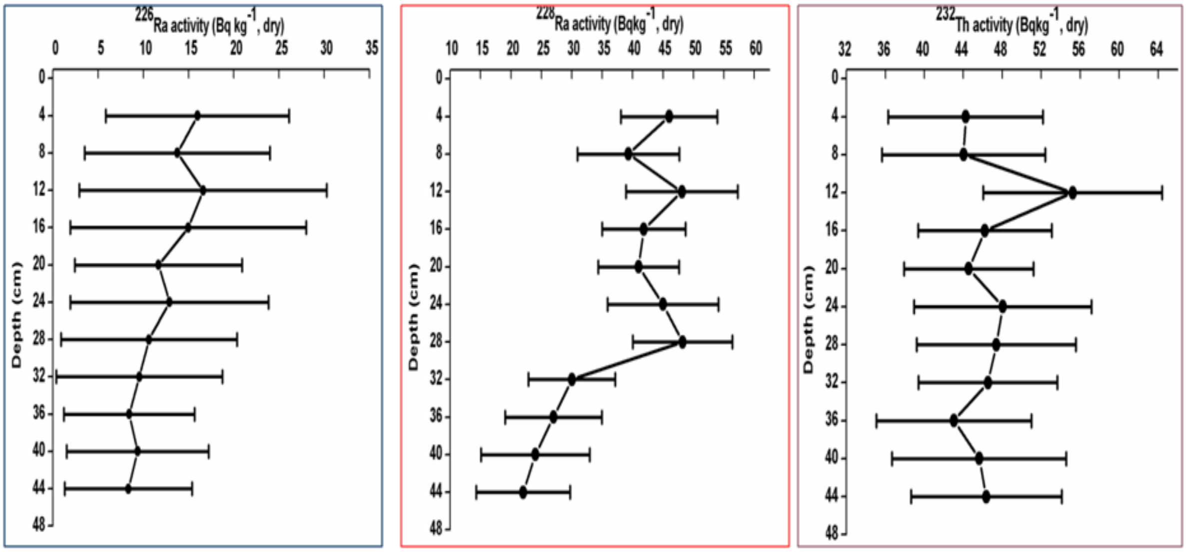

Fig.7.5: Depth profile distribution of mean activity of ^{226}Ra, ^{228}Ra and ^{232}Th throughout the all cores

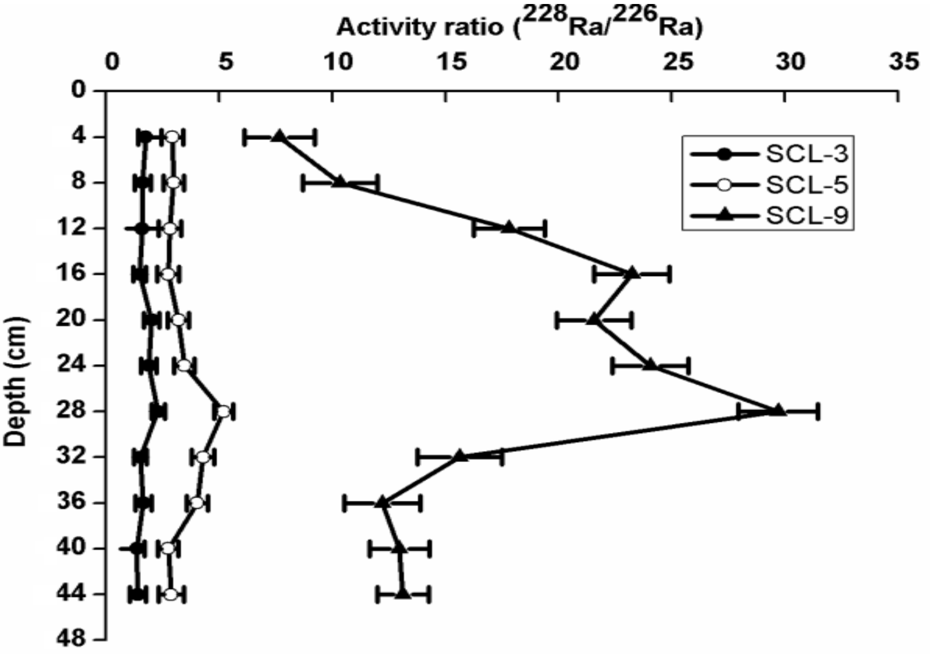

Fig.7.6: Depth profile distribution of activity ratio of ^{228}Ra/^{226}Ra in cores of SCL-3, SCL-5 and SCL-9

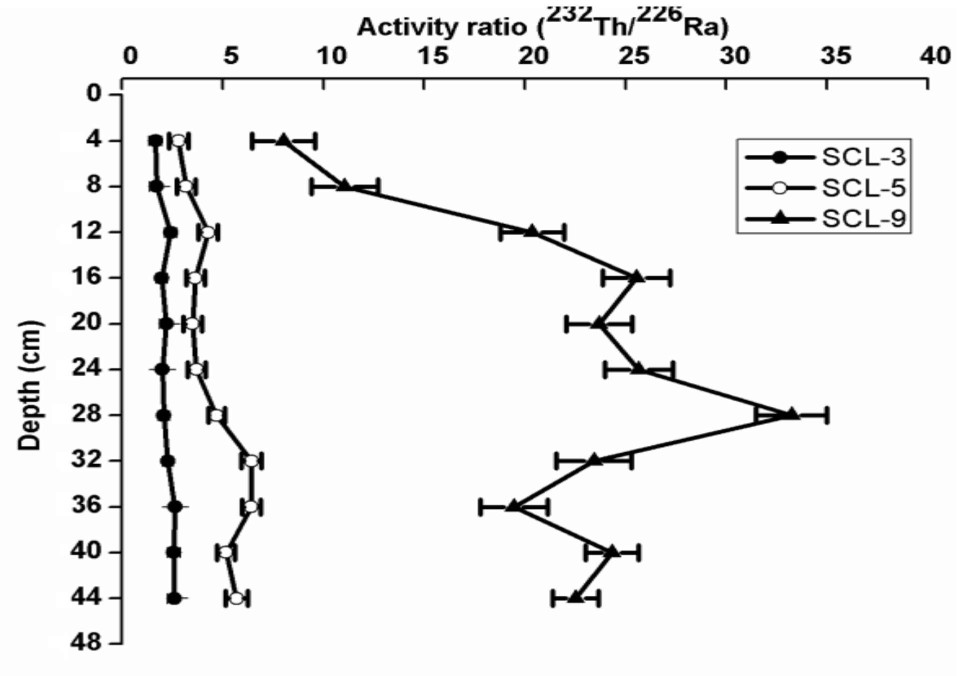

Fig.7.7: Depth profile distribution of activity ratio of ^{232}Th/^{226}Ra in cores of SCL-3, SCL-5 and SCL-9

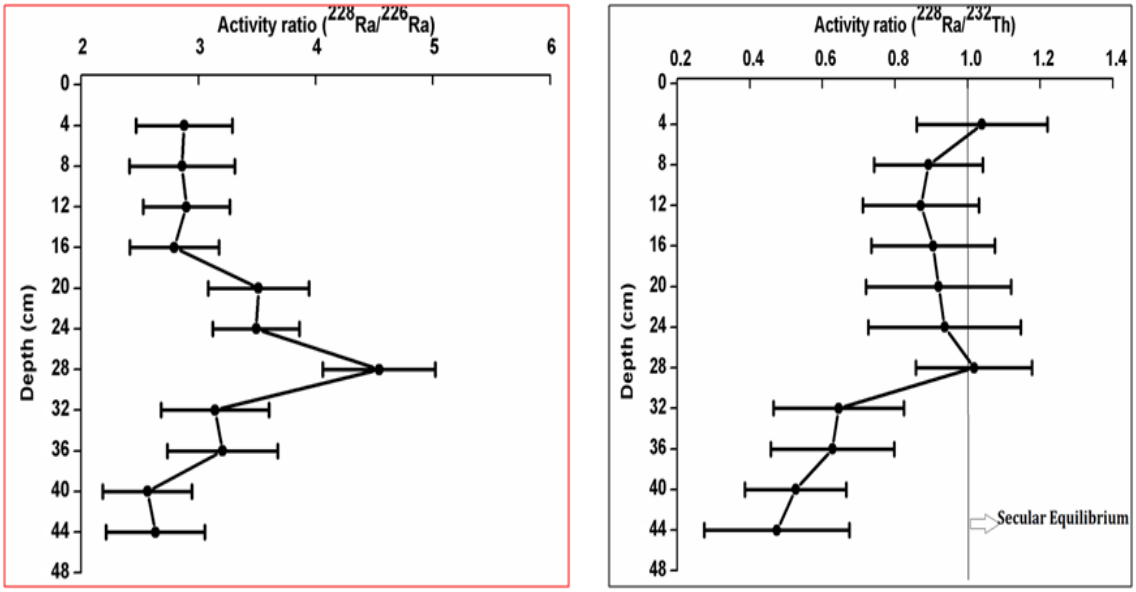

7.8: Depth profile distribution of mean activity ratio of ^{228}Ra/ ^{226}Ra and ^{232}Th/ ^{228}Ra in all the three cores

For constant sedimentation rate, a logarithmic plot of activity levels of $^{210}Pb_{ex}$ **(Fig.7.9)** verses arithmetic sediment depth yielded a straight line and the sedimentation rate was determined from the slope of lines obtained from the depth profile of radionuclides. Trend of graphs were tested by establishing the linear relationship between the two parameters (activity and depth) using Karl Pearson's correlation coefficient analysis. The correlation of ^{210}Pb concentrations with depth in all cores showed a very high degree of negative correlation coefficient of $r > -0.90$ and the lines were sufficiently fit.

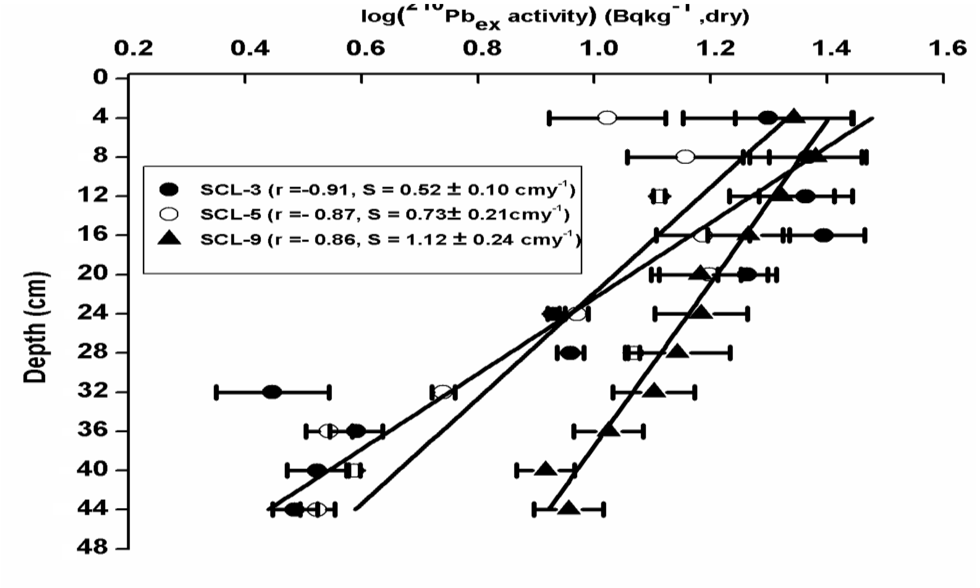

Fig.7.9: A plot of log $^{210}Pb_{ex}$ activity against linear depth of cores

The sedimentation rate of ^{210}Pb was determined to be 0.52±0.10 cmy^{-1}, 0.73± 0.21cmy^{-1} and 1.12 ± 0.24 cmy^{-1} by the slope of lines obtained in cores of SCL-3, SCL-5 and SCL-9 respectively. The corresponding age of collected core sediment samples of SCL-3, SCL-5 and SCL-9 was representative of 77 ± 15 y, 55 ± 16 y and 36 ± 8 y time spans respectively. The age of top layers (upto 4cm) of same cores were estimated to be 7.74 y, 5.48 y and 3.57 y respectively. The lower the sedimentation rate indicates the older age of sediment. To avoid any influence of sediment compaction on the results, the overall sediment accumulation rate of ^{210}Pb in same cores was calculated to be 1.73 gcm^{-2}y^{-1}, 1.54 gcm^{-2}y^{-1} and 1.89 gcm^{-2}y^{-1} using the **Eq. (7.10).** The significant differences in sedimentation rates or sediment accumulation rates indicate that ^{210}Pb depositions to sediments have the distinct characters.

7.3.2.2. ^{137}Cs

Similarly for constant sedimentation rate, a logarithmic function of activity levels of ^{137}Cs was also plotted against arithmetic core sediment depth and yielded a straight line using a least-square fit procedure ((**Fig.7.10)**. The sedimentation rate of ^{137}Cs was obtained to be 1.04 ± 0.18 cmy^{-1}, 0.69 ± 0.25 cmy^{-1}, 1.25 ± 0.28 cmy^{-1} in cores of SCL-3, SCL-5 and SCL-9 respectively.

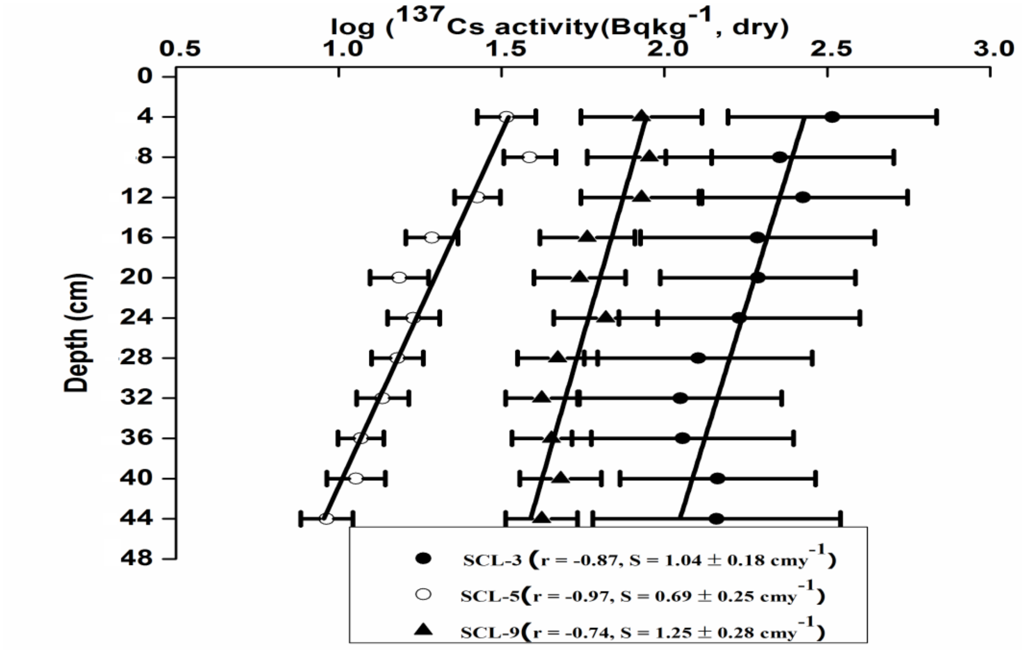

Fig.7.10: A plot of log ^{137}Cs activity against linear depth of cores

The corresponding age of collected cores of same location was representative of 38 ± 6.7 y, 58 ± 21, y, and 32 ± 7 y time spans respectively. The overall sediment accumulation rate of ^{137}Cs for the same was calculated to be 1.43 gcm^{-2}y^{-1}, 1.15 gcm^{-2}y^{-1} and 1.95 gcm^{-2}y^{-1}

respectively**.** These values appeared to be highly compatible with the results of the ^{210}Pb dating. The minor discrepancy in the sedimentation rate or sediment accumulation rate between ^{210} Pb and ^{137}Cs dating might be due to continual mixing of the top several centimeters of the sediment column by the action of organisms.

7.3.2.3. ^{228}Ra/ ^{226}Ra

In addition to the traditional methods (^{210}Pb and ^{137}Cs profiles), the sedimentation rate was also determined using a new geo-chronometer as ^{228}Ra/^{226}Ra and found to be 1.76 ± 0.30 cmy^{-1}, 2.52 ± 0.21 cmy^{-1} and 2.05 ± 0.29 cmy^{-1} in cores of SCL-3, SCL-5 and SCL-9 respectively as depicted in (**Fig.7.11).** The corresponding age of collected core sediments over the length of 40 cm for the same was calculated to be 23 ± 4 y, 16 ± 1.4 y and 19.5 ± 2.8 y respectively. As determined from ^{137}Cs or ^{210}Pb , the average age of sediment was found to be about 45 to 56 years prior to core collection and over this time scale, ^{226}Ra ($t_{1/2}$ = 1600 yr) would not in-grow appreciably. This indicates that the changes in vertical profiles of ^{228}Ra/^{226}Ra activity ratio are mainly controlled by in-growth of ^{228}Ra ($t_{1/2}$ = 5.8 yr).

7.3.3. Total inventory and fluxes

The cumulative inventory of deposited ^{210}Pb and ^{137}Cs in cores of SCL-3, SCL-5 and SCL-9 was fitted by least square method and approximated using **(Eq.7.8).** The measured inventory of ^{210}Pb **(Fig.7.12 - 7.14)** and ^{137}Cs **(Fig.7.15 - 7.17)** in cores expressed as a percentage of the total inventory in the sediment profile were plotted as a function of h_0 (kgm^{-2}). The total inventory of ^{210}Pb in cores of SCL-3, SCL-5 and SCL-9 was obtained to be 13.5 kBqm^{-2}, 7.85kBqm^{-2} and 7.7 kBqm^{-2} respectively. However, the total inventory of deposited ^{137}Cs in cores of SCL-3, SCL-5 and SCL-9 was determined to 14.5 kBqm^{-2}, 6.45 kBqm^{-2} and 6.97 kBqm^{-2} respectively.

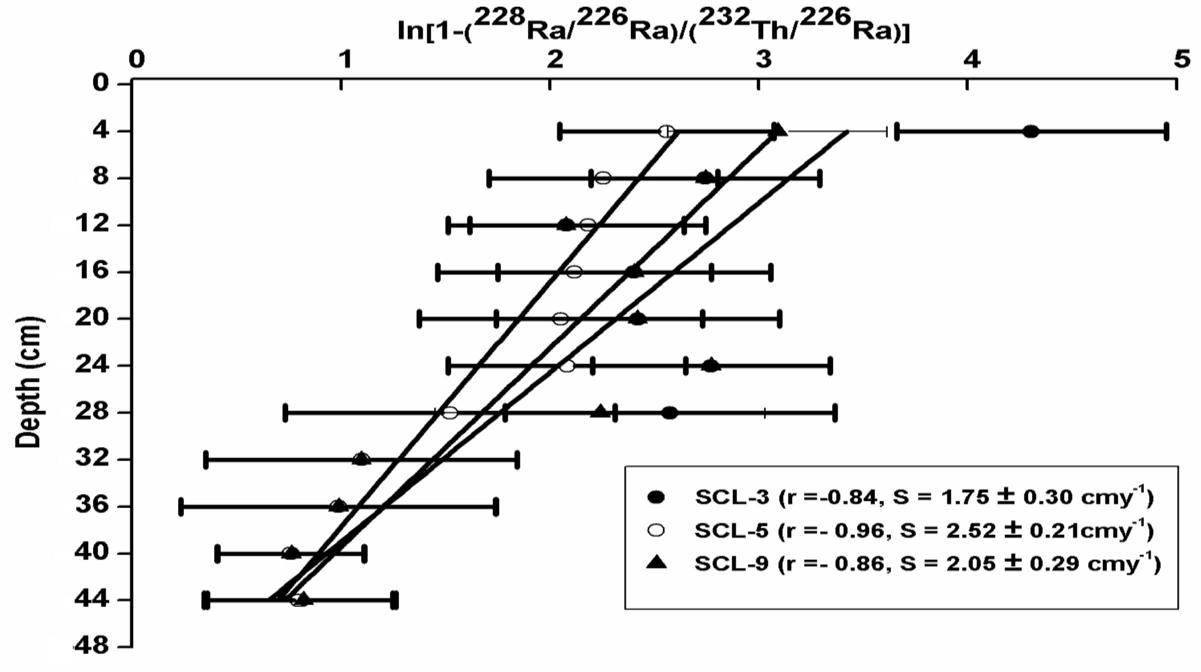

Fig.7.11: A Plot of ln {1 - [(^{228}Ra/^{226}Ra)/(^{232}Th/^{226}Ra)]} versus linear depth of cores

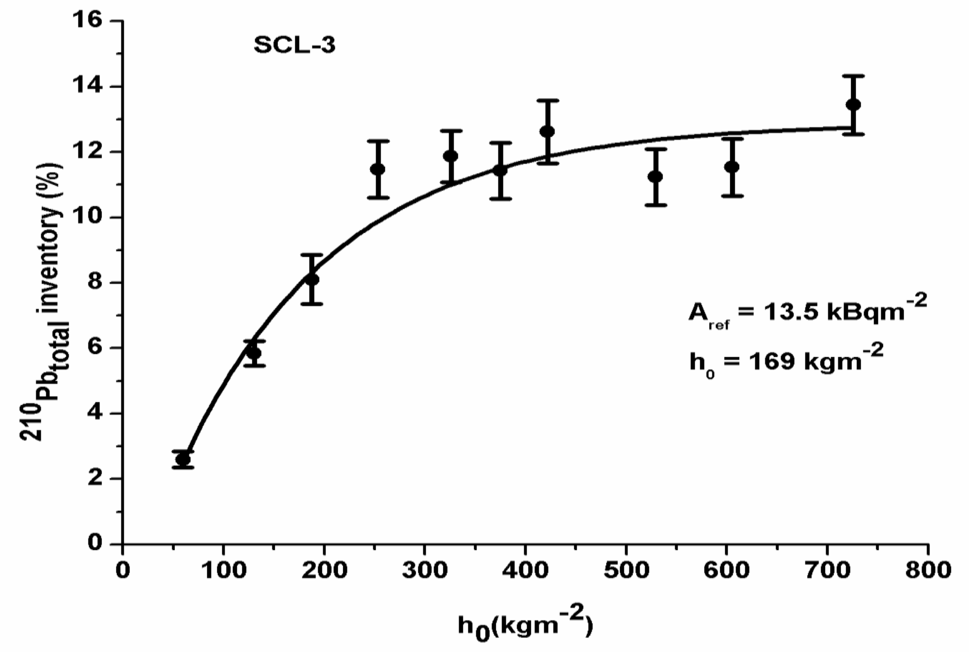

Fig.7.12: Total ^{210}Pb inventory (%) as a function of mass depth in the sediment profile of core SCL-3

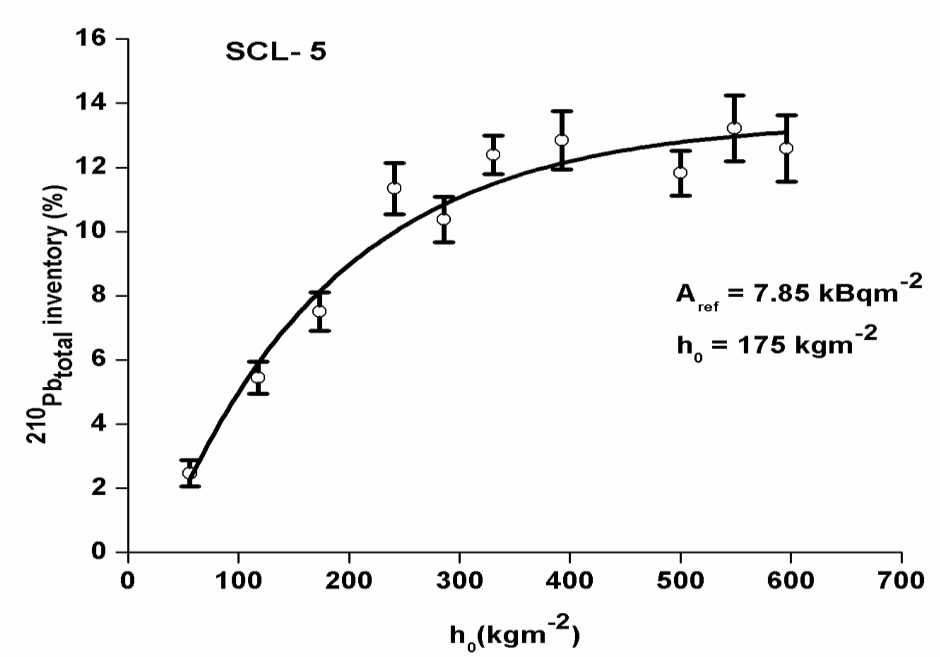

Fig.7.13: Total ^{210}Pb inventory (%) as a function of mass depth in the sediment profile of core SCL-5

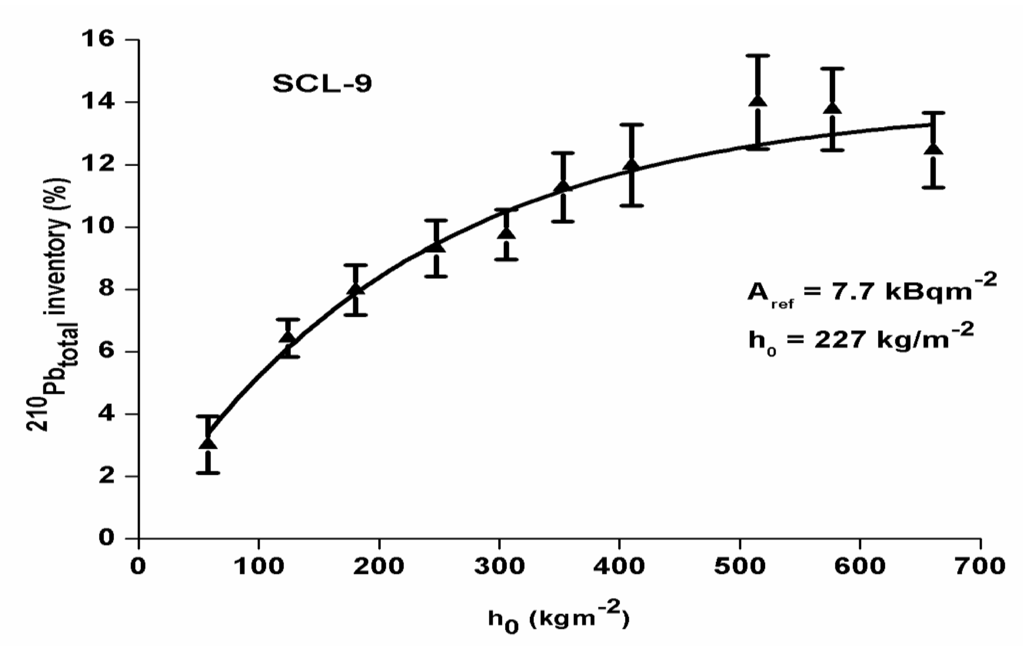

Fig.7.14: Total ^{210}Pb inventory (%) as a function of mass depth in the sediment profile of core SCL-9

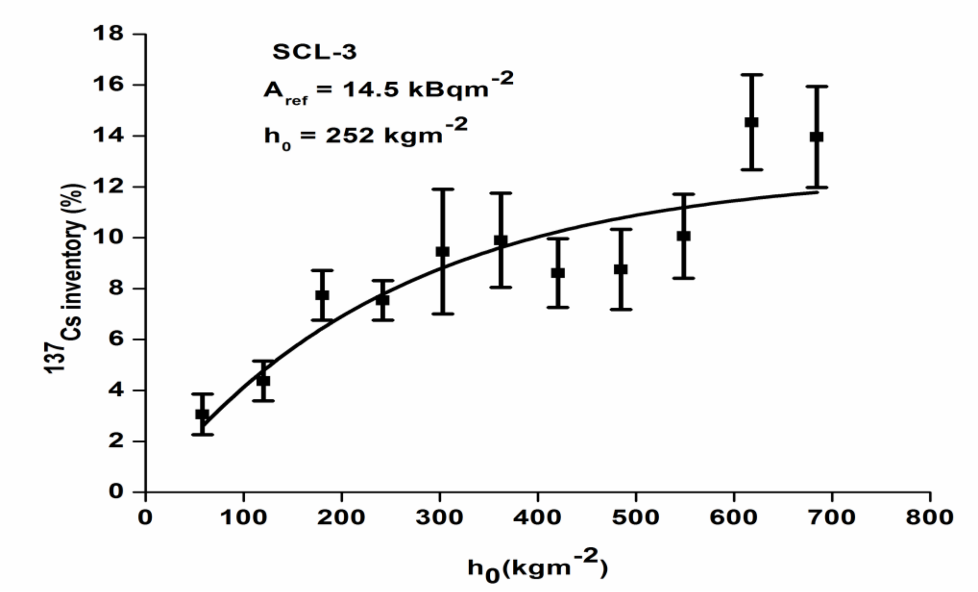

Fig.7.15: Total ^{137}Cs inventory (%) as a function of mass depth in the sediment profile of core SCL-3

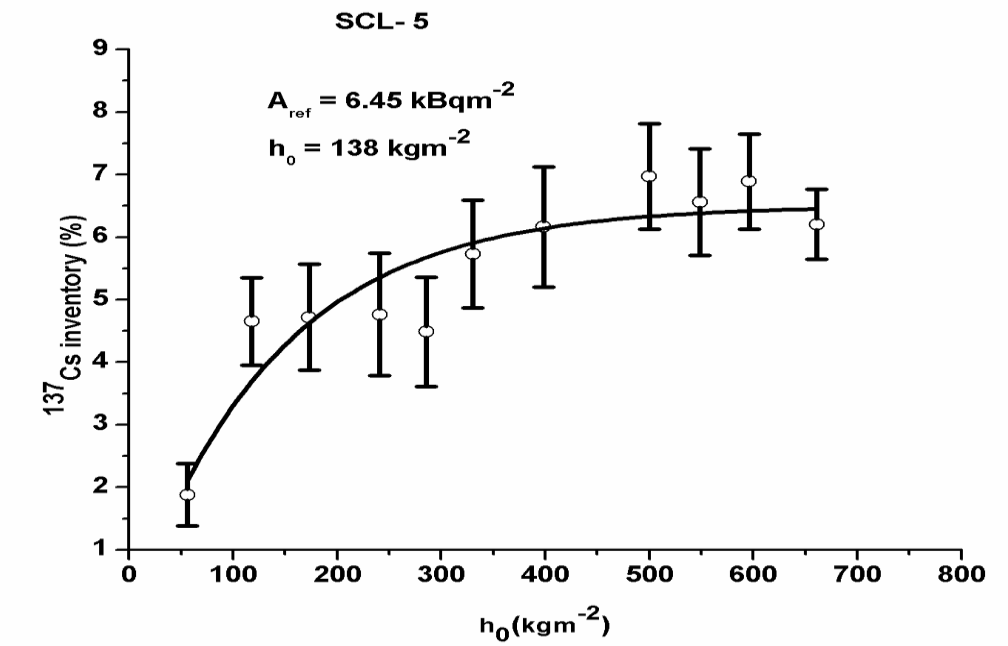

Fig.7.16: Total ^{137}Cs inventory (%) as a function of mass depth in the sediment profile of core SCL-5

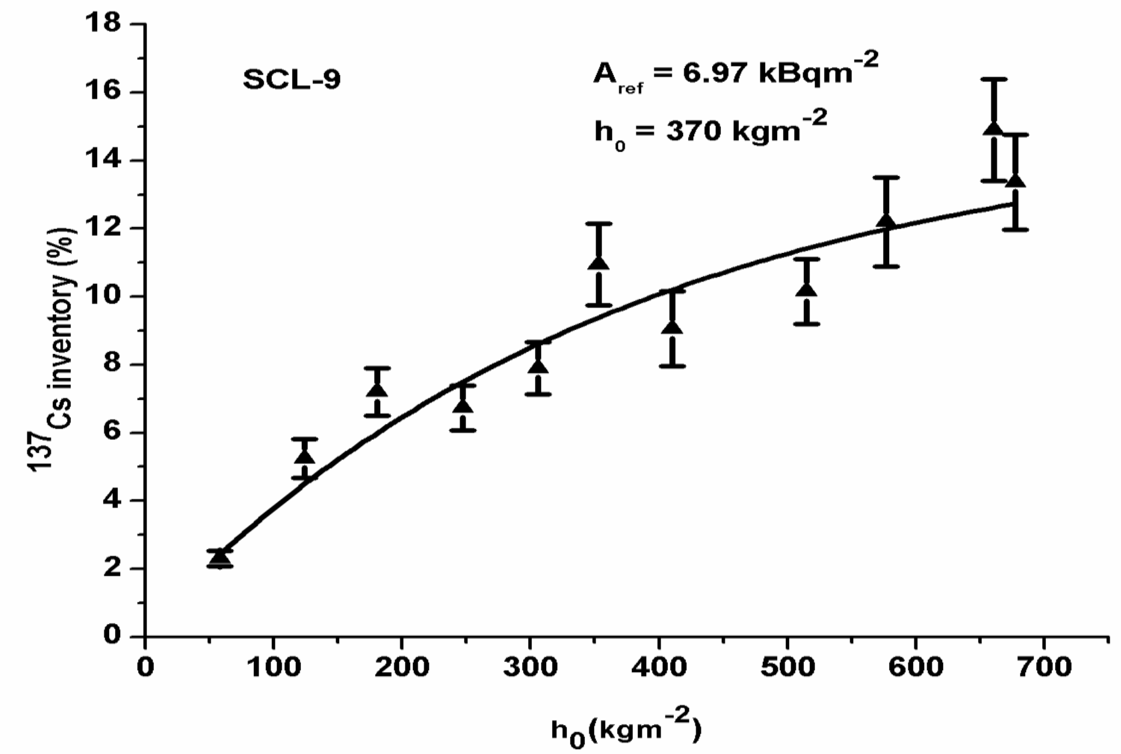

Fig.7.17: Total ^{137}Cs inventory (%) as a function of mass depth in the sediment profile of core SCL-9

Similarly, the cumulative flux of total ^{210}Pb (^{210}Pb$_{total}$) and excess ^{210}Pb (^{210}Pb$_{ex}$) in cores of SCL-3, SCL-5 and SCL-9 as depicted in Figs.7.18 -7.20 respectively, were obtained by fitting the depth profiles distribution using least square methods and approximated using (Eq.7.11). The flux of total ^{210}Pb and excess ^{210}Pb in cores of SCL -3, SCL-5 and SCL-9 was observed to be 0.48kBqm^{-2}y^{-1}, 0.53kBqm^{-2}y^{-1} and 0.76kBqm^{-2}y^{-1} respectively. The corresponding ^{210}Pb$_{ex}$ flux (atmospheric flux) was obtained to be 0.21 kBqm^{-2}y^{-1}, 0.19 kBqm^{-2}y^{-1} and 0.57 kBqm^{-2}y^{-1} for the same respectively. Whereas for ^{137}Cs, the flux using (Eq. 7.12), derived to be 0.35 kBqm^{-2}y^{-1}, 0.15 kBqm^{-2}y^{-} and 0.16 kBqm^{-2}y^{-1} for the cores of SCL-3, SCL-5 and SCL-9 respectively.

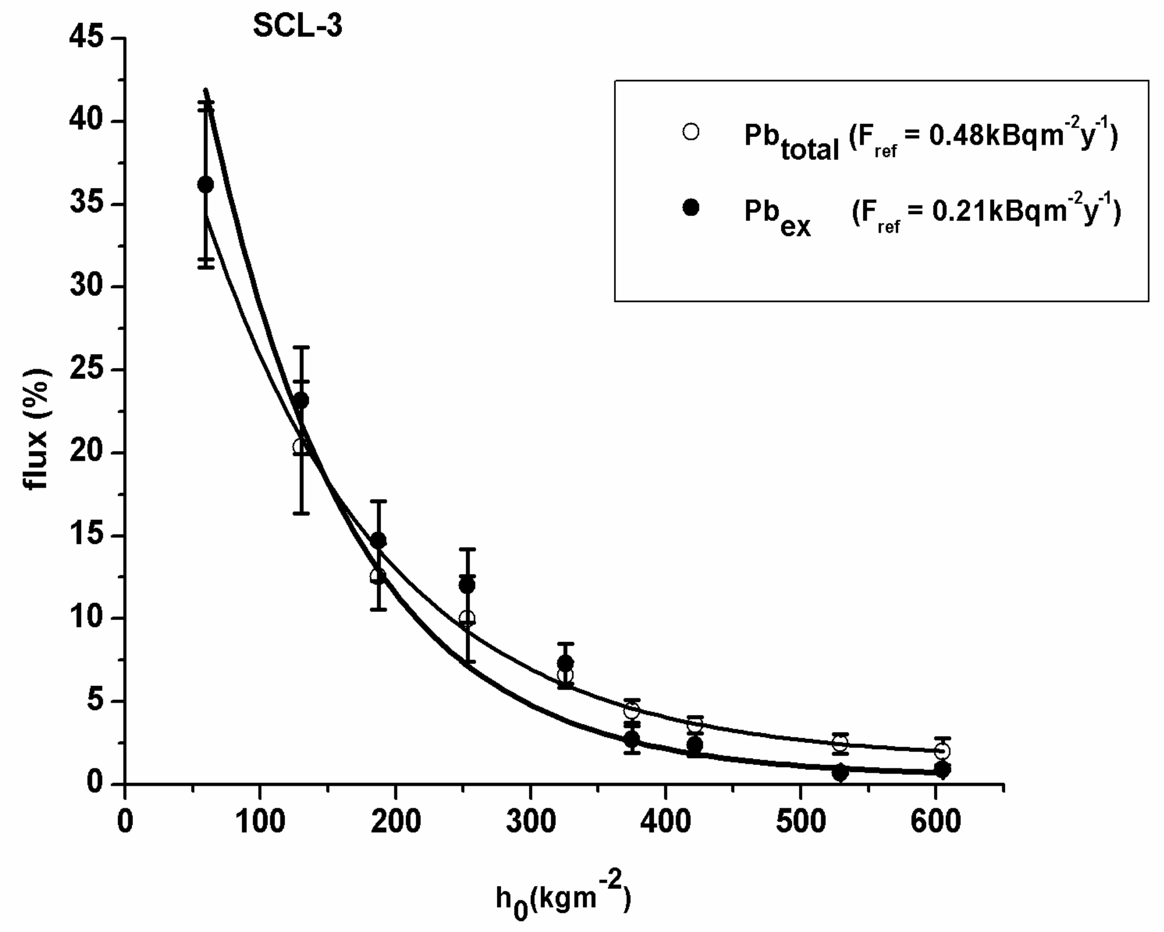

Fig.7.18: Depth distribution of flux (% of the total flux) for ^{210}Pb (total) and ^{210}Pb (excess) in the sediment profile of core SCL-3

The atmospheric fluxes ($^{210}Pb_{ex}$) accounted to be about 44%, 36% and 75% of the total ^{210}Pb flux for SCL -3, SCL-5 and SCL-9 respectively. Although the inventory of $^{210}Pb_{total}$ in core SCL-5 and SCL-9 was almost similar, the atmospheric fluxes in core SCL-9 credited to be higher. Though, the $^{210}Pb_{total}$ inventory in core SCL-3 showed 72% higher than SCL-5, the atmospheric flux accounted to be almost similar.

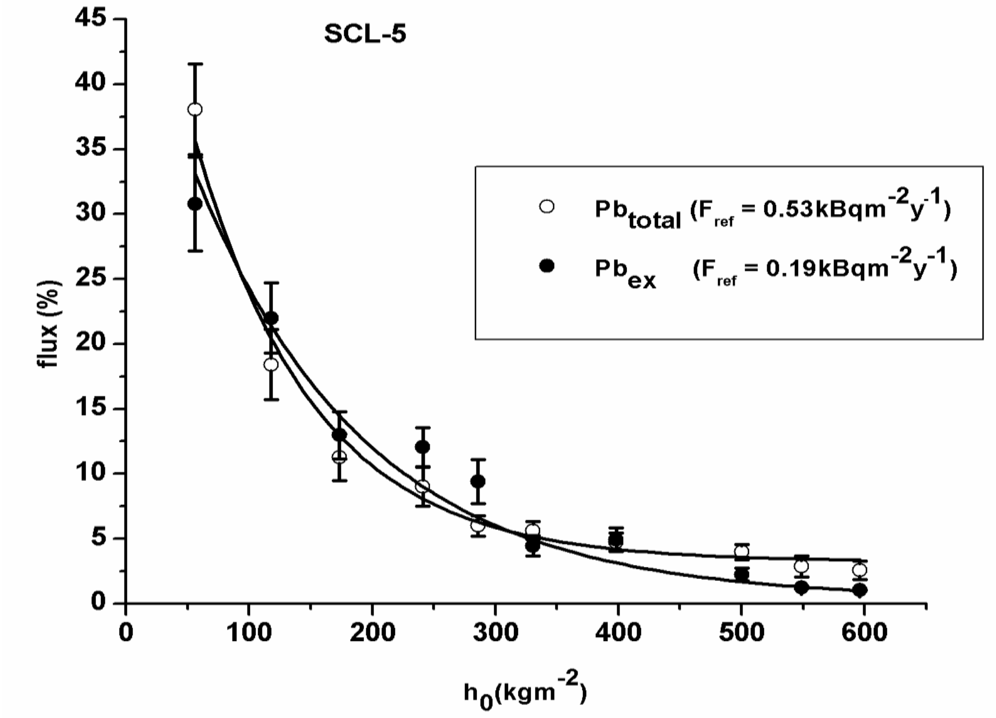

Fig.7.19: Depth distribution of flux (% of the total flux) for ^{210}Pb (total) and ^{210}Pb (excess) in the sediment profile of core SCL-5

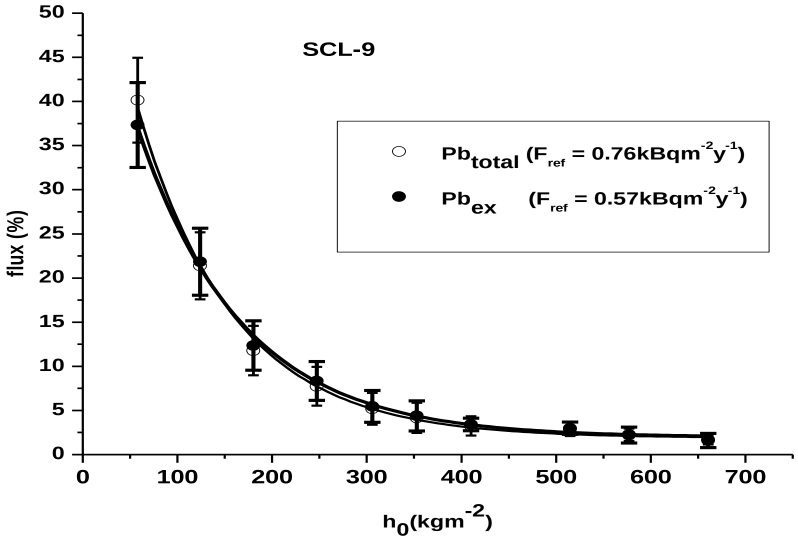

Fig.7.20: Depth distribution of flux (% of the total flux) for ^{210}Pb (total) and ^{210}Pb (excess) in the sediment profile of core SCL-9

Differences in fluxes might be resulted from highly significant different in the activity levels between ^{210}Pb and ^{226}Ra in cores SCL-9 as seen by high activity ratio. The mean global atmospheric flux and inventory of ^{210}Pb fallout was about 0.165kBqm^{-2}y^{-1} and 5.3kBqm^{-2} respectively [361].

Joshi et al. (1969) have reported the atmospheric deposition flux and the inventory of ^{210}Pb at Thane Creek of Mumbai Harbour Bay to be 0.25kBqm^{-2}y^{-1} and 8kBqm^{-2} respectively [422]. Appleby and Oldfield reported the global average atmospheric flux value of 0.185kBqm^{-2}y^{-1}[362]. ^{210}Pb deposition from the atmosphere of Poland varied between 10 and 0.5kBqm^{-2}y^{-1} in aquatic environment of Poland and southern Baltic Sea [423, 424]. Despite the same geology of all sampling locations, atmospheric fluxes in core SCL-3 and SCL-5 were significantly different from SCL-9. Therefore, it is concluded that the atmospheric fluxes were the dominant factor controlling the ^{210}Pb supply.

7.3.4. Scavenging rate and residence time

7.3.4.1. Total ^{210}Pb

The vertical profile of ^{210}Pb scavenging rate can be measured directly in the open ocean through measurements of ^{210}Pb in sediment trap material or inventories of excess ^{210}Pb in deep-sea sediments. Under steady-state conditions, the inventory of excess ^{210}Pb (unsupported by ^{226}Ra), in a deep-sea sediment core represents the flux of ^{210}Pb to the sea floor averaged over about 4-5 half-fives or 100 years. The flux required to support the inventory is obtained by multiplying by the decay constant for ^{210}Pb and represents the mean flux of ^{210}Pb to the seafloor. But, it is noted that the ^{210}Pb flux measured in near bottom sediment traps may not equal to derived from excess ^{210}Pb inventories in bottom sediments if scavenging of ^{210}Pb at the sediment-water interface is occurring [425 – 427]. In this study, vertical profile of scavenging rate of ^{210}Pb in cores of SCL-3, SCL-5 and SCL-9 were estimated and ranged to be 0.0044-0.033 y^{-1} (mean: 0.013 y^{-1}), 0.014 – 0.038 y^{-1} (mean: 0.023 y^{-1}) and 0.024 – 0.028 y^{-1} (mean: 0.027 y^{-1}) respectively. The corresponding residence time of ^{210}Pb for the same (**Fig.7.21)** ranged from 30 to 226 y (mean: 78 y), 26 to 72 y (mean: 43 y) and 35 to 41 y (mean: 37 y) respectively. Comparatively higher residence time obtained in core SCL-3 indicates that the rate of removal of ^{210}Pb from sediment is slower than in both cores SCL-5 and SCL-9. The depth profile variation in residence time of ^{210}Pb for core SCL-3 showed almost constant values in the range of 30 – 42 years up to the depth of 4-20 cm and onwards increased sharply in the higher depth fractions. Similarly, for core SCL-5, the residence time generally decreases as depth increases upto 4 -28 cm and onwards increases in the succeeding downward core fractions. Overall, residence time in both cores increases as depth increases. The core SCL-9 did not show any significant variation in the residence times of ^{210}Pb as seen by almost uniform values throughout the core depth. It is also obvious that larger the residence time, lower the scavenging rate of radionuclides.

The residence time of ^{210}Pb with respect to scavenging is short in the surface ocean, in the order of 1 year, while in the deep ocean the value is 30-100 years [428 – 430]. This relatively long residence time in the deep ocean permits ^{210}Pb to be transported from areas of low scavenging intensity to areas of more rapid removal. Cochran et al. (1989) reported the value of residence time of ^{210}Pb with respect to scavenging in the North Atlantic and North Pacific oceans in the range of 15 - 260 y [431].

7.3.4.2. ^{137}Cs

For ^{137}Cs, residence half-time were calculated using the multi compartment model by assuming the sediment depth into a series of N horizontal layers (compartments) which are connected by a downward transport. The time dependence (for t > 0) of ^{137}Cs concentrations in the compartments is then written as

$$\frac{dc_1(t)}{dt} = -[\lambda + k_{1,2}]c_1(t) \qquad \textbf{(Eq. 7.17)}$$

$$\frac{dc_i(t)}{dt} = -[\lambda + k_{i,i+1}]c_i(t) + k_{i-1,}c_{i-1,i}c_{i-1}(t), i = 2,........, N, \qquad \textbf{(Eq. 7.18)}$$

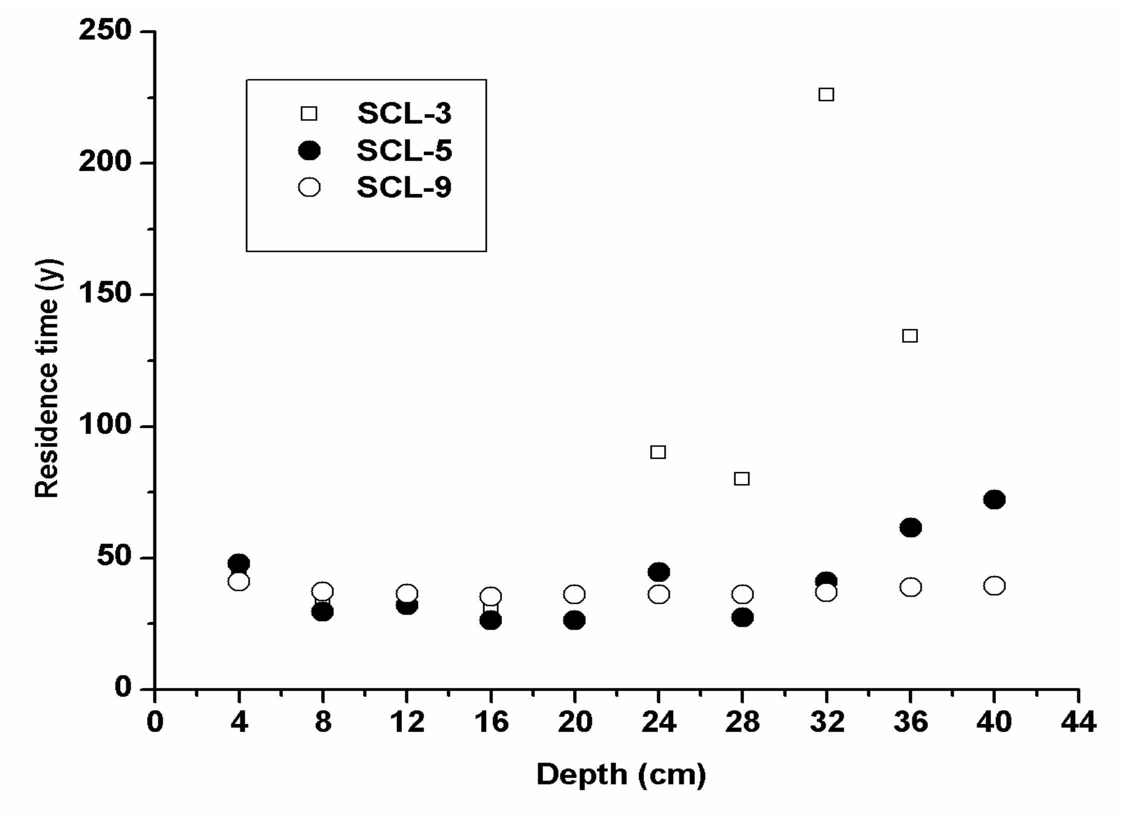

Fig.7.21: Residence time of ^{210}Pb (total) as a function of cores depth

Where c_i is the concentration of the radionuclide in sediment layer i, $k_{i,i+1}$ is its transport rate from sediment layer *i* to i+1. The solution of **Eq. (7.18)** is fitted to measured concentrations in sediment layers taken at a field site in order to estimate the unknown $k_{i,i=1}$. From these one can deduce a residence half-time in layer *i* as $\tau_i = \ln 2/k_{i,i+1}$.

The values of k in each compartment of cores were derived from the least square fits to the depth distributions observed at the various sites [432]**.** The residence half-times were observed to be the highest at the top layers of all the three cores and decreased with sediment depth with a mean ranging from 1.06 at top layer (0 - 4 cm) to 35.35 years at the bottom layer (32 - 36 cm) throughout the cores [432]**.** This might be due to occurrences of high content of finer particles in the form of clay and silt in the upper layers and coarser particles in the deeper layers. Generally, ^{137}Cs migration is a complicated process which is affected by a number of factors like the type of sediments, its chemical properties, organic matter content and climatic conditions such as rainfall, temperature or humidity and biological activity of microorganisms. It was also observed that the adsorption of cesium is decreased by the presence of competing ions of K or Na ions in the sediments.

7.3.5. Linear attenuation coefficient (α) and relaxation mass depth (h_0)

7.3.5.1. ^{210}Pb

The parameter α (cm^{-1}) obtained by fitting the depth profile distribution of ^{210}Pb in the cores of SCL-3, SCL-5 and SCL-5 using **(Eq.7.1)** were derived to be 0.028 cm^{-1}, 0.027 cm^{-1} and 0.027 cm^{-1} respectively. The resulting h_0 (kgm^{-2}) of ^{210}Pb computed using (**Eq.7.8)** was found to be 169 kgm^{-2}, 175 kgm^{-2} and 227 kgm^{-2} respectively**.** The high value of h_0 obtained in core SCL-9 indicates a deeper penetration into the sediment profile. The greater is the value of the relaxation mass depth (h_0), the deeper the ^{210}Pb penetrates into the sediment profile [403]**.** The penetration of ^{210}Pb in SCL-3 and SCL-5 cores was fairly similar. The obtained mean values of h_0 at each layer of all the three cores were plotted against the clay and silt content as shown in **Fig.7.22**. Overall, the clay showed a significant negative correlation (r =-0.70) with the values of h_0 indicating that as the clay content increases, the penetration depth of deposited radionuclides in sediment profile decreases. Since the clay content increases the aggregate stability of sediment [433, 434], therefore the infiltration rate of sediment is not a simple function of clay content. ^{210}Pb is selectively adsorbed by fine sediment particles, thus it is expected that it concentrates at the sediment surface. However, the silt did not show any significant correlation (r = - 0.22) with h_0 values indicating that penetration depth of ^{210}Pb is not very much influenced by the coarse particles. Though, it was reported that coarse particles also adsorb particle reactive radionuclides, such as ^{137}Cs and ^{210}Pb especially when their relative percentage in the sample is high [435].

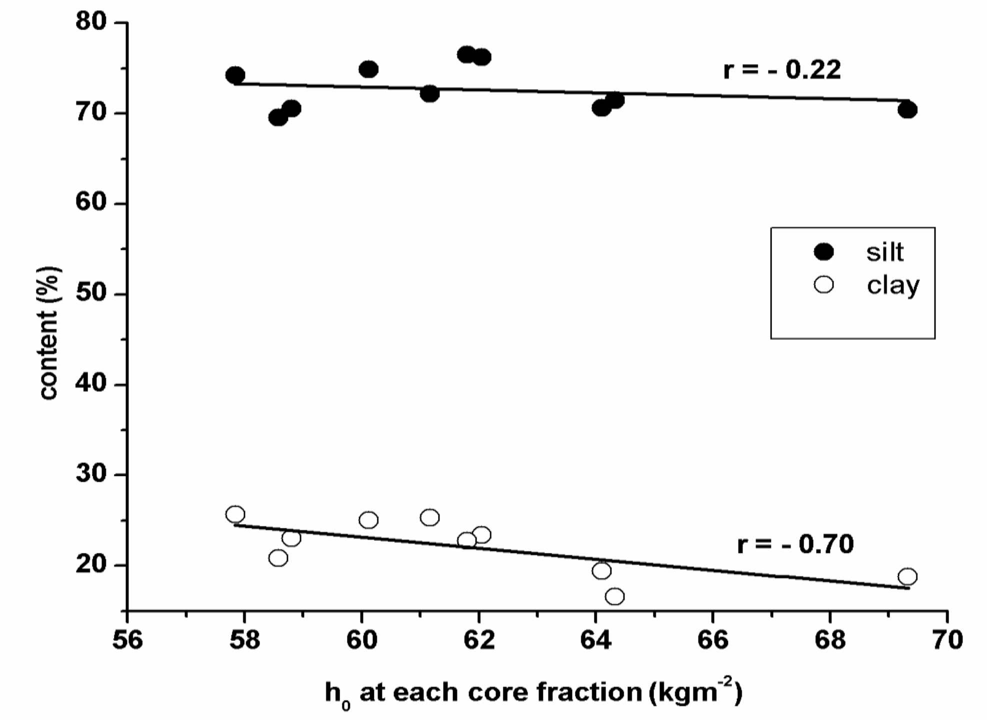

Fig.7.22: The silt and clay content as a function of h_0 values in the studied area

7.3.5.2. ^{137}Cs

The values of α for ^{137}Cs in cores of SCL-3, SCL-5 and SCL-9 were found to be 0.022, 0.033 cm^{-1} and 0.020 cm^{-1}. The resulting h_0 values for the same computed to be 252 kgm^{-2}, 138 kgm^{-2} and 370 kgm^{-2} respectively. A greater h_0 values obtained at SCL-9 for the ^{137}Cs than ^{210}Pb indicates deeper penetration of ^{137}Cs into the sediment. The h_0 value of 4.6 kgm^{-2} for ^{137}Cs was calculated for a silty - clay soil in a pasture in Skogsvallen, Sweden [436], whereas the h_0 value for the same silty clay soil in grasslands in Bavaria and Munich, Germany was 10.3kgm^{-2} [437, 438]. For loamy sand soils of cultivated lands in the proximity of the Chernobyl NPP, the h_0 values of ^{137}Cs ranged 5.6-9.1 kg/m^{2} [439]. Kato et al., 2011, reported the h_0 value of 9.1kgm^{-2} for ^{137}Cs in cultivated soil of Kawamata, Fukushima after FDNPP accident [440]. **Table 7.1** shows the various migration parameters obtained from the depth profile distribution of ^{210}Pb, ^{137}Cs and ^{228}Ra/ ^{226}Ra in cores of studied area.

Table 7.1: Parameters obtained from the depth profile distribution of ^{210}Pb, ^{137}Cs and ^{228}Ra/ ^{226}Ra in cores of studied area

Parameters		**SCL-3**		**SCL-5**			**SCL-9**		
	^{210}Pb	^{137}Cs	^{228}Ra/^{226}Ra	^{210}Pb	^{137}Cs	^{228}Ra/^{226}Ra	^{210}Pb	^{137}Cs	^{228}Ra/^{226}Ra
Sedimentation rate (cmy^{-1})	0.52± 0.10	1.04± 0.18	1.75± 0.30	0.73± 0.21	0.69± 0.25	2.52± 0.21	1.12± 0.24	1.25± .28	2.05± 0.29
Sediment accumulation rate (gcm^{-2}y^{-1})	1.73	1.43	-	1.54	1.15	-	1.89	1.95	-
Age of sediment (y)	77± 15	38± 6.7	23± 4	55± 16	58± 21	16± 1.4	36± 8	32± 7	19.5± 2.8
Total inventory (kBqm^{-2})	13.50	14.5	-	7.85	6.45	-	7.70	6.97	-
Total flux (kBqm^{-2}y^{-1})	0.48	0.35	-	0.53	0.15	-	0.76	0.16	-
Excess ^{210}Pb flux or atmospheric flux (kBqm^{-2}y^{-1})	0.21	-	-	0.19	-	-	0.57	-	-
Mean residence time (years)	78		-	43	-	-	37	-	-
Mean scavenging rate (y^{-1})	0.013		-	0.023	-	-	0.027	-	-
Linear attenuation coefficient (cm^{-1})	0.028	0.022	-	0.027	0.033	-	0.027	0.020	-
Relaxation mass depth (kgm^{-2})	169	252	-	175	138	-	227	370	-

7.4. Conclusions

Various data evaluated under this study clearly indicates that ^{210}Pb dating appeared to be a valid and powerful technique for establishing the age of recently deposited sediments and also useful for predicting the chronicle deposition of actinides of interest in Mumbai Harbour Bay. Companion ^{137}Cs profiles indicate that the coring technique was probably recovering the uppermost levels of the deposit and that the mobility of radionuclides within the sediments is small. Although ^{210}Pb technique applied to dating sediments is effective and precise but the analysis of ^{137}Cs is also useful to corroborate the results. The application of these methods under the dynamic conditions of such systems is used carefully because it usually determines a relatively poor accumulation of such radioelements into marine sediments.

In addition to the traditional methods (^{210}Pb, ^{234}Th and ^{137}Cs profiles), the use of ^{228}Ra/^{226}Ra activity ratios, based on the in-growth of ^{228}Ra into secular equilibrium with ^{232}Th, also permits the determination of sediment accumulation rates on an approximate 30-year time scale. Constant initial activity deficit, insignificant diffusion of ^{228}Ra and the accurate determination of ^{232}Th are essential for the reliability of this technique, which fills the geochronological gap created by the ^{210}Pb dating. Therefore, this method is a valuable asset in the investigation of rapidly accumulating, fine grained sediments in other areas. Even where the traditional methods of determining sediment deposition and accumulation rates are valid, this new approach has the potential of providing information on an intermediate time scale, which can enhance our understanding of the process of strata formation.

The ^{210}Pb activity levels in all cores were comparatively higher than ^{226}Ra indicated that ^{210}Pb is more particles reactive, immobile and less soluble than radium. This might be resulted from atmospheric fall-out by ^{222}Rn decay, addition of significant amount of rainwater by heavy rainfall and preferential accumulation in the mud containing fine particles from industrial activities. However ^{226}Ra has comparatively lower persistent in the surface of sediment grains because it readily undergoes ion exchange with other dissolved cations at sediment – seawater interface leading to increase in dissolved Ra activities in coastal waters or activity lost from sediment to seawater by diffusion. Overall, a decreasing trend (linear or exponential) of the depth profile distribution of ^{210}Pb or ^{137}Cs in all cores observed from top to bottom suggesting that the bottom layers of cores are in more compact undisturbed sedimentary environment. Another reason for elevated levels of these radionuclides on the surface sediment might be caused by the settling particles produced from the atmosphere and land or the older sediment issued from the resuspension processes.

In general, the ^{210}Pb derived sedimentation rates were highly compatible with the results of the ^{137}Cs dating. However, dating model of ^{226}Ra/ ^{228}Ra was observed to be highly significant different from both radiometric methods. The discrepancy in sedimentation rates in all the three cores might be due to many factors : concurrent between a fresh discharge and the sampling time, sediment composition, pre and post-depositional processes such as physical mixing, redox changes and bioturbation, the adsorption on oxides of heavy metals and hydroxides from the seawater, re-mineralisation under the highly reducing conditions, incorporation inside the carbonates framework, scavenging during tidal mixing and as a detrital phase from the downstream floods with different intensities.

In the studied area, the excess ^{210}Pb appeared to be originated primarily from atmospheric fallout but a further inventory of the ^{210}Pb distribution in cores must be made to properly assess the significance of other sources. It was also observed that input of atmospheric fluxes of ^{210}Pb to the cores was not only dependent on total inventory but also the sedimentation rate and abundances of its parent radionuclides (^{226}Ra) in such cores. In general, the depth profile distribution of residence time of ^{210}Pb in cores showed an increasing trend with depth suggesting that higher the residence time, lower the scavenging/removal rate of radionuclides. However, for ^{137}Cs, the residence half-times decreased sharply upto 16 cm and thereafter an almost constant trend observed from one sediment layer to another suggesting that the radionuclide dwelled for longer times in the upper sediment layers and shorter in the deeper layers before migrating downward. The high residence time at upper layers of sediment indicates that there could be the presence of high content of K or Na or clay minerals in that layer.

The h_0 derived from the sediment profile of radionuclides at the studied area were highly distinct indicating a different penetration rate of radionuclides into the sediment profile at all the three cores. A negative relationship of clay with the h_0 values indicates that as the clay content increases, the penetration depth of deposited radionuclides in sediment profile decreases.

CHAPTER 8
THERMODYNAMICS PARAMETERS OF U (VI) SORPTION ONTO SEDIMENTS/SOILS IN VARIOUS AQUATIC SYSTEMS

8.1. Introduction

It is well known that thermodynamic parameters viz. the standard free energy (ΔG^o), standard enthalpy change (ΔH^o) and standard entropy change (ΔS^o) are important parameters in sorption-desorption process of any element under the natural environment. They can affect the adsorption, microstructure, fate and transport of environmental contaminants in natural soil and water. Therefore, in this chapter, efforts have been made to evaluate the key thermodynamic parameters during uranium sorption onto sediment/soil in various aquatic systems. However, owing to experimental limitations with Th and Pu, study was carried out with uranium only.

The sorption of uranium onto sediments/soils is a result of several processes such as adsorption, chemisorptions and ion exchange [441]**.** The sorption mechanisms are controlled by aqueous solution properties (pH, Eh, ionic strength and presence of complexing ligands) and characteristics of sorbing materials (mineral compositions, surface area, density of sorptive surface sites, solid/solution ratio [442, 443]**.** The behavior and mobility of radionuclides in sediments/soils is a major consideration for distribution coefficients which have also been observed to vary depending on sediments/ soil properties such as texture, organic matter content, bacterial action, pH, redox potential and physicochemical speciation. In addition, there are two parameters i.e. temperature and atmospheric pressure which can influence the sorption processes. Increasing temperature increases the overall energy in the system and this favours a more energetic phase i.e., usually a progression is seen from solid to liquid to gas as temperature is increased. In fact, U solubility with increasing temperature may not follow the general rule, i.e. the solubility decreases with increasing temperature for certain uranium species. This means that the solid phase is favoured over the liquid at elevated temperatures [444]**.** Similarly, atmospheric pressure also plays an important role in systems that include a gas phase, especially surface waters that are in direct contact with the atmosphere. This can affect the distribution of elements between air and water over time. Hence, increasing pressure acts to drive more gas into the aqueous phase, leading to increase of the dissolved atmospheric gasses in the aqueous phase and tends to favour the formation of the more compact aqueous and mineral phases. Most thermodynamic data regarding species of interest used to determine a given equilibrium constant is produced at standard temperature and pressure (STP) or at a temperature of 298.15 K and a pressure of 101.325 kPa [445, 446]**.**

Uranium as hexavalent state is the thermodynamically stable in oxic natural water and interacts strongly with solid phases. The transport of uranium in the natural waters is governed by its interactions with adsorbed phases and a variety of sorption reactions are involved in the dynamic systems. Iron-containing minerals in particular strongly adsorb uranium [447, 448] and its interactions with pure Fe–mineral phases such as ferrihydrite [449]**,** goethite [450, 451]**,** amorphous iron hydroxide [452] and hematite [453] have been thoroughly investigated. In most cases, these studies have focused on the pH-dependent adsorption of uranium in batch experiments and have used different surface complexation model (SCM) formulations to describe the data. The sorption of uranium onto clay minerals is more complex, due to the larger variety of potential sorption sites [454, 455] and their sorption on other pure mineral phases such as sulfides [456] and carbonates [457] have also been investigated.

As with the adsorption of most dissolved metals, aqueous pH has a significant effect on U(VI) adsorption due to the consequence of pH on U(VI) aqueous speciation and the number of exchange sites on variable charged surfaces of solids such as iron, aluminum-oxides and natural organic matter. Depending on the adsorbent, the measured adsorption of U(VI) by soil and single-mineral phases in carbonate-containing aqueous solutions is low at pH values less than 3, increases rapidly with increasing pH from pH 3 to 5, reaches a maximum in adsorption in the pH range from pH 5 to 7 – 8 and then decreases with increasing pH at pH values greater than 7. The increase in U(VI) adsorption onto soil from acidic to near neutral pH values is a consequence of the dominant U(VI) aqueous species being cationic and neutral over this pH range. However, the subsequent decrease in U(VI) adsorption with increasing basic pH values results from the dominant U(VI) aqueous species being anionic U(VI) carbonate complexes. In the absence of dissolved carbonate, uranium sorption to iron oxide and clay minerals has been shown to be extensive and remain at a maximum at pH values near and above neutral pH [458 - 460]**.** However, in the presence of carbonate and organic complexants, U(VI) adsorption has been shown to be substantially reduced or inhibited. Surface complexation studies of uranium adsorption [458, 461 – 465] have shown that the formation of strong anionic U(VI) carbonate complexes decreases U(VI) adsorption at basic pH conditions. Even differences in partial pressures of CO_2 have a major effect on uranium adsorption at neutral pH conditions. **Waite et al (1992),** show that the percent of U(VI) adsorbed onto ferrihydrite decreases from approximately 97 to 38% when CO_2 is increased from ambient (0.03%) to elevated (1%) partial pressures [462]**.**

The sorption behavior of uranium on geologic materials is the subject of extensive study. The majority of these studies deal with the sorption of U (VI). Sorption studies of U(IV) are limited relative to those for U(VI), because U(IV) is considered relatively immobile due to its low solubility under reducing conditions. Studies of U(IV) sorption typically are conducted in support of safety assessments for the geologic disposal of high level radioactive waste in deep crystalline rock formations. These U(IV) sorption studies are usually carried out using crushed rock or single mineral phase(s) relevant to the geologic formation. Because such geologic materials are not relevant to sediments or soils present at the vadose zone in the groundwater. The dominant U(IV) aqueous species are expected to be cationic and neutral over the complete pH range. Therefore, the sorption of U(IV) on sediment is minimal at very acidic conditions, increases with increasing pH especially in the near-neutral pH range and be at a maximum at basic pH conditions. It is noted that uranium sorption measurements conducted under reducing conditions that resulted in very large adsorption (k_d) values are likely affected by U(IV) precipitation reactions and not representative of uranium sorption on mineral surfaces. **Kaplan et al. (1995)** notes that U(VI) adsorption typically increases with increasing ionic strength of an oxidized aqueous solution [468]**.** The presence of increasing concentrations of other dissolves ions, such as Ca^{2+}, Mg^{2+}, and K^{+}, will displace the U(VI) ions adsorbed onto mineral surface sites, and release U(VI) into the aqueous solution. Therefore, the mobility of U(VI) is expected to increase in high ionic-strength solutions.

Naturally occurring organic matter in sediments/soils is also important in the adsorption of uranium. Several mechanisms have been proposed for U(VI) adsorption by organic matter [466]. The adsorption of uranium to humic substances may occur through ion exchange and complexation processes that result in the formation of stable U (VI) complexes involving the acidic functional groups [467, 468]**.** Alternatively, **Nash et al (1981)** has suggested that organic material may act to reduce dissolved U (VI) species to U(IV). Organic matter generally reduces anion adsorption due to the formation of organic coatings on the surface anion adsorbing minerals [469]**.**

Batch sorption methods in various configurations provides the largest fraction of sorption data because of their relative simplicity, lower cost and lack of complicating factors associated with dynamic experiments that involve diffusion and advective transport. In batch experiments the sorbing solid and the solution containing the sorbate (usually dissolved) are contained in a vessel. After a given reaction time the solid and liquid are separated and the liquid (or solid) are characterized for sorbate concentration or chemical form. Batch methods are used for both adsorption and desorption reactions. In the present study, the distribution coefficients of U for sediments in seawater were obtained at three particular temperatures (298 K, 323K and 343 K) and compared with other geochemical environments such as soils (disturbed and undisturbed) under different aqueous media (groundwater and deionised water) using a batch equilibrium experiment. Subsequently, the thermodynamic parameters viz. the standard free energy (ΔG^o), standard enthalpy change (ΔH^o) and standard entropy change (ΔS^o) were determined.

8.2. Experimental

Two bulk composite marine sediment samples collected from Mumbai Harbour Bay and two bulk composite surface (depth upto15cm) soil samples representing undisturbed and disturbed soil of 1 kg each were collected from two different sites in Mumbai. The collected sediments/soil samples were dried at 110° C for 24 h, powdered, homogenized and sieved through 110 mesh sizes. The powdered samples were thoroughly mixed with each other and washed thrice with deionised water for 7 days. The solid phase was allowed to settle by gravity and the washing solution was discarded. After washing, samples were further dried at 110°C, placed in conical flasks and stored as stock samples for experimental work.

A batch equilibrium experiment was conducted to determine the distribution coefficient of U in sediment – seawater system and soils under two different aqueous media viz. groundwater and deionised water. Each of 5 g dried sediment/soil samples was placed in PTFE containers with lid to avoid significant sorption at higher pH on glass ware and equilibrated for 7 days with each of 150 mL seawater (for sediment) and groundwater and deionised water (for soils) containing 10 mgL^{-1} of uranium prepared from standard solutions (1 gL^{-1}) of uranyl nitrate hexahydrate (USA make) followed by shaking at 298, 323 and 343 K using an incubator-cum shaker. After equilibration time, the samples of each set were centrifuged, filtered through 0.45 µm filter paper and concentration of U in the equilibrium solution was determined using laser fluorimetery as discussed in **chapter 3**.. The pH of the equilibrated solution ranged from 7.8 to 8.0. Prior to the experiments, U concentrations in dissolved phases (seawater, groundwater, deionised water) and adsorbed phases (sediment and soils) as a background concentration were also determined. Finally, the sorption of uranium onto sediment/soil in terms of distribution coefficient (k_d) was calculated by batch method formula using **Eq. (6.1)** in **chapter 6.**

8.2.1. Thermodynamic parameters (ΔG^0, ΔH^0 and ΔS^0)

The thermodynamic parameters viz. the standard free energy (ΔG^o), standard enthalpy change (ΔH^o) and standard entropy change (ΔS^o) were determined using the obtained values of k_d of U (VI) in soil/sediment under various aquatic systems. The thermodynamic equilibrium constant, K^0 (or the thermodynamic distribution coefficient) is defined as

$$K^0 = \frac{a_s}{a_e} = \frac{\gamma_s}{\gamma_e}\frac{C_s}{C_e} \qquad \textbf{(Eq. 8.1)}$$

where a_s = activity of adsorbed U on adsorbed phases, a_e = activity of U in solution at equilibrium, γ_s = the activity coefficient of adsorbed U, γ_e = the activity coefficient of U in equilibrium solution, C_s = concentration of adsorbed U on adsorbed phases.

The expression of K^0 can be simplified by assuming that the concentration in the solution approaches zero resulting in $C_s \rightarrow 0$ and $C_e \rightarrow 0$ and the activity coefficients approach unity at these very low concentrations [470, 471]. The above equation can be written as

$$C_s \rightarrow 0 \frac{C_s}{C_e} = \frac{a_s}{a_e} = K^0 = k_d$$

(Eq. 8.2)

Hence, ΔG^0 (kJ mol^{-1}) at temperature T (in Kelvin) was calculated as follows:

$$\Delta G^0 = -RT \ln k_d$$

(Eq. 8.3)

Where R is the universal ideal gas constant (8.314 $Jmol^{-1}K^{-1}$), T is the temperature in Kelvin

Moreover, since the adsorption isotherms have been measured at three temperatures, the heat of adsorption can be calculated. The temperature dependency of distribution coefficient (k_d) obeyed the van’t Hoff equation which can be written in the form of ΔH^0

$$\ln\left(\frac{k_{d(1)}}{k_{d(2)}}\right) = \frac{\Delta H^0}{R}\left[\frac{1}{T_2} - \frac{1}{T_1}\right]$$

(Eq. 8.4)

and $k_{d(1)}$ and $k_{d(2)}$ are the distribution coefficients at particular temperatures T_1 and T_2 (in Kelvin) respectively. ΔS^0 (J $mol^{-1}K^{-1}$) was calculated as [472 – 474]

$$\Delta S^0 = \left(\frac{\Delta H^0 - \Delta G^0}{T}\right)$$

(Eq. 8.5)

Finally, the values of ΔHº and ΔSº can be calculated from the slope and y-intercept of the plot of $\ln k_d$ versus 1/T **(Fig. 8.1 – 8.3)** using the following equations

$$\ln k_d = \frac{\Delta S^0}{R} - \frac{\Delta H^0}{RT}$$

(Eq. 8.6)

8.3. Results and discussions

8.3.1. Sediment/Soil texture

Table 8.1 depicts the estimated values of physical parameters, % C and % N in sediment/ soil. In general, the sediments were mainly composed of silt and clay. The mean content of sand, silt and clay in the sediment were observed to be 2% (> 63µm), 79% (>2 - < 63µm) and 19% (< 2µm) respectively. The mean of bulk density and porosity of sediment were determined to be 1.27 gcm^{-3} and 48% respectively. Disturbed soils were sandy- silt loam in the form of 56% sand, 41 % silt and 3 % clay whereas undisturbed soils were found to be silty-sand loam with the distribution as 23% sand, 72 % silt and 5 % clay. The mean of bulk density, porosity and moisture content of both soils were determined to be 1.64 gcm^{-3}, 36% and 2.21% respectively. Average soil particle density was assumed to be 2640 kg/m^3.

Table 8.1: Estimated values of physical parameters, % C and % N in sediment/ soil

Samples	Bulk density (gmcm $^{-3}$)	Porosity (%)	Moisture content (%)	Sand (%)	Silt (%)	Clay (%)	C (%)	N (%)
Sediment	1.27	48	60	2	79	19	2.28	1.88
Undisturbed soil	1.72	35	1.62	34	61	5	1.95	2.50
Disturbed soil	1.67	37	2.80	56	41	3	0.84	1.74

8.3.2. Uranium sorption onto sediments/soils as a function of temperatures

The sorption of U onto sediment in seawater in terms of k_d values was initially examined at three different temperatures viz 298 K, 323 K and 343 K under the similar laboratory conditions and it was compared with other geochemical environments such as undisturbed and disturbed soil in groundwater and deionised water system. **Table 8.2** illustrates k_d values of U in three different geological environments at 298 K, 323 K and 343 K. In sediment-seawater system, the average extraction rate of U at 298 K was found to be 0.0098 % d^{-1} and reduced to 0.0083 % d^{-1} at 343 K. However for undisturbed soil, at 298 K, the average extraction rate in deionised water and groundwater was obtained to be 0.156 % d^{-1} and 0.081% d^{-1} respectively and at 343 K, it was reduced to 0.107% d^{-1} and 0.074% per d^{-1} for the same respectively. Similarly for disturbed soil, at 298 K, the extraction rate in deionised water (0.162 % d^{-1}) was about 15% more than in groundwater (0.141 % d^{-1}), while at 343 K, the extraction rate decreased to about 50% in both medium. Overall, at 298 K, the extraction rate of uranium in sediment-seawater system was about ten to fifteen times slower than soil-groundwater/deionised water system. Similarly, for undisturbed soil, the extraction rate in groundwater was about 50% slower than in deionised water suggesting that groundwater was observed to be more favorable for high surface sorption of U onto soils. Prior to the experiments, concentrations of U in seawater, groundwater, deionised water, sediment and soils as a background concentration were determined to be 2.5 μgL^{-1}, 3μgL^{-1}, < 0.2 μgL^{-1}, 1 $\mu g\ g^{-1}$ (^{238}U) and 1.7$\mu g\ g^{-1}$respectively.

The measured mean k_d value of uranium in sediment– seawater, soils – deionised water and soils - groundwater system at 298 K was found to be 43448 ± 5280 Lkg^{-1}, 2673 ± 415 $Lkg^{-1}$and 4127± 565 Lkg^{-1}respectively whereas at 343 K, the values were increased to 51381 ± 4800 Lkg^{-1}, 4635 ± 673 $Lkg^{-1}$and 6013 ± 848 L/kg for the same respectively. This clearly indicates that sediment surface is more favorable for U sorption. The high sorption onto sediment may be due to presence of high amount of finer particles in the form of silt and clay. Due to fine particles, the availabilty of exchange surfaces onto sediment will be higher for U which leads to high binding capacity. The another reason might be due to high exchange of U with the calcium bearing minerals present as Ca- montmorillonite, dolomite and calcite in sediments.

Table 8.2: The obtained distribution coefficients of uranium as a function of temperature under various aquatic systems

Samples	Distribution coefficients (k_d, Lkg^{-1})								
	Seawater			Deionised water			Groundwater		
	298 K	323 K	343 K	298K	323K	343K	298 K	323K	343 K
Sediment	43448 ± 5280	48470 ± 4760	51381 ± 4800	NA			NA		
Undisturbed soil	NA			2725 ± 342	3543 ± 365	3985 ± 423	5246 ± 460	5612 ± 572	5814 ± 517
Disturbed soil				2620 ± 235	4362 ± 325	5285 ± 523	3008 ±324	4982 ± 452	6212 ± 672

NA – Not Available

Similarly, the ratio of obtained k_d values of U for undisturbed soil in groundwater to deionised water was found to be 1.92 and 1.46 at 298 K and 343 K respectively whereas for disturbed soil, this ratio was almost insignificant different (differed by 1.7%) for both temperatures. This indicates that the undisturbed soil has stronger sorption capacity than disturbed soil in both aqueous systems. The low sorption onto disturbed soil may be due to presence of high amount of coarse particles in the form of sand (56%). Due to high content of sand, availability of exchange surfaces for U in soil is small and subsequently it released into the dissolved phases leading to low k_d. The another reason for low k_d in disturbed soil might be due to low abundances of total carbon content caused for the poor sorption and complexation processes on organic soil constituents.

The ratio of carbon content in undisturbed to agricultural soil was observed to be 2.32. Overall, it was observed that as temperature increases, sorption of U onto soils/ sediment increases **(see Fig. 8.1 – Fig.8.3)**. This may be due to increase in diffusion rate of U(VI) into the pores of soils/sediments [475, 476]**.** Changes in the soils/sediments pore sizes as well as an increase in the number of active sorption sites near soil/sediment surface edge (due to breaking of some internal bonds) are generally expected at higher temperatures. Thus, the increase in temperature may result in the increase in proportion or concentration of U(VI) in solution, the affinity of U(VI) to the soil surface and the potential charge of soil surface [477].

Kaplan et al. (1998) investigated the adsorption of U (VI) on natural sediment (a silty loam and very coarse sand) containing carbonate minerals in groundwater system and found the k_d values greater than 400 Lkg^{-1} at pH > 10 [478]. **Gamerdinger et al. (1998)** conducted a series of experiments to measure the adsorption of U(VI) on sediments (medium coarse sand, fine sand and silt loam) in groundwater at pH 8.4 under partial moisture saturation conditions and found as increasing trend of k_d values with moisture saturation content [479]. **US EPA, 1999**, has reported the soil- water k_d values in the range of 0.4 – 250000 Lkg^{-1} at pH 8 for U in the look-up-table [480].

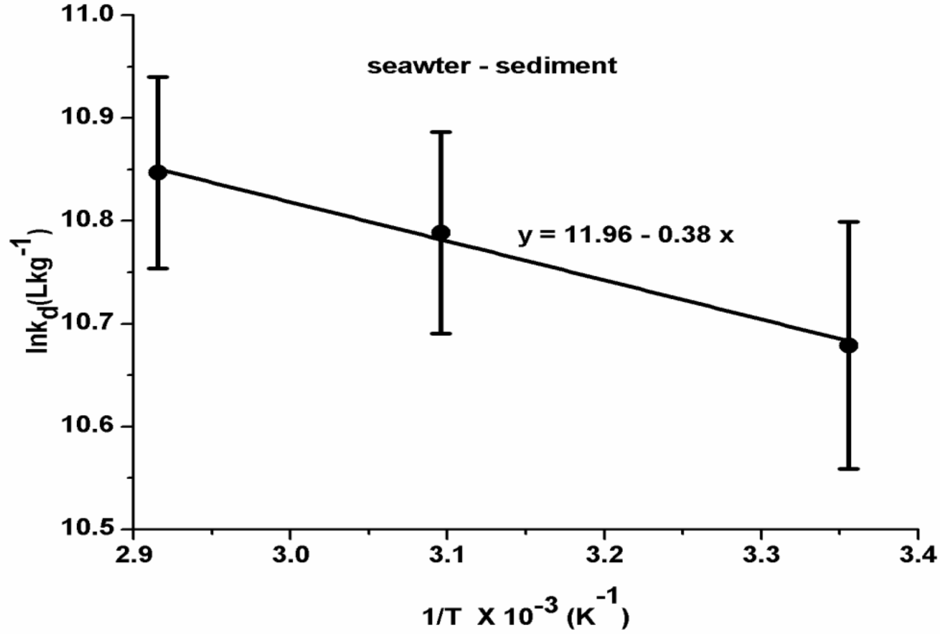

Fig. 8.1: The linear plot of $\ln k_d$ versus 1/T for U(VI) sorption onto sediments in seawater

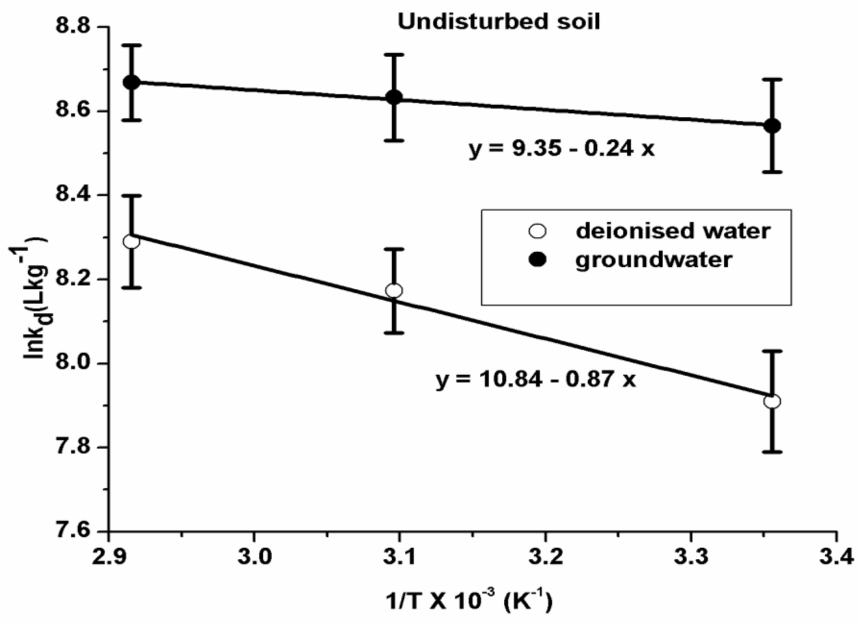

Fig. 8.2: The linear plot of $\ln k_d$ versus 1/T for U(VI) sorption onto undisturbed soil in groundwater and deionised water

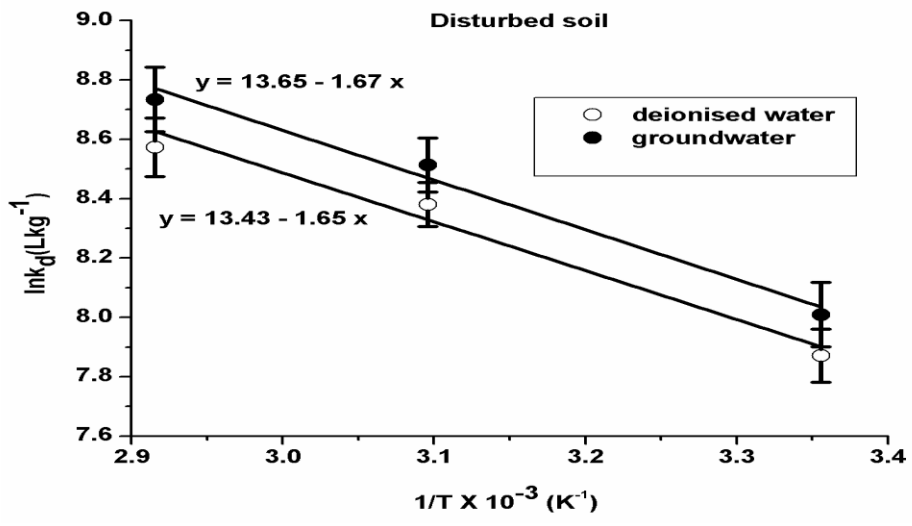

Fig. 8.3: The linear plot of $\ln k_d$ versus 1/T for U(VI) sorption onto disturbed soil (agricultural) in groundwater and deionised water

8.3.3. Thermodynamic studies

The determination of the thermodynamic parameters (ΔH°, ΔS° and ΔG°) for U(VI) as given in **Table 8.3** can provide mechanism insights into U(VI) adsorption onto soils/sediments. The values of ΔH° were positive in soils/sediments, indicating that it is an endothermic process for U adsorption onto them. One possible interpretation for the endothermic process is that U(VI) ions are well solvated in water. In order to adsorb onto soils/sediments, U (VI) ions are denuded of their hydration sheath to some extent and this dehydration process needs energy. It is assumed that the needed energy for dehydration exceeds the exothermicity of the ions attaching to soil/sediment surfaces. The implicit assumption herein is that the adsorbed U(VI) ions are less hydrated than those in solution. The removal of water molecules from U(VI) ions is essentially an endothermic process and the endothermicity of the desolvation process exceeds the enthalpy of sorption to a considerable extent [472, 473, 481]**.**

The values of ΔG° were all negative at all temperatures studied herein as expected for a spontaneous process under our experimental conditions. The higher the reaction temperature, the more negative the value of ΔG°, indicating that the adsorption reaction is more favorable at elevated temperatures [472]. At high temperature, U(VI) ions are readily dehydrated and thereby their sorption becomes more favorable. The ΔG° values for sediments were found to more negative than soils.

However, the values of ΔS° in soils/sediments were all positive, which indicates that during the whole adsorption process, some structural changes occurs on soils/sediments surface and thus leading to an increase in the disorderness at the soil- water interface [472] **[32].** In addition, whether or not a surface adsorption reaction is an associative or dissociative mechanism, strongly depends on the value of ΔS°. When the value of ΔS° is higher than -10 kJ mol^{-1}, a dissociative mechanism controls adsorption [472, 473, 481]**.** The present study confirms that the dissociative mechanism is not responsible for U(VI) adsorption onto soils/sediments. The relatively higher values of ΔSº in disturbed soil revealed a more efficient sorption at higher temperature [476, 482 – 484].

8.3.4. FTIR spectroscopy

The FTIR spectra of undisturbed soil (**see Fig. 6.19**) and sediment (**see Fig. 6.20**) **in chapter 6** have shown the main absorption band at the range of 3361-3374 cm^{-1}, 1634-1674 cm^{-1} and 996 cm^{-1} indicating that they represent H-bonded OH groups (alcohols, phenols, water molecules), C=O stretching vibration of carboxylic and ketonic groups. In addition, the band at 996 cm^{-1} represents due to symmetric stretching vibration of silicate group. However the disturbed soil did not show any significant intensity of absorption band except at 1002 cm^{-1} **(Fig. 8.4)** which also indicates a silicate group.

8.3.5. Speciation of uranium in equilibrium solution

The mean concentration of uranium in equilibrium solution of sediment in seawater was determined to be 7 μgL^{-1} (3.3×10^{-8} M) at 25^0C whereas for soils in deionised water and groundwater was to be 111 μgL^{-1}($\sim 4.7 \times 10^{-7}$ M) and 78 μgL^{-1}($\sim 3.3 \times 10^{-7}$M) respectively as shown in **Table 8.4.** The equilibrium aqueous speciation of U as a function of pH in seawater and groundwater as depicted in **Fig. 8.5 and Fig. 8.6**. The predicted aqueous species as $(UO_2)_2CO_3\ (OH)_3^-(aq)$ accounted for about 68% and 90% of the total dissolved U at measured pH range of equilibrium solution of seawater and groundwater respectively. The mixed hydroxo-carbonato species of U, might be assumed to adsorb onto sediment/soil surface and caused the removal of U under alkaline conditions.

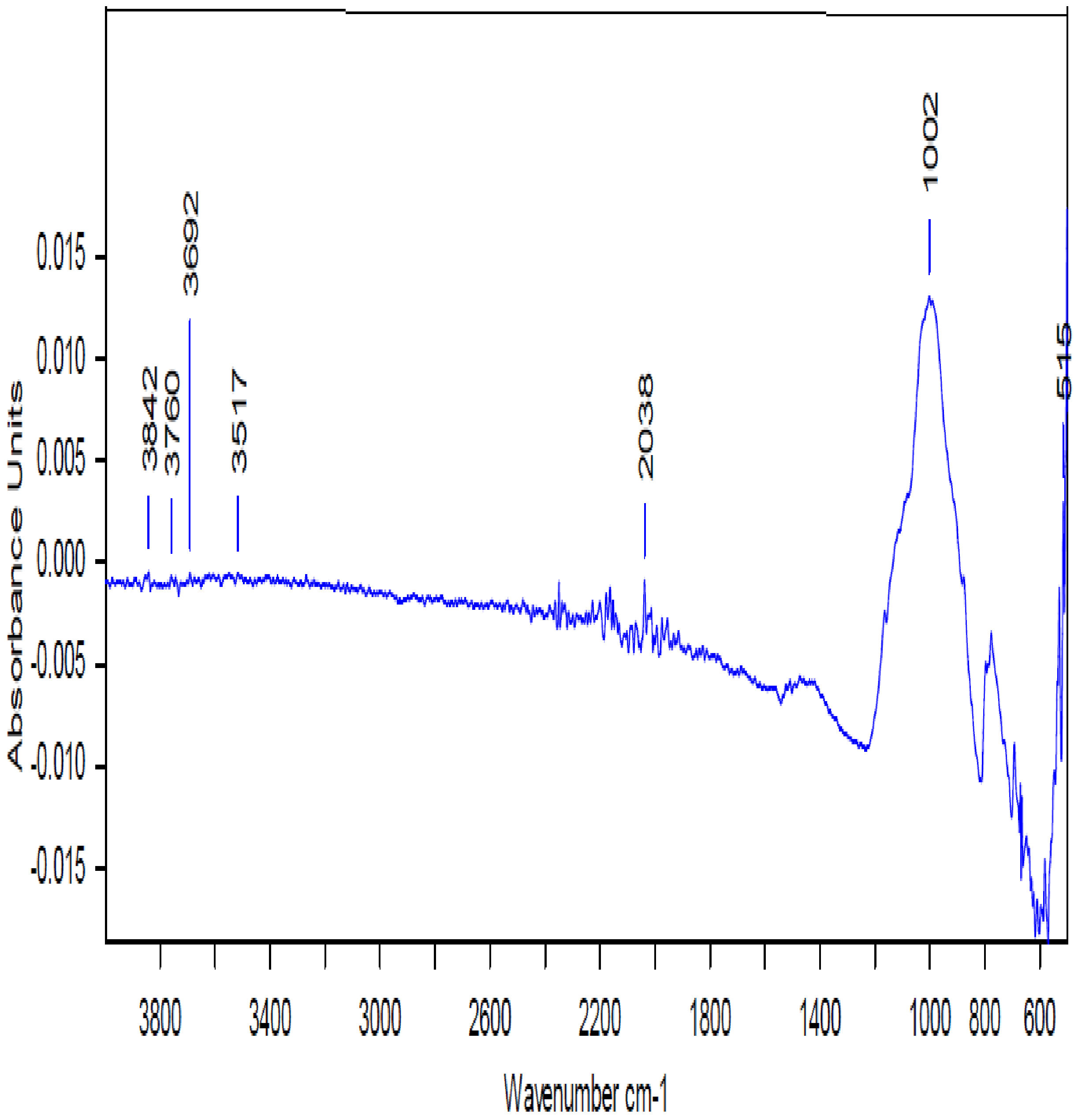

Fig. 8.4: FTIR spectra of disturbed soil at 298 K

Table 8.3: The Obtained thermodynamic parameters for U sorption onto sediment/soils as a function of temperature under different aqueous media

Samples	ΔH^0 (kJ/mol)			ΔS^0 (J/ mol/°K)			ΔG^0 (kJ/mol)								
							SW			DW			GW		
	SW	DW	GW	SW	DW	GW	298 K	323 K	343 K	298 K	323 K	343 K	298 K	323 K	343 K
Sediment	3.16	-	-	99.60	-	-	-26.45	-28.96	-30.91	-			-		
Undisturbed soil	-	7.23	2.00	-	90.00	77.74	-			-19.60	-21.95	-23.64	-21.22	-22.50	-24.72
Disturbed soil	-	13.72	13.88		111.66	113.48	-			-19.50	-22.50	-24.43	-19.84	-22.86	-24.91

SW – Seawater, DW – Deionised water, GW - Groundwater

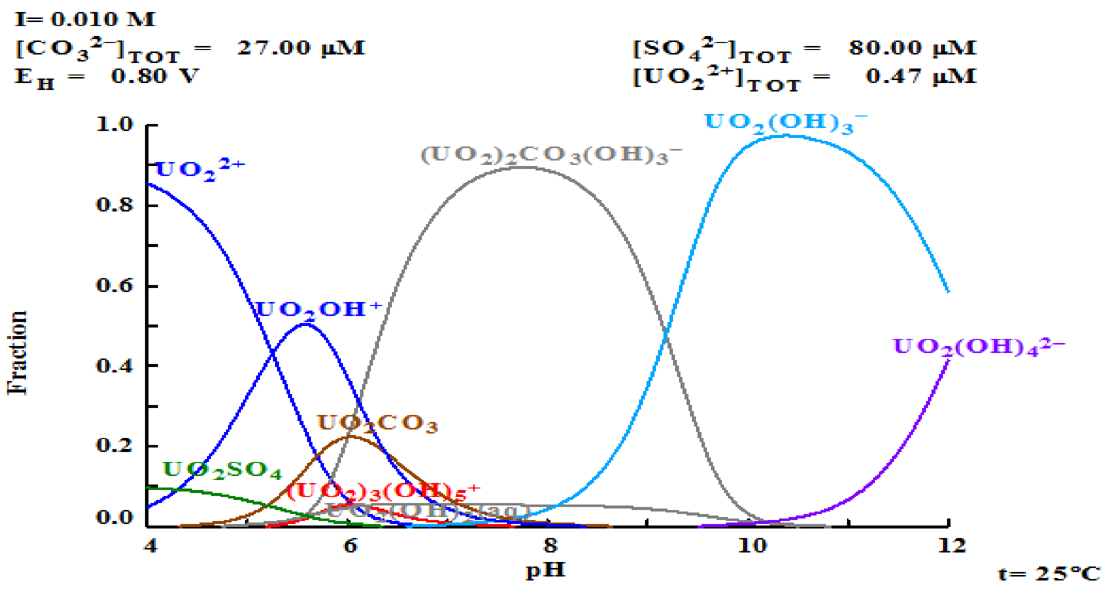

Fig. 8.5: The fraction of uranium species as a function of pH in equilibrium solution of groundwater

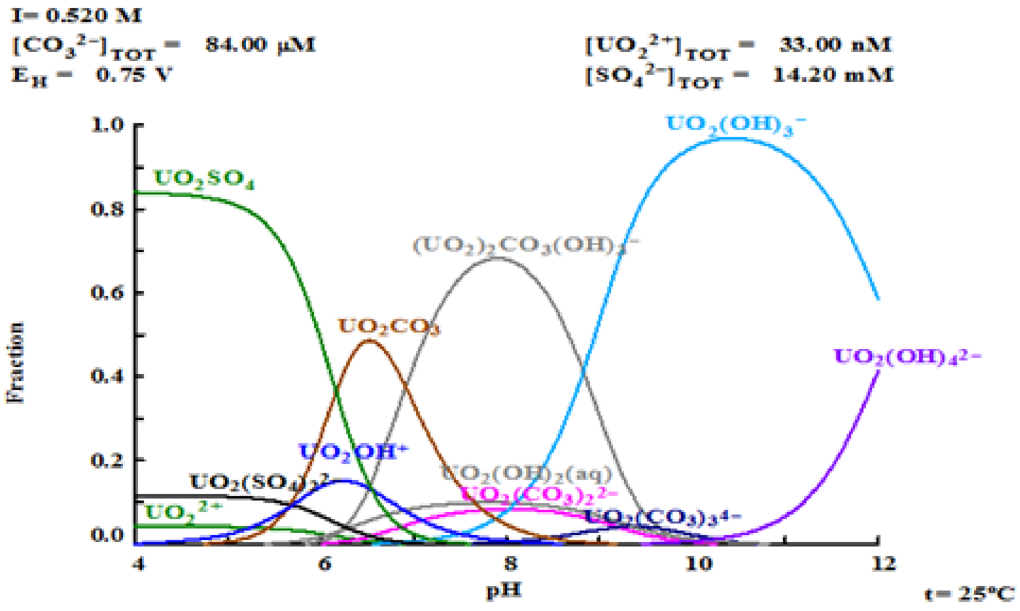

Fig. 8.6: The fraction of uranium species as a function of pH in equilibrium solution of seawater

Table 8.4: Ionic composition of equilibrium solutions in soils under different aqueous media at 298 K

Ionic components	Mean Values		
	Groundwater	Deionised water	Seawater
U (µg L^{-1})	78	111	7
Cl^{-1} (mgL^{-1})	12	6	16812
NO_3^{-1}(mgL^{-1})	2	ND	ND
SO_4^{-2}(mgL^{-1})	8	2	1364
HCO_3^{-1} (mgL^{-1})	308	ND	150
CO_3^{2-}(mg/L)	1.6	ND	5
Na^{+1}(mgL^{-1})	14	5	9310
K^{+1}(mgL^{-1})	1.8	1.2	312
Mg^{+2}(mgL^{-1})	6	2.4	971
Ca^{+2}(mgL^{-1})	7	2	538
Eh (V)	0.8	NA	0.75
Ionic strength (molal)	0.1	0.001	0.52

8.4. Conclusions

In this work, the obtained values of ΔSº for soils and sediment were all positive indicating that that there are some structural changes at their surfaces during the complete adsorption process. Moreover, the relatively higher values of ΔSº in disturbed soil revealed a more efficient sorption at higher temperature due to increased randomness at solid-solution interface. The experimental results have shown that as temperature increases, sorption of U onto soils/ sediment increases. This might be due to increase in diffusion rate of U(VI) into the pores of soils/sediments. this leads to change their pore sizes as well as an increase in the number of active sorption sites (due to breaking of some internal bonds near soil/sediment surface edge).

Batch adsorption results indicated that U sorption onto soils/sediments was promoted at higher temperature and an endothermic and spontaneous interfacial process. Thus it can be concluded that the thermodynamic parameters are related to both the nature of sorbate and the nature of solid particles. The low sorption onto soil may be due to presence of high amount of coarse particles. On the other hand, it can be predicted that, the enhanced k_d values at high temperatures are less susceptible to U mobility in soils/sediments. Thus, temperature dependent physical properties of soil or sediment need to be studied in the assessment of thermodynamic parameters. Geochemical modeling predicted that mixed hydroxocarbonato complexes of uranium were the most stable and abundant complexes in equilibrium solution during experimental. The data and modeling calculations illustrate that it is important to take into account the effect of geochemical parameters on U aqueous speciation when predicting its sorption and mobility at contaminated soil/sediment. The findings in this study are quite important to understand the physicochemical behavior of radionuclides of interest in the natural environment.

REFERENCES

1. Bruno, J. and Montoya, V. (2012), From aqueous solution to solid solutions: A process oriented review of the work performed within the Fundamentals of Radionuclide Migration (FUNMIG) project, Applied Geochemistry, 27, 444–452.
2. Cowart, J.B. and Burnett, W.C. (1994), The distribution of uranium and thorium decay – series radionuclides in the environment: a review, Journal of. Environmental Quality, 23, 651− 662.
3. Gascoyne, M. (1992), Geochemistry of the actinides and their daughters; In uranium-series disequilibrium: Applications to earth, marine and Environmental Sciences, 2nd ed., Ivanovich, M., Harmon, R.S., Eds., Oxford University Press, Oxford, U.K., 34−61.
4. Cowan, G.A. and Adler, H.H. (1976). The variability of the natural abundances of ^{235}U, Geochimica Cosmochimica Acta, 40, 1487−1490.
5. Gauthier-Lafaye, F., Holliger, P. and Blanc, P.L. (1996), Natural fission reactors in the Franceville basin, Gabon: a review of the conditions and results of a ‘critical event’ in a geologic system, Geochimica Cosmochimica Acta, 60 (23), 4831−4852.
6. Smellie, J. (1995), The fossil nuclear reactors of Oklo, Gabon, Journal of Radwaste Magazine, 2(2), 18-22.
7. Burbidge, E.M., Burbidge, G.R., Fowler, W.A. and Hoyle, F. (1957), Synthesis of the elements in Stars, Reviews of Modern Physics, 29 (4): 547–650.
8. Baruah, R., Duorah, K., and Duorah, H.L. (2012), Isotopic r-process abundances produced by supernova explosions, Astrophysics Space Science, 340 (2), 291−305.

9. Cowan, J.J., Thielemann, F.K. and Truran, J.W. (1991), The r-process and nucleochronology, Physics Reports, Review Section Physics Letters, 208 (4-5), 267−394.
10. Kuroda, P.K. (1996), Extraterrestrial radioactivity, Journal of Radioanalytical Nuclear Chemistry, 203, 591−599.
11. Kimura, T., Choppin, G.R., Kato, Y. and Yoshida, Z. (1996), Determination of the hydration number of Cm(III) in various aqueous solutions, Radiochimica Acta, 72 (2), 61 - 64.
12. Runde, W. and Neu, M.P. (2010), Actinides in the Geosphere, In the chemistry of the actinide and transactinide elements, 4th ed., Morss, L.R., Edelstein, N.M., Fuger, J., Eds., Springer : Dordrecht, The Netherlands, 3475−3593.
13. Choi, J.S. and Pigford, T.H. (1981), Water dilution volumes for high-level wastes, Transactions of the American Nuclear Society, 39, 176−177.
14. Perkins, R.W. and Thomas, C.W. (1980). In: Hanson, W.C. (Ed.), Transuranic elements in the environment worldwide fallout. NTIS, Springfield, M.O., 53–82. DOE/TIC-22800.
15. Pentreath, R.J., Lovett, M. B., Jefferies, D.F., Woodhead, D.S., Talbot, J.W. and Mitchell, N. T. (1984), Impact on public radiation exposure of transuranium nuclides discharged in liquid waste from fuel element reprocessing at Sellafield Radioactive Waste Management, IAEA, Vienna.
16. Holm, E., Fukai, R. and Whitehead, N.E. (1986), Radiocesium and transuranium elements in the mediterrancan sea: Conferencia International sobre radioactividad Ambiental en ei Area del Mediterranco, Socie-dad Nuclear Espafiola, Madrid, 601-617

17. Neuefeind, J., Soderholm, L. and Skanthakumar, S. (2004), Uranyl nitrate complex migration into TBP/Dodecane organic solution: A molecular dynamics study, Journal of Physical Chemistry, A, 108, 2733−2739.
18. Denning, R.G. (1992), Electronic structure and bonding in actinyl ions, Structural Bonding (Berlin), 79, 215−276.
19. Denning, R.G. (2007), Electronic structure and bonding in actinyl ions and their analogs, Journal of Physical Chemistry, A, 111, 4125−4143.
20. Choppin, G.R. and Jensen, M.P. (2010), Actinides in solution: Complexation and kinetics, In the chemistry of the actinide and transactinide elements, 4th ed., Morss, L.R., Edelstein, N. M., Fuger, J., Eds., Springer: Dordrecht, The Netherlands, 2524−2621.
21. Reed, D.T., Deo, R.P. and Rittmann, B. (2010), Subsurface interactions of actinide species with microorganisms, In the chemistry of the actinide and transactinide elements, 4th ed., Morss, L.R., Edelstein, N.M., Fuger, J., Eds., Springer: Dordrecht, The Netherlands, 3595− 3663.
22. Christensen, H. and Sunder, S. (2000), Current state of knowledge of water radiolysis effects on spent nuclear fuel corrosion, Nuclear Technology, 131, 102−123.
23. Sattonnay, G., Ardois, C., Corbel, C., Lucchini, J. F., Barthe, M.F., Garrido, F. and Gosset, D. (2001), Alpha-radiolysis effects on UO_2 alteration in water, Journal of Nuclear Materials, 288, 11−19.
24. Langmuir, D. and Herman J.S. (1980), The mobility of thorium in natural waters at low temperatures, Geochimica Cosmochimica Acta, 44, 1753–1766.
25. Guillaumont, R., Fanghanel, T., Volker, N., Fuger, J., Palmer, M.R., Grenthe, I. and Rand, M.H. (2003), Update on the chemical thermodynamics of uranium, neptunium,

plutonium, americium and technicium, Chemical Thermodynamics, 5, Elsevier, Amsterdam, The Netherlands .

26. Dong, W. and Brooks, S.C. (2006), Determination of the formation constants of ternary complexes of uranyl and carbonate with alkaline earth metals (Mg^{2+}, Ca^{2+}, Sr^{2+}, and Ba^{2+}) using anion exchange method, Environmental Science Technology, 40, 4689− 4695.
27. Berto, S., Crea, F., Daniele, P.G., Gianguzza, A., Pettignano, A. and Sammartano, S. (2012), Advances in the investigation of dioxo-uranium (VI) complexes of interest for natural fluids, Coordination Chemistry Reviews, 256, 63−81.
28. Soderholm, L., Skanthakumar, S., Gorman-Lewis, D., Jensen, M.P. and Nagy, K.L. (2008), Characterizing solution and solid-phase amorphous uranyl silicates, Geochimica Cosmochim.Acta, 72, 140−150.
29. Rajan, K.S. and Martell, A.E. (1965), Equilibrium studies of uranyl complexes, III: Interaction of uranyl Ion with citric acid, Inorganic Chemistry, 4, 462−469.
30. Rajan, K.S. and Martell, A.E. (1964), Equilibrium studies of uranyl complexes—I: Interaction of uranyl ion with some hydroxy-carboxylic and amino carboxylic acids, Journal of Inorganic Nuclear Chemistry, 26, 789−798.
31. Rajan, K.S. and Martell, A.E. (1964), Equilibrium studies of uranyl complexes—II: Interaction of uranyl ion with tartaric and malic acids, .Journal Inorganic Nuclear Chemistry, 26, 1927−1944.
32. Crea, F., De Robertis, A., De Stefano, C. and Sammartano, S. (2007), Dioxouranium (VI)-carboxylate complexes, A calorimetric and potentiometric investigation on the interaction towards oxalate at infinite dilution and in NaCl aqueous solution at I = 1.0 $molL^{-1}$ and t = 25 °C, Talanta, 71, 948−963.

33. Ulrich, K.U., Veeramani, H., Bernier-Latmani, R. and Giammar, D.E. (2011), Speciation-dependent kinetics of uranium (VI) bioreduction, Geomicrobiology Journal, 2011, 28, 396−409.
34. Stewart, B.D., Amos, R.T., Nico, P.S. and Fendorf, S. (2011), Influence of uranyl speciation and iron oxides on uranium biogeochemical redox reactions, Geomicrobiology Journal, 28, 444−456.
35. Stewart, B.D., Neiss, J. and Fendorf, S. (2007), Speciation-dependent microbial reduction of uranium within iron-coated sands, Journal of Environmental Quality, 36, 363−372.
36. Singer, D.M., Chatman, S.M., Ilton, E.S., Rosso, K.M., Banfield, J.F. and Waychunas, G.A. (2012), Identification of simultaneous U(VI) sorption complexes and U(IV) nanoprecipitates on the magnetite (111) surface, Environmental Science Technology, 46, 3811− 3820.
37. Brooks, S.C., Fredrickson, J.K., Carroll, S.L., Kennedy, D.W., Zachara, J.M., Plymale, A. E., Kelly, S.D., Kemner, K.M. and Fendorf, S. (2003), Inhibition of bacterial U(VI) reduction by calcium, Environmental Science Technology, 37, 1850−1858.
38. Rajan, K.S. and Martell, A.E. (1967), Equilibrium studies of uranyl complexes—IV: Reactions with carboxylic acids, Journal of Inorganic Nuclear Chemistry. 29, 523−529.
39. Meinrath, G. (1997), Uranium (VI) speciation by spectroscopy, Journal of Radioanalytical Nuclear Chemistry, 224, 119−126.
40. Bernhard, G., Geipel, G., Reich, T., Brendler, V., Amayri, S. and Nitsche, H. (2001), Uranyl (VI) carbonate complex formation: Validation of the $Ca_2UO_2(CO)_3$(aq.) species, Radiochimica Acta, 89, 511−518.

41. Guenther, A., Steudtner, R., Schmeide, K. and Bernhard, G. (2011), Luminescence properties of uranium(VI) citrate and uranium(VI) oxalate species and their application in the determination of complex formation constants, Radiochimica Acta, 99, 535−541.
42. Pasilis, S.P. and Pemberton, J.E. (2003), Speciation and coordination chemistry of uranyl (VI)-citrate complexes in aqueous solution, Inorganic Chemistry, 42, 6793− 6800.
43. Goldstein, S.J., Abdel-Fattah, A.I., Murrell, M.T., Dobson, P.F., Norman, D. E., Amato, R. S. and Nunn, A.(2010), Uranium-series constraints on radionuclide transport and groundwater flow at the Nopal I uranium deposit, Sierra Peña Blanca, Mexico, Journal of Environmental Science Technology, 44, 1579−1586.
44. Dodge, C.J. and Francis, A.J. (2003), Structural characterization of a ternary Fe(III)-U(VI)-citrate complex, Radiochimica Acta, 91, 525−532.
45. Bailey, E.H., Mosselmans, J.F.W. and Schofield, P.F. (2005), Uranyl-citrate speciation in acidic aqueous solutions—an XAS study between 25 and 200° C, Chem. Geology, 216, 1−16.
46. Bailey, E. H., Mosselmans, J.F.W. and Schofield, P.F. (2004), Uranyl acetate speciation in aqueous solutions—an XAS study between 25° C and 250° C, Geochimica Cosmochimica Acta 68, 1711−1722.
47. Hennig, C., Schmeide, K., Brendler, V., Moll, H., Tsushima, S. and Scheinost, A.C. (2007), EXFAS investigation of U(VI), U(IV) and Th(IV) sulfato complexes in aqueous solution, Inorganic Chemistry, 46, 5882−5892.
48. Hennig, C., Tutschku, J.,Rossberg, A., Bernhard, G. and Scheinost, A.C. (2005), Comparative EXFAS investigation of Uranium(VI) and - (IV) aquochloro complexes in

solution using a newly developed spectroelectrochemical cell, Inorganic Chemistry, 44, 6655−6661.

49. Ray, R.S., Krueger, S. and Roesch, N. (2009), Ternary Complexes of Uranyl monocarboxylate: Structure, Energetic and Stability Constant, Inorganic Chimica Acta, 363, 263−269.
50. Thurman, E.M. (1985), Organic geochemistry of natural waters, Springer, Dordrecht, The Netherlands,
51. Kharaka, Y.K. and Hanor, J.S. (2003), Deep Fluids in the Continents: I. Sedimentary Basins, Elsevier: Amsterdam, The Netherlands, 5, 1−48.
52. Jones, D.L. (1998), Organic acids in the rhizopshere, Plant and Soil, 205, 25−44.
53. Kantar, C. (2007), Heterogeneous processes affecting metal ion transport in the presence of organic ligands: Reactive transport modeling, Earth-Science Reviews, 81, 175−198.
54. De Stefano, C., Gianguzza, A., Pettignano, A., Piazzese, D. and Sammartano, S. (2011), Uranium (VI) sequestration by polyacrylic and fulvic acids in aqueous solution, Journal of Radioanalytical Nuclear Chemistry, 289, 689−697.
55. Allen, P. G., Shuh, D. K., Bucher, J.J., Edelstein, N.M., Reich, T., Denecke, M.A. and Nitsche, H. (1996 a), EXFAS determinations of uranium structures: The uranyl ion complexed with tartaric, citric and malic acids, Inorganic Chemistry, 35,784 -787.
56. Crea, F., Foti, C. and Sammartano, S. (2008), Sequestering ability of polycarboxylic ligands towards dioxouranium (VI), Talanta, 75, 775−785.
57. Pompe, S., Schmeide, K., Bubner, M., Geipel, G., Heise, K.H., Bernhard, G. and Nitsche, H.(2000), Investigation of humic acid complexation behavior with uranyl ions using modified synthetic and natural humic acids, Radiochim.Acta, 88, 553−558.

58. Schild, D. and Marquardt, C.M. (2000), Analysis of Th (IV)-humate by XPS, Radiochimica Acta, 88, 587−591.
59. Kantar, C. and Honeyman, B.D. (2006), Citric acid enhanced remediation of soils contaminated with uranium by soil flushing and soil washing, Journal of Environmental Engineering, (American Society of Civil Engineering), 132, 247−255.
60. Landais, P., Dubessy, J., Poty, B. and Robb, L. (1990), Preliminary chemical analyses and Raman spectroscopy on selected samples of Witwatersrand kerogen, Journal of Organic Geochemistry, 16, 601−608.
61. Wood, S.A. (1996), The role of humic substances in the transport and fixation of metal of economic interest (Au, Pt, Pd, U, V), Ore Geology Reviews, 11, 1−31.
62. Crancon, P. and van der L. (2003), Speciation and mobility of uranium (VI) in humic containing soils, Radiochimica. Acta, 91, 673−679.
63. Zhou, P. and Gu, B.H. (2005), Humics impact uranium bioreduction and oxidation, Environmental Science Technology, 39, 4435−4440.
64. Bencheikh-Latmani, R. and Leckie, J.O. (2003), Association of uranyl with the cell wall of Pseudomonas fluorescens inhibits metabolism, Geochimica Cosmochimica Acta, 67, 4057−4066.
65. Matsunaga, T., Nagao, S., Ueno, T., Takeda, S., Amano, H. and Tkachenko, Y. (2004), Association of dissolved radionuclides released by the Chernobyl accident with colloidal materials in surface water, Applied Geochemistry, 19, 1581−1599.
66. Choppin, G.R. (1992), The role of natural organics in radionuclide migration in natural aquifer systems, Radiochimica Acta, 58−59, 113−120.

67. Zeh, P. and Kim, J.I., Marquardt, C.M. and Artinger, R. (1999), The reduction of Np(V) in groundwater rich in humic substances, Radiochimica Acta, 87, 23−28.
68. Andre, C. and Choppin, G. R. (2000), Reduction of Pu(VI) by humic acid, Radiochimica Acta, 88, 613−616.
69. Zavarin, M., Powell, B.A., Bourbin, M., Zhao, P. and Kersting, A.B. (2012), Np(V) and Pu(V) ion exchange on Montmorillonite, Environmental Science Technology, 46, 2692−2698.
70. Keeney-Kennicutt, W.L. and Morse, J.W. (1985), The redox chemistry of $Pu(V)O_2^+$ interaction with common mineral surfaces in dilute solutions and seawater, Geochimica Cosmochimica Acta, 49, 2577−2588.
71. Powell, B.A., Fjeld, R.A., Kaplan, D.I., Coates, J.T. and Serkiz, S.M. (2005), Pu $(V)O_2^+$ adsorption and reduction on synthetic Goethite (α-FeOOH) and Hematite (α-Fe_2O_3), Environmental Science Technology, 39, 2107−2114.
72. Powell, B.A., Fjeld, R.A., Kaplan, D.I., Coates, J.T. and Serkiz, S.M. (2004), Pu $(V)O_2$ adsorption and reduction on synthetic magnetite (Fe_2O_3), Environmental Science Technology, 38, 6016−6024.
73. Soderholm, L., Almond, P.M., Skanthakumar, S., Wilson, R.E. and Burns, P.C. (2008), The structure of the plutonium oxide nanocluster $[Pu_{38}O_{56}Cl_{54}(H_2O)_8]_{14,}$ Angew. Chemistry, Intern. Ed., 47, 298−302.
74. Schmeide, K., Reich, T., Sachs, S. and Bernhard, G. (2006), Plutonium (III) complexation by humic substances studied by X-ray absorption fine structure spectroscopy, Inorganic Chimica Acta, 359, 237−242.

75. Degueldre, C. (2010), Identification and speciation of actinides in the environment, In the chemistry of the actinide and transactinide elements, 4th ed., Morss, L.R., Edelstein, N.M., Fuger, J., Eds., Springer: Dordrecht, The Netherlands, 3013−3085.
76. Kaszuba, J.P. and Runde, W.H. (1999), The aqueous geochemistry of neptunium; Dynamic control of soluble concentrations with applications to nuclear waste disposal, Environmental Science Technology, 33, 4427−4433.
77. Rai, D., Serne, R.J. and Moore, D.A.(1980), Solubility of Plutonium compounds and their behavior in soils, Soil Science Society American Journal, 44, 490−495.
78. Qafoku, N.P. and Icenhower, J.P. (2008), Interactions of aqueous U(VI) with soil minerals in slightly alkaline natural systems, Reviews of. Environmental Science Bio-Technology, 7, 355−380.
79. Geckeis, H. and Rabung, T.J. (2008), Actinide geochemistry: From molecular level to the real system, Contaminant Hydrology, 102, 187−195.
80. Allard, T., Calas, G. and Ildefonse, P. (2007), Reconstruction of past uranium migration in a sedimentary deposit (Coutras, France): implications for a radwaste repository, Chemical Geology, 239, 50−63.
81. Allard, T., Ildefonse, P., Beaucaire, C. and Calas, G. (1999), Structural chemistry of uranium associated with Si, Al, Fe gels in a granitic uranium mine, Chemical Geology, 158, 81−103.
82. Choppin, G.R. (2006), Environmental behavior of actinides, Czechoslovakia Journal of Physics, 56, D13.

83. Clark, M.W.,; Harrison, J.J. and Payne, T.E. (2011), The pH-dependence and reversibility of uranium and thorium binding on a modified bauxite refinery residue using isotopic exchange techniques, Journal of Colloid Interface Science, 356, 699-705.
84. Landa, E.R., Le, A.H., Luck, R.L. and Yeich, P. (1995), Sorption and coprecipitation of trace concentration of Thorium and various minerals under conditions simulating an acid uranium mill effluent environment, Journal of Inorganic Chimica Acta, 229-247.
85. Murphy, R.J., Lenhart, J.J. and Honeyman, B.D (1999), The sorption of thorium (IV) and uranium (IV) to hematite in the presence of Natural organic matter, Colloids Surface A, 157, 47-62.
86. Da□hn, R., Scheidegger, A.M., Manceau, A., Curti, E., Baeyens, B., Bradbury, M.H.and Chateigner, D. (2002), Th uptake on montmorillonite : A powder and polarized extended X-Ray absorption fine structure (EXAFS) study, Journal of Colloid Interface Science, 249, 8-21.
87. Carroll, S.A., Bruno, J., Petit, J.C. and Dran, J.C. (1992), Interaction of U(VI) Nd and Th(IV) at the calcite-soltionnterface, Radiochimica Acta, 58−59, 245-252.
88. Neck, V., Altmaier, M. and Fangha□nel, T.C. (2003), Solubility of plutonium hydroxides/hydrous oxides under reducing conditions and in the presence of oxygen, Comptes Rendus Chimie, 10, 959-977.
89. Reiller, P., Moulin, V., Casanova, F. and Dautel, C. (2003), On the study of Th(IV)-humic acid interactions by competition sorption studies with silica and determination of global interaction constant, Radiochimica Acta, 91, 513-524.

90. Bradbury, M.H. and Baeyens, B. (2005), Experimental measurements and modeling of sorption competition on montmorillonite, Geochimica Cosmochimica Acta, 69, 4187-4197.
91. Seco, F., Hennig, C., de Pablo, J., Rovira, M., Rojo, I., Marti,V., Gimenez, J., Duro, L., Grive, M. and Bruno, J. (2009), Sorption of Th(IV) onto iron corrosion products : EXAFS study, Environmental Science Technology, 43, 2825-2830.
92. Yamaguchi, T., Nakayama, S. and Yoshida, T. (2004), Interactions between anionic complex species of actinides and negatively charged mineral surfaces, Radiochimica Acta, 92, 677-682.
93. Davis, J.A., Meece, D.E., Kohler, M. and Curtis, G.P. (2004), Approaches to surface complexation modeling of uranium(VI) adsorption on aquifer sediments, Geochimica Cosmochimica Acta, 68, 3621-3641.
94. Gabriel, U., Charlet, L., Schläpfer, C.W., Vial, J.C., Brachmann, A. and Geipel, G. (2001), Uranyl surface speciation on silica particles studied by Time-Resolved Laser-Induced Fluorescence Spectroscopy, Journal of Colloid Interface Science, 239, 358-368
95. Walter, M., Arnold, T., Geipel, G., Scheinost, A. and Bernhard, G.J. (2005), An EXAFS and TRLFS investigation on uranium(VI) sorption to pristine and leached albite surfaces, Journal of Colloid Interface Science, 282 (2), 293-305.
96. Kowal-Fouchard, A., Drot, R., Simoni, E. and Ehrhardt, J.J. (2004), Use of spectroscopic techniques for uranium (VI)/montmorillonite interaction modeling, Environmental Science Technology, 38, 1399-1407.

97. Katsoyiannis, I.A. (2007), Carbonate effects and pH-dependence of uranium sorption onto bacteriogenic iron oxides: Kinetic and equilibrium studies, Journal of Hazardous Materials, 139 (1), 31-137,
98. Dong, W.M., Ball, W.P., Liu, C.X., Wang, Z.M., Stone, A.T., Bai, J. and Zachara, J.M. (2005), Influence of calcite and dissolved calcium on uranium (VI) sorption to a Hanford subsurface sediment, Environmental Science and Technology 39(20), 7949-7955.
99. Alliot, C., Vitorge, P.,Bion, L. and Mercier, F. (2005), Effect of aqueous acetic, oxalic and carbonic acids on the adsorption of uranium(VI) onto alpha-alumina, New Journal of Chemistry, 29, 1409-1415.
100. Hartmann, E., Geckeis, H., Rabung, T., Lu□tzenkirchen, J. and Fangha□nel, T. (2008), Th. Sorption of radionuclides onto natural clay rocks, Radiochim.Acta, 96, 699-707.
101. Stoliker, D. L., Kent, D.B. and Zachara, J.M. (2011), Quantifying differences in the impact of variable chemistry of equilibrium uranium (VI) adsorption properties of aquifer sediments, Environmental Science Technology, 45, 8733 - 8740.
102. Shang, J., Liu, C., Wang, Z., Zachara, and J.M. (2011), Effect of grain size on Uranium(VI) surface complexation kinetics and adsorption additivity, Environmental Science Technology, 45 (14), 6025 -6031.
103. Fo□rstendorf, H., Heim, K. and Rossberg, A. (2012), The complexation of uranium(VI) and atmospherically derived CO_2 at the ferrihydrite–water interface probed by time-resolved vibrational spectroscopy, Journal of Colloid and Interface Science, 377 (1) , 299 - 306,

104. Elzinga, E.J., Tait, C.D., Reeder, R.J., Rector, K.D., Donohoe, R.J. and Morris, D.E. (2004), Spectroscopic investigation of U (VI) sorption at the calcite-water interface, Geochimica Cosmochimica Acta, 68, 2437-2448.

105. Singer, D.M., Chatman, S.M., Ilton, E.S., Rosso, K.M., Banfield, J.F. and Waychunas, G.A. (2012), U(VI) sorption and reduction kinetics on the magnetite (111) surface, Environmental Science Technology, 46 (7), 3811 -3830.

106. Tochiyama, O., Endo, S. and Inoue, Y. (1995), Sorption of neptunium (V) on various ironoxides and hydrous iron oxides, Radiochimica Acta, 68, 105-111.

107. T. Hiemstra, Van R.W.H., Rossberg, A. and Ulrich, K.U. (2009), A surface structural model for ferrihydrite, II, Adsorption of uranyl and carbonate, Geochimica Cosmochimica Acta, 73, 4437-4451.

108. Sato, S., Niitsu, Y., Ohashi, H., Sakamoto, Y., Nagao, S., Ohnuki, T. and Muraoka, S. (1997), Effects of humic acid on the sorption of neptunium (V) on kaolinite, Journal of Nuclear Materials, 248, 328 – 332.

109. Chisholm-Brause, C., Conradson, S.D., Buscher, C.T., Eller, P.G. and Morris, D.E. (1994), Speciation of uranyl sorbed at multiple binding sites on montmorillonite, Geochimica Cosmochimica Acta, 58 (17), 3625-3631.

110. Stumpf, T., Bauer, A., Coppin, F. and Kim, J.I. (2002a), Time-resolved laser fluorescence spectroscopy study of the sorption of Cm(III) onto smectite and kaolinite, Environmental Science Technology, 35, 3691-3694.

111. Stumpf, T., Bauer, A., Coppin, F., Fangha□nel, T. and Kim, J.I. (2002b), Inner-sphere, outer-sphere and ternary surface complexes: a TRLFS study of the sorption process of Eu(III) onto smectite and kaolinite, Radiochimica Acta, 90, 345 -349.

112. Schmidt, M., Lee, S.S., Wilson, R.E., Soderholm, L. and Fenter, P. (2012), Sorption of tetravalent thorium on muscovite, Geochimica Cosmochimica Acta, 88, 66 -76.

113. Miller, A.W. and Wang, Y. (2012), Radionuclide interaction with clays in dilute and heavily compacted systems: a critical review, Environmental Science Technology, 46, 1981-1994.

114. Bradbury, M. H. and Baeyens, B. (2005), Modelling the sorption of Mn(II), Co(II), Ni(II), Zn(II), Cd(II), Eu(III), Am(III), Sn(IV), Th(IV), Np(V) and U(VI) on montmorillonite : Linear free energy relationships and estimates of surface binding constants for some selected heavy metals and actinides, Geochimica Cosmochimica Acta , 69, 875 -892.

115. Bradbury, M. H. and Baeyens, B. (2009), Sorption modelling on illite. Part II: Actinide sorption and linear free energy relationships, Geochimica Cosmochimica Acta, 73, 1004 -1013.

116. Dähn, R.,Scheidegger, A.M., Manceau, A., Curti, E., Baeyens, B., Bradbury, M.H. and Chateigner, D.J. (2002), Th uptake on montmorillonite : A powder and polarized extended X-ray absorption fine structure (EXAFS) study, Journal of Colloid Interface Science, 249, 8 -21.

117. Zavarin, M., Powell, B.A., Bourbin, M., Zhao, P. and Kersting, A.B. (2012), Np(V) and Pu(V) ion exchange on montmorillonite, Environmental Science Techology, 46, 2692-2698,

118. Müller, K., Förstendorf, H., Meusel, T., Brendler, V., Lefevre, G., Comarmond, M.J. and Payne, T.E. (2012), Sorption of U (VI) at the TiO_2 – water interfaces: An in situ vibrational spectroscopic study, Geochimica Cosmochimica Acta, 76, 191-205.

119. Chang, H.S., Korshin, G.V., Wang, Z.M. and Zachara, J.M. (2006), Adsorption of uranyl on gibbsite: A time-resolved laser-induced fluorescence spectroscopy study, Environmental Science Technology, 40, 1244.

120. Zingde, M.D. and Desai, B.N. (1981), Mercury in Thane creek, Bombay harbor, Marine Pollution Bulletin, 12, 237-241.

121. Jha, S.K., Chavan, S.B., Pandit, G.G. and Sadasivan, S. (2003), Geochronology of Pb and Hg pollution in a coastal marine environment using global fallout ^{137}Cs, Journal of Environmental Radioactivity, 69, 145-157.

122. Bhosale, U. and Sahu, K.C. (1991), Heavy metal pollution around the island city of Bombay, India. Part II, distribution of heavy metals between water, suspended particles and sediments in a polluted aquatic regime, Chemical Geology, 90, 285-305.

123. Sharma, P., Borole, D.V. and Zingde, M.D. (1994), ^{210}Pb geochronology and trace element composition of the sediments in the vicinity of Bombay, west coast of India, Marine Chemistry 47, 227-241.

124. Pilaai, K.C., Subraratnam, T. and Ganguly, A.K. (1958), Tidal movement and water renewal rate in Bombay Harbour Bay, AEET/HP/RWD/2.

125. Ganguly, A.K. (1983), Tracing the radionuclides in a tropical near – shore environment, Proceedings of 30 years" commemoration symposium, Saha Institute of Nuclear Physics, Calcutta.

126. Desai, M.V.M., Kulkarni, V.V, Dey, N.N., Rao, S.R., Borker, M.D., More, A.K., Sathi Kumar, Chhapgar, B.F. and Pillai, K.C. (1985). Role of sediments in accumulation and transport of radionuclides in waterways, Final report of IAEA research contract No. 3334/R2/RB.

127. MMRDA (Mumbai Metropolitan Region Development Authority), (2001), basic statistics

128. Kulkarni, V.A., Jagtap, T.G., Mhalsekar, N.M. and Naik, A.N. (2010), Biological and environmental characteristics of mangrove habitats from Manori creek, West Coast, India, Environmental Monitoring and Assessment, 168 (1-4), 587-596.

129. Baumgartner, A. and Reichel, E. (1975), The World Water Balance, Elsevier Science, Amsterdam, Oxford, New York.

130. Perkins, R.W. and Thomas, C.W. (1980), In: Hanson, W.C. (Ed.), Transuranic Elements in the Environment Worldwide Fallout, NTIS, Springfield, M.O., 53–82, DOE/TIC-22800.

131. Bacon, M.P., Rutgers V. D. and Loeff, M.M. (1989), Removal of Thorium- 234 by scavenging in the bottom nepheloid layer of the ocean, Earth Planetary Science Letters, 92, 157– 164.

132. Clegg, S.L. and Whitfield, M. (1990), A generalized model for the scavenging of trace metals in the open ocean: I. Particle cycling, Deep Sea Research, 37, 809– 832.

133. Clegg, S.L. and Whitfield, M. (1991), A generalized model for the scavenging of trace metals in the open ocean: II. Thorium scavenging, Deep Sea Research, 38, 91– 120.

134. Dunne, J.P., Murray, J.W., Young, J., Balistrieri, L.S. and Bishop, J. (1997), ^{234}Th and particle cycling in the central equatorial Pacific, Deep-Sea Research, II 44, 2049–2084.

135. Moore, W.S. (1981), The thorium content of ocean water, Earth Planetary Science Letters, 53, 419– 426.

136. Anderson, R.F., Fleisher, M.Q. and Biscaye, P.E. (1994), Anomalous boundary scavenging in the Middle Atlantic Bight—evidence from ^{230}Th, ^{231}Pa, ^{10}Be, and ^{210}Pb, Deep-Sea Research, II 41, 537–561.

137. Santschi, P.H., Guo, L., Walsh, I.D., Quigley, M.S. and Baskaran, M. (1999), Boundary exchange and scavenging of radionuclides in continental margin waters of the Middle Atlantic Bight, Implications for organic carbon fluxes, Continental Shelf Research, 19, 609– 636.

138. Smoak, J.M., Moore, W.S., Thunell, R.C. and Shaw, T.J. (1999), Comparison of ^{234}Th, ^{228}Th, and ^{210}Pb fluxes with fluxes of major sediment components in the Guaymas Basin, Gulf of California. Marine Chemistry, 65, 177–194.

139. Yu, E.-F., Francois, R. and Bacon, M.P. (1996), Similar rates of modern and last-glacial ocean thermohaline circulation inferred from radiochemical data, Nature, 379, 689– 694.

140. Marchal, O., Francois, R., Stocker, T.F. and Joos, F. (2000), Ocean thermohaline circulation and sedimentary ^{231}Pa/^{230}Th ratio, Paleoceanography, 15, 625–641.

141. Moran, S.B., Shen, C.-C., Edmonds, H.N., Weinstein, S.E., Smith, J.N. and Edwards, R.L. (2002), Dissolved and particulate ^{231}Pa and ^{230}Th in the Atlantic Ocean: constraints on intermediate/deep water age, boundary scavenging, and ^{231}Pa/ ^{230}Th fractionation, Earth Planetary Science Letters, 203, 999–1014.

142. Mitchell, P.E., Batlle, J.V., Downes, A.B., Condren, O.M., Vintro, L.L., and Sanchez-Cabeza, J.A. (1995), Recent Observations on the physico-chemical speciation of plutonium in the Irish Sea and the Western Mediterranean, Applied Radiation and Isotopes, 46(11), 1175–1190.

143. Starik, I.E. and Kolyadnin, L.B. (1957), The occurrence of uranium in ocean water, Geochemistry, 2, 245 -256.

144. Miyake, Y, Sugimura, Y. and Uchida, T. (1972), A new method of spectrophotometric determination of uranium in sea water and uranium content with $^{234}U/^{238}U$ ratio in the Pacific water, Records Oceanography Works Japan, 11, 53-63.

145. Hodge, V.F., Koide, M. and Goldberg, E.D. (1979), Particulate uranium, plutonium and polonium in biogeochemistries o the coastal zone, Nature, 277, 206 -209.

146. Anderson, R.F. (1982), Concentration, vertical flux, and remineralization of particulate uranium in seawater, Geochimica Cosmochimica Acta, 46, 1293 - 1299.

147. Hirose, K. (1990), Chemical speciation of trace metals in seawater : implication of particulate trace meals, Marine Chemistry, 28, 267-274.

148. Ku,T.L., Knauss, K.G. and Mathieu G.G. (1977), Uranium in open ocean : concentration and isotopic composition, Deep Sea Research., 24, 1005-1017.

149. Sugimura, Y. and Maeda, M. (1980), in: Isotope Marine Chemistry, E. D. Goldberg, Y. Horibe, K. Saruhashi (Eds), Uchida Rokakuho, Tokyo, p. 211.

150. Langmuir, D. (1978), Uranium solution-mineral equilibria at low temperatures with applications to sedimentary ore deposits, Geochimica Cosmochimica Acta, 42, 547-569.

151. Kim, J.I. (1986), Chemical behaviour of transuranic elements in natural aquatic systems, In Handbook on the Physics and Chemistry of the Actinides, Freeman, A.J. and Keller, C., Eds. Elsevier, Amsterdam, 413-455.

152. Osmond, J.K. and Ivanovich, M. (1992), Uranium-series mobilisation and surface hydrology. In Uranium Series Disequilibrium: Applications to Environmental Problems, 2nd ed. Ivanovich, M. and Harmon, R.S.,Eds. Clarendon Press, Oxford, 259 – 289.

153. Cochran, J.K. (1992), The oceanic chemistry of the uranium- and thorium-series nuclides. In Uranium Series Disequilibrium: Applications to Environmental Problems, 2nd ed. Ivanovich, M. and Harmon, R.S., Eds. Clarendon Press, Oxford. 334- 396.

154. Skwarzec, B., Boryło, A. and Strumińska, D.I. (2004), Activity disequilibrium between ^{234}U and ^{238}U isotopes in southern Baltic, Water, Air and Soil Pollution, 159, 165-173.

155. Ku, T.L., Knauss, K.G. and Mathieu, G.G. (1977). Uranium in Open Ocean: concentration and isotopic composition, Deep-Sea Research, 24, 1005-1017.

156. Skwarzec, B. (1995), Polon, uran i pluton w ekosystemie południowego Bałtyku. (Polonium, uranium and plutonium in the southern Balic ecosystem), Rozpr. i monogr., IO PAN, 6, Sopot, (in Polish).

157. Palmer, M.R. and Edmond, J.M. (1993), Uranium in river water, Geochimica Cosmochimica Acta, 57**,** 4947- 4955.

158. Windom, H., Smith, R., Niencheski, F. and Alexander, C. (2000), Uranium in rivers and estuaries of globally diverse, smaller watersheds, Marine Chemistry, 68**,** 307.321.

159. Gascoyne, M. (1992), Geochemistry of the actinides and their daughters, In Uranium Series Disequilibrium: Applications to Environmental Problems. 2nd ed. Ivanovich, M. and Harmon, R.S., Eds. Clarendon Press, Oxford, 34 - 61.

160. Moore, W.S. (1992), Radionuclides of the uranium and thorium decay series in the estuarine environment. In Uranium Series Disequilibrium: Applications to Environmental Problems. 2nd ed. Ivanovich, M. and Harmon, R.S., Eds. Clarendon Press, Oxford, 396 - 422.

161. Bacon, M.P., Rutgers V.D. and Loeff, M.M. (1989), Removal of Thorium- 234 by scavenging in the bottom nepheloid layer of the ocean, Earth Planetary Science Letter, 92, 157– 164.

162. Clegg, S.L. and Whitfield, M. (1990), A generalized model for the scavenging of trace metals in the open ocean: I. Particle cycling, Deep- Sea Research, 37, 809– 832.

163. Clegg, S.L. and Whitfield, M. (1991), A generalized model for the scavenging of trace metals in the open ocean: II. Thorium scavenging, Deep-Sea Research, 38, 91– 120.

164. Murray, J.W., Downs, J., Strom, S., Wei, C.-L. and Jannasch, H. (1989), Nutrient assimilation, export production and ^{234}Th scavenging in the Eastern Equatorial Pacific, Deep-Sea Research, 36, 1471– 1489.

165. Anderson, R.F., Fleisher, M.Q. and Biscaye, P.E. (1994), Anomalous boundary scavenging in the Middle Atlantic Bight—evidence from Th-230, Pa-231, Be-10, and Pb-210. Deep-Sea Research, II 41, 537–561.

166. Santschi, P.H., Guo, L., Walsh, I.D., Quigley, M.S. and Baskaran, M. (1999), Boundary exchange and scavenging of radionuclides in continental margin waters of the Middle Atlantic Bight, Implications for organic carbon fluxes, Continental Shelf Research, 19, 609– 636.

167. Smoak, J.M., Moore, W.S. and Thunell, R.C. (2000), Influence of boundary scavenging and sediment focusing on Th-234, Th-228 and Pb- 210 fluxes in the Santa Barbara Basin, Estuarine Coastal Shelf Science, 51, 373–384.

168. Yu, E.-F., Francois, R. and Bacon, M.P. (1996), Similar rates of modern and last-glacial ocean thermohaline circulation inferred from radiochemical data, Nature, 379, 689– 694.

169. Marchal, O., Francois, R., Stocker, T.F. and Joos, F. (2000), Ocean thermohaline circulation and sedimentary ^{231}Pa/^{230}Th ratio, Paleoceanography, 15, 625–641.

170. Moran, S.B., Shen, C.-C., Edmonds, H.N., Weinstein, S.E., Smith, J.N. and Edwards, R.L., (2002), Dissolved and particulate Pa-231 and Th-230 in the Atlantic Ocean: constraints on intermediate/deep water age, boundary scavenging, and Pa-231/Th-230 fractionation, Earth Planetary Science Letters, 203, 999–1014.

171. Choppin, G. and Morgernstern, A. (2001), Distribution and movement of environmental plutonium. In: Kudo A (ed.). Plutonium in the Environment, edited Proceeding of the second invited international symposium. November 9-12, 1999 Osaka, Japan, Elsevier/Netherland, 91-105.

172. Pilviö, R. (1998), Methods for the determination of low-level actinide concentrations and their bahaviour in the aquatic environment, Dissertation, Report Series in Radiochemistry 10, Helsinki, Yliopistopaino,

173. Watters, R., Edgington, D., Hakonson, T., Hanson, M., Smith, M., Whicker, F. and Wildung, R. (1980), Synthesis of the research literature. In: Hanson W (ed.), Transuranic elements in the environment, Springfield, Virginia, U.S. Department of Commerce, 1-44.

174. Emery, R., Klopfer, D. and McShane, M. (1980), The migration of plutonium from a freshwater ecosystem at Hanford, In: Hanson W (ed.), Transuranic elements in the environment. Springfield, Virginia, U.S. Department of Commerce, 625-643.

175. Fucai, R., Yamato, A., Thein, M. and Bilinski, H. (1981), Speciation of plutonium in the Mediterranean environment, In: International Atomic Energy Agency, Techniques for identifying transuranic speciation in aquatic environments, Vienna, IAEA, 37-42.

176. Molero, J., Sanchez-Cabeza J., Merino, J., Vives Battle, J., Mitchell, P. and Vidal-Quadras, A. (1995), Particulate distribution of plutonium and americium in surface waters from he Spanish Mediterranean coast, Journal of Environmental Radioactivity, 28, 271-283.

177. Ikäheimonen, T.K., Mattila. J., Klemola, S. and Ilus, E. (1997), A study on the behavior ofcesium and plutonium in the sedimentation process under varying redox-conditions, In: Walderhaug, T., Gudlausson, E. (eds.). Proceedings of NordiskSelskap For Strålevern, det 11, ordinare møtet, Det 7, Nordiske Radioøkologi Seminar, 26 – 29, August 1996, Reykjavik, Island. Reykjavik: ODDI, 443-448.

178. Allard, B., Olofsson, U., Torstenfelt, B. (1984), Environmental actinide chemistry, Inorganic Chimica Acta, 94, 205-221.

179. Sholkovitz, E. (1983), The geochemistry of plutonium in fresh and marine water environment, Earth - Science Reviews, 1983 19, 95-161.

180. International Atomic Energy Agency (1985), Sediment K_ds and concentration factors for radionuclides in the marine environment, Technical Report Series No. 247, Vienna, IAEA.

181. National Council on Radiation Protection and Measurements (2001), Scientific basis for evaluating the risks to populations from space applications of plutonium, NCRP Report No.131, Bethesda, NCRP.

182. Noshkin, V. (1980), Transuranium radionuclides in components of the benthic environment of Enewetak Atoll, In: Hanson W (ed.), Transuranic elements in the environment, Springfield, Virginia, U.S. Department of Commerce, 578-601.

183. Hallstadius, L., Aarkrog, A., Dahlgaard, H., Holm, E., Boelskifte, S., Duniec, S. and Persson B. (1986), Plutonium and americium in the Arctic waters, the Nort Sea and Scottish and Irish coastal zones, Journal of Environmental Radioactivity, 4, 11-30.

184. Holm, E., Aarkrog, A., Ballestra. S. and Dahlgaard, H. (1986), Origin and isotopic ratios of plutonium in the Barents and Greenland Seas, Earth Planetary Science Letters, 79, 27-32.

185. Ilus, E., Sjöblom, K.L, Ikäheimonen, T., Saxén, R. and Klemola, S. (1993), Monitoring of radionuclides in the Baltic Sea in 1989 – 1990, STUK-A103., Helsinki: Painatus-keskus Oy.

186. Yamato, A. (1992), Concentration levels and behaviour of transuranium nuclides inJapanese coastal marine environment, Journal of Radioanalytical Nuclear Chemistry, 156, 349-360.

187. Taylor, D. (2001), Environmental plutonium - creation of the universe to twenty-first century mankind, In: Kudo A (ed.), Plutonium in the Environment. Edited Proceeding of the second invited international symposium, November 9-12,1999, Osaka, Japan. Netherlands, Elsevier, 1-14.

188. Matsunaga, T., Ueno, T., Amano, H., Tkatchenko, Y., Kovalyov, A., Watanabe, M. and Onuma, Y. (1998), Characteristics of Chernobyl-derived radionuclides in particulate form in surface waters in the exclusion zone around the Chernobyl Nuclear Power Plant, Journal of Contaminant Hydrology, 35, 101-113.

189. Baskaran, M., Shaunna, A., Santschi, P., Davis, T., Brooks, J., Champ, M., Makeyev, V. and Khlebovich, V. (1995), Distribution of ^{239,240}Pu and ^{238}Pu concentrations in sediments from the Ob and Yenisey rivers and the Kara Sea, Applied Radiation Isotopes, 46, 1109-1119.

190. Davies, D. and Gorsline, D. (1976), Oceanic sediments and sedimentary processes, In: Riley, J., Skirrow, G. (eds.). Chemical Oceanography, 2nd Edition, 5, London, Academic Press, 1-80.

191. Grasshoff, K. and Voipio, A. (1981), Chemical oceanography, In: Voipio, A. (ed.), The Baltic Sea, Netherlands: Elsevier Scientific Publishing Company, 183-218.

192. Kankaanpää, H. (1997), Sedimentation, distribution, sources and properties of organic halogen material in the Gulf of Finland, Monographs of the Boreal Environment Research, 6, Helsinki, Finnish Institute of Marine Research.

193. Kuenen, H. (1965), Geological conditions of sedimentation, In: Riley J, Skirrow G.(eds.), Chemical Oceanography, 2, London, Academic Press, 96 1-21.

194. Leivuori, M. (2000), Distribution and accumulation of metals in sediments of the Northern Baltic Sea, Contributions 2, Helsinki, Finnish Institute of Marine Research.

195. Vallius, H. (1999), Recent sediments of the Gulf of Finland: An environment affected by the accumulation of heavy metals, Department of Geology and Mineralogy, Åbo Akademi University., Espoo, Libella Painopalvelu, O.Y.

196. Struminska, D.I. and Skwarzec, B. (2004), Plutonium concentrations in waters from the southern Baltic Sea and their distribution in cod (Gadus morhua) skin and gills, Journal of Environmental Radioactivity, 72, 355–361.

197. Livingston, H.D. and Povinec, P.P. (2002), A millennium perspective on the contribution of global fallout radionuclides to ocean science. Health Physics, 82, 656–668.

198. Mattila, J., Kankaanpa¨a¨, H. and Ilus, E. (2006), Estimation of recent accumulation rates in the Baltic Sea using artificial radionuclides ^{137}Cs and $^{239, 240}$Pu as time markers, Boreal Environmental Research, 11, 95–107.

199. Suplinska, M.M. (2002), Vertical distribution of ^{137}Cs, ^{210}Pb, ^{226}Ra and ^{239,240}Pu in bottom sediments from the Southern Baltic Sea in the years 1998–2000, Nukleonika, 47, 45–52.

200. Wanner, H. and Forest, I. (Eds.) (1992), Chemical Thermodynamics of Uranium, North Holland, Amsterdam.

201. His, C.D. and Langmuir D. (1985), Adsorption of uranyl onto ferric oxyhydroxides, Application of the surface-complexation site-binding model, Geochimica Cosmochimica Acta, 49 (9), 1931–1941.

202. Choppin, G.R. (2007), Actinide speciation in the environment, Journal of Radioanalytical Nuclear Chemistry, 273(3), 695–703.

203. Grenthe, I. and Lagerman, Bo. (1991), Studies on metal carbonate equilibria: Complex formation in the Th(IV)–H_2O–CO_2(g) system, Acta Chemistry Scand, 45, 231– 238.

204. Osthols, E., Bruno, J. and Grenthe, I. (1994), On the influence of carbonate on mineral dissolution: the solubility of microcrystalline ThO_2 in CO_2–H_2O media, Geochimica Cosmochimica Acta, 58, 613–623.

205. Choppin, G.R. and Wong, P.J. (1998), The chemistry of actinide behavior in marine systems, Aquatic Geochemistry, 4, 77–101.

206. Bruno, J. (1990), The influence of dissolved carbon dioxide on trace metal speciation in seawater, Marine Chemistry, 30, 231– 240.

207. Murphy, R.J., Lenhart, J.J. and Honeyman, B.D. (1999), The sorption of thorium (IV) and uranium (VI) to hematite in the presence of natural organic matter, Colloids and Surfaces A : Physicochemical and Engineering Aspects, 157, 47–62.

208. Fanghanel, T. and Neck, V. (2002), Aquatic chemistry and solubility phenomena of actinide oxides/hydroxides, Pure Applied Chemistry, 72, 1895–1907.

209. Neck, V., Altmaier, M., Muller, R., Bauer, A., Fanghanel, Th. and Kim, J.I. (2003), Solubility of crystalline thorium dioxide, Radiochimica Acta, 91, 253– 262.

210. Huh, C.A., Moore, W.S. and Kadko, D.C. (1989), Oceanic ^{232}Th: a reconnaissance and implications of global distribution from manganese nodules, Geochimica Cosmochimica Acta, 53, 1357– 1366.

211. Nash, K.L. and Choppin, G.R. (1980), Interaction of humic and fulvic acids with Th(IV), Journal of Inorganic Nuclear Chemistry. 42, 1045– 1050.

212. Choppin, G.R. and Nash, K.L. (1981), Dissociation kinetics of thorium and humic acid, Journal of Inorganic Nuclear Chemistry, 43, 357– 359.

213. Artinger, R., Buckau, G., Zeh, P., Geraedts, K., Vancluysen, J., Maes, A. and Kim, J.I. (2003), Humic colloid mediated transport of tetravalent actinides and technetium, Radiochimica Acta, 91, 743– 750.

214. Reiller, P., Moulin, V., Casanova, F. and Dautel, C. (2003), On the study of Th(IV)–humic acid interactions by competition sorption studies with silica and determination of global interaction constants, Radiochimica Acta, 91, 513– 524.

215. Guo, L., Chen, M. and Gueguen, C. (2002), Control of Pa/Th ratio by particulate chemical composition, Geophysical Research Letter, 29 (20), 1961.

216. Quigley, M.S., Santschi, P.H., Hung, C.-C., Guo, L. and Honeyman, B.D.(2002), Importance of polysaccharides for ^{234}Th complexation to marine organic matter, Limnology Oceanography, 47, 367– 377.

217. Passow, U., Dunne, J., Murray, J.W., Balistrieri, L. and Alldredge, A.L. (2006), Organic carbon to ^{234}Th ratios of marine organic matter, Marine Chemistry, 100, 323 – 336.

218. Guo, L., Santschi, P.H. and Baskaran, M. (1997), Interaction of thorium isotopes with colloidal organic matter in oceanic environments, Colloids and Surfaces A: Physicochemical and Engineering Aspects, 120, 255–272.

219. Hunter, K.A. and Liss, P.S. (1979), The surface charge of suspended particles in estuarine and coastal waters, Nature, 282, 823– 825.

220. Nelson, D.M., Carey, A.E. and Bowen, V.T. (1984), Plutonium oxidation state distributions in the Pacific Ocean during 1980–1981, Earth Planetary Sciience Letters, 68, 422– 430.

221. Mitchel, P.I., Battle, J.V., Ryan, T.P., Schell, W.R., Sanchez-Cabeza, J.A. and Vidal-Quadras, A. (1991), In: Kershaw, P.J., Woodhead, D.S. (Eds.), Radionuclides in the Study of Marine Processes. Elsevier, London.

222. Nelson, D.M. and Lovett, M.B. (1978), Oxidation state of plutonium in the Irish Sea, Nature 276, 599–601.

223. Holm, E. and Fukai, R. (1986), Actinides isotopes in the marine environment, Journal of Less Common Metals, 122, 487– 497.

224. Morse, J.W. and Choppin, G.R. (1991), The chemistry of transuranic elements in natural waters, Review in Aquatic Sciience 4, 1– 22.

225. Mattigod, S.V. (1995), Validation of geochemical equilibrium models. In Chemical Equilibrium and Reactive Models. Loepport, R.H., Schwab, A.P., and Goldberg, S., Eds. Soil Society of America and American Society of Agronomy, Madison, WI., 201- 218.

226. Nordstrom, D.K. and Ball, J.W. (1984), Chemical models, computer programs and metal complexation in natural waters. In Complexation of Trace Metals in Natural Waters. Kramer, C.J.M. and Duinker, J.C., Eds. Martinus Nijhoff/Dr. W. Junk Publishers, The Hague, 149.164.

227. Markich, S.J. and Brown, P.L. (1999), Thermochemical Data (log K) for Environmentally Relevant Elements, 1. H, Na, K, Ca, Mg, Fe, Mn, U, Al, Pb, Cu and Cd with Model Fulvic

Acid (aspartate, citrate, malonate, salicylate and tricarballyate). ANSTO/E735, Australian Nuclear Science and Technology Organisation, Sydney.

228. Campbell, P.G.C. and Tessier, A. (1987), Current status of metal speciation studies. In Metal Speciation, Separation and Recovery, Patterson, J.W. and Passino, R., Eds. Lewis Publishers, Chelsea, MI, 201 - 224.

229. Nordstrom, D.K. and Munoz, J.L. (1994), Geochemical Thermodynamics. 2nd ed. Blackwell Scientific, Oxford.

230. Cochran, J.K. (1992), The oceanic chemistry of the uranium- and thorium-series nuclides. In Uranium Series Disequilibrium: Applications to Environmental Problems. 2nd ed. Ivanovich, M. and Harmon, R.S.,Eds. Clarendon Press, Oxford, 334 -396.

231. Nordstrom, D.K. (1996), Trace metal speciation in natural waters: computational vs. analytical, Water Air Soil Pollution, 90**,** 257 - 267.

232. Grenthe, I., Fuger, J., Konings, R.J.M., Lemire, R.J., Muller, A.B., Nguyen-Trung, C. and Wanner, H. (1992), Chemical Thermodynamics of Uranium, Wanner, H. and Forest, I., Eds. North-Holland, Amsterdam.

233. Choppin, G.R. (1992), The role of natural organics in radionuclide migration in natural aquifer systems, Radiochimica, Acta, 58/59, 113-120.

234. Markich, S.J. (1998), Effects of Biological and Physicochemical Variables on the Valve Movement Responses of Freshwater Bivalves to Mn, U, Cd and Cu [Ph.D. Thesis], University of Technology, Sydney.

235. Puigdomenech I, (1999), MEDUSA: Make Equilibrium Diagrams Using Sophisticated Algorithms, version 2. Inorganic Chemistry. Stockholm7 Royal Institute of Technology (KTH).

236. IAEA TECHDOC-265 (1982), Behavior of transuranic nuclides in coastal environment.

237. Alberts, J.J., Tilly, L.J. and Vigerstad, T.J. (1979), Seasonal cycling of Cesium-137 in a reservoir, Science, 203, 649–651.

238. Bird, G.A., Schwartz, W.J., Motycka, M. and Rosentreter, J. (1998), Behavior of ^{60}Co and ^{134}Cs in a Canadian Shield lake over 5 years, Science of the Total Environment, 212, 115–135.

239. Hakonson, T.E. and Whicker, F.W. (1975), Cesium kinetics in a Montana lake ecosystem, Health Physics, 28, 699–706.

240. Kennedy, V.H., Sanches, A.L., Oughton, D.H. and Rowland, A.P. (1997), Use of single and sequential chemical extractants to assess radionuclide and heavy metal availability from soils for root uptake, Analyst, 122, R89 – R-100.

241. Stumm, W. (1992), Chemistry of the solid-water interface; John Wiley & Sons, Inc.: New York.

242. Brady, N.C. (1990), The Nature and Properties of Soils; MacMillian: New York.

243. Osmond, J.K. and Ivanovich, M. (1992), Uranium-series mobilisation and surface hydrology. In Uranium Series Disequilibrium: Applications to Environmental Problems. 2nd ed. Ivanovich, M. and Harmon, R.S.,Eds. Clarendon Press, Oxford, 259.289.

244. Silva, R.J., Nitsche, H. (1995), Actinide environmental chemistry, Radiochimica Acta, 70/71, 377– 396.

245. Bard, E.B., Hemlin, R.G., Fairbanks and Zindler, A. (1980), Calibration of the ^{14}C time scale over the past 30,000 years using mass spectrometric U-Th ages from Barbados corals, Nature, 345, 405-410.

246. Yu, E.F., Francois, R and Bacon, M.P. (1996), Similar rates of modern and last glacial ocean thermohaline circulation inferred from radiochemical data, Nature, 3779, 689-694.

247. Anderson R.F., .Lehuray, A.P., Fleisher, M.Q. and Murray, J.W. (1989), Uranium deposition in Saanich Inlet sediments, Vancouver Island, Geochemica et Cosmochimca Acta, 53, 2205-2213.

248. Cochran, J.K., Carey, A.E., Scholkovitz, E.R. and Suppenant, L.D. (1986), The geochemistry of uranium and thorium in coastal marine sediments and sediment pore waters, Geochemica et Cosmochimca Acta, 50, 663-680.

249. Colley, S. and Thomson, J. (1985), Recurrent uranium relocations in distal turbidities emplaced in pelagic conditions, Geochemica et Cosmochimca Acta, 49, 2339-2348.

250. Wallace, H.E., Thomson, J., Wilson, T.R.S., Weaver, P.P.E., Higgs, N.C. and Hydes, D.J. (1988), Active diagenetic formation of metal-rich layers in N-E., Atlantic sediments, Geochemica Cosmochimca Acta, 52, 1557-1569.

251. Andersson, R.F., Fleisher, M.O. and Lehuray, A.P. (1989), Concentration, oxidation state and particulate flux of uranium in the Black Sea, Geochimica et Cosmochimica Acta, 53, 2215-2224.

252. Scott, M.R. (1968), Thorium and uranium concentrations and isotope ratios in river sediments, Earth Planetary Science Letters, 4, 245- 252.

253. Huh, C.A. and Kadko, D.C. (1992), Marine sediments and sedimentation process. In: Uranium-series Disequilibrium: Applications to Earth, Marine and Environmental Sciences, M. Ivanovich and R.S. Harmon (Eds). Clarendon Press, Oxford, pp. 460.

254. Nozaki, Y. and Horibe, Y. (1981), The water column distributions of thorium isotopes in the western north Pacific, Earth Planetary Science Letters, 54, 203 – 216.

255. Bacon, M.P. and Anderson, R.F. (1982), Distribution of thorium isotopes between dissolved and particulate forms in the deep sea, Journal of Geophysical Research, 87(C3), 2045 – 2056.

256. Murnane, R., Sarmiento, J.L. and Bacon, M.P. (1990), Thorium isotopes, particle cycling models and inverse calculations of model rate constants, Journal of Geophysical Research, 99 (C2), 3393- 3405.

257. Bhat, S.G., Krishnaswami, S., Rama Lal, D. and Moore, W.S. (1669), ^{234}Th/ ^{238}U ratios in the ocean, Earth Planetary Science Letters, 5, 483 – 491.

258. Kaufman A., Li, Y.H. and Turekian, K.K. (1981), The removal rates of ^{234}Th and ^{228}Th from water of the New York Bight, Earth Planetary Science Letters, 54, 385-392.

259. Choppin, G.R. and Bond, A. H. (1996), Actinide oxidation state speciation, Journal of Analytical Chemistry, 51 (12), 1129 - 1138.

260. Choppin, G.R. (2006), Actinide speciation in aquatic systems, Marine Chemistry, 99, 83 - 92.

261. Choppin, G.R. (1991), Redox speciation of plutonium in natural waters, Journal of Radioanalytical Nuclear Chemistry, 147 (1), 109−116.

262. Nelson, D.M. and Lovett, M.B. (1978), Oxidation state of plutonium in the Irish Sea, Nature (London), 276, 599--601.

263. Holm, E. and Fukai, R. (1986), Actinide isotopes in the marine environment, Journal of Less Common Metals, 122, 487-497.

264. McCubbin, D. and Leonard, K.S.(1993), A preliminary study to assess the effect of some seawater components on the speciation of plutonium, Journal of Radioanalytical and Nuclear Chemistry, Articles, 172(2), 363–370.

265. Morse, W.A and Chopin, G.R. (1991), The chemistry of transuranic elements in natural water, Review in Aquatic Science, 4 (1), 1-22.

266. Edgington, D. (1981), Characterization of transuranic elements at environmental levels. In: International Atomic Energy Agency. Techniques for Identifying Transuranic Speciation in Aquatic Environments, Vienna, IAEA, 3-25.

267. McKay, W. and Pattenden, N. (1993), The behaviour of plutonium and americium in the shoreline waters of the Irish Sea: A Review of Harwell studies in 1980s, Journal of Environmental Radioactivity, 18, 99-132.

268. McKenzie, A., Cook, G. and McDonald P. (1999), Radionuclide distribution and particle size associations in Irish Sea surface sediments: implications for actinide dispersion, Journal of Environmental Radioactivity, 44, 275 - 296.

269. Leonard, K., McCubbin, D., Blowers, P. and Taylor, B. (1999), Dissolved plutonium and americium in surface waters of the Irish Sea, 1973 – 1996, Journal of Environmental Radioactivity, 44,129-158.

270. Assinder, D.J, Mudge, S.M. and Bourne, G.S. (1997), Radiological assessment at the Ribble Estuary- I, Distribution of radionuclides in surface sediments, Journal of Environmental Radioactivity, 36 (1), 1-19.

271. Ilus, E., Niemistö, L. and Bojanowski, R. (1995), Radionuclides in sediment and suspended particulate matter. In: Helsinki Comission, Radioactivity in the Baltic Sea, Baltic Sea Environment Proceedings, No.61. Hamburg: Bundesamt fürSeeschiffahrt and Hydrographie, 69-91.

272. Cook, G., Baxter, M., Duncan, H. and Malcolmson, R. (1984), Geochemical association of plutonium and gamma-emitting radionuclides in caithness soil and marine particulates, Journal of Environmental Radioactivity, 1, 119-131.

273. Loyland, S., LaMont, S., Herbison, S. and Clark, S. (2000), Actinide partitioning to an acidic, sandy lake sediment, Radiochimica Acta, 88, 793-798.

274. McDonald, P., Vives, I., Battle, J., Bousher, A., Whittall, A. and Chambers, N. (2001), The availability of plutonium and americium in Irish Sea sediments for re-dissolution, Science of Total Environment, 267, 109-123.

275. Ilus, E., Mattila, J., Klemola, S., Ikäheimonen, T. and Niemistö L. (2001), Sedimentation rate in the Baltic Sea. In: Palsson S. (ed). NKS-8, Marine Radioecology, Final reports from sub-projects within the Nordic Nuclear Safety Research Project EKO-1.Roskilde: Pitney Bowes Management Services, 38-60.

276. Baskaran, M., Shaunna, A., Santschi, P., Davis, T., Brooks, J., Champ, M., Makeyev, V. and Khlebovich, V. (1995), Distribution of ^{239,240}Pu and ^{238}Pu concentrations in sediments from the Ob and Yenisey rivers and the Kara Sea, Applied Radiation Isotopes, 46, 1109-1119.

277. Livingstone, H. and Povinec, P. (2000), Anthropogenic marine radioactivity, Ocean and Coastal Management, 43, 687-712.

278. Environmental radiological Laboratory Procedure manual, (1998), HPD/BARC.

279. Narayana, Y., Rajashekara, K.M. and Siddappa, K. (2007), Natural radioactivity in some major rivers of coastal Karnataka on the southwest coast of India, Journal of Environmental Radioactivity, 95, 98–106.

280. Canadian Water Quality Guidelines. Canadian Council of Resource and Environment Ministers (CCREM), (1991), Inland Waters Directorate, Environment Canada, Ottawa.

281. Veeh, H.H. (1967), Deposition of uranium from the ocean, Earth Planetary Science Letters 3, 145-150.

282. Scott, M.R. (1982), The chemistry of U and Th series nuclides in rivers. In Uranium Series Disequilibrium: Applications to Environmental Problems. Ivanovich, M. and Harmon, R.S., Eds. Clarendon Press, Oxford, 181-201.

283. Sam, A.K., Ahamed, M.M.O., Khangi, F.A. and Nigumi , Y.O. (2000), Uranium and thorium isotopes in some red sea sediments, Radiochimica Acta, 88, 307-312.

284. McCartney, M., Kershaw, P.J., Allington, D.J., Young, A.K. and Turner, D. (1992), Industrial sources of naturally occurring radionuclides in the eastern Irish Sea, Radiation Protection Dosimetry, 45 (1/4), 711-714.

285. McDonald, P., Cook, G.T. and Baxter, M.S. (1991), Natural and artificial radioactivity in coastal regions of UK. In: Radionuclides in the study of marine processes, Kershaw, P.J. and Woodhead, D.S. (Eds). Elsevier Applied Science, London, 329-339.

286. Nedwell, D., Parkes, S., Upton, A. and Assinder, D.J. (1993), Seasonal fluxes across the sediment-water interface and processes within North Sea sediments, Phil. Trans. R. Soc. Lond. A 343, 519-529.

287. IAEA TECHDOC- 265 (1982), Behavior of transuranic nuclides in coastal environment.

288. IAEA Technical Report Series No.247 (1985), Sediment k_ds and concentration factors for radionuclides in the marine environment.

289. Pillai, K.C. and Matkar, V.M. (1983). Determination of Pu and Am in environmental samples and assessment of Th in bone samples from normal and background area, Journal of Radioanalytical chemistry, 115(2), 217-229.

290. M. Scott, in Uranium Series Disequilibria: Applications to Environmental Problems, ed. M. Ivanovich and R. S. Harmon, Clarendon Press, Oxford, 1982, 181—201.

291. Keating, G.E., McCartney M. and Davidson, C.M. (1996), Investigation of the technological enhancement of natural decay series radionuclides by the manufacture of phosphates on the Cumbrian coast, Journal of Environmental Radioactivity, 32 (1-2), 53-66.

292. Anderson, R.F. (1982), Concentration, vertical flux and remineralization of particulate uranium in seawater, Geochimica et Cosmochimica Acta, 46, 1293-1299.

293. Yehia, H. D. (2010), Factors controlling uranium and thorium isotopic composition of the streambed sediments of the River Nile, Egypt, Earth Science, 21 (2), 77-103.

294. Ergin, M., Saydam, C., Basturk, O., Erdem, E. and Yoruk, R. (1991), Heavy metal concentrations in surface sediments from the two coastal inlets (Golden Horn Estuary and Izmit Bay) of the Northeastern Sea of Marmara, Chemical Geology, 91, 269–285.

295. Zhu, F.G., Wang, Z.F. and Zhang, B.Z. (1990), Clay mineral distributions and their effects on the transfer of the polluting elements in the Changjiang Estuary and the adjacent shelf. In:YuGH,Martin JM, Zhou JY, editors. Biogeochemical study of the Changjiang Estuary. Beijing: China Ocean Press, 437–449.

296. Breslin, V.T. and Sanudo-Wilhelmy, S.A. (1999), High spatial resolution sampling of metals in the sediment and water column in Port Jefferson Harbor, New York. Estuaries, 22, 669–680.

297. Horowitz, A.J. (1991), A Primer on Sediment–Trace Element Chemistry, Chelsa, MI: Lewis Publishers, 136.

298. Hedges, J. and Keil, R., (1995), Sedimentary organic matter preservation: an assessment and speculative synthesis. Marine Chemistry 49, 81-115.

299. Kumar, A., Singhal, R.K., Rout, S., Narayanan, U., Karpe, R. and Ravi, P.M. (2013), Adsorption and kinetic behavior of uranium and thorium in seawater-sediment system, Journal of Radioanalytical Nuclear Chemistry, 295, 649-656.

300. Kumar, A., Karpe, R., Rout, S., Joshi, V.M., Singhal, R.K., Ravi, P.M. (2013), Spatial Distribution an accumulation of ^{226}Ra, ^{228}Ra, ^{40}K and ^{137}Cs in bottom sediments of Mumbai Harbour Bay, Journal of Radioanalytical Nuclear Chemistry, 293(1), DOI: 10.1007/s10967-012-2166-3.

301. Muthu Raj, S. and Jayaprakash, M. (2007), Distribution and enrichment of trace metals in marine sediments of Bay of Bengal, off Ennore, southeast coast of India, Environmental Geology, 56(1), 207–217.

302. Santos, I. R., Silva- Filho, E. V., Schaefer, C. E., Albuquerque-Filho, M. R. and Campos, L. S. (2005), Heavy metal contamination in coastal sediments and soils near the Brazilian Antarctic Station, King George Island, Marine Pollution Bulletin, 50, 185–194.

303. Bellucci, L. G., Moumni, E.I., Collavini, B., Frignani, F. and Albertazzi, M. (2003), Heavy metals in Morocco Lagoon and river sediments. Journal of Physics, 107 (1), 139-142.

304. Buccolieri, A., Buccolieri, G., Cardellicchio, N., Dell Atti, A., Di Leo, A. and Maci, A. (2006), Heavy metals in the marine sediments of Taranto Gulf (Ionian Sea, Southern Italy), Marine Chemistry, 99, 227–235.

305. Gonzalez-Macias, C., Schifter, I., Liuch-Cota, D. B., Mendez-Rodriguez, L. and Hernandez-Vazquez, S. (2006), Distribution, enrichment and accumulation of heavy metals in coastal sediments of Salina Cruz Bay, Mexico, Environmental Monitoring and Assessment, 118, 211–230.

306. Ip, C. C. M., Li, X. D., Zhang, G., Wai, O.W. H. and Li, Y. S. (2007), Trace metal distribution in sediments of the Pearl River Estuary and the surrounding coastal areas, South China, Environmental Pollution, 147, 311–323.

307. Szefer, P., Glasby, G.P., Pempkowiak, J. and Kaliszan, R., 1995. Extraction studies of heavy-metal pollutants in surficial sediments from the southern Baltic Sea off Poland. Chemical Geology 120, 111–126.

308. Förstner, U. and Salomons, W. (1980), Trace metal analysis on polluted sediments. Part 1: assessment of sources and intensities, Environmental Technology Letter, 1, 494–505.

309. Fedo, C.M., Eriksson, K. and Krogstad, E.J. (1996), Geochemistry of shales from the Archean Abitibi greenstone belt, Canada: implications for provenance and source area weathering, Geochim et Cosmochim Acta, 60, 1751–63.

310. Nesbitt, H.W, Young, G.M., Mc Lennan, S.M. and Keays, R.R.(1996), Effects of chemical weathering and sorting on the petrogenesis siliclastic sediments, with implications for provenance studies, Journal of Geology, 104, 525–42.

311. Nath, B.N., Kunzendorf., H. and Pluger, W.L. (2000), Influence of provenancer weathering, and sedimentary processes on the elemental ratios of the fine-grained fractions of the bed load sediments from the Vembanad Lake and the adjoining continental shelf, south west coast of India, Jounal of Sediment Petrol, 70, 1081–94.

312. Valette-Silver, H.J. (1993), The use of sediment cores to reconstruct historical trends in contamination of estuarine and coastal sediments, Estuaries, 16 (3B), 577–588.

313. Clark, R.B.(2001), Marine Pollution Oxford: Oxford University Press, 5th ed., 237 pp.

314. Förstner, U. and Wittman, G.T.W. (1979), Metal pollution in the aquatic environment, Berlin, Springer–Verlag, 486 pp.

315. Zhang, J. and Liu, C. L. (2002), Riverine composition and estuarine geochemistry of particulate metals in China—weathering features, anthropogenic impact and chemical fluxes, Estuarine, Coastal and Shelf Science. 54, 1051–1070.

316. Zhang, L., Ye, X., Feng, H., Jing, Y., Ouyang, T. and Yu, X. (2007), Heavy metal contamination in western Xiamen Bay sediments and its vicinity, China, Marine Pollution Bulletin, 54, 974–982.

317. Simeonov, V., Massart, D. L., Andreev, G. and Tsakovski, S. (2000), Assessment of metal pollution based on multivariate statistical modeling of "hot spot" sediments from the Black Sea, Chemosphere, 41, 1411– 1417.

318. Covelli, S. and Fontolan, G. (1997), Application of normalization procedure in determining regional geochemical baselines, Environmental Geology, 30(1/2), 34–45.

319. Nolting, R.F., Ramkema, A. and Everaarts, J.M. (1999), The geochemistry of Cu, Cd, Zn, Ni and Pb in sediment cores from the continental slope of the Banc d'Arguin (Mauritania), Continental Shelf Research, 19, 665–91.

320. Taylor, S. R. and McLennan, S.M. (1985), The continental crust: its composition and evolution, Blackwell Scientific Publications. Geoscience texts.

321. McLennan, S.M., Hemming, S., McDaniel, D.K. and Hanson, G.N. (1993), Geochemical approaches to sedimentation, provenance, and tectonics. In: Johnsson, M.J., Basu, A.

(Eds.), Processes Controlling the Composition of Clastic Sediments, Geological Society of America Special Paper, 284, 21–40.

322. Canuel, E.A. and Martens, C.S. (1993), Seasonal variability in the sources and alteration of organic matter associated with recently deposited sediments, Organic Geochemistry, 20(5), 563–77.

323. Sirocko, F., Garbe-Schönberg, D. and Devey, C. (2000), Processes controlling trace element geochemistry of Arabian Sea sediments during the last 25,000 years, Global and Planetary Change, 26, 217–303.

324. Das, A. and Krishnaswami, S. (2006), Barium in Deccan Basalt Rivers: Its abundance, relative mobility and flux, Aquatic Geochemistry, 12, 221–238.

325. Collier, R. and Edmond, J. (1984), The trace element geochemistry of marine biogenic particulate matter, Progress in Oceanography. 13, 113–199.

326. Buckley, D.E. and Winters, G.V. (1992), Geochemical characteristics of contaminated surficial sediments in Halifax Harbour: impact of waste discharge, Canadian Journal of Earth Sciences, 29, 2617– 2639.

327. Gobeil, C., Silverberg, N., Sundby, B. and Cossa, D. (1987), Cadmium diagenesis in Laurentian Trough sediments, Geochimica et Cosmochimica Acta, 51(3), 589-596.

328. Rubio, B., Nombela, M.A. and Vilas, F. (2000), Geochemistry of major and trace elements in sediments of the Ria de Vigo (NW Spain): an assessment of metal pollution, Marine Pollution Bulletin, 40, 968–80.

329. Johnson, K.S., Berelson, W.M., Coale, K.H., Coley, T.L., Elrod, V.A., Fairey, W.R., Iams, H.D., Kilgore, T.E. and Nowicki, J.L. (1992), Manganese flux from continental margin sediments in a transect through the oxygen minimum, Science, 257, 1242-1245.

330. Abu-Hilal, A.H. and Badran, M.M. (1990), Effect of pollution sources on metal concentration in sediment cores from the Gulf of Aqaba (Red Sea), Marine Pollution Bulletin, 21, 190–197.

331. El-Sayed M. Kh. (1982), Effect of sewage effluent on the sediment of Nordasvatnet (a land-locked fjord), Norway, Marine Pollution Bulletin, 13, 85–88.

332. Nohara M. and Yokota, S. (1978), The geochemistry of trace elements in pelagic sediments from the central Pacific Basin, Journal of Geological Society, Japan, 84(4), 165–175.

333. Choppin, G.R. and Pamela, J.W. (1998), The chemistry of actinide behavior in marine systems, Aquatic Geochemistry, 4, 77–101.

334. Sheppard, M.I., Thibault, D.H. and Mitchell, J.H. (1987), Element leaching and capillary rise in sandy soil cores, experimental results, Journal of Environmental Quality, 16, 273-284.

335. Abdelouas, A., Lutze, W. and Nuttall, E. (1998), Chemical reactions of uranium in ground water at a mill tailings site. Journal of Contaminant Hydrology, 34 (4), 343–361.

336. Langmuir, D. (1978), Uranium solution-mineral equilibria at low temperatures with applications to sedimentary ore deposits. Geochimica et Cosmochimica Acta, 42 (96), 547–569.

337. Syed, H.S. (1999), Comparison studies adsorption of thorium and uranium on pure clay minerals and local Malaysian soil sediments, Journal of Radioanalytical and Nuclear Chemistry, 241 (1), 11-14.

338. Choppin, G.R. (2007), Actinide speciation in the environment, Journal of Radioanalytical and Nuclear Chemistry, 273 (3), 695–703.

339. Hsi, C.D. and Langmuir, D. (1985), Adsorption of uranyl onto ferric oxyhydroxides : Application of the surface-complexation site-binding model, Geochimica et Cosmochimica Acta, 49, (9), 1931–1941.

340. UNEP, (2001), Possible effects of DU on groundwater, UNEP Balkans Report of March, 119 – 122.

341. Unsworth, E.R. (2001), Measurement and modelling of uranium and thorium in natural waters, Ph.D. Thesis, University of Plymouth, Plymouth, United Kingdom.

342. Stevenson, F.J. (1982), Humus chemist: Genesis, composition and reactions, John Wiley & Sons, New York.

343. Franke K., Rössler, D., Gottschhalch, U. and Kupsch, H. (2000), Mobilization and retardation of uranium DOC species at Three Mine Piles in Schlema/Alberoda, Saxony, Germany, Isotope in Environmental and Health Studies, 36, 223 – 239.

344. Wood, S.A., (1996), The role of humic substances in the transport and fixation of metals of economic interest (Au, Pt, U, V), Ore Geology Reviews, 11(1-3), 1–31.

345. Schmeide, K., Jander, R., Haise, K.H. and Berhard, G. (1999), Effect of humic acid on the uranium (VI) sorption onto phylite and its mineralogical constituents. In: FZKA 6324, Wissenshaftliche Berichte Forschungszentrum Karlsruhe, G. Buckau (ed.), Karlsruhe 1999, pp. 199.

346. Pompe, S., Bubner, M., Schmeide, K., Heise,K.H., Bernhard, G. and Nitsche, H. (1999), Influence of humic acids on the migration behavior of radioactive and non-radioactive substances under conditions close to nature –synthesis, radiometric determination of functional groups, complexation-, Wissenschaftlich-Technische Berichte/Forschungszentrum Rossendorf; FZR-290.

347. United States Environmental Protection Agency (1999), Understanding variation on partition coefficient, K_d, values: II. Review of geochemistry and gvailable K_d values for cadmium, caesium, chromium, lead, plutonium, radon, strontium, thorium, tritium (^3H) and uranium, Rep. 402-R-99-004B, USEPA, Washington, DC

348. Langmuir, D. and Herman, J.S. (1980). The mobility of thorium in natural waters at low temperatures, Geochim et Cosmochimica Acta, 44, 1753–1766.

349. Felmy, A.R., Rai, D. and Mason, M.J. (1991), The solubility of hydrous thorium (IV) oxide in chloride media: Development of an aqueous ion-interaction model, Radiochimica Acta, 55, 177–185

350. Sparks, D.L. (1995), Environmental Soil Chemistry. Academic Press, San Diego, CA.

351. Goldberg S. (2002), Competitive adsorption of arsenate and arsenite on oxides and clay minerals, Soil Science Society of America Journal, 66, 413– 421.

352. Sposito, G. (1980), Derivation of the Freundlich equation for ion exchange in soils, Soil Science Society of America Journal, 44, 652– 654.

353. Shaheen, S.M. (2009), Sorption and lability of cadmium and lead in different soils from Egypt and Greece, Geoderma, 153, 61-68.

354. Basta, N.T. and Tabatabai, M.A. (1992 a), Effect of cropping systems on sorption of metals by soils: III. Competitive sorption, Soil Sciience, 153, 331–337.

355. Ticknor, K.V. (1994), Uranium sorption on geological materials, Radiochimica Acta, 64, 229–236.

356. Alloway, B.J. (1995), Soil processes and the behavior of metals. In: Heavy Metals in Soils, Alloway, B.J. (Ed.) Blackie Academic & Professional, London, 11–37

357. Shaheen, S.M, Tsadilas, C.D. and Eskridge, K.M. (2009), Effect of common ions on phosphorus sorption and lability in Greek Alfisols with different pH, Soil Science, 174 (1), 21-26

358. Saha, U.K., Taniguuchi, S., and Sakurai K. (2002), Simultaneous sorption of cadmium, zinc, and lead on hydroxyaluminum- and hydroxyaluminosilicate- montmorillonite complexes, Soil Sciience Society of America Journal, 66, 117–128.

359. Schneider, P., Neitzel, P.L., Osenbrück, K., Noubacteb, C., Merkel, B. and Hurst, S. (2001), In-situ treatment of radioactive mine water using reactive materials – result of laboratory and field experiments in uranium ore mines in Germany, Acta Hydrochimica Hydrobiology, 29(2-3), 129-138.

360. Ehdwall H., Holmberg, B.T. and Farzar, K. (1985), Radiological and legal aspects of energy production by burning peat, The Science of the Total Environment, 45(10), 69 - 75.

361. Krishnaswami, S. and La1, D. (1978), Radionuclide limnochronology in Lerman, A., ed., Lakes-Chemistry, Geology, Physics. Springer- Verlag, New York, p. 153-177.

362. Appleby, P.G. and Oldfield, F. (1992), Application of lead-210 to sedimentation studies. Uranium Series Disequilibrium: Application to Earth, Marine and Environmental Science, Oxford Science Publications, pp. 731–783.

363. Goldberg, E.D. (1963), Geochronology with lead-210 radioactive dating, STI/PUB/68. International Atomic Energy Agency, Vienna, pp. 121–131.

364. Oldfield F. and Appleby P.G. (1984), Empirical testing of ^{210}Pb dating models for lake sediments. In: Haworth E.Y. and Lund J.W.G., eds., Lake Sediments and Environmental History, Leicester University Press, 93-124.

365. Krishnaswami L.D., Martin J.M. and Meybeck M. (1971), Geochronology of lake sediments, Earth Planet. Science Letter, 11, 407-414.

366. Koide, M., Soutar, A. and Goldberg, E.D. (1972), Marine geochronology with ^{210}Pb, Earth Planetary Science Letter, 14, 442– 446.

367. Lesueur P., Jouanneau J.M., Boust D., Tastet J.P. and Weber O. (2001), Sedimentation rates and fluxes in the continental shelf mud fields in the Bay of Biscay (France), Continental Shelf Research 21 (13-14), 1383-1401.

368. Alperin, M.J., Ismail, B., Suayah, L.K., Benninger, C.S., Martens, 2002, Modern organic carbon burial fluxes, recent sedimentation rates, and particle mixing rates from the upper continental slope near Cape Hatteras, North Carolina, Deep-Sea Research II 49, 4645-4665.

369. Oguri, K., Matsumotob, E., Yamada, M., Yoshiki Saito, Y., Iseki, K. (2003), Sediment accumulation rates and budgets of depositing particles of the East China Sea, Deep-Sea Research, 50, 513-528.

370. Owen and Lee (2004), Human impacts on organic matter sedimentation in a proximal shelf setting, Hong Kong, Continental Shelf Research 24, 583-602.

371. Zuo, Z., Eisma, D., Gieles, R. and Beks, J. (1997), Accumulation rates and sediment deposition in the northwestern Mediterranean, Deep Sea Res.,Part II, 44, 597– 609.

372. Palanques, A., Sanchez-Cabeza, J. A., Masque, P. and Leon L. (1998), Historical record of heavy metals in a highly contaminated Mediterranean deposit: The Besos prodelta, Mar. Chem., 61, 209– 217.

373. Radakovitch, O., Cherry, R.D. and Heussner, S. (1999), Particulate fluxes on the Rhoˆne continental margin (NW Mediterranean). Part III: ^{210}Po and ^{210}Pb data and the particle transfer scenario, Deep Sea Res., Part I, 46, 1539– 1563.

374. Sanchez-Cabeza, J. A., Masque, P., Martı´nez-Alonso, M., Mir, J. and Esteve, I. (1999b), ^{210}Pb atmospheric flux and growth rates of a microbial mat from the northwestern Mediterranean Sea (Ebro River Delta), Environmental Science Technology, 33, 3711 – 3715.

375. Masque, P., Fabres, J., Canals, M., Sanchez-Cabeza, J.A., Sanchez-Vidal, A., Cacho, I., Calafat, A.M. and Bruach, J.M. (2003), Accumulation rates of major constituents of hemipelagic sediments in the deep Alboran Sea: A centennial perspective of sedimentary dynamics, Marine Geology, 193, 207–233.

376. Nozaki, Y., Tsubota, H., Kasemsupaya, V., Yashima, M. and Ikuta, N. (1991), Residence times of surface-water and particle-reactive ^{210}Pb and ^{210}Po in the East China and Yellow seas, Geochimica Cosmochimica Acta, 55, 1265–1272.

377. Wei, C. L., and Murray, J. W., (1994), The behavior of scavenged isotopes in marine anoxic environments: ^{210}Pb and ^{210}Po In the water column of the Black Sea, Geochimica Cosmochimica Acta, 58, 1795–1811.

378. Shotyk, W., Weiss, D., Heisterkamp, M., Cheburkin, A.K., Appleby, P.G. and Adams, F.C. (2002), New peat bog record of atmospheric lead pollution in Switzerland: Pb concentrations, enrichment factors, isotopic composition, and organolead species, Environmental Science Technology, 33, 3893– 3900.

379. Kaste, J. M., Friedland, A.J. and Sturup, S. (2003), Using stable and radioactive isotopes to trace atmospherically deposited Pb in montane forest soils, Environmental Science Technology, 37, 3560–3567.

380. DeMaster, D. J., Brewster, D.C., McKee, B.A. and Nittrouer, C.A. (1991), Rates of particle scavenging, sediment reworking and longitudinal ripple formation at the Hebble site based on measurements of the ^{234}Th and ^{210}Pb, Marine Geology, 99, 423–444.

381. Roberts, K. A., Cochran, J. K. and Barnes, C. (1997), ^{210}Pb and ^{239,240}Pu in the northeast water polynya, Greenland: Particle dynamics and sediment mixing rates, Journal Marine System., 10, 401– 413.

382. Benninger, L. K., Aller, R.C., Cochran, J.K. and Turekian, K.K. (1976), Lead-210 Geochronology of contemporary near-shore sediments: Status and problems transactions (abstract), Eos Trans. AGU, 57(12), 931–932.

383. Sanchez-Cabeza, J. A., Masque, P., Ani-Ragolta, I., Merino, J., Frignani, M., Alvisi, F., Palanques, A., P. and Puig, P. (1999a) , Sediment accumulation rates in the southern Barcelona continental margin (NW Mediterranean Sea) derived from ^{210}Pb and ^{137}Cs chronology, Prog. Oceanography, 44, 313–332.

384. Benoit, G. and Rozan, T. F. (2001), ^{210}Pb and ^{137}Cs dating methods in lakes: A retrospective study, Journal. Paleolimnology, 25, 455–465.

385. Orson, R. A., Simpson, R. L. and Good, R. E. (1992), A mechanism for the accumulation and retention of heavy metals in tidal freshwater marshes of the upper Delaware River estuary, Estuarine Coastal and Shelf Science, 34: 171-186.

386. Amano, H. and Onuma, Y. (2003), Depth profiles of long lived radionuclides in Chernobyl soils sampled around 10 years after the accident, Journal of Radioanalytical and Nuclear Chemistry, 255 (1): 217-222.

387. Ambers, R. K. R. (2001), Using the sediment record in a western Oregon flood-control reservoir to assess the influence of storm history and logging on sediment yield. Journal of Hydrology, 244 (3-4): 181-200.

388. Thomson, J., Dyer, F.M. and Croudace, I.W. (2002), Records of radionuclides deposition in two salt marshes in the United Kingdom with contrasting redox and accumulation conditions, Geochimica et Cosmochimica Acta 66 (6):1011-1023.

389. Preiss, N., Melieres, M. A. and Pourchet, M., 1996, A compilation of data on lead 210 concentration in surface air and fluxes at the air-surface and water-sediment interfaces, Journal Geophysical Research, 101, 28,847–28,862.

390. Turekian, K. K., Benninger, L.K. and Dion, E.P. (1983), ^{7}Be and ^{210}Pb total deposition fluxes at New Haven, Connecticut and at Bermuda, Journal of Geophysical Research, 88, 5411 –5415.

391. Durham, R. W. and Joshi, S.R. (1980). The ^{210}Pb and ^{137}Cs profiles in sediment cores from Lakes Matagami and Quevillon, Northwest Quebec, Canada, Canadian Journal of Earth Science 147, pp. 1746-1750.

392. Wise, S. M. (1980). Caesium-137 and Lead-210:. A review of the techniques and some applications in geomorphology, in R. A. Cullingiord, D. A. Davidson, and J. Lewin, editors, Timescales in Geomorphology. John Wiley and Sons, London, pp. 109-127.

393. Livens F. R. and Rimmer D. U. (1988), Physico-chcmical controls on artificial radionuclides in soils, Soil Use Manage, 4, 63- 69

394. Ritchie J. C. and McHenry J. R. (1990), Application of radioactive fallout cesium-137 for measuring soil erosion and sediment accumulation rates and patterns: a review, Journal of . Environmental Quality, 19, 215-233.

395. Ely L. U, Webb R. H. and Enzel Y. (1992), Accuracy of post-bomb : ^{137}Cs and ^{14}C in dating fluvial deposits, Quat. Res. 38, 196 -204.

396. Robbins, J. A., and Edgington, D.N. (1975), Determination of recent sedimentation rates in Lake Michigan using Pb-210 and CS-137. Geochimica et Cosmochimic Acta 39, 285-304.

397. Benninger, L. K. (1978), Pb-210 balance in Long Island Sound, Geochimica et Cosmochimica Acta 42, pp. 1165-1174.

398. Smith, J. N. and Walton, A. (1980), Sediment accumulation rates and geochronolpgies measured in the Sanguenay Fjord using the Pb - 210 dating method. Geochimica et Cosmochimica Acta, 44, 225-240.

399. Goldberg, E. D., Hodge, V., Koide, M., Griffin, J.J., Gamble, E., Bricker, O.P., Matisoff, G., Holdren, G.R. and Braun, R. (1978), A pollution history of Chesapeake Bay, Geochimica et Cosmochimica Acta, 42, pp. 1413-1425.

400. Burton, W. M. and Steward, N.G. (1960), Use of long-lived natural radioactivity as an atmospheric tracer, Nature, 186, 584-589.

401. Kuehl, S.A., Nittrouer, C.A. and DeMaster, D.J. (1982), Modem sediment accumulation and strata formation on the Amazon Continental Shelf, Marine Geology, 49, 279-300.

402. Kuehl, S.A., DeMaster, D.J. and Nittrouer, C.A. (1986a), Nature of sediment accumulation on the Amazon continental shelf, Continental Shelf Research, 6, 209 - 225.

403. Crook, C.L. (1992), Solid phase activities of ^{228}Ra, ^{226}Ra, and ^{228}Th in the Amazon mixing zone, M.S. Thesis, University South Carolina, 108 pp.

404. Appleby, P.G. (2001), Chronostratigraphic techniques in recent sediments. In: Last WM, Smol JP Editors Tracking Environmental Change Using Lake Sediments 1. Springer Nedherlands: E-Publishing Inc. pp.366 171-203.

405. McDonald C.P. and Urban, N.R. (2007), Sediment radioisotope dating across a stratigraphic discontinuity in a mining-impacted lake, Journal of Environmental Radioactivity, 92, 80-95.

406. Walling, D.E. and He, Q. (1999), Improved models for estimating soil erosion rates from Caesium-137 measurements, Journal of Environmental Quality, 28, 611- 622.

407. Walling, D.E. and Quine, T.A. (1990), Calibration of caesium-137 measurements to provide quantitative erosion rate data, Land Degradation and Rehabilitation, 2, 161-175.

408. Zhang, X.B., Higgitt, D.L. and Walling, D.E. (1990), A preliminary assessment of the potential for using caesium-137 to estimate rates of soil erosion in the Loess Plateau of China, Journal of Hydrological Science, 35, 26-276.

409. Walling, D.E., He, Q. and Appleby, P.G. (2002), Conversion models for use in soil-erosion. Soil-redistribution and sedimentation investigations. In: Zapata, F. (Ed.), Handbook for the Assessment of Soil Erosion and Sedimentation using Environmental Radionuclides. Kluwer Academic Publishers, Dordrecht, Netherlands, pp. 111-164.

410. Sutherland R.A. (1992), Caesium-137 estimates of erosion in agricultural areas, Hydrological Processes, 6, 215-225.

411. Poręba, G., Bluszcz, A. and Śnieszko, Z. (2003), Concentration and vertical distribution of ^{137}Cs in agricultural and undisturbed soils from Chechło and Czarnocin areas, Geochronometria, 22, 67-72.

412. Pillai, P. M. B., Paul, A. C., Komalan Nair, S. and Pillai, K. C. (1988), Indian Journal of Environmental Health, 30, 253.

413. Hamilton, T.F., Ballestra,.S., Baxter, M.S., Gastaud, J., Osvath, I., Parsi, P., Povince, P.P. and Scott, E.M. (1994), Radiometric investigations of Kara Sea sediments and preliminary radiological assessment related to dumping of radioactive wastes in the Arctic Seas, Journal of Environmental Radioactivity, 25 (1994) 113.

414. Miralles, J., Radakovitch, O. and Aloisi, C. (2005).^{210}Pb sedimentation rate from the Northwestern Mediterranean margin, Elsevier Science, Marine Geology, 216: 155-167.

415. Chung, Y., Chang, H. C. and Hung, G. W. (2004), Particulate flux and ^{210}Pb determined on the sediment trap and core samples from the northern South China Sea, Elsevier Science Ltd., Continental Shelf, 24, 673-691.

416. Wang, A., Shu, G. and Jianjun, J. (2005), Contemporary sedimentation rates on salt marshes at Wanggang, Jiangsu, China. Acta Geographica Sinica, 60 (1), 61-70. (In Chinese).

417. Andrew, B.C., Lan, W.C. and Alejandro, C. (2003), Reconstructing historical trends in metal input in heavily-disturbed, contaminated estuaries: studies from Bilbao, Southampton Water and Sicily, Applied Geochemistry, 18, 311-325.

418. Kryshev, I.I. and Sazykina, T.G. (1995), Radiological Consequences of Radioactive Contamination of the Kara and Barents Seas, Journal of Environmental Radioactivity, 29, (3),.213-223.

419. Noureddine, A. and Baggoura, B. (1997), Plutonium Isotopes, ^{137}Cs, ^{90}Sr and Natural Radioactivity in Marine Sediments from Ghazaouet (Algeria), Journal of Environmental Radioactivity, 34 (1997) 127-138.

420. Strand, P., Trand, A., Nikitin, A., Rudjord, A.L., Salbu, B.,Christensen,G., Foyn,L., Kry dhev, I.I., Chumichev, V.B., Dahlgaard, H. and Holm, E. (1994), Survey of artificial radionuclides in the Barents Sea and the Kara Sea, Journal of Environmental Radioactivity, 25 (1994) 99 -112.

421. Cundy, A. B. and Croudace, I. W. (1995) Sedimentary and geochemical variations in a saltmarsh/mudflat environment from the mesotidal Hamble Estuary, southern England. Marine Chemistry, 51, 115-132.

422. Joshi, L.V., Rangarajan, C., Gopalakrishnan, S. (1969), Measurement of ^{210}Pb in surface, air and precipitation, Tellus, 21, 107–112.

423. Carvalho F.P. (1997). Distribution, cycling and mean residence time of ^{226}Ra, ^{210}Pb and ^{210}Po in the Tagus estuary, Portugal. Science of the Total Environment, 196, 151-161.

424. Skwarzec B., Boryło A. and Strumińska D.I. (2002), Isotopes of ^{234}U and ^{238}U in sediments of the southern Baltic, Journal of Environmental Radioactivity, 61, 345-363.

425. Bacon, M. P., Spencer, D.W. and Brewer, P.G. (1976), ^{210}Pb/^{226}Ra and ^{210}Po/^{210}Pb disequilibria in seawater and suspended particulate matter, Earth Planet. Science Letter, 32, 277-296.

426. Spencer, D.W., Bacon, M.P. and Brewer, P.G. (1980 a), Models of the distribution of ^{210}Pb in a section across the North Equatorial Atlantic Ocean, Journal of Marine Research, 39, 119-138.

427. Nozaki, Y. (1986), ^{226}Ra-^{222}Rn-^{210}Pb systematics in seawater near the bottom of the Ocean, Earth Planetary Science Letter, 80, 36-40.

428. Rama, M .K. and Goldberg, E.D. (1961), Lead-210 in natural waters, Science, 134, 98-99.

429. Goldberg, E.D. (1963), Geochronology with lead-210 radioactive dating, STI/PUB/68. International Atomic Energy Agency, Vienna, pp. 121–131.

430. Craig, H., Krishnaswami, S. and Somayajulu, B.L.K. (1973), ^{210}Pb, ^{226}Ra: Radioactive disequilibrium in the deep sea, Earth Planet. Science Letter, 17, 295-305.

431. Cochran, J. K., McKibbin-Vaughan, T., Mark M. Dornblaser, M. M., Hirschberg, D., Livingston, H.D. and Buesseler, K.O. (1990), ^{210} Pb scavenging in the North Atlantic and North Pacific Oceans, Earth and Planetary Science Letters, 97, 332-352.

432. Ajay, K., Sabyasachi R., Chopra, M.K., Mishra, D.G.,.Singhal, R.K., Ravi, P.M. and Tripathi, R.M. (2014), Modeling of ^{137}Cs migration in cores of marine sediments of Mumbai Harbor Bay, Journal of Radioanalytical Nuclear Chemistry, DOI: 10.1007/s10967-012-2166-3.

433. Levy, G.J. and Mamedov. A.I., (2002), High-energy-moisture-characteristic aggregate stability as a predictor for seal formation, Soil Science Society, American Jounal, 66, 1603–1609.

434. Norton, L.D., Mamedov, A.I., Levy, G.J. and Huang , C. (2006), Soil aggregate stability as affected by long-term tillage and clay mineralogy, Advance Geoecology, 38, 422–429.

435. He, Q. and Walling, D.E. (1996), Interpreting particle size effects in the adsorption of ^{137}Cs and unsupported ^{210}Pb by mineral soils and sediments, Journal of Environmental Radioactivity, 30 (2), 117-137.

436. Rosén, K., Öborn, I. and Lönsjö, H. (1999), Migration of radiocaesium in Swedish soil profiles after the Chernobyl accident, 1987-1995, Journal of Environmental Radioactivity 46, 45-66.

437. Bunzl, K., Schimmack, W., Krouglov, S.V. and Alexakhin, R.M. (1995), Changes with time in the migration of radiocaesium in the soil, as observed near Chernobyl and in Germany, 1986-1994, Science of the Total Environment, 175, 49-56.

438. Schimmack, W. and Schultz, W. (2006), Migration of fallout radiocaesium in a grassland soil from 1986 to 2001, Part I: activity-depth profiles of ^{134}Cs and ^{137}Cs, Science of Total Environment, 368, 853- 862.

439. Ivanov, Y.A., Lewyckyj, N., Levchuk, S.E., Prister, B.S., Firsakova, S.K., Arkhipov, N.P., Arkhipov, A.N., Kruglov, S.V., Alexakhin, R.M., Sandalls, J., and Askbrant, S. (1997), Migration of ^{137}Cs and ^{90}Sr from Chernobyl fallout in Ukrainian, Belarussian and Russian soils, Journal of Environmental Radioactivity, 35 (1), 1-21.

440. Kato, Y., Fujinaga K., Nakamura, K., Takaya, Y., Kitamura, K., Ohta, J., Toda, R., Nakashima, T. and Iwamori, H. (2011), Deep-sea mud in the Pacific Ocean as a potential resource for rare-earth elements , Nature Geo-science, 4, 535–539.

441. Sheppard, M.I., Thibault, D.H. and Mitchell, J.H. (1987), Element leaching and capillary rise in sandy soil cores, Experimental results, Journal of Environmental Quality, 16,273-284.

442. Bibler, J.P. and Marson, D.B. (1999), Behaviour of mercury, lead, ceasium and uranyl ions on four SRS soils (U). In: toxicological profile for uranium (Eds. Keiths S, Spoo, W, Corporan).

443. Prikryl, J.D., Pabalan, R.T., Turner, D.R. and Leslie, B.W. (1994), Uranium sorption on alpha-alumina: effects of pH and surface-area/ solution-volume ratio, Chemistry and migration behaviour of actinides and fission products in the geosphere, 295–300, 841.

444. Ritherdon, B., Phelps, C., Neff, H., Sowder, A.G. and S.B. Clark, (2003), Stability of U(VI) solid phases in the U(VI)-Ca^{2+}-SiO_2-OH system, Radiochimica Acta, 91, 93–96.

445. Grenthe, I., Fuger, J., Konings, R. J. M., Lemire, R. J., Muller, A. B., Nguyen-Trung, C. and Wanner, H. (1992), Chemical Thermodynamics of Uranium: Issy-les-Moulineaux (France), Nuclear Energy Agency - Organization for Economic Co-Operation and Development, 715 p.

446. Guillaumont, R., Fanghanel, T., Fuger, J., Grenthe, I., Neck, V., Palmer, D. and Rand, M., (2003), Update on the Chemical Thermodynamics of Uranium, Neptunium, Plutonium, Americium, and Technetium: Amsterdam, Elsevier, ISBN: 0-444-51401-5.

447. Casas, I., Casabona, D., Duro, L. and Depablo, J. (1994), The influence of hematite on the sorption of uranium (VI) onto granite filling fracture, Chemical Geology, 113, 319-326.

448. Ticknor, K.V. (1994), Uranium sorption on geological materials, Radiochimica Acta, 64, 229–236.

449. Waite, T.D., Davis, J.A., Payne, T.E., Waychunas, G.A. and Xu, N. (1994), Uranium (VI) adsorption to ferrihydrite: application of a surface complexation model, Geochimica et Cosmochimica Acta, 58, 5465–5478.

450. Kohler, M., Wieland, E. and Leckie. J.O. (1992), Metal–ligand–surface interactions during sorption of uranyl and neptunyl on oxides and silicates. p. 51–54. In Y.K. Kharaka and A.S. Maest (ed.) Water–rock interaction. Balkema, Rotterdam, the Netherlands.

451. Tripathi, V.S. (1983), Uranium (VI) transport modeling: Geochemical data and submodels, PhD. dissertation Stanford University palo Alto, CA (Dissertation Abstrct, 8412891)

452. Morrison, S.J., Spangler, R.R. and Tripathi, V.S. (1985), Adsorption of U (VI) on amorphous ferric oxyhydroxide at high concentrations of dissolved carbon (IV) and Sulphur (VI), Journal of Contaminant Hydrology, 17, 333-346.

453. Hsi, C.D. and Langmuir, D. (1985), Adsorption of uranyl onto ferric oxyhydroxides: application of the surface complexation site-binding model, Geochimica et Cosmochimica Acta, 49, 1931–1941.

454. McKinley, J.P., Zachara, J.M., Smith, S.C. and Turner, G.D. (1995), The influence of uranyl hydrolysis and multiple site-binding reactions on adsorption of U (VI) to montmorillonite, Clays Clay Minerology, 43(5), 586–598.

455. Turner, G.D.,, Zachara, J.M., McKinley, J.P. and Smith, S.C. (1996), Surface charge properties and UO_2^{2+} adsorption of a subsurface smectite. Geochimica et Cosmochimica Acta, 60 (18), 3399–3414.

456. Wersin, P., Hochella, M.F., Persson, Jr. P., Redden, G., Leckie, J.O and D.W. Harris, D.W.(1994), Interaction between aqueous uranium(VI) and sulfide minerals: Spectroscopic evidence for sorption and reduction, Geochimica et Cosmochimica Acta, 58, 2829–2843.

457. Morse, J.W., Shanbhag, P.M., Saito, A. and Choppin, G.R. (1984), Inter- action of uranyl ions in carbonate media, Chemical Geology, 42, 85–99.

458. Langmuir D., (1997), Actinides and their daughter and fission products. In: Aqueous environmental geochemistry. Prentice-Hall, Inc., Upper Saddle River, NJ, pp 487–547

459. Kent, D.B., Abrams, R.H., Davis, J.A., Coston, J.A. and LeBlanc, D.R.(2000), Modeling the influence of variable pH on the transport of zinc in a contaminated aquifer using semiempirical surface complexation models, Water Resources Research, 36, 3411–3425.

460. Ames, L.L. and D. Rai. D. (1978), Radionuclide interactions with rock and soil media, Vol. 1. USEPA 520/6-78-007-a. USEPA, Las Vegas, NV.

461. Tripathi, V.S. (1984) Uranium (VI) transport modeling: Geochemical data and submodels. PhD diss Stanford Univ. Palo Alto CA (Diss Abstract, 841- 891)

462. Waite, T.D., Davis, J.A., Payne, T.E., Waychunas, G.A. and Xu, N. (1994), Uranium (VI) adsorption to ferrihydrite: application of a surface complexation model, Geochimica et. Cosmochimica Acta, 58, 5465–5478.

463. Duff, M.C. and Amrhein, C. (1996), Uranium (VI) adsorption on goethite and soil in carbonate solutions. Soil Science Society American Journal, 60, 1393–1400.

464. McKinley J.P, Zachara, J.M., Smith, S.C. and Turner, G.D. (1995), The influence of uranyl hydrolysis and multiple site-binding reactions on adsorption of U(VI) to montmorillonite, Clays Clay Minerology, 43(5), 586–598.

465. Turner, G.D., Zachara, J.M., McKinley, J.P. and Smith, S.C. (1996), Surface charge properties and UO_2^{2+} adsorption of a subsurface smectite, Geochimica et Cosmochimica Acta, 60 (18), 3399–3414.

466. Kaplan, D.I. and Serne, R.J. (1995), Distribution coefficient values describing iodine, neptunium, selenium, technetium, and uranium sorption to Hanford Sediments, PNL - 10379, Pacific Northwest Laboratory, Richland, Washington.

467. Idiz, E.F., Carlisle, D. and Kaplan, I.R. (1986), Interaction between organic matter and trace metals in uranium-rich bog Kern County California, Applied Geochemistry, 1, 573 - 590.

468. Shanbhag, P.M. and Choppin, G.R. (1981), Binding of Uranyl by humic acid, Journal of inorganic and nuclear chemistry, 43 (12), 3369-3372.

469. Nash, J.T., Granger, H.C. and Adams, S.S. (1981), Geology and concepts of genesis of important types of uranium deposits: Economic Geology, 75th Anniversary, Volume, 63-116.

470. Biggar, J.W. and Cheung, M.W. (1973), Adsorption of picloram (4-amino- 3,5,6-trichloropicolinic acid) on Panoche, Ephrata, and Palouse soils—thermodynamic approach to adsorption mechanism, Soil Sciience Society American Journal, 37, 863–868.

471. Calvet, R. (1989), Adsorption of organic-chemicals in soils, Environmental Health Perspective, 83, 145–177.

472. Hu, B.W., Cheng, W., Zhang, H. and Yang, S.T. (2010), Solution chemistry effects on sorption behavior of radionuclide ^{63}Ni (II) in illite-water suspensions, Journal of Nuclear Materials, 406, 263–270.

473. Yang, S., Zhao, D., Zhang, H., Lu, S., Chen, L. and Yu, X. (2010), Impact of environmental conditions on the sorption behavior of Pb(II) in Na-bentonite suspensions, Journal of Hazardous Materials, 183, 632–640.

474. Yang, S., Guo, Z., Sheng, G. and Wang, X. (2012), Investigation of the sequestration mechanisms of Cd(II) and 1-naphthol on discharged multi-walled carbon nanotubes in aqueous environment, Science of the Total Environment, 420, 214–221.

475. Chen, C.L., Wang, X.K. and Nagatsu, M. (2009), Europium adsorption on multiwall carbon nanotube/iron oxide magnetic composite in the presence of polyacrylic acid, Environtal Science Technology, 43, 2362-2367.

476. Zhao, D.L., Yang, X., Zhang, H., Chen, C.L. and Wang, X.K. (2010), Effect of environmental conditions on Pb(II) adsorption on b-MnO_2, Chemical Engineering Journal, 164, 49-55.

477. Ghosh, S., Mashayekhi, H., Pan, B., Bhowmik, P. and Xing, B.S. (2008), Colloidal behavior of aluminum oxide nanoparticles as affected by pH and natural organic matter, Langmuir, 24, 12385-12391.

478. Kaplan, D. I., Gervais, T.L. and Krupka, K.M. (1998), Uranium (VI) sorption to sediments under high pH and ionic strength conditions, Radiochimica Acta, 80, 201-211.

479. Gamerdinger, A.P., Resch, C.T. and Kaplan. D.I. (1998), Uranium (VI) sorption and transport in unsaturated, subsurface Hanford Site sediments - effect of moisture content and sediment texture: Final Report for Subtask 2b. PNNL-11975, Pacific Northwest National Laboratory, Richland, Washington.

480. E.P.A. (U.S. Environmental Protection Agency) (1999), Understanding variation in partition coefficient, K_d, values: Volume I. The K_d model, methods of measurement and application of chemical reaction codes. EPA 402-R-99-04A, prepared for the U.S. Environmental Protection Agency, Washington, D.C. by Pacific Northwest National Laboratory, Richland, Washington.

481. Yang, S., Sheng, G., Tan, X., Hu, J., Du, J., Montavon, G. and Wang, X. (2011), Determination of Ni(II) uptake mechanisms on mordenite surfaces: a combined macroscopic and microscopic approach, Geochimica et Cosmochimica Acta, 75, 6520–6534.

482. Yang, S., Li, J., Shao, D., Hu, J. and Wang, X. (2009b), Adsorption of Ni (II) on oxidized multi-walled carbon nanotubes: effect of contact time, pH, foreign ions and PAA, Journal of Hazardous. Materials, 166, 109-116.

483. Yang, S., Zhao, D., Sheng, G., Guo, Z. and Sun, Y. (2011b), Investigation of solution chemistry effects on sorption behavior of radionuclide ^{64}Cu (II) on illite, Journal of Radioanalytical Nuclear Chemistry, 289, 467-477.

484. Yang, S., Hu, J., Chen, C., Shao, D. and Wang, X. (2011c), Mutual effect of Pb (II) and humic acid adsorption onto multiwalled carbon nanotubes/poly(acrylamide) composites from aqueous solution, Environmental Science Technology, 45, 3621-3627.

Summary

Genesis of actinides in the aquatic environment is either due to natural process or anthropogenic activities. The work carried out under this dissertation deals with interaction of three important members of the actinides i.e. Uranium (U), Thorium (Th) and Plutonium (Pu) in the marine ecosystem of Mumbai Harbour Bay. Observed concentration of U and Th in the aquatic environment is mainly due to natural process whereas Pu has mainly due to anthropogenic activities like atmospheric/underground nuclear weapon testing and major nuclear accidents like Chernobyl (Russia) in 1986 and Fukishima (Japan) in 2011. It is estimated that 1.6 $x10^{16}$ Bq of plutonium have been deposited in the oceans of the world from these tests. Subsequently, plutonium concentration in open ocean waters is in the order of 10^{-5} Bq L^{-1}, indicating that most of the plutonium released from natural waters is rather quickly sorbed to suspended particles or to the bottom sediments. Pu may also come into environment through discharges of ultra low level effluents generated at the back end of nuclear fuel cycle.

As of now more than 70 percent of the reactors are on coastal region. Therefore, it is very important to study the impact of environmental releases of long lived radionuclides on the various matrices of the coastal environment, since bays and estuaries are known to be biologically productive and strongly influenced by human activities. Coastal bay is the region of strong land-ocean interaction and their ecological functions are more complicated and vulnerable to the influence by human activities and land-source pollution than the open ocean. The bay at Trombay is called as Mumbai Harbor Bay (MHB). The average area of seawater surface of the bay is about 215 km^2 at high tide level and about 160 km^2 at low tide level. The samples of seawater and sediment were collected from sixteen different locations of MHB. All the necessary precaution were taken into account for spatial and temporal variation in the concentration of ^{232}Th, ^{238}U and $^{239+240}$Pu.

The activity concentrations of U, Th and $^{239 + 240}$Pu in seawater were ranged from 1 - 4.4 µg L^{-1} (mean: 2.6 ± 0.83 µg L^{-1}), 70 – 250 ng L^{-1} (mean: 143 ± 51 ng L^{-1}) and 47 – 138 µBq L^{-1} (mean: 86 ± 30 µBq L^{-1}) respectively. These levels are on lower side compared to others equivalent scenario internationally like La hague, France and Sellafield, UK reprocessing. Whereas in case of bottom (grab) sediments, concentrations of ^{238}U, ^{232}Th and $^{239+240}$Pu ranged from 8.5 to 14 Bqkg^{-1}, dry (mean:11.5 ± 1.7 Bq kg^{-1}, dry), 21.5 to 61.2 Bq kg^{-1}, dry (mean: 40 ± 11.4 Bq kg^{-1}, dry) and 0.16 to 1.5 Bq kg^{-1}, dry (mean: 0.7 ± 0.4 Bq kg^{-1}, dry). The spatial variability of ^{238}U, ^{232}Th and $^{239+240}$Pu in terms of coefficient of variation (CV) throughout the studied area has been found to be 15.4%, 28.5% and 63 %.

Experimental results clearly indicate that distribution of ^{238}U, ^{232}Th and $^{239+240}$Pu in the marine ecosystem is highly influenced by the concentration profiles of major and minor elements in different matrices of marine ecosystem. The linear association relationship between the spatial and vertical concentration profile of ^{238}U, ^{232}Th and $^{239+240}$Pu and heavy elements (Fe, Cu, Ni, Co and Mn) in bottom sediments was established using Karl Pearson's correlation coefficient analysis. Among heavy metals, in general, the spatial concentration profiles of Fe showed a negative correlation with all elements including ^{238}U and ^{232}Th suggesting a distinguishable behaviour during transport in the sediment system. This reveals that that once Fe ions enter into the sediment profile, other metals are removed out from sediments to seawater column. While in the case of K, Mg and $^{239+240}$Pu, Fe containing minerals are seen to be as scavengers/adsorbent as obtained by a positive correlation. Other ions like Na^{+}, K^{+}, Ca^{2+} and Mg^{2+} in marine sediments may also interfere with actinide sorption. In the marine environment, sorption is generally known to take place primarily as an exchange reaction with metal ions, particularly Ca^{2+}, Na^{+} and K^{+} present in the clay minerals such as Ca -montmorillonite, Na-montmorillonite and illite respectively.

To understand the role of sediments in scavenging and removing actinides (^{232}Th, ^{238}U and $^{239+240}$Pu) from the seawater, k_d values were evaluated under different geochemical conditions. The distribution coefficient (k_d) was calculated using batch method formula. For sediment-seawater system, k_d for U and Th ranged from 24970 to 55526 L kg^{-1} (mean: 42140 ± 12865 L kg^{-1}) and 24926 to 38561 L kg^{-1} (mean: 34256 ± 4665 L kg^{-1}) respectively. The resulting coefficient of variation (CV) around mean of k_d values for uranium and thorium determined to be 30.53% and 13.62% respectively. Subsequently, at equilibrium condition, the rate constants (k) for uranium and thorium in seawater-sediment were determined by assuming the first order of kinetics reaction and observed to be very narrow range of 0.96 – 1.07 d^{-1} for uranium and 0.96 – 1.02 d^{-1} for thorium. The variation of k_d as a function of U and Th dosages indicates that initially, at low concentration, k_d increased as a function of their concentration till achieving the saturation stage. After achieving the saturation stage, it observed to be almost constant and at sufficiently high concentration, k_d values decreased because the partitioning behavior deviates from ideality due to removal of species by precipitation. The higher k_d values obtained in the experiments with lower U and Th concentrations, may be due to their strong association with the sorption sites of sediment/soil leading to relatively strong bonding energies. The sorption parameters of U and Th obtained from the experimental results for sediment-seawater and soil-groundwater systems were fitted to Freundlich, Linear and Langmuir models.

To predict the long term behavior of actinides in the marine environment, it is essential to know their chronological deposition in the bottom sediment of Mumbai Harbour Bay. ^{210}Pb and ^{137}Cs was used as tracer to evaluate the sedimentation rate in the MHB. The total signal of ^{210}Pb in recent sediment profile consists of, supported $^{210}\text{Pb}_{\text{sup}}$, which is present due to autigenic material of the sediment and unsupported (excess) ^{210}Pb, which originates from the atmospheric deposition. $^{210}\text{Pb}_{\text{sup}}$ is usually assumed to be in radioactive equilibrium with its parent nuclide ^{226}Ra (half-life 1600 y). The activity of ^{226}Ra in core fractions was determined by taking the average activity of two separate photopeaks of two radon daughters: ^{214}Pb at 352 keV and ^{214}Bi at 609 keV after attaining the secular equilibrium and the activity of ^{137}Cs was determined using photopeak at 662 keV using gamma spectrometry systems. In the case of ^{210}Pb dating model, the sedimentation rate was determined to be 0.52 ± 0.10 cmy^{-1}, 0.73 ± 0.21 cmy^{-1} and 1.12 ± 0.24 cmy^{-1} by the slope of lines obtained in cores of SCL-3, SCL-5 and SCL-9 respectively.Besides the ^{210}Pb dating models, ^{137}Cs method utilized to confirm the sedimentation rates in core SCL-3, SCL-5 and SCL- 9 obtained to be 1.04 ± 0.18 cmy^{-1}, 0.69 ± 0.25 cmy^{-1}, 1.25 ± 0.28 cmy^{-1}respectively.

Thermodynamic parameters were also evaluated to understand the sorption of uranium onto sediment in seawater and compared with other geochemical environments such as soil – groundwater/deionised water. The negative value of ΔG^o and positive value of ΔH^o reflects that sorption of uranium onto both sediment/soil systems are a spontaneous and endothermic process under experimental conditions. However, the values of ΔS^o were positive, which indicates that during the whole adsorption process, some structural changes occurs on soils/sediments surface and thus leading to increase in the disorderness at the soil/sediment - water interface. Overall, it was observed that as temperature increases, sorption of U onto soils/ sediment increases. This may be due to increase in diffusion rate of U(VI) into the pores of soils/sediments. The speciation of U, Th and Pu at various physico-chemical parameters of marine environment was calculated by the speciation code MEDUSA. This code includes an extensive thermodynamic data base along with HYDRA (hydrochemical equilibrium constant database) speciation program and three main different algorithms for creating chemical equilibrium diagrams. The ligands such as hydroxide, chloride, nitrate, carbonate, fluoride, sulphate, phosphate and silicate are included. Using HYDRA model, the Eh-pH diagram of uranium, thorium and plutonium was drawn at measured composition of seawater. Since there are many constraints while working with Pu as the concentration were very small, therefore various conclusions were drawn on the basis of uranium.

As far as the future scope of research in measurement of ^{232}Th, ^{238}U and $^{239+240}$Pu in various matrices of marine environment of this region is concerned, early detection of deterioration is necessary to efficiently protect marine ecosystem quality. As any anthropogenic contamination once mobilized may take several decades for amelioration. Detailed laboratory experiments are needed to study the leaching of ^{232}Th, ^{238}U and $^{239+240}$Pu from in situ sediment cores under different physiochemical conditions such as pH, Eh, salt content, etc., which would give information on leachable fraction of ^{232}Th, ^{238}U and $^{239+240}$Pu which are available in seawater. There is an immediate need to study the direct determination of speciation of ^{232}Th, ^{238}U and $^{239+240}$Pu in marine environment which would give a clearer picture on contaminant dynamics and immensely help to the local marine ecosystem to take precautionary remedial measures.